THE UNIVERSITY OF HULL

Exploring the interaction between rivers and sand dunes – implications for fluvial-aeolian geomorphology

being a Thesis submitted for the Degree of Doctor of Philosophy

in the University of Hull

by

Baoli Liu
MSc from Xiamen University, China

September, 2014

For my mum Chunrong（杨春荣）*and young brother Zehua*（刘泽华）

And in memory of my father Kefu（刘克富）

Abstract

The interaction between fluvial and aeolian processes can significantly influence landforms. When rivers and sand dunes meet, the interaction of sediment transport between the two systems can lead to change in either one or both systems. However, these two systems are usually studied independently which leaves many questions unresolved in terms of how they interact. This study investigated interactions between fluvial and aeolian processes, focusing on the triggers that switch the dominance between one process and the other, and the consequent changes in geomorphology that may occur.

Firstly, a global inventory of fluvial-aeolian interactions at 230 globally distributed locations was collected using satellite imagery. At each site, the following attributes were measured: net sand transport direction, fluvial-aeolian meeting angle, dune type and river channel pattern. From these data, six different types of interaction were classified that reflect a shift in dominance between the fluvial and aeolian systems. Results from this classification confirm that only certain types of interaction were significant: the meeting angle and dune type, the meeting angle and interaction type and finally the channel pattern and interaction type. These results show the importance of fluvial – aeolian interactions, but also reveal the difficulties of understanding dynamic geomorphic systems from images taken at a single moment in time.

A highly novel cellular fluvial and aeolian/dune model was then developed to simulate the process interactions over longer periods of time. Results from the global inventory were used to set up the computational domain and different flow regimes (perennial and ephemeral) were simulated interacting with different magnitudes of aeolian sand transport. The model results demonstrated the same six types of interaction that were identified in the global survey, and also provided a better understanding of the dynamics of landform change which cannot be interpreted from single 'snapshot' images. In perennial fluvial systems, when the ratio between fluvial discharge (R_s) and aeolian sand transport rate (D_c) was in a range of critical values, the landscape exhibited cyclic behaviour with abrupt large-scale changes in the absence of external forcing. River channels would avulse around dunes significantly altering the river/dune

configuration and affecting sediment output. The interaction types observed in the modelled scenarios also exhibited transient characteristic with gradual or rapid shifts between various interaction types even under stable conditions. In contrast, landform evolution in ephemeral fluvial systems was very different from perennial environments. Dunes crossed the river channel more easily in ephemeral environments and channel development was more irregular with wetland areas developing and frequent changes in channel pattern. The results suggest that the duration of the wet season is more important than the timing of the wet season on the sediment output rates.

This study has demonstrated the importance of fluvial-aeolian interactions for understanding landform development in certain fluvial-aeolian environments and has shown that these systems may show complex responses even with constant input conditions.

Acknowledgements

I cannot express enough thanks to my principle supervisor Professor Tom Coulthard for his continued support and encouragement. The inspiration, thoughtful guidance and critical comments from every meeting and discussion with him not only helped me to get through my PhD study and finish writing my thesis but also altered my perception about research. The considerable help of my second supervisor, Dr Stuart McLelland, has also been invaluable, for which I am very grateful. The encouragement, comprehensive advice and feedback from Dr Andreas Baas (King's College London, UK), Professor Martin Williams (University of Adelaide, AU), Professor Jonathan Phillips (University of Kentucky, USA) and all the other researchers I have met have enriched my research - it means so much to a junior researcher like me.

I would like to extend my grateful thanks to all of the people from the department of Geography, Environment and Earth Sciences at University of Hull. Sincerely thanks to Dr Malcolm Lillie, for equipment, advice, mentoring, and help during the final stage of corrections. Thanks also to Dr Jane Reed, Mike Dennett, Dr Sonja Boehmer-Christiansen and Dr Jane Bunting, for their good advice, support and friendship all of which have been so valuable on both academic and personal levels. The understanding and help from other PhD students, especially Tim Horsfield with whom I shared an office and faced the challenge of writing together to the end, have been very important and made my PhD a bit easier.

Also, I would like to take this opportunity to thank the joint scholarship from the University of Hull and China Scholarship Council, and the support from Professor Wenzhi Cao (Xiamen University, China). Without this support, I would not have been able to come to study in England, which has been one of the most important experiences in my life.

Heartfelt thanks also go to all the friends and people I have met during my PhD life, for their help and good wishes for the successful completion of this study.

Finally, I am forever indebted to my mum and my young brother for their understanding, endless support and love.

To all of the above and any I have forgotten to mention, my sincere thanks.

Contents

List of figures

List of tables

List of symbols

w	Dune width
h	Dune height
h'	Flow depth in flow model
L	Dune length
l	constant transport length of a slab in model
r_d	Dune migration rate
r_d	Dune average sand flux/sand flow rate/sand transport rate in real world
Q_{ia}	Total aeolian sediment input volume
Q_{oa}	Total aeolian sediment output volume
Q_{of}	Total fluvial sediment discharge volume
R_{ia}	Aeolian sediment input rate per width in model ($m^3\ m^{-1}\ t^{-1}$)
R_{oa}	Aeolian sediment output rate per width in model ($m^3\ m^{-1}\ t^{-1}$)
R_{of}	Fluvial sediment discharge rate ($m^3\ t^{-1}$)
R_{out}	Sediment output rate ($m^3\ d^{-1}$)
R_p	Potential sediment flux on a perfect flat surface
R_s	Potential sediment flux (sediment transport rate) in model
h_a	Slab added/input depth in dune model
h_s	Max slab thickness in dune model
θ	Shadow check angle in dune model
d	Shadow check distance in dune model
P_d	Deposition probability in dune model
P_e	Erosion probability in dune model
t	Time step between dune call in dune model (*minute*)
t'	Time step in flow model
D_c	River discharge
g	Grid size in dune model (*m*)
η	Dune field density
A'	Sand dune area
A	Whole dune field area
A_p	Polygon area of a barchan in network spacing measurement method

A_f	Sand free area of a barchan in network spacing measurement method
Q	Dune volume
ρ	Defect density
q	Sediment transport rate in flow model ($m^3 s^{-1}$)
α	Ratio between aeolian sand transport rate and flow discharge (R_s/D_c)
T	Simulated time
ϕ	Dimensionless bedload transport rate
ψ	Amount of sediment eroded by fluvial action
z	Bed elevation in flow model (m)
x	Grid cell size in flow model (m)
h_{flow}	Difference in elevation between the maximum water surface elevation and maximum bed elevation of the two cells where water is being routed between
U_*	Shear velocity in flow model
F_i	Fractional volume of the i-th sediment in the active layer in flow model
W_i^*	Function that relates the fractional transport rate to the total transport rate in flow model
τ	Shear stress of the cell adjacent to the bank in flow model
τ_{rm}	Critical shear stress for the mean size of the bed sediment in flow model
υ	Flow velocity
Ci	Drag coefficient in flow model
R_{ca}	Local radius of curvature in flow model
ζ	Lateral erosion in flow model
Λ	Lateral erosion rate in flow model
λ	In-channel lateral erosion rate in flow model
Ψ_n	Lateral sediment flux in flow model
Z	Cell elevation in flow model
E	Volume of material eroded in flow model
C_{rate}	Rate of soil creep ($m\ yr^{-1}$)
i	Number of image series saved from models

Chapter 1 Introduction

1.1 Fluvial and aeolian systems versus geomorphologys

The interaction between fluvial and aeolian processes can significantly change Earth surface morphology. When rivers and aeolian systems meet, the interaction of sediment transport between the two systems can lead to change in either or both systems. However, these two systems are usually studied independently and very little previous work has been done to study fluvial-aeolian interactions, which leaves many questions unresolved in terms of how they interact.

To sketch out the wide existence of fluvial-aeolian interaction and the impact on landform evolution, there is a need to examine, describe and classify the interaction between fluvial and aeolian processes at a large (regional/global) scale to identify the issues that might have been ignored before. Furthermore, the difficulties of studying the interaction and corresponding geomorphology lie in the wide temporal and spatial scale that the interactions take place over and the limits of accessible field locations. Numerical modelling offers an alternative solution to this problem, although there are no previous studies on simulating the interaction between rivers and sand dunes, and their impact on the landscape.

1.2 Aims and contributions

1.2.1 Aims

The aims of this thesis are to:

1. Investigate, describe and classify the interaction between fluvial and aeolian processes in the field and their impact on geomorphology.
2. Numerically model the dynamic processes between fluvial and aeolian systems in comparison with field observation.
3. Examine the important factors that affect fluvial-aeolian interactions and landform evolution, and determine the critical values at which the profound geomorphological changes occur.

1.2.2 Contributions

In this study, the first systematic classification of fluvial-aeolian interaction at the global scale has been undertaken; numerical flow and dune modelling have been integrated for the first time to simulate the dynamic process of fluvial-aeolian interaction and landscape evolution; the modelling results present new insights into landform change.

1.3 Approach

The approach adopted in this study would address the research aims by applying a combination of numerical simulation with a global field survey.

1.4 Summary

This thesis has seven chapters. Following this introduction, reviews of previous research examining fluvial or aeolian processes and findings on fluvial-aeolian interactions are presented in Chapter two. From this review contemporary issues and the context for this study are identified. In Chapter three, a global survey on the interaction between rivers and sand dunes are presented, and the implication for fluvial and aeolian geomorphology are analysed. Results from Chapter three not only display the worldwide located fluvial-aeolian interaction which strongly support the importance of this study, but also provide the precise objectives for model simulation and abundant information in assisting the interpretation of model results. Following this, Chapter four details the implementation of a sand dune model. The integration of a flow model and the sand dune model is then introduced in Chapter five which also presented the observation and interpretation on the simulated interaction between perennial river and dunes. Chapter six further tested the interaction between ephemeral/intermittent rivers with dunes to find out what different results could be by changing the flow regime. Finally, Chapter seven summarises the important findings from the results chapters and outlines the future directions for research.

Chapter 2 Literature review

2.1 Introduction

Historically, research on aeolian and fluvial processes has usually been carried out separately, with their interaction rarely the central subject of investigation (Bullard and Livingstone, 2002). In this literature review, therefore, current research into aeolian and fluvial processes are firstly reviewed separately, followed by an overview of fluvial-aeolian interaction studies and relevant research methods. In aeolian dominated areas, dune morphology reflects not only field pattern characteristics, but also field dynamics, which is important in terms of field identification, dune model sentivity analysis and validation (Nishimori and Ouchi, 1993; Lima et al., 2002; Herrmann et al., 2005). Therefore, a comprehensive systhesis of current dune morphometry, morphology and dynamics research is conducted first, as this will be applied in field work and dune model validation in the current research (section 2.2). Correspondingly, a summary of current research on river morphology and dynamics is conducted in respect of identifying fluvial system characteristics (section 2.3). A review of current work in relation to fluvial and aeolian interactions will help in the identification of current research problems and assist in the identification of new approaches in respect of the study of fluvial-aeolian interaction processes (section 2.4), along with current developments in relation to computational modelling of landscape evolution. This will be integrated in order to determine which models are the most appropriate and how these can be developed to ensure their suitability to be applied in this research (section 2.5).

2.2 Aeolian geomorphology

There are four aeolian depositional landforms: sand seas, sand sheets, dunes and ripples (von Karman, 1947; Sharp, 1963; Wilson, 1972; Breed and Grow, 1979; Breed et al., 1987; Lancaster, 2011), in which dunes are important features and have been studied extensively. Dunes can be found in different climate zones world wide, and over 60% of the total area of the Earth's sand seas are covered by dunes of various

forms and sizes (Lancaster, 2011). These aeolian bodies are not only impressive in the field but can be also recognised clearly from satellite images (Breed and Grow, 1979; Daniel and Alan, 2007; Vermeesch and Drake, 2008; Hesse, 2009b; Hugenholtz et al., 2012; Al-Masrahy and Mountney, 2013).

2.2.1 Dune type classification

Dunes in the field exhibit many types of shape and classifications of dune types have been proposed mostly based on their form or dynamics (Melton, 1940; Wasson and Hyde, 1983; Mainguet, 1984).

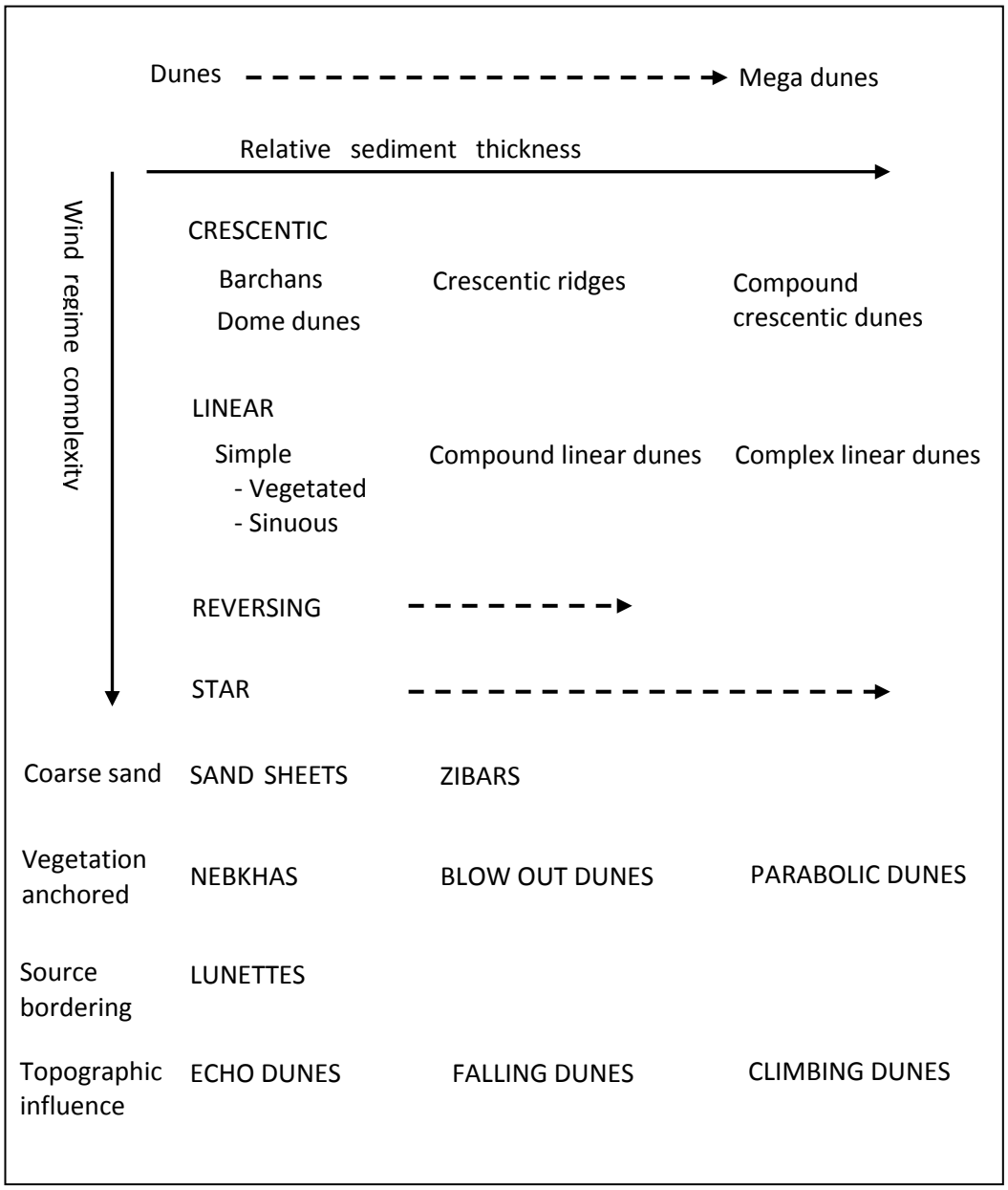

Figure 2-1 A scheme for the classification of desert dunes (Lancaster, 2011).

One of the main classifications is based on the form and relation to formative winds with dunes being classified as transverse, longitudinal or oblique (Wilson, 1972; Lancaster, 1995). Another morphological classification groups dunes on the basis of their shape and number of slip faces into five major types: crescentic (barchans), linear, reversing, star, and parabolic (McKee, 1979). Other workers have attempted to order dunes by including aspects of their mobility and relation to sediment budgets and thus to distinguish between erosional types (parabolic dunes, sand ridges) and purely depositional forms (barchanoid dunes, transverse chains, linear dunes and star dunes) (McKee, 1979). Recently, Tsoar et al. (2004) consolidated the classification of dune forms based on morphodynamics by proposing a three-fold division: *migrating* dunes (exemplified by transverse forms), *elongating* dunes (exemplified by linear dunes) and *accumulating* dunes (exemplified by star dunes). A modified scheme for the classification of desert dunes is reviewed by Lancaster (2011) based on external morphology, sediment volume and other key parameters (Figure 2-1). Broadly speaking these equate, respectively, to dunes formed in uni-modal wind regimes, those formed in bi-modal wind regimes and those formed in annual wind regimes with more than two modes which are sometimes called 'complex'.

2.2.2 Dune morphology

In reality, all dunes shapes may occur in three forms: simple, compound and complex (Breed and Grow, 1979; Hunter et al., 1983; Lancaster, 1985). Simple dunes are basic forms with the minimum number of slip faces that define the geometric type. Compound dunes are larger dunes on which smaller dunes of similar shape and slip face orientation are superimposed. Complex dunes are combinations of two or more dune shapes. Simple dunes represent a wind regime that has not changed in intensity or direction since the formation of the dune, while compound and complex dunes suggest that the intensity and direction of the wind has changed (Havholm and Kocurek, 1988). There are so many varieties in the field, that in this section dune types based on Tsoar et al. (2004)'s classification are summarised, which are also the main and most common dune types that can be seen in the field. These research provide the fundamental information in terms of field identification and evaluating performance of numerical models.

2.2.2.1 Crescentic dunes

Crescent-shaped dunes are generally wider than they are long (Figure 2-2 and Figure 2-3). The slip faces are on the concave sides of the dunes. These dunes form under winds that blow consistently from one direction where the directional variability is 15° or less about a mean value, in the absence of vegetation (Lancaster, 1995).

1) Barchan dunes

Barchan dunes are found to be formed in wind regimes characterised by a narrow range of wind directions (less than 15°) and limited sand availability (Warren, 1972; Hunter et al., 1983; Wasson and Hyde, 1983; Herrmann et al., 2005). Barchans are one of the simple dune forms, and many researchers have conducted extensive studies on the morphology and dynamics via field observation, wind tunnel simulation or aerial and satellite images (Bagnold, 1941; Finkel, 1959; Wiggs et al., 1996; Parker Gay Jr, 1999; Hugenholtz et al., 2012). Recently numerical models have also been applied these dune types (Howard et al., 1978; Momiji and Warren, 2000; Sauermann et al., 2003; Hersen, 2004; Parsons et al., 2004; Herrmann et al., 2005; Klaus et al., 2005; Durán et al., 2010; Mousavi et al., 2010).

Barchan dunes morphometric characteristics are illustrated in Figure 2-2 (Beadnell, 1910; Melton, 1940; Bagnold, 1941; Hesp and Hastings, 1998; Hesse, 2009a)(Bourke, 2010). To quantify a barchan dune, the length L along the central axis (parallel to the wind direction), the dune height h and the width w are the parameters used and close relationships between them are explored in many studies (Hesp and Hastings, 1998; Herrmann et al., 2005; Klaus et al., 2005; Parteli et al., 2007; Wang et al., 2007). It has been found that the barchan height is normally approximately one-tenth of the dune width (Mabbutt, 1977; Lancaster, 1995: 52; Hesp and Hastings, 1998), and in general, the relationship between dune height and width takes the form (2.1):

$$w = a + bh \tag{2.1}$$

The relationship between dune height and length could be expressed in the form (2.2) (Finkel, 1959; Sauermann et al., 2000):

$$L = c + dh \tag{2.2}$$

Where b and d is dimensionless coefficients and a and c is length dimensions.

The relationships of barchan morphometry parameters are important because they are closely linked to the three-dimensional morphology of the dune, and barchan dune width and length are well characterised by dune height h. This suggests that it would be more practical to measure dune height when dealing with large numbers of dunes in the field.

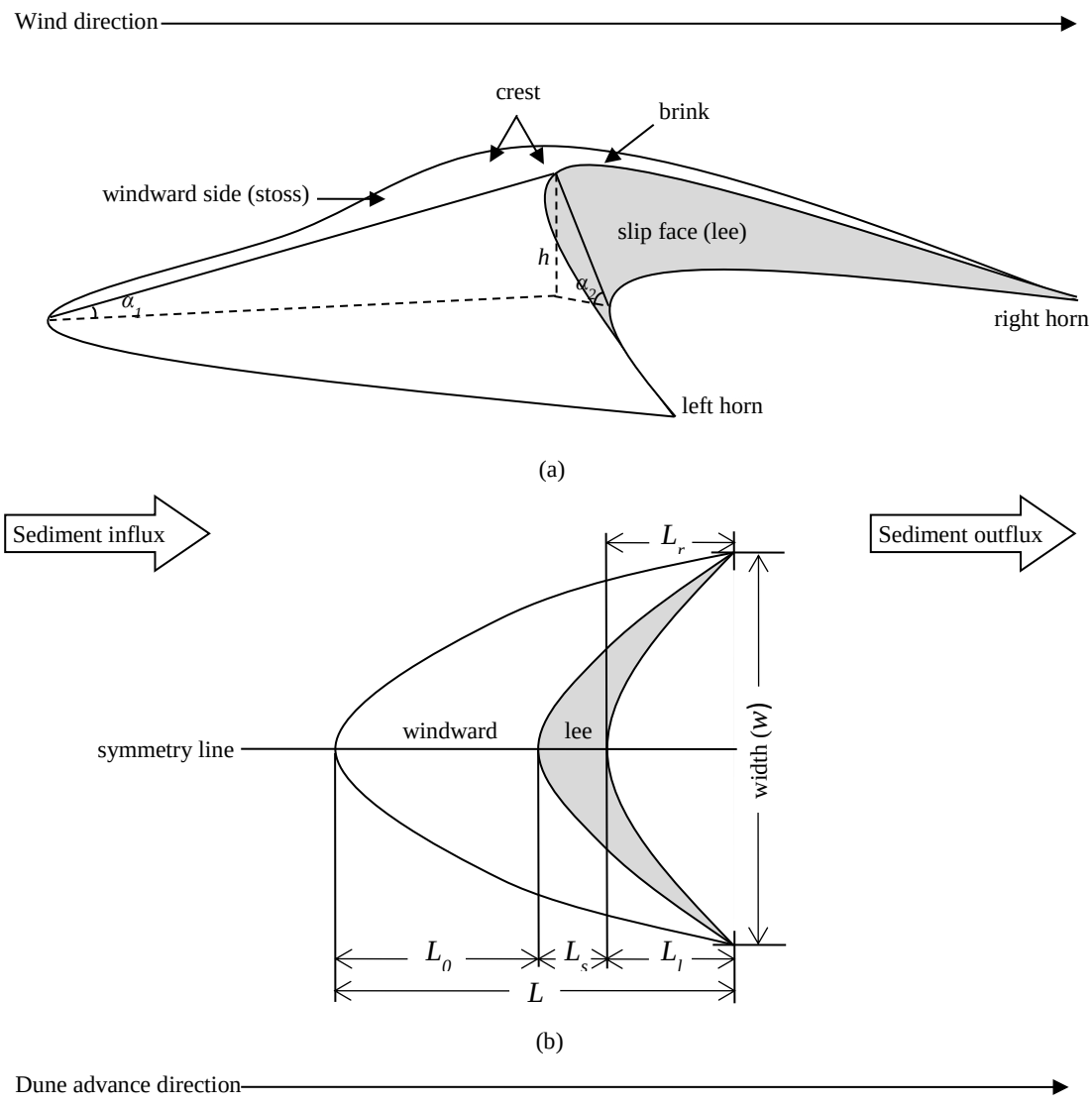

Figure 2-2 Sketch of barchan dunes morphology and morphometry. (a) three-dimension view; (b) plan view.

2) Transverse ridge dunes

As the amount of available sand increases, barchans merge (coalesce) laterally to form transverse ridges or barchanoids that consist of a series of connected crescents in planview (Wilson, 1972; Mulligan, 1988; Lancaster, 1995: 50; Van Boxel et al., 1999; Van Dijk et al., 1999; Walker and Nickling, 2003; Schatz and Herrmann, 2006). Transverse dunes are found to occupy about 40 per cent of the area of sand seas world-wide (Breed and Grow, 1979).

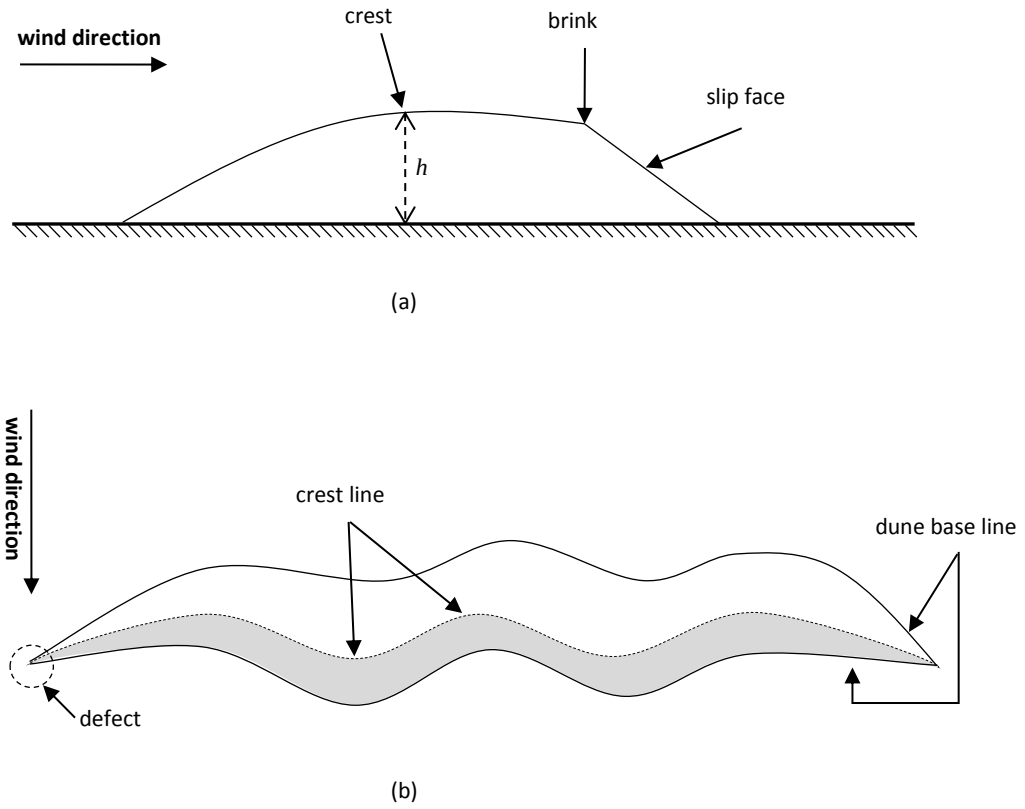

Figure 2-3 Sketch of transverse dune morphology and morphometry: (a) profile view; (b) plan view.

Transverse dunes are thought to be one of the simplest dunes in terms of shape and configuration, therefore, there were very few studies on transverse dune morphometry. Essentially, transverse dune profiles are similar to barchan dunes, the distance from the crest to the base ground being the dune height (Figure 2-3a). However, transverse dunes have more than 2 crest points as they may form from coalesced barchans, and the line connecting the crests is called the crest line (Figure 2-3b). The height at different crest points can vary which could generate an average dune height of transverse ridges. In reality, transverse ridge heights vary across a very wide range from half metre high in a simple ridge to over hundreds of metres high in

compound ridges. From some published data, which were shown and explored in Chapter 4 section 4.4.1, transverse ridge heights on the earth could be from few metres to over 200 metres with a median height of 15 m.

In plan view, the typical shape of transverse ridges is straight or very gently curved (Figure 2-3b). The width which is also referred as the wavelength of transverse ridge is the distance between the two toes which could be from few to thousand metres (Lancaster, 1995: 56; Stokes and Bray, 2005; Parteli et al., 2006).

2.2.2.2 Longitudinal dunes

Longitudinal dunes, can also be called Linear dunes if vegetated or Seifs if they are more sinuous, and can be characterised by their length, straightness and parallelism (Figure 2-4) (Price, 1950; Tsoar, 1983; Lancaster, 1995; Hesse and Simpson, 2006). Many longitudinal dunes are found to be partly vegetated which inevitably decreases the sand mobility (Tsoar and Moller, 1986).

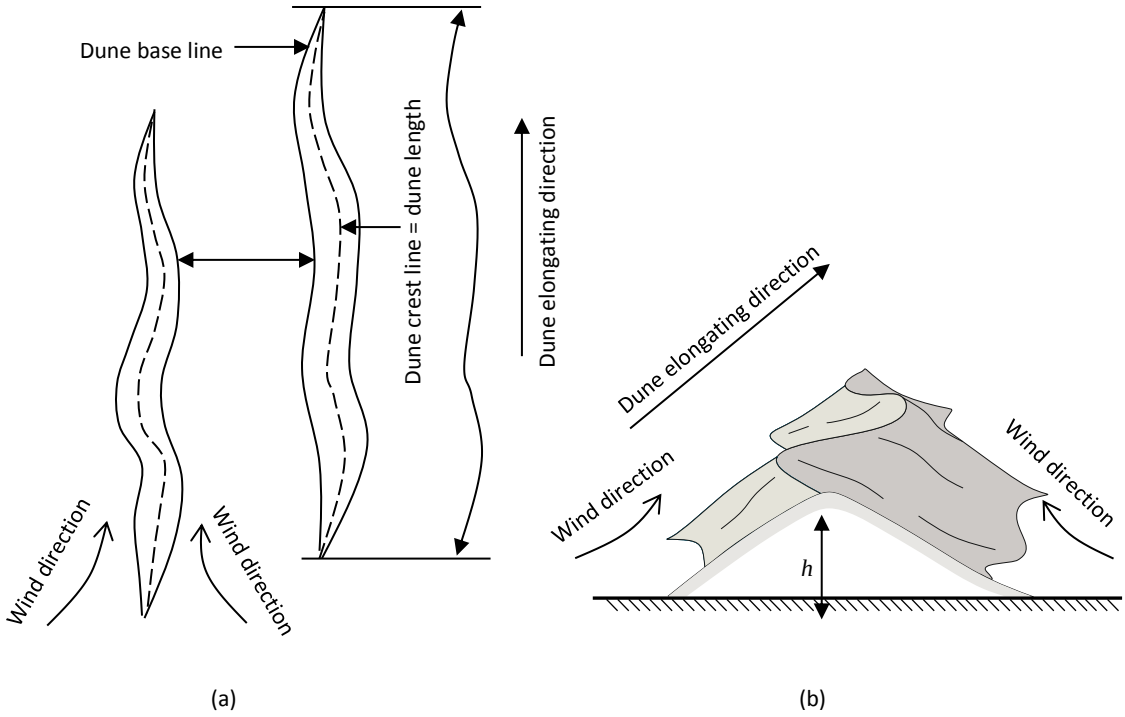

Figure 2-4 Sketch of longitudinal dune morphology and morphometry: (a) plan view; (b) cross-section view.

In terms of the dynamic process, longitudinal dunes are defined as dunes whose trend lies within 15˚ of the long-term resultant or vector sum sand transport direction, in

comparison with crescentic dunes which trend perpendicular to the resultant transport direction (Hunter et al., 1983). The causes of their formation are related to the bi- or multi-directional wind regime under which the dunes formed (Fryberger, 1979). As a result, longitudinal dunes elongate (extend in length) along the crest lines more than migrate laterally (Figure 2-4), and their level of activities are relatively lower than migrating dunes such as transverse and barchan dunes (Livingstone, 1989; Livingstone, 2003; Tsoar et al., 2004).

2.2.2.3 Star dunes

Star dunes, sometimes called pyramid dunes because of their shape, are characterised by their large size and pyramidal morphology with three or four arms radiating from a central summit (Figure 2-5) (Lancaster, 1989). This is the result of the complex wind regime under which they typically form where within multi-directional or complex wind regimes, sand-transporting winds blow from different directions from season to season. The annual resultant or net sand transport in these dune areas is subsequently often low and sand collects in the depositional centre (Nielson and Kocurek, 1987). Being an accumulating sand body, star dunes grow vertically with a very minor or no component of net lateral migration, therefore, they are considered as a stable dune (Tsoar et al., 2004). They are in many cases the highest dunes found in a sand sea (Wasson and Hyde, 1983).

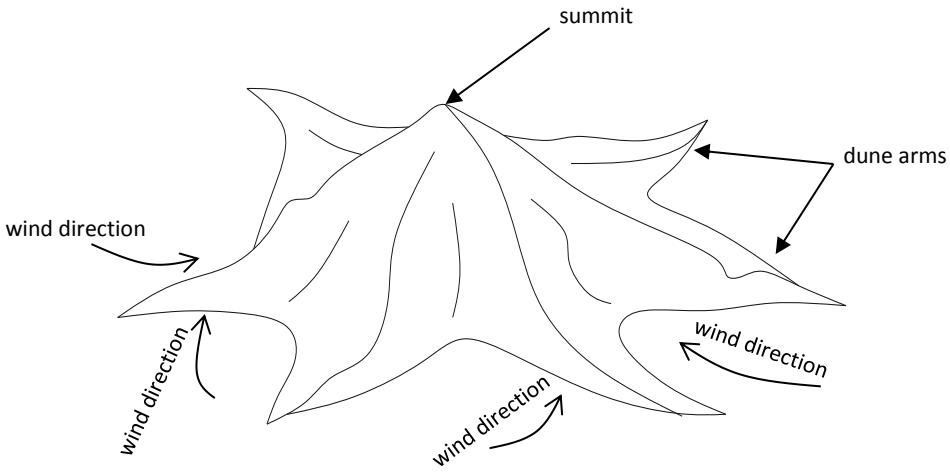

Figure 2-5 Sketch of star dune morphology.

2.2.2.4 Other dune types

There are some other types of dunes that have received considerable attention, including parabolic dunes, nebkhas, lunettes and dome dunes. These dunes are less common and usually developed under certain narrow environment constraints.

Parabolic dunes are crescentic-like with partly vegetated parallel arms pointing upwind whereas the active crest migrates forward in downwind direction (Hack, 1941; Tsoar and Blumberg, 2002). Therefore, parabolic dune arms are almost always stabilised because of vegetation.

Nebkhas are mounds composed mostly of silt and clay but less sand that accumulate around vegetation clumps (Thomas and Tsoar, 1990; Link et al., 1994; Wang et al., 2006). Therefore, they are more fixed with low migration rates and their morphology are, to a large extent, controlled by the growth patterns of the shrubs that are trapped in (Tengberg and Chen, 1998; El-Bana et al., 2003; Ardon et al., 2009).

Lunettes are another crescent-shaped, fixed dunes formed on the downwind margin of playas or river valleys (Holliday, 1997). Unlike barchans, their horns point upwind in similar with parabolic dunes (Telfer and Thomas, 2006). They are considered as a type of source-bordering dunes as their sand sources are mainly from the adjacent water body (Chen, 1995).

Dome dunes are round without slipfaces most of the time. They have been interpreted as the equilibrium dunes formed under strong unidirectional winds and from an abundant sand supply (McKee, 1979).

2.2.3 Dune field metrics

The land surface of Earth shows both scale-specific and scaling behaviour, in where the regularity of sand dunes is well known, although size and spacing vary regionally (Cooke et al., 1993; Evans, 2003). Focusing on the morphology of patterns, some researchers suggest that the dune fields could be interpreted as a self-organizing complex system (Werner, 1995; Werner and Kocurek, 1999). Their development is influenced by boundary conditions, for example the wind regime and sediment supply as well as sand source-area geometry (Ewing and Kocurek, 2010a; Eastwood et al.,

2011). The dune size and field structure can be inferred and described qualitatively, and a systematic and quantitative characterisation of dune fields would allow the easy characterisation of a dune-field as well as providing a bench-mark for testing numerical model results.

There are two factors which have been applied in previous research to quantify a dune-field, one is the dune-field density and another is inter-dune spacing which is considered to be limited by the area of a dune field within a given space (Ewing and Kocurek, 2010a). Especially, compared to the other types of dunes, the field pattern of crescentic dunes (including barchan and transverse ridges) have received more attention (Hersen et al., 2004; Beveridge et al., 2006; Ewing et al., 2006; Elbelrhiti et al., 2008; Durán et al., 2009; Durán et al., 2011).

2.2.3.1 Dune-field density

One definition of dune-field density is defined in Equation (2.3),

$$\eta = \frac{A'}{A} \tag{2.3}$$

in which, η is the dune density, A' is the sand dune area, A is the whole area of the field (Durán et al., 2011). However, the dune-field density value obtained from equation (2.3) is likely to reflect the sediment volume in the field but may not reflect the dynamics. A field with few large dunes may have same density as a field with numerous small dunes but the latter will have very different formation dynamics from the former.

Another definition of dune-field density is the number of dunes per unit area, as defined below,

$$\eta = \frac{N}{A} \tag{2.4}$$

in which, N is the number of dunes, A is the area of dune fields (Elbelrhiti et al., 2008). Again, the value obtained from equation (2.4) may not reflect the dynamics in the field neither. For example, two dune fields with the same dune density measured by equation (2.4) may have larger dunes in one field but smaller dunes in another field

with different distance between dunes. However, applying equation (2.4) is more practical if it is difficult to obtain the dune area value.

2.2.3.2 Inter-dune Spacing

To investigate the spatial distribution of the dunes, the spacing between each dune has been used in previous research, although different measurement methods were applied (Beveridge et al., 2006; Ewing et al., 2006; Elbelrhiti et al., 2008; Durán et al., 2011). The inter-dune spacing provides additional information on the total amount of sand transportation beyond the size distribution, and the relationships between spacing and controlling dynamic parameters have attracted more studies (Elbelrhiti et al., 2008; Durán et al., 2009; Ewing and Kocurek, 2010a). The spacing characteristics and measurement of crescentic dune fields has received considerable research (Hersen et al., 2004; Al-Masrahy and Mountney, 2013).

2.2.3.2.1 Barchan dune fields

When groups of barchan dunes are found in large fields, all the dunes orient along the wind direction forming corridor-like structures with the remarkable feature being their coherent and homogeneous in scale within any one area (Finkel, 1959; Lima et al., 2002). Three measurement methods have been used to determine the spacing of barchan dunes: *Network* (Durán et al., 2011), *Rectangular* (Elbelrhiti et al., 2008) and *Longitudinal* methods (Al-Masrahy and Mountney, 2013). By applying *Network* method, a dune was selected as the centre of a Cartesian coordinate system, then four of its nearest neighbours were connected to this centre dune with each one located at each quadrant of the coordinate system, thus composing a planar dune network as sketeched in Figure 2-6b. The *rectangular* method is to measure the horizontal and longitudinal distance between a dune and its adjacent neighbours as illustrated in Figure 2-6a.

In some studies, only the longitudinal distance, d_v in Figure 2-6a, of the dune spacing has been measured which reduces the work required for field pattern analyses (Al-Masrahy and Mountney, 2013). Compared to the rectangular spacing method, network spacing may indicate the relationship between specific dune morphometry with the field spacing, but apparently increases the measurement and calculation workload at

the same time – that may not prove practical when facing a field with thousands of dunes. In addition, one study showed that there was no clear trend of a function of the dune size *w* with the inter-dune spacing *L(w)* (Durán et al., 2011).

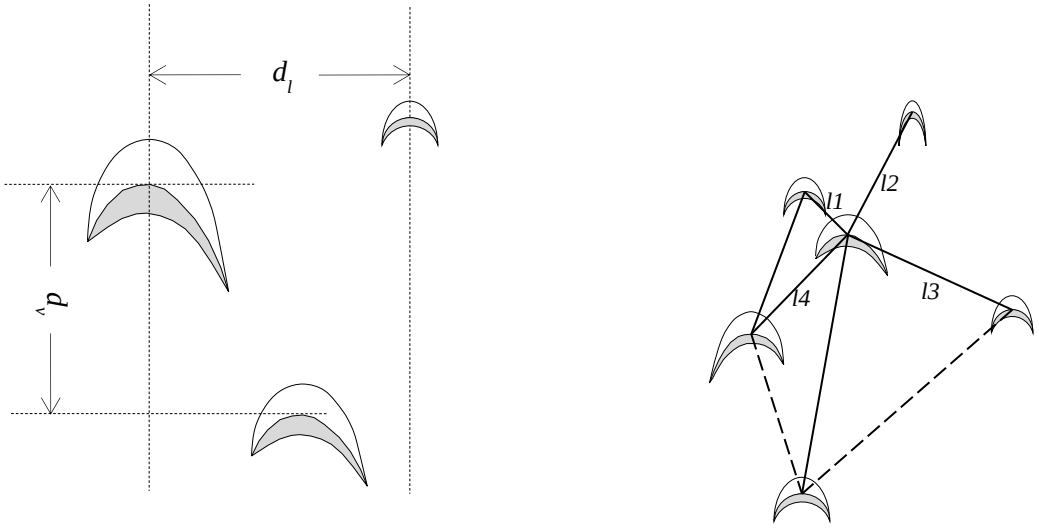

(a) (b)

Figure 2-6 Schematic illustration of the barchan dune field spacing measurement methods: (a) rectangular spacing; (b) network spacing (modified after Durán et al. (2011)).

2.2.3.2.2 Transverse ridge fields

In comparison to the barchan dune spacing measurement method, transverse ridges spacing measurement is simpler. In transverse ridges field, the dune spacing is usually measured between crestlines (Figure 2-7), perpendicular to the orientation of the dune, which is similar to the vertical distance measurement of barchan dune spacing illustrated in Figure 2-6a. Orientation is measured along a straight line parallel to the overall trend of the crestlines. Crest wavelength can be measured along the entire length of the crestline between terminations, the terminations of crestlines are pattern defects (Figure 4-6) (Ewing et al., 2006; Ewing and Kocurek, 2010b).

Unlike in barchan dune spacing, there is no lateral distance that needs to be measured in transverse ridge fields, but instead another factor called the defect density. The

defect density is a field-scale parameter that expresses the number of defect pairs per unit length of crestline, as defined in equation (2.5),

$$\rho = \frac{N}{L} \tag{2.5}$$

in which, ρ is the defect density, N is the number of defect pairs, L is the length of crestline (Werner and Kocurek, 1999; Beveridge et al., 2006).

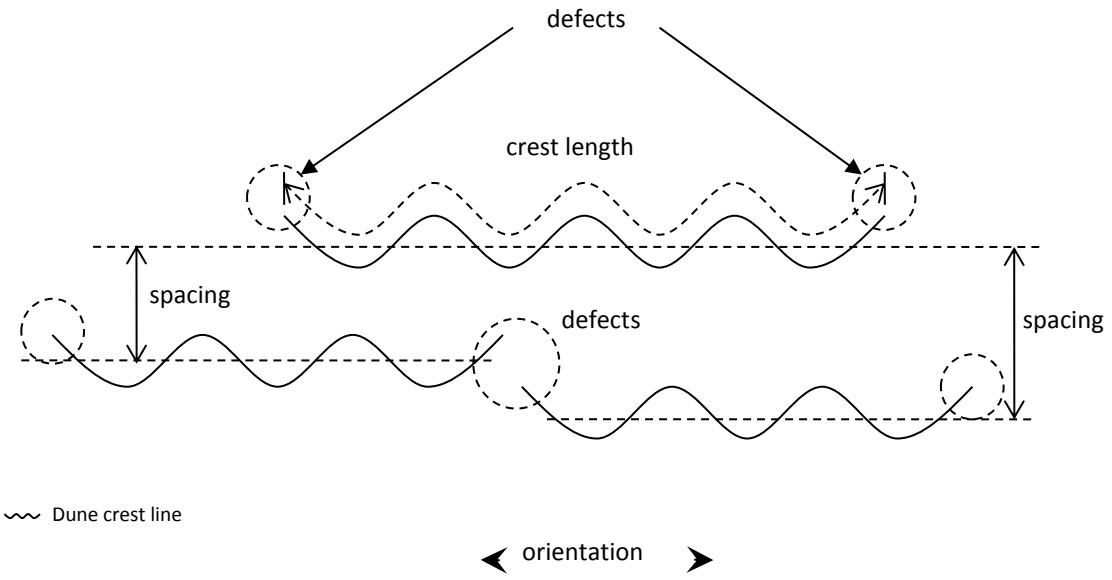

Figure 2-7 Morphometry of transverse ridges pattern and their measurement (modified after Ewing et al. (2006)).

2.2.4 Dune dynamics and migration

Dunes are primarily composed of accumulated sand grains. Finer silt and clay are carried further by the wind leaving the heavier sand grains behind. Saltating grains move up the windward slope and then come to rest at their angle of repose on the downwind side in a zone of stagnant air (Bagnold, 1941; Wilson, 1972; Tsoar, 1983; Hersen, 2004). In fact, dunes are a product of interactions between the wind and sediment surfaces and their dynamics have been found to be closely related to the environment sediment state, and one of the important features that results from this dynamic process is dune migration.

2.2.4.1 Sediment state

The aeolian sediment state is commonly quantified by the *sediment supply*, *sediment availability* and the transport capacity of the wind which is usually expressed as the *sand transport rate* or sand flow rate (Kocurek and Lancaster, 1999).

Sediment supply is the sediment of suitable grain size that can be used as the source material to create the dune field, though some researchers suggest that it is a limiting factor on the formation of dunes (Glennie et al., 1994). *Sediment availability* represents the sediments that are available to be entrained by the wind. So it is the dimensionless percentage of the dune-field surface covered by grains that can be entrained and is less than the sediment supply. Barchans occur where there is very little sand and almost unidirectional winds: crescentic dunes where sand is abundant and winds slightly more variable; linear dunes occur where sand supply is small, but winds more variable still; and star dunes are found in complex wind regimes with abundant sand supply (Nickling and Wolfe, 1994; Lancaster, 1995).

Sand transport rate, or sand flow/flux rate, is the volume of sediment entrained by the wind that passes through a sectional area during given time period. The initiation, development, and equilibrium morphology of all dunes are determined by changes in sediment transport rates in time and space that give rise to either erosion or deposition (Bagnold, 1935; Wilson, 1971; Mainguet, 1984; Sauermann et al., 2003).

The sand transport rate will vary on different parts of individual dunes or dune fields. It can be influenced by sand grain texture, the local moisture levels and vegetation (Lancaster, 1995). The maximum amount of sand that a wind can possibly carry over a bed of similar grain size is called the potential sand flux rate ($kg \cdot m^{-1}$ *per unit time*). Usually, the resultant sand flux is smaller than the potential sand flux because in reality the wind regime is complex with alternating and opposing winds cancelling each other out (Wilson, 1971).

2.2.4.2 Dune migration rate

One of the important features of dunes is their movement, which is important for many environmental issues. Transverse and barchan dunes are the common examples of migrating dunes and have been studied extensively by many researchers (Bagnold,

1941; Wilson, 1972; Momiji and Warren, 2000; Wang et al., 2009; Hugenholtz et al., 2012). On crescentic dunes, erosion and deposition patterns are characterized by erosion on the stoss slopes and deposition in the lee. This pattern leads to a migration of the dune downwind. There are three methods to measure the dune migration rate.

(1) Calculating dune migration rate via sediment flux

The difference between sediment influx and outflux can determine the different dynamic behaviour of dunes (Tsoar et al., 2004).The erosion and deposition patterns on transverse dunes lead to a migration of the dune downwind (Wilson, 1972). The migration rate (r_d) of transverse dunes can be described by:

$$migration\ rate = \frac{sand\ transport\ rate}{height \times bulk\ density} \quad (2.6)$$

To use notation instead of words to express the equation, Equation (2.6) becomes Equation (2.7):

$$r_d = \frac{R_d}{\gamma h} \quad (2.7)$$

Where R_d is the sand transport rate ($kg\ m^{-1}s^{-1}$) (when the bedform has a large slipface nearly all the sand crossing the ridge is trapped on it), γ is sand bulk density in the dune ($kg\ m^{-3}$), and h is dune height (m) (Bagnold, 1941). For most dune sands, the bulk density is ca. 1,700 $kg\ m^{-3}$ (Wilson, 1972), although it various in different regions because of variations in sand grain size and properties, for example, the average bulk density of dunes near Jericoacoara of Brazil is 1,650 $kg{\cdot}m^{-3}$ (Sauermann et al., 2003) whereas some other researchers adopt 2,650 $kg{\cdot}m^{-3}$ as an average value for most sand dunes (Momiji and Warren, 2000). From this formula, it is obvious that there is an inverse relation between migration speed and dune height, which has been confirmed in many studies (Momiji and Warren, 2000).

(2) Measuring dune migration rate

In the early studies, barchan dune migration rates are measured by using probes or pins inserted into the dunes to measure movement and erosion rates (Bagnold, 1941; Ould Ahmedou et al., 2007). In this way, relationships between dune migration rate

and dune morphometry were established, for example the correlation between dune movement and dune height or width.

With accessible sequential image data, e.g. aerial photography, photogrammetry, remote sensed data etc. it is easier to calculate the short-midterm change of dune migration. Comparison of the position of dunes on time-series images provides the data to calculate dune migration rates, mostly for small crescentic (transverse) or barchan dunes (Dong et al., 2000; Bailey and Bristow, 2004; Ojeda et al., 2005; Daniel and Alan, 2007). However, only dune width, not height can be readily measured from images. Therefore, the dune movement is usually correlated with dune width which is found in an inverse linear relationship, as follows (Parker Gay Jr, 1999):

$$c = Rw^2 \tag{2.8}$$

or

$$R = cw^{-1} \tag{2.9}$$

Where, *R*=rate of movement in metres per year; *w*=width in metres (on transverse line through bottom of slip face); c=a constant, with dimensions of $m^2\ yr^{-1}$.

However, the dune velocity is very different from one place to another, and it strongly depends on time (Andreotti et al., 2002). Formulae developed to estimate dune migration rate have been expressed in many forms, but there is no universe formula that can be applied to estimate the actual movement rate of dunes with reliable accuracy, because of the specific boundary conditions in which these formula have been calculated. In general, Barchan dunes are found move in proportion to the wind velocity and inversely in proportion to their height, which means that smaller barchans move faster (Finkel, 1959; Cooke et al., 1993; Nishimori et al., 1998; Parker Gay Jr, 1999; Sauermann et al., 2000). After examining published field data, Momiji and Warren (2000) found that dune migration rate could be approximated as:

$$r_d = a + b\frac{1}{h} \qquad (a > 0) \tag{2.10}$$

Where a and b are positive constants and h is dune height.

By using image based measurements, dune evolution studies are time limited from short to mid-term because of the lack of historical data (Vermeesch and Drake, 2008). Some researchers have combined statistical approaches such like Empirical Orthogonal Functions (EOF) to obtain the long-term evolution of dunes migration (Muñoz-Perez et al., 2009). However, this method is usually used in the coastal science field and amelioration is need to improve the accuracy of its results (Navarro et al., 2011).

(3) Dating dune migration rate

Longer-term (centuries to millennia) perspective on dune migration cannot be gained from time-series images but have now become possible by applying luminescence dating technologies (Kar et al., 1998).

Sand dunes structures are firstly identified by ground penetrating radar (GPR) technique which provides information on their sedimentary structure. Based on this sand samples from the same depth in the same type of sedimentary units at intervals across the dune (usually lee face cross strata) are luminescence dated parallel to the inferred migration direction and thus shows the advance of dunes (Bristow et al., 2005; Lancaster, 2008).

2.3 River geomorphology

Rivers can be found in many different climatic zones, from humid to arid, from equatorial to arctic. In this section, the hydrodynamics of various river channel patterns and the factors that may influence the channel geomorphology have been reviewed.

2.3.1 River and channel pattern

Perennial rivers flow for all or most of the year, while many of those in dryland environments only transmit water at certain times which are terminated as **intermittent** flow (seasonal floods followed by little or no flow) or **ephemeral** flow (occasional floods being interspersed with longer periods of no flow) (Muhs et al., 2003).

River channels may cut into rock and sediment. The three chief types of river channel are bedrock channels, alluvial channels, and semi-controlled or channelized channels (Huggett, 2007). **Bedrock channels** are eroded into rock. They are resistant to erosion and tend to persist for long periods. **Alluvial channels** form in sediment that has been, and is being, transported by flowing water. They are usually deep and narrow. The main patterns of alluvial channels are commonly classified as *Straight*, *Meandering* and *Braided* (Leopold and Wolman, 1957). The dividing line between *Straight* and *Meandering* is arbitrarily defined by a sinuosity of:

$$sinuosity = \frac{channel\ length}{valley\ length} \tag{2.11}$$

Whereas in *Braided* channels, the flow is divided into a series of anabranches separated by bars of accumulated sediment. There are also some other channel patterns such as *Anabranching*, *Wandering* and *Anastomosing* which are not as common as the three main patterns. *Anabranching* is used to describe all planforms that are characterised by more than one separate channel (Nanson and Knighton, 1996). The *Wandering* style (Church, 1983) represents a transitional morphology between braiding and meandering (Ferguson and Werritty, 1983) with irregular sinuosity that generally is lower than in freely meandering river but where channel division is less continuous and less intense than in braided rivers (Rice et al., 2009). The comparatively rare *Anastomosing* channels exhibit the branching and rejoining of the river courses with numerous waterholes (Schumm, 1985; David Knighton and Nanson, 1993; Knighton and Nanson, 1994; Gibling et al., 1998).

2.3.2 Channel dynamics

Channel form and behaviours are directly controlled by flow regime and sediment supply. Characteristics of the flow regime include seasonal variations, flood frequency-magnitude relationships and the frequency and duration of low flows (Charlton, 2008). Sediment supply includes the volume of sediment and the sediment size distribution. Rivers shape and reform their channels continuously by erosion of the channel boundary (bed and banks) and deposition (Muhs et al., 2003). There are internal basin controls as well as external basin controls that can lead to changes in fluvial system. Internal driving variables include drainage density, hillslope angle, soil type, flow

discharge, sediment yield, channel pattern and channel depth. External variables, at the basin scale, are climate, base level, tectonics and human activity. All of these external and internal drivers can lead to long-term changes in channel form and behaviour.

2.3.2.1 River processes

Transportation of sediment within the channel occurs when friction is overcome and occurs in three ways: suspension, saltation and traction. (Charlton, 2008). In river hydraulics, one of the most important problems is the determination of the rate of movement of bed material.

Researchers have sought ways to quantify sediment transport and there are a range of expressions or equations that can be used to model or predict sediment transport (Gomez and Church, 1989). For example, the well-known Einstein (1950) equation provides the bed-load function to calculate the rates of transport for various sediment sizes found in channel bed and initiated a probabilistic approach to modelling sediment transport in rivers. Since then, other studies have been attempted to complement for wider application under various channel characteristics (Parker et al., 1982; Parker, 1990; Church and Hassan, 1992; Habersack, 2001; Troendle et al., 2001; Kleinhans and van Rijn, 2002). Wilcock and Crowe (2003) presented a function for mixed sand and gravel bed that can not only provides a more complete description of the transport/bed surface interaction, but allows incorporation of the previously unmodelled nonlinear effect of sand content on gravel transport rate.

2.3.2.2 Discharge

Sediment entrainment, transport and deposition all involve the interaction of forces. To carry out geomorphological work, energy is needed. The energy availability is dependent on two things: the flow discharge and the channel slope which is related to the topography. The channel discharge is the volume rate of water flow, dependent upon the velocity of water and cross-sectional area of channel at a given point. The discharge of a channel can be calculated by equation of continuity:

$$Q = va \tag{2.12}$$

Where Q is the discharge ($m^3 \cdot s^{-1}$), a is the cross-sectional area of the stream (m^2) obtained by simplifying the geometry and calculating the area or by drawing cross-sections to scale and measuring the area, and v is the average velocity of flowing water ($m \cdot s^{-1}$). Discharge has a significant influence on in channel sediment transport. At any location, channel form is dependent on the discharge and supply of sediment from upstream. Increases in discharge lead to a general increase in the size of the channel, with discharge acting as a control on the gross dimensions (Knighton, 2014).

River discharge can vary considerably. Rivers in humid areas receive more water resources maintaining a more stable discharge level, whereas dryland river discharges can be more variable (Bull and Kirkby, 2002). For example, the Barwon-Darling River in Australia has recorded discharge in the range of 4.9 – 125 $m^3 \cdot s^{-1}$ (Thoms and Sheldon, 2000). Tarim River in China is one of the longest inland rivers in the world, its discharges are various significantly that it can be as low as less than 10 $m^3 \cdot s^{-1}$ but sometimes can reach up to an average value of 235 $m^3 \cdot s^{-1}$ (Xu et al., 2004; Hailiang et al., 2005; Zhang et al., 2010). The William river in Canada run through an active dune field is recorded of discharge in between 5-30 $m^3 \cdot s^{-1}$ (Smith and Smith, 1984). A study in Oman estimates the bankfull palaeodischarge of local rivers could vary between 59 – 30720 $m^3 \cdot s^{-1}$ (Tooth, 2000).

2.3.2.3 Channel pattern change

The three classical channel patterns have different dynamic characteristics. *Straight* channels are usually structurally controlled by faults or joints so that they are relatively static with steep channel slopes. Meandering channels are caused by the intrinsic instabilities of turbulent water against a movable channel bank. They may change form substantially as discharge, sediment supply, and other factors change because alluvium is normally unable to resist erosion to any great extent (Huggett, 2007). *Braided* channels tend to form where (1) stream energy is high; (2) the channel gradient is steep; (3) sediment supply from hillslopes, tributaries, or glaciers is high and a big portion of coarse material is transported as bedload; and (4) bank material is erodible, allowing the channel to shift sideways with relative ease (Leopold and Wolman, 1957; Rust, 1972; Lenzi et al., 2003). Some studies have suggested that thresholds exist between the three classical patterns that once a threshold is crossed, the shape of the

channel pattern changes rapidly to another, whereas some oppose the existence of a threshold but suggest that transitions may be gradual (Ackers and Charlton, 1970; Schumm, 1981; van den Berg, 1995; Alabyan and Chalov, 1998; Bledsoe and Watson, 2001).

The results of channel change include adjustments of pattern, pronounced widening, rapid lateral migration, entrenchment, and floodplain erosion and deposition (Tooth, 2000). Five bedform modes of behaviour have been recognised as migrating bedforms approach each other in the streamwise direction: (1) simple merging, (2) off-center collision, (3) repulsion, (4) cannibalisation, and (5) bedform splitting (Kocurek et al., 2010).

Factors that influence channel patterns include tectonic activities, climate change, sediment supply, discharge, bank stability and vegetation. Tectonics is an external control which will influence the flow and sediment regimes therefore lead to long-term change in river channel development. It can lead to large scale uplift, localised subsidence, warping, tilting, fracturing and faulting of river valley which may in turn affect channel pattern and location (Yang, 1990; Li et al., 1999; Wang et al., 2004; Charlton, 2008). Climate change will lead to changes in water and sediment inputs into rivers (Yang et al., 2002). For example, a study on Neales River on the western shore of lake Eyre indicates that mild epeirogenic forces have deformed sediments of Miocene age while climate change associated with the Last Glacial maximum caused the ancestral Neales River to incise (Croke et al., 1998). Sediment supply is another important factor influencing channel form and behaviour because it is closely connected with river aggradation or degradation.

2.4 Fluvial-aeolian interaction

There is normally a clear distinction between fluvial and aeolian research. A literature search using ISI Web of Knowledge (www.webofscience.com) shows that most studies only consider the aeolian or fluvial transport component – very few explicitly considering both (Field et al., 2009). Notably, as research into Quaternary environmental change in drylands has developed, oscillations between periods of

predominantly aeolian activity and predominantly fluvial activity have been recognised (Bullard and McTainsh, 2003). In particular, the work of Tricart (1965) in Niger documents the impact of fluvial-aeolian interactions resulting from quaternary climate changes on the development of the Niger River and delta and has been cited as 'one of the most eloquent treatments of fluvial-aeolian interaction in the dry tropics' (McIntosh, 1983). Sedimentological research has also shown that there are interbedded fluvial-aeolian sediments in the stratum record of arid environment (Langford, 1989; Langford and Chan, 1989; Thomas, 1991). Different sedimentary characteristics indicate a change from an environment where aeolian deposition dominates to one where fluvial deposition dominates, or *vice versa*, and plays an important role in the reconstruction of palaeoenvironments. However, the temporal and spatial differentiation of dominant processes is not always clear, since mixed fluvial-aeolian deposits can be identified as sequences where the interplay of fluvial and aeolian depositional processes is very subtle (Mountney et al., 1998). Based on previous work, Bullard and Livingstone (2002) summarise how changes in moisture can affect the balance between aeolian and fluvial processes with the highest levels of fluvial-aeolian interaction occurring where neither fluvial nor aeolian processes dominate (Figure 2-8).

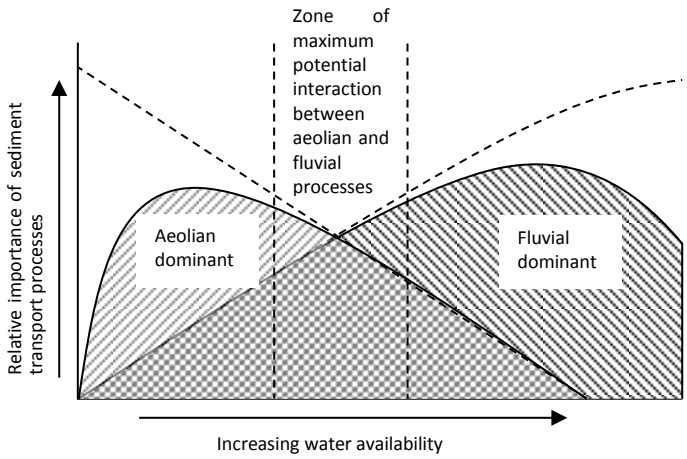

Figure 2-8 Balance between aeolian and fluvial processes according to the water availability (Kirkby, 1978; Bullard and Livingstone, 2002).

But, field process studies of contemporary interactions are still very rare. Whilst there may be many more areas where there is an interplay between fluvial and aeolian processes than a single process dominating, the interaction is rarely the main subject

of investigation (Cooke et al., 1993). Additionally, the role of rivers in shaping the dryland landscape has generally been underestimated (Reid et al., 1998). There are a range of existing studies looking at fluvial/aeolian interactions and these can be grouped into those viewing from a fluvial and an aeolian perspective.

2.4.1 Fluvial-aeolian interaction examples

From a fluvial perspective, researchers have observed how flow can affect the development of aeolian features. By the action of fluvial erosion, sand dunes bordering channels can be changed in both size and location. Alternatively, dune sand can slump into rivers as a result of over-steepening of dune flanks from river erosion and the sand is then transported and re-deposited by the river which in turn determines the location of new dunes sourced by this sediment (Langford, 1989; Han et al., 2007; Maroulis et al., 2007). These types of dunes are named source-bordering dunes as they closely border the downwind side of their sediment supply from sand bed streams (Cooke et al., 1993). In addition, some river systems can intercept the sediment transported from dune fields to the extent that they block dune movement. For example, from landscape observations, it can be clearly seen that the dunefields in Northern Sudan are terminated by the Nile River (Bullard and McTainsh, 2003), the Namib Sand Sea is terminated by the ephemeral Kuiseb River (Thomas et al., 1997), the Skeleton Erg ends at the Hoarusib River (Krapf et al., 2003) and the perennial Orange River marks the downwind margin of the southwest Kalahari dunefield (Ward, 1987; Thomas et al., 1997; Bullard and McTainsh, 2003; Krapf et al., 2003). The Colorado River was found to be not only the boundary of the Algodones dunefield, but also to be at the end of the Mojave Desert (Sweet et al., 1988; Muhs et al., 2003). Interestingly, although the Colorado River terminates the sand transport path from the Mojave Desert (feldspar-rich sediments), which is on the western river bank, it does supply the distinct (quartz-rich) sediments to the dune fields on the eastern river bank, which is sourced from the alluvium in the river, and as a consequence two different sediment sources for the dune fields on each side of the river were identified by mineralogical, geochemical and magenetic sediment analyses by Muhs *et al*., Muhs et al. (2003). However, how the river valley affects the aeolian process, e.g. wind regimes – the aeolian sediment transport on western bank is eastward but changed to northeastward on the eastern bank, has not been determined. Unlike the Colarado River valley, Bouse Wash in the

Parker dune field has not been found to exert any influence on the aeolian sand transport pathways (Muhs et al., 2003).

The majority of the studies considered above focus more on general descriptions of surface processses and the development of landforms, being predetermined by the research methodologies such as landscape orremote sensing imagary observation, or stratigraphical or sedimentological record analyses, with very few studies providing empirical information about how, and the extent to which, fluvial systems contribute to the origin and development of dunefields. Some researchers have noticed that the presence of a valley has the potential to impact on the development of smaller scale landforms, in particular aeolian bedforms, by affecting wind velocity and direction (Sierputowski et al., 1995; Wiggs et al., 2002). In particular, valleys in low relief landscapes act in a similar manner to a hill, having an effect on wind direction due to the incident angle of the approaching wind to the axis of the valley (Bullard et al., 2000; Wiggs et al., 2002; Garvey et al., 2005). These factors may help to explain the widely observed phenomena of the association of particular sand dune patterns with river valleys in desert environments (Bullard and Nash, 1998).

Contrastingly, aeolian processes can heavily influence fluvial processes. Sand dunes can deflect and confine overbank flows, and dam and divert river courses, and thus determine the position of many contemporary waterholes and channels (Langford, 1989; Loope et al., 1995; Maroulis et al., 2007). By studying the stratigraphy, sedimentology, paleogeography and tectonic setting of an erg in South Central Utah, USA, Jones and Blakey (1997) observed that an ephemeral stream flowing along the edge of the erg was diverted several times until it was forced to take a different route to the sea, leaving relic dry channels. The channel diversions were inferred to be the result of avulsion, possibly caused by aeolian blockage, although no direct evidence for these inferrences are available (Jones and Blakey, 1997).

Similar phenomena are recorded in central Australia, where the Todd River is found to have partially abandoned its paleochannel course to its present position by avulsing, which is supported by evidence of alluviation data. This major event may have been caused by shifting aeolian dunes obstructing narrow fluvial routeways, but detailed chronological precision is needed to separate the impacts of climate change,

infrequent catastrophic flooding and aeolian damming in this system (Hollands et al., 2006).

Additionally, some river systems can dramatically change pattern and behaviour when they encounter features created by aeolian processes, although it is not clear whether there are contributions from other environment factors. For example, the lower William River in Canada undergoes a rapid adjustment from a relatively narrow and deep single-channel to a braided pattern when it encounters a large dune field (Smith and Smith, 1984). The authours found that the width, width/depth, and braiding intensity all increase independent of discharge, but associate this with the bedload which is increased more than 40-fold with sediment that is provided by the dune field. These authors conclude that all of the important channel modifications that they observed result from the massive infusion of sand from the dune field (Smith and Smith, 1984). Fundamentally, Smith and Smith (1984) have not convincingly shown that sediment supply is the sole cause of braiding in the system, as it is unlikely that such changes are monocausal. The analysis of grain size only confirms that the river is flowing through a dune field rather than proving that sediment supply is the cause of the braiding. Furthermore, the analysis of low steady June/July flow ignores spring melt when the middle reaches have high flows in a constrained gravel/boulder bed single channel, and as this high discharge hits the dune field the braided channel forms are a logical outcome. Whilst discharge may look stable in the summer months there are significant seasonal influences. The authors failed to assess peak flow influences and only assessed the river discharge between June 30 to July 3, 1982, a period of only 4 days; at a time of low discharge. Longer and comprehensive field work and analyses, therefore, are needed. In addition, this study does not provide information relating to aeolian processes and how dune movements interact and affect channel pattern and location at different times of the year.

Huisink's (2000) study demonstrates the need for a more holistic approach to understanding the interaction of rivers in dune fields in that the author has provided more comprehensive explanations of channel change in such environments as opposed to inferring a single causal factor such as high sediment inputs. By studying change in the lithological and sedimentological characteristics of the Vecht valley from the Middle Pleniglacial to the Holocene, Huisink (2000) found a correspondence

between historical changes in channel pattern and aeolian activity, where low energy meandering rivers were associated with periods of low aeolian activity and high energy braided systems were associated with periods of high aeolian activity. However, high aeolian activity can also cause a high influx of sediment as well as loss of vegetation and subsequent bank stability, and changes in the water-sediment discharge ratio, especially when climatic changes are also considered. Hence, it is not easy to exclude the influence of other environment factors on channel pattern as opposed to the single factor of extra sedment input. Furthermore, aeolian processes can rework fluvial sediments by deflation so that fluvial systems become the primary sediment sources for many sand seas and dunefields. For example in Israel, Roskin et al. (2011) found the sand supply and storage in Sinai was initiated by exposure of the Nile Delta sands during the Late Pleistocene, which not only supplied the sediment but were suggested to be transported by strong southeasterly winds blowing across Sinai and into the northwestern Negev. The sediment source was identified by optically stimulated luminescence (OSL) dating, however, the mechanism of sediment delivery from the Nile Delta to northwest Sinai has not been investigated in detail. In particular, the strong Later Pleistocene aeolian sand transport drift potentials were only inferred from modern meteorological data (1987-1993), which are obviously not sufficient to suggest the palaeoclimate conditions in the late Pleistocene.

Petrographic analysis of sand mineralogy undertaken by Ramsey *et al*., (1999) at Kelso Dunes in California showed that a percentage of the sand in the dunefield may have originated from alluvial material deposited at the surrounding Kelso Wash, Devils Playground Wash and Mojave River Wash to the west, by the prevalent winds from the northwest(Ramsey et al., 1999). Similarly, sedimentological, mineralogical, geochemical and magnetic properties occur in at least three of the major dune fields of the Sonoran desert of western Arizona and northern Mexico. These were found to closely resemble the composition of the Colorado River, which is, therefore, considered to be the sediment source, under a northeastward wind regime (Muhs et al., 2003; Draut, 2012). Sedimentological and mineralogical analyses were also carried out in two major dune areas on the Ordos Plateau in China, and it was found that the dune sands were derived from local fluvial and lacustrine sediments (Peterov II, 1959; Zhu et al., 1980; Wu, 1987; Liu et al., 2005).

Along the palaeochannel of the Todd River in Australia, dune sands were shown, through sedimentological and chronological analyses, to be transported by southerly winds from the floor of the Todd river channel during seasonal dry periods. The westward migrating channel of the river, results in the occurrence of relict dunes of different chronological age on the palaeofloodplain to the east, which reduce in age as they approach the present channel position (Hollands *et al.*, 2006).

The above studies have provided historical evidence to show how aeolian processes have changed and been reworked by fluvial interactions, however, only a limited number of these studies have demonstrated the machanisms of interaction between fluvial and aeolian processes, especially in a modern environmental context.

Some modern fluvial-aeolian interaction processes can be observed in locations where the balance between fluvial and aeolian action has alternated over relatively short time scales, which may correspond to seasonal changes (for example ephemeral rivers) (Krapf et al., 2003). This presents the scenario wherein during dry seasons, blown sands may travel over a dried up river channel that crosses its transport pathway, subsequently the river may then forms an obstacle to aeolian transport when river flow levels rise (Muhs et al., 2000). For example, Xu et al. (2006) studied water-wind processes in the middle Yellow River basin, a region that covers various climatic zones including arid, semi-arid and sub-humid. Between November and June, the weather is dry and windy, and strong winds, with maximum velocities greater than 17 ms^{-1}, are shown to be transporting aeolian sand and weathered bedrock perpendicular to the dry river channel. This material covers the dry river bed, and some small gullies are also in-filled; from July to October, strong rainstorms cause runoff from the adjacent loess covered hillslopes, which flows into the previously dry gullies and channels so that the coarser aeolian material stored in these features is rapidly entrained and a hyperconcentrated flow forms (400-600 kgm^{-3}), which removes the infill material. It is suggested that the fluvial process can transport the aeolian sediments due to the optimal grain size composition of this material, which includes 40% of coarse sediment (>0.05 mm fractions) from aeolian sand and bank erosion, and 20% of <0.01 mm fractions from the loess.

On the basis of their field observations, Xu *et al.* (2006) further suggest that the sand cannot cross the river as wind-blown sands are mainly located on the upwind side of river banks. However, without sedimentological analysis of material on the opposite sie of the river, and an understanding of the prevailing wind pattern within the valley system itself, this suggestion remains to be proven: as unlike the Colorado River this system is seasonally dry, and the wind regimes may differ between the dry and wet seasons. As such, the nature of the fluvial-aeolian interactions in this system need to be understood in greater detail in order to understand the interaction between the two processes over annual timescales, as variability can occur during periods of greater aridity due to changes in vegetation type, bank stability and erodability, and the available sediment source.

Seasonal fluvial-aeolian interactions were also observed in polar deserts (Good and Bryant, 1985). At the Sachs River in the Canadian Arctic, the annual hydrology is high during spring flood followed by lower summer discharges, and the maxium mean wind velocities ocurr from July to September. Therefore, the fluvial deposits of the ephemeral streams and the main channel are subject to aeolian modification during the arid summer months. Importantly, the presence of permafrost during winter indicates that sand transport does not occur, and fluvial sediments from spring flooding were able to overlay this surface; as the thaw-front reaches a greater depth, the permeability of the seasonally frozen sands increases such that no run-off occurs during summer within the channels, and the previous fluvial deposits were buried by wind blown sand; the damp sediment layer further limits the quantity of mobile sand available for aeolian transport and dune formation, such that another layer of aeolian sediment was formed. This new layer was subsequently frozen and covered by fluvial sediment in the following spring flood. These annual cycles of sediment accumulation, through alternating fluvial and aeolian depositional processes, result in the development of interbedded fluvial-aeolian sediments sequences (Good and Bryant, 1985).

Although various fluvial-aeolian interaction phenomena, as outlined above, have been observed in the field, very few studies have systematically classified these relationships. Langford (1989) documented six types of modern fluvial-aeolian interaction after observing the ways in which the Medano Creek intermixed with the aeolian landforms

in the Great Sand Dunes in America, these included: (1) aeolian landforms damming streams; (2) interdune areas being flooded, particularly alongside channels and behind aeolian dams; (3) dunes bordering flooded channels and interdunes being eroded; (4) fluvial sediment being deposited in interdune areas; (5) interdunes being flooded by groundwater derived from the fluvial system; and (6) fluvial sediment being eroded by the wind and blown into the aeolian system. However, these six types only described interaction behaviours in temperate climates and at a local scale. Therefore, there is a clear need to examine, describe and classify the interactions between fluvial and aeolian processes at a large (global) scale, reflecting geomorphological characteristics and corresponding dynamic processes.

2.4.2 Current approaches to the study of fluvial-aeolian interactions

In many desert regions, over longer time scales, there are shifting boundaries between fluvial-dominated and aeolian-dominated areas with the interaction varying, which produce some distinctive sedimentological and geomorphological features. Hence, various research methods have been applied to study the complex ancient (palaeoenvironmental) or modern (contemporary) interacting processes.

2.4.2.1 Chronological dating of sedimentation

Deposits in rocks, dunes and fluvio-lacustrine faces become the important indicators for ancient erosion processes (Cooke et al., 1993; He et al., 1996; Thomas et al., 1997; Robinson et al., 2006; Miao et al., 2010). Moreover, by dating and analysing the deposits in different chronological ages, researchers can study the relationship between deposits and corresponding climate; further infer the paleoclimate changes and ancient fluvial-aeolian interactions.

The researches on ancient processes mainly focus on the measurement and analysis of ancient geographical records to reveal the fluvial-aeolian interactions and the advance-inverse processes of desertification since Quaternary, and reconstruct past climate. For example, by optical luminescence dating two dunes in Ras Al Khaimah of United Arab Emirates are found to be accumulated in response to the transgression of the Persian Gulf by rising sea levels in late Pleistocene and Holocene times or periodically reactivated after erosion by fluvial action (Goudie et al., 2000). Harrison and Yair (1998)

thermoluminescence dated and identified buried palaeosols in the interdune areas in the Nizzana linear sand dune field and suggest that the sands buried in the late Pleistocene were fluvially reworked and are not primary aeolian deposits. Clarke and Rendell (1998) applied the luminescence dating techniques to determine the timing of sand dune formation in the Mojave Desert and conclude that storm events are the controlling factor for periods of sand dune formation in desert areas of the south western U.S.A. In Sahara, El-Baz et al. (2000) illustrates the sand origin are mainly from fluvial processes and was deposited in inland lacustrine depressions by palaeo-rivers and streams.

2.4.2.2 Field observation of geomorphology and stratigraphy

These studies focus on the seasonal changes, dynamic states of fluvial-aeolian interactions and the distribution of landforms. These studies are normally conducted through simultaneous observations of erosion processes and landforms or remote sensing as the interaction systems are evident on Landsat images (Breed and Grow, 1979; Langford, 1989; Rendell et al., 2003). Farraj and Harvey (2004) investigated the landforms and fluvial-aeolian interactions in the northern UAE, and pointed out that the assemblages of alluvial fans and dunes may contain paleoclimatic signals and so can be expected to indicate the drying-wetting alternation. Newell (2001) found two contrasting types of fluvial/aeolian bounding surface (planar and incised) in the Wessex Basin, SW UK. In this area, planar bounding surfaces separate tabular bodies of fluvial conglomerate and aeolian dune sandstone. They were produced primarily by wind scour to groundwater table, with the later emplacement of conglomerates resulting in local fluvial erosion of cemented aeolian dune sandstone. Incised bounding surfaces were produced by fluvial downcutting. The erosive relief was infilled with mixed aeolian/fluvial deposits. In central Australia, Bourke (2002) observed the fluvial-aeolian interactions at paleoflood termini and found that late Pleistocene and Holocene floods have strongly influenced the assemblage of fluvial, aeolian and lacustrine landforms along the desert margin. A series of high magnitude floods eroded longitudinal dunes, emplaced sandy-gravel bars and formed clay pans in inter-dune areas. Aeolian processes subsequently reworked the abandoned flood channels. Aeolian dunes located proximal to fluvial systems are therefore repositories of information on past episodes of fluvial activity. These adjustments in aeolian landform

to fluvial events provide key geomorphic signatures of pulsed high-energy climatic events.

In the Kuqa Basin of China, the work of Mingxiang et al. (2004) illustrates a set of arid red beds of the Lower Cretaceous strata that several types of sedimentary facies were identified: mudstones of the plaza, aeolian sandstones, sandy conglomerates from intermittent rivers, conglomerates from fluvial fan. These types of sedimentary facies constitute a typical desert system. Some coarse sands and fine conglomerates are found in aeolian sandstone with distinct sorting features. It denotes that aeolian sandstones are reworked by fluvial action with the humid-arid changes and interbedded fluvial-aeolian depositing.

2.4.2.3 Process observations

The association of particular sand dune types and patterns with river valleys has been widely observed from a number of desert environments (Bullard and Nash, 1998). To identify the relationship between sand dunes and valleys, some researchers have conducted process observations in both field and laboratory settings (Bullard et al., 2000; Wiggs et al., 2002; Garvey et al., 2005). It was found that the presence of a valley has no significant influence on airflow direction when the approach angle of the wind is perpendicular to the valley axis, but that marked deflection of airflow can be caused with any wind approach angle of less than 90°. However, it is uncertain as to whether valley-induced boundary-layer modification can be invoked as an explanation for less-localised valley-marginal dune pattern changes. This research provides an explanation for the evolution of valley-marginal dune patterns, as well as offering insights into the approaches that can be applied when conducting simulations of fluvial-aeolian interactions using different interacting angles.

2.5 Numerical modelling of landscape development

Modelling can be classified into physical models (laboratory models) and computational (numerical) models. Physical models, usually operating within a laboratory, use appropriate tools and scaling laws to measure and assess some

environmental phenomena which are hard to observe in the field. Computational models provide an alternative approach to compensate the limits of physical models. Computational models can simulate large spatial scale and longer time scales, improving the understanding of the natural systems and predict future states of a system so that they have been developed extensively. However, current numerical modelling focuses on either fluvial or aeolian dynamics, with no model simulating fluvial-aeolian interactions.

2.5.1 Computational simulation of dune field development

To study the morphology, dune growth, downwind migration and spatial patterns that form in a sand field, numerical modelling of individual dune dynamics and dune field evolution has been developed since 1970s (Howard et al., 1978; Wippermann and Gross, 1986; Nishimori et al., 1998; Kroy et al., 2002; Lima et al., 2002; Livingstone et al., 2007; Hugenholtz et al., 2012). In these models, geomorphological understanding of sand transport was combined with computer models of wind flow over dunes. However, most of the studies failed to model the patterns of erosion and deposition on sand dunes completely, and were generally unable to provide reliable predictions of dune movement and growth (Wiggs, 2001). This is because most of the models were built up on empirical data which inevitably limits their application (Werner, 1995).

Nevertheless, the regularity and patterning of dune fields, as have been viewed in section 2.2.3, inspired modellers to simulate the field development by self-organisation using cellular automata. Significant progress has been made by the introduction of two models by Werner (1995) and Nishimori and Ouchi (1993; 1995). Both models assumed that a dune field can be considered as an accumulation of sand "slabs" piled in a two-dimensional horizontal lattice, and the movement of these slabs can be used to simulate wind directional sand transport and deformational shaping by gravity. Different from Nishimori's model, Werner's model takes into account the time scale difference between bulk sand transport and avalanching (Bishop et al., 2002). Nishimori et al. (1998) further improved the model by using a different mathematical formulation which presents a more complicated relationship between bed form size and migration rate than in the Werner (1995) model.

Werner's model is simple, with only a few rules, but powerful. The model space consists of a grid with each location containing a number of slabs (Figure 2-9). Slabs are conceptualised to be a packet of sand, rather than a single grain (Werner, 1995). Slabs sit on a non-erodible basement, which can assume any configuration. Shear stress from the wind is abstracted with a simple shadow zone rule. From each point of topography a line is traced down at of the 'shadow zone angle' (θ_s), typically θ_s=15^0. Any slabs that are below the height of the wind shadow are deemed to be in a shadow zone. The slab is moved a specified number of lattice sites, l, in the transport direction and is deposited at this site with a probability that depends upon the number of sand slabs there. The probability of deposition at a site with no sand slabs, p_{ns}, is less than the probability of deposition at a site with at least one sand slab, p_s. if the slab is not deposited, then it is repeatedly moved '*l*' sites in the transport direction until deposition, following which another slab is chosen randomly for transport. This procedure is repeated to construct the time evolution of the surface. Slab movement not parallel to the transport direction originates only from enforcement of the angle of repose (Werner, 1995). The simulations result in this model can strongly resemble the actual development of a dune field (barchan, transverse ridge, linear and star dunes) by varying the directions and duration of transport (Werner, 1995; Bishop et al., 2002; Barchyn and Hugenholtz, 2012).

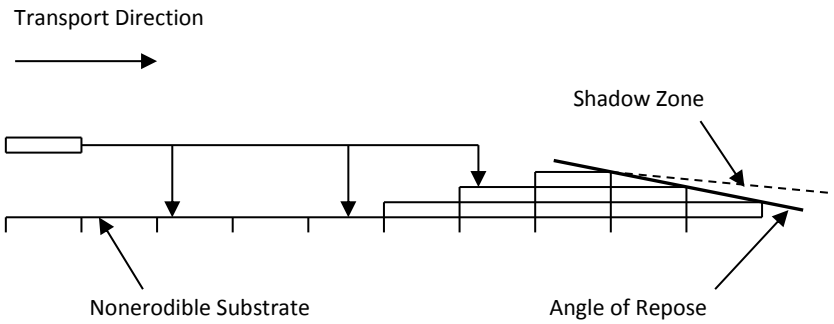

Figure 2-9 Side view illustrating dune-simulation transport algorithm in Werner's cellular dune model (Werner, 1995).

Following upon Werner's work, further studies have been undertaken to implement Werner's model or apply it to investigate the sediment fluxes and evolution of dune fields (Baas and Nield, 2007; Narteau et al., 2009; Eastwood et al., 2011). Momiji et al. (2000) and Bishop et al. (2002) introduced a wind speedup factor on the stoss slope to

solve the problem of non-erosion in wind shadows, which would lead to the endless dune growth tendency, and simulated more realistic dune shapes than in the original Werner model. Pelletier (2009) further enhances Werner's model along the lines of (Momiji et al., 2000), but instead of adjusting the saltation length based on height, Pelletier's model adjusts the probability of erosion and deposition at each grid point, at each time step, according to the local sand flux, which is dependent on bed shear stresses of the then-current topography. This results in bedforms that evolve into a dynamic steady-state train of bedforms (unlike earlier models where the bedforms coalesce into one transverse ridge), and suggests a linkage between physical parameters and bedform size. These models improvement more accurately simulate the evolution of real-world dune fields, for example, they have been used to replicate the precursor of a vegetated dune landscape or employed to investigate the historical evolution of a compound and multi-episodic dune fields (Baas, 2002; Kocurek and Ewing, 2005; Nield and Baas, 2008).

2.5.2 Computational simulation of fluvial landscapes

In the past decades, different types of computational models have been developed to simulate the response of river systems to environmental change in different time and spatial scales, from decades to millennia, from reach scale to catchment scale. These models focus on different aspects of fluvial systems, e.g. hydrological models, flood inundation models, channel morphology models, channel network models, models of river meandering and river braiding, alluvial stratigraphy models, and landscape evolution models (LEMs) (Lancaster, 1982). LEMs have become the most functional tool for the study of coupled interactions between surface processes and external forcing factors, e.g. tectonics, climate change, to replicate the processes that form the landscape (Ahnert, 1976; Willgoose et al., 1994; Goren et al., 2014). A number of LEMs have been developed to cope with various issues that arise in simulating different processes operating over a wide range of spatial and temporal scales (Coulthard, 2001). The computational simulations of the landscape evolution have been especially facilitated by adoption of cellular approaches (Murray and Paola, 1994; Murray and Paola, 1997; Martin and Church, 2004; Nicholas, 2005; Willgoose, 2005). In cellular models, the landforms are represented by a lattice of cells and the routing of water

and sediment are the results of the interaction between cells which are simply ruled by abstractions of governing physics.

Several LEMs have been developed to date and some are available as open source codes. GOLEM (Tucker and Slingerland, 1994)and SIBERIA (Willgoose et al., 1991; 1994) are two of the earlier LEMs and still have been studied and applied by other researchers (Hancock et al., 2002). Both models use a grid of square cells to represent the simulation domain. GOLEM was developed to explore the effects of different combinations of erosion processes and tectonics on long-term landscape evolution (100 000 to 10 000 000 yrs) so that the grid cell size is large (*c*. 1 *km* × 1 *km*). Whereas SIBERIA is to model the long-term interaction between hydrology and catchment form, and how tectonics and erosion combine to form channel network morphology, the grid size could be much smaller. In SIBERIA, a diffusion term is added to the continuity equation that operates in fluvial channel to erode the material from slope cells into channels. However, the treatment of hillslopes and channels at the same scale might not represent adequately the physics of erosion in steep fluvial channels, though it is computationally efficient (Attal et al., 2008). The same problem exists with the SIGNUM model (Refice et al., 2012). SIGNUM is a TIN-based (Triangular Irregular Network) landscape evolution model. It was built to simulate topography development at various space and time scales. There are other TIN-based LEMs including CASCADE (Braun and Sambridge, 1997) and CHILD (Tucker and Bras, 2000). CASCADE was designed to simulate large-scale landscape evolution on tectonic time scales. The uses of the irregular mesh (TIN) have great geometrical flexibility to solve problems involving complex boundaries, such as radially symmetrical uplift functions and horizontal tectonic transport across strike-slip faults. This algorithm can greatly improve the computational efficiency. But the large time and spatial scales used in the models results in extremely wide spacing (approximately 1km). CHILD was designed to simulate the erosion and sedimentation in a drainage basin and long-term geomorphic impact of natural variability in storm size.

However, in most models, fluvial flow processes are represented by routing water only to the lowest neighbouring grid cell, which rules out the divergent flow patterns required by analysis of alluvial fans and braided river (Coulthard and Van De Wiel, 2012). To solve this problem, CAESAR (Coulthard et al., 2000; Coulthard et al., 2002;

Van De Wiel et al., 2007; Van De Wiel et al., 2011) adopted the multiple flow routing approach which allows the simulation of alluvial fans (Pelletier, 2004). CAESAR is a two dimensional flow and sediment transport cellular automaton LEM which can simulate morphological changes in river catchments or reaches, over periods from decades up to millennia. Alternatively, CAESAR used a larger number of much smaller regular grid cell (2-5 m as opposed to 25-50 m or even higher) to concentrate most of the computation time on the active cells near the channel, whilst periodically checking the hill slopes. Another feature is CAESAR model can incorporate and simulate many of the complex non-linear fluvial processes, e.g. in-channel and overbank flow, sediment entrainment and deposition, multiple grainsize sediment transport, lateral erosion and bank failure, divergent flow and bed armouring to simulate fluvial response to environmental change, e.g. climate and/or land cover change.

Another notable issue in most of the LEMs lies in the assumption of the steady flow, which is clearly controversial to the fact of hydrodynamic variability's impact on landscape dynamics (Tucker and Hancock, 2010). To address this issue, CASEAR was improved by merging with an 2D hydrodynamic flow model LISFLOOD-FP (Coulthard et al., 2013). LISFLOOD -FP flow model is notable in its fast operation time among many flow models (Neal et al., 2012). It is a simplified one dimensional inertial model that is applied in a coordinate space to simulate two dimensional flow depths and velocities over a raster grid (Bates et al., 2010). Incorporating an inertia term enables the model to increase the simulation time steps considerably to seconds to tens of seconds thus significantly accelerate the operation time. The integrated CASEAR-Lisflood allows, for the first time, hydrodynamic effects (tidal flows, lake filling, alluvial fans blocking valley floor) to be represented in an LEM, as well as producing noticeably different results to steady flow models (Coulthard et al., 2013).

2.6 Synthesis

The current research on fluvial and aeolian processes, as reviewed in this chapter, clearly indicates that there is a need for further study into the interactions between these two systems. As shown in section 2.4, the important impacts of fluvial-aeolian interactions on landforms has been gradually recognised by many researchers, but despite this, no systematic work has been carried out in order to describe or classify

the interaction phenomena that being observed in the field. Furthermore, in the majority of previous studies, despite general descriptions of the resulting landform characteristics and suggested surface processes, usually based solely on sediment records studied using sedimentology, stratigraphic, mineralogical, geochemical analyses, etc., relatively little empirical information is provided about how, and the extent to which, coupled fluvial and aeolian processes contribute to the origin and development of landforms. As a consequence, five preliminary research questions can be developed:

1) How do fluvial-aeolian interactions influence landform evolution?

2) What are the dominant environmental factors and geomorphic features that characterise these environments?

3) Based on modern environmental context, can a comprehensive classification of fluvial-aeolian interaction types be set up that can reflect geomorphological characteristics and corresponding dynamic processes?

4) Can modelling provide insights into the nature of, and processes involved in, fluvial-aeolian interactions?

5) What are the threshold values that are exceeded when dominant regimes shift?

These questions clearly indicate that a greater understanding of fluvial-aeolian interactions is required. In order to address these questions here,initially a comprehensive investigation at the global scale will provide a basis for the identification of possible environmental influencing factors, and the classification of various types of fluvial-aeolian interactions. This study will incorporate various resources; both imagery and the available literature to enable the observation, analysis and classification of these landforms in order to generate an initial of the possible range of fluvial-aeolian interaction processes, provide references for field observation, and consequently assist in the development of additional research questions about fluvial-aeolian interactions.

Additionally, in order to find out how fluvial and aeolian processes affect each other, and the impact that these interactions have on landform geomorphology, long term

observations of interaction processes and landform development is clearly needed. However, given general time and financial constraints this fundamental data is usually very hard to obtain. With this in mind, it is clear that computational modelling, could provide a realistic approach which can enable the simulation of long-term interaction processes between fluvial and aeolian systems, and facilitate and assessment of the subsequent impacts on geomorphological processes. To date no combined fluvial-aeolian model has been developed, even though plenty of independent fluvial or aeolian models have been established; as reviewed in section 2.5. To carry out both an assessment of the available field data that is available for study, and to delineate the parameters of the modelling work, previous independent studies on aeolian/channel processes and landform evolution, as reviewed in section 2.2 and 2.3, are very important. This work would provide the context for these interactions and provide baseline information to inform field investigations, and ultimately provide the contextual data to feed into the evaluation of the simulation results.

Therefore, the main aims of this research are:

1) To carry out a large scale investigation to illustrate the distribution of interactions between fluvial and aeolian processes and assess possible impact factors;

2) From the investigation, identify the most frequent dune/river types, and categorize the fluvial-aeolian interaction types, which would be applied in further numerical simulations;

3) Develop dune/river models that can be applied in this research;

4) Conduct numerical simulation with two aims; one is to verify the fluvial-aeolian interaction types observed in the investigation, and the other is to observe the dynamic processes between fluvial and aeolian systems and the impacts that these have on landforms,

and finally, to:

5) Identify if there are threshold values that are connected to shifts in the dominant regimes.

Chapter 3 Mapping fluvial-aeolian interaction

3.1 Introduction

A number of researchers have identified the importance of fluvial-aeolian interactions as reviewed in Chapter two (section 2.4), but there has been limited work to understand these interaction and the resulting landscape. To illustrate the wide distribution of interactions between fluvial and aeolian processes and their impact on landform evolution, there is a need to identify, describe and classify the interaction between fluvial and aeolian processes over a large (regional/global) scale to enable the identification of new issues that have been ignored previously. Furthermore, current research in disciplines ranging from sedimentology to geomorphology and studying across timescales that range from ancient to modern processes, need contemporary analogues to assist with the interpretation of landform evolution. Therefore, it is necessary to examine current interactions between fluvial and aeolian systems to establish modern analogues (Bullard and McTainsh, 2003).

Hence, a global inventory of fluvial-aeolian interactions has been undertaken to provide a global classification of existing types of interaction and their frequency. The factors that may contribute to the interactions that have been identified from remote-sensing data and a variety of published information and statistical techniques have been used to interpret the relationships between forms and processes. The bulk of this chapter is presented in Liu and Coulthard (2014).

3.2 Methodology

3.2.1 Field identification

Regularity of morphology (form and pattern) has long been used to infer process and satellite images provide the opportunity to observe the forms and patterns from a synoptic view. This constitutes the bulk of the global mapping presented in this chapter. During the survey, areas of fluvial-aeolian interactions were detected visually using remote sensed imagery hosted by Google Earth (GE). Using remote sensed

images does present some difficulties since these images can only identify surface features and landforms – in effect the symptoms of aeolian and fluvial action. For this reason the study focussed on the interaction between sand dunes and rivers as both features are readily identifiable.

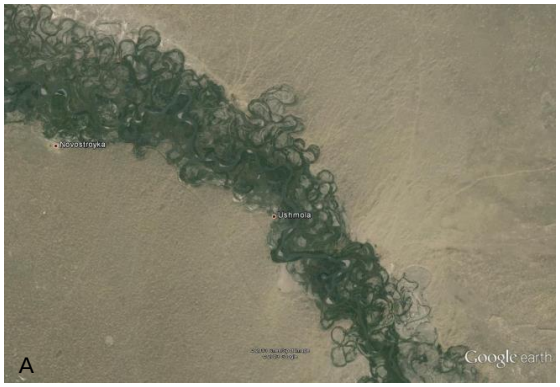

A) Ushtobe, Kazakhstan (45°34'20.34" N 77°36'15.54" E);

B) Paiku Co, China (28°42'26.59" N 85°33'22.02" E);

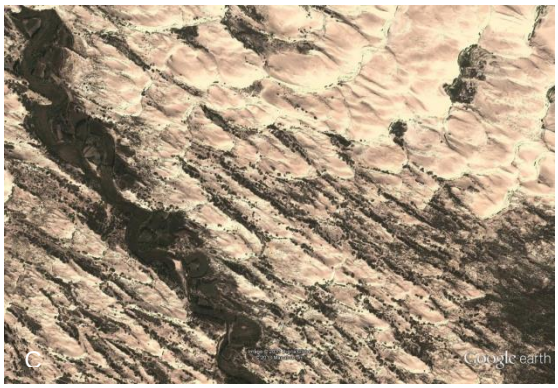

C) Shanhou, China (43°08'32.34" N 118°57'49.65" E);

D) North Panamint valley, America (36°27'49.79" N 117°26'55.98" W);

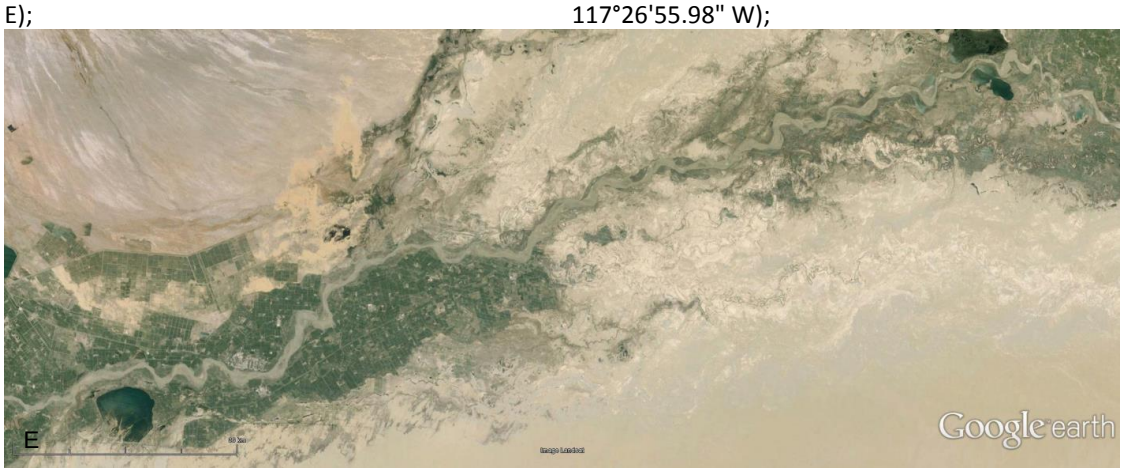

E) Tarim River on the north border of Taklamakan Desert, China (40°44'01.28" N 81°51'37.67" E).

Figure 3-1 Examples where fluvial-aeolian interactions are difficult to identify (Landsat image source: Google Earth).

Sand sheets were not recorded since it is difficult to distinguish them from bare or scrub ground at the resolution of the imagery used here (e.g. Figure 3-1A, B). The survey also excluded vegetated dunes as vegetation adds a level of uncertainty to the

behaviour of the dunes that is difficult to interpret from satellite imagery (Figure 3-1C, D). To augment the visual search examples from published studies were also used where available.

In order to determine local wind direction, visual identification based on local dune morphologies were mainly used and meteorological records from government or private sources were used when the images resolution were not high enough to determine the dune morphologies (Weather Underground, 2013). The wind direction in some locations could be accessed directly from onsite or nearby weather stations and was checked repeatedly during our survey period (Figure 3-2A). Some remote locations were too far away from the nearest stations so meteorological data from nearby stations was used to identify the wind direction (Figure 3-2B).

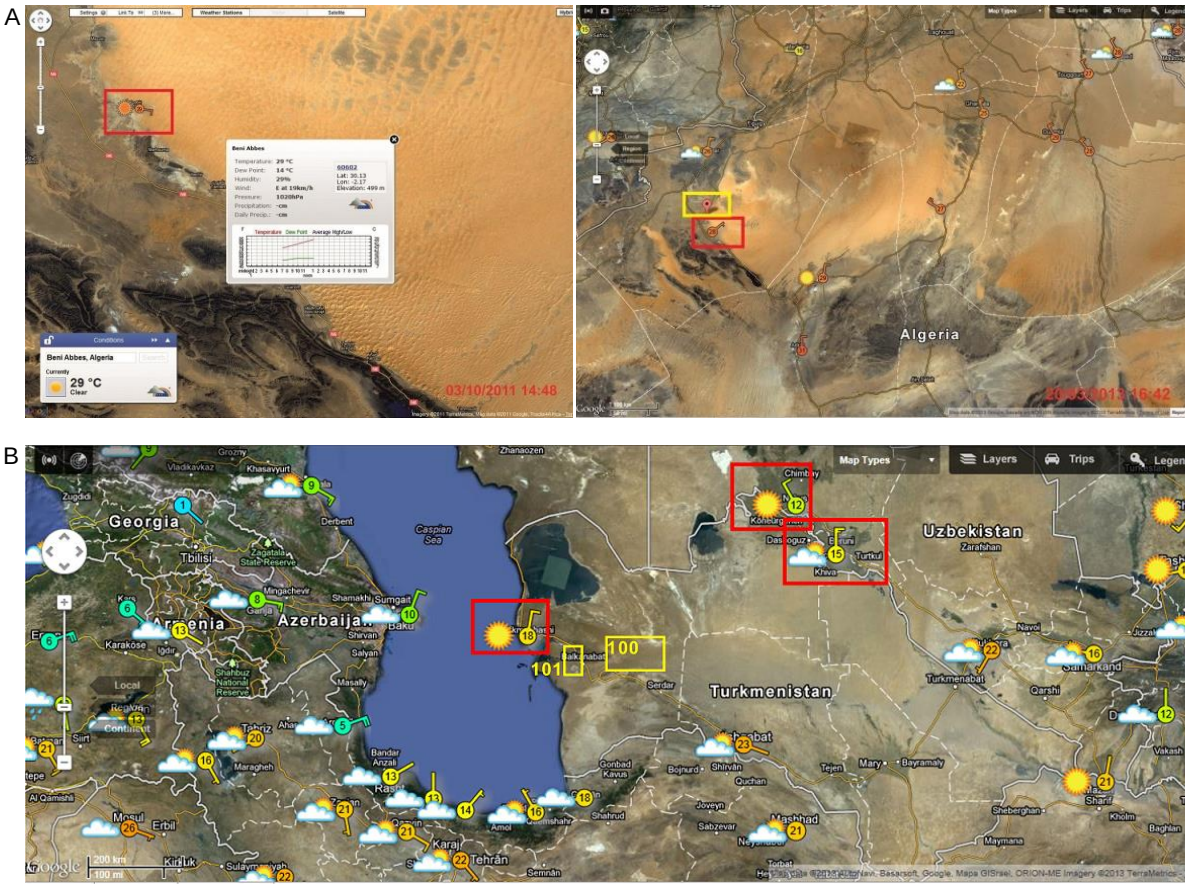

Figure 3-2 Identification of wind direction by referring to metrological station records. Study sites are circled in yellow rectangles and stations that have been referred to are circled in red rectangles. A) Igli, Algeria (30°31'05.99" N 2°19'48.04" W). The metrological records had been referred from nearby station and been accessed on 3rd October, 2011 and 20th March, 2013, separately; B) Two sites in Turkmenistan (39°42'51.53" N 55°33'35.18" E and 39°37'31.05"N 54° 9'55.13"E). Three metrological stations records had been compared. (data source: weatherunderground.com).

The search methodology started at the margins of dryland areas identified visually using Google Earth (image spatial resolutions of about 15m per pixel). The identification work was conducted across the period April 2011 to June 2013. The margins of these areas are where the aeolian and fluvial processes are most likely to interact with each other (Bullard and Livingstone, 2002). Identifiable river channels were then traced up- and down-stream to identify locations where aeolian dunes interacted with river channels. The identification of dune forms were based on the unique dune morphological characteristics (as reviewed in Chapter 2) that can be seen in the images, as well as other sources of information such as the published literature, local images, etc. These interactions were classified at a regional scale, where the interaction for a single river will be recorded as one case (Figure 3-3A, B). For some very large river catchments which may cross a wider range of landscapes or even different climatic zones, examples were selected from distinct regions or where there were clear examples of different interaction types at different location (Figure 3-3C). In some locations many small streams flow down from mountains and dissipate into dune fields and, to prevent double counting, these cases were recorded as a single example since the small streams are located in the same region and all exhibit similar behavior when they interact with the local aeolian processes (Figure 3-3D).

To further reduce uncertainty, the locations studied must be outside of the influence of obvious human activity. As a result many places with fluvial and aeolian interactions have been excluded from the final dataset due to the high population densities found along many rivers, for example, the Tarim River on the north border of Taklamakan Desert in China (Figure 3-1E).

At each site, several basic variables were recorded to describe the landscape and the controls on geomorphological processes: the channel type, the dune type, the channel flow direction and the aeolian transport direction. These allowed further analysis of possible causes of different types of fluvial/aeolian interaction. The following sections describe the classification method, as well as how channel pattern, dune type, channel flow direction and wind direction were determined.

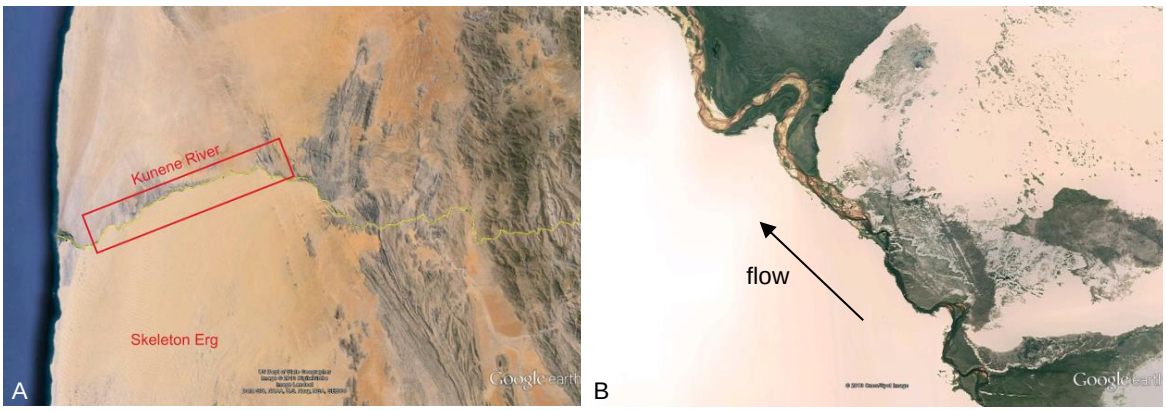

A) The downstream of Kunene River on the North border of the Skeleon Coast erg in Namibia (17°11'12.99" S 11°57'03.13" E);

B) William River, Canada (59°01'40.19" N 109°10'58.41" W);

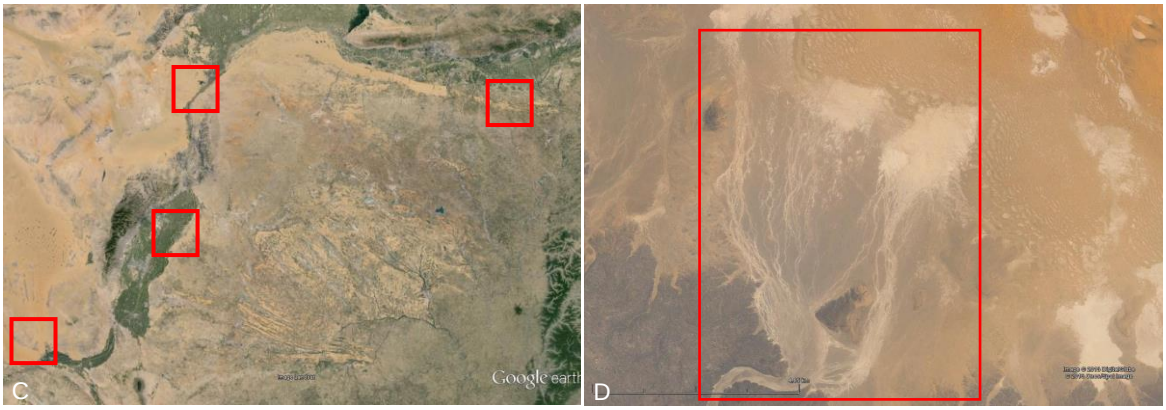

C) Four study sites were selected along Yellow River in China which are located separately at Gansu (37°27'17.09" N 104°58'52.45" E), Ningxia (38°42'13.11"N 106°36'16.14"E), Neimenggu (40°04'49.78" N 106°44'43.07" E and 40°07'51.00" N 111°18'54.10" E);

D) Streams on the edge of Erg Atafaitafa in Algeria (26°17'09.21" N 6°45'52.67" E).

Figure 3-3 Examples of the identification of study sites under different scales and environmental conditions (highlighted in the rectangle) (Landsat image source: Google Earth). A) and B) single river meets various size of dune fields at one place; C) single river meets dunes at different sections and have different interaction processes; D) multi streams meet dune field at one place.

3.2.2 Interaction type classification

The aim of this study is to categorize fluvial-aeolian interactions across a range of regional and local scales – which are mainly decided by the scale of the interacting dune field. Therefore we need to carefully consider the criteria necessary for the classification. These categories should be:

a) Comprehensive and universal- the categories should account for most of the interaction types that can be visually identified and be widely applicable

b) Reflect the processes in operation

c) Simple and where possible compatible with existing fluvial and aeolian classifications

To establish the categories, firstly a scoping survey using the field identification method (section 3.2.1) was carried out on Google Earth identifying global locations where fluvial activity has an impact on aeolian processes and landforms (e.g. dune size and pattern), and where aeolian activity triggers a response in the fluvial regime (e.g. channel change including width, length and location), as well as areas where the two systems are co-dependent. Following this, the six most frequent modes of interaction were classified based on this initial survey, and these are outlined below in Table 3-1 and illustrated in Figure 3-4(a-f). The interpretation of the satellite images, and the mode of classification, is subjective, and limitations associated with this process are considered further in the discussion.

Table 3-1 Classification of interaction types.

Interaction type	Geomorphological characteristics
Fully fluvial dominant (FF)	Dunes are located on only one side of river, with the river acting as a barrier to dune movement
Mostly fluvial dominant (MF)	Dunes are present on both sides of river but are smaller on the downwind side of the river due to sediment depletion. The river flows through the dune field with little or no change in the channel course.
Balanced (B)	The river flows through the dune field and dunes of similar size can be observed on both sides of the river channel. There are no obvious changes in channel width/length/location and dune type/size.
Mostly aeolian dominant (MA)	River flows through the dune field but notable changes on channel width/length/location are observed. The channel may be pushed across in the direction of aeolian transport and /or partially obstructed by dunes.
Fully aeolian dominant (FA)	Dunes block or terminate the river. The river flows into the dune field but its path is blocked by sand dunes preventing it from flowing further.
Alternating (Al)	A system where dominance alternates seasonally between fluvial and aeolian processes over short timescales (monthly to annually). E.g. Dunes may occupy the dry ephemeral/intermittent river bed during dry seasons but are eroded by water flow during wet seasons.

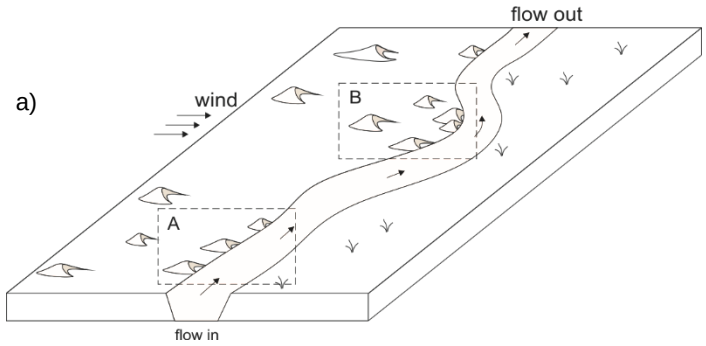

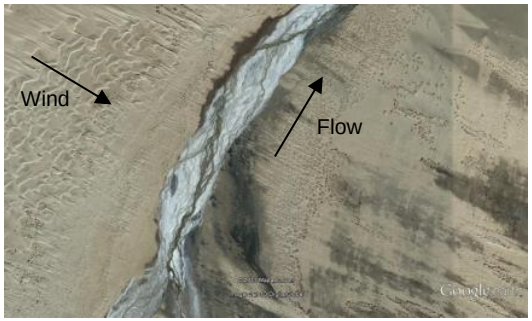

Fully fluvial dominant (*FF*). In the diagram, area A - a location where the river stops dune movement without changing the channel location and type; Area B - a location where the river stops dune movement but the channel location is pushed in downwind direction. The example shows the Tuolahai River in China, the inward dunes moving from NW while the river flows to NE. There are dunes present on NW side of river whereas only bare surface or sand sheet exhibit on NE side of river, and there are no significant changes on channel pattern and location (36°40'22.88" N 94°29'08.16" E);

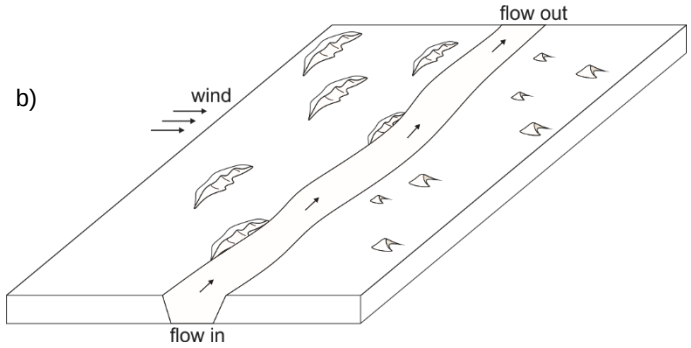

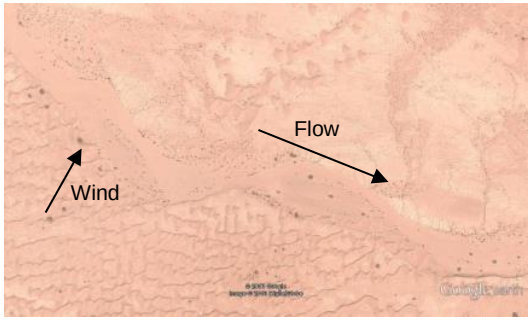

Mostly fluvial dominant (*MF*). The example shows a river in Morroco, there are dense transverse dunes on the SW side of the channel moving towards the river, whereas only barchans present sparsely on the NE side of channel moving apart from the river (31°32'53.04" N 4°30'50.88" W);

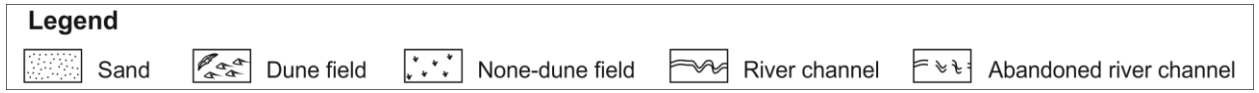

Figure 3-4 Diagrams of different types of interaction (the wind/flow meeting angle, the type of dune and river in real may not exactly as the same as it shows in the graphs).(Landsat image source: Google Earth) (to be continued).

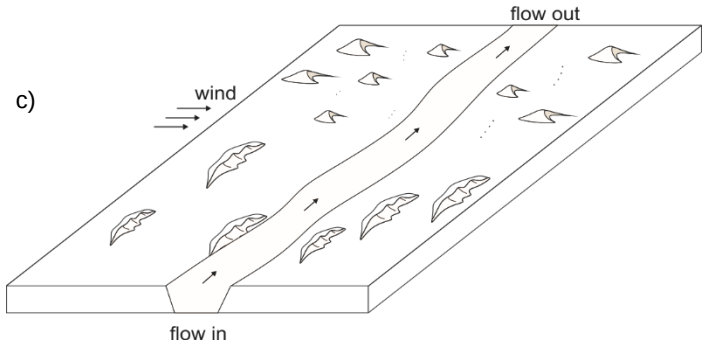

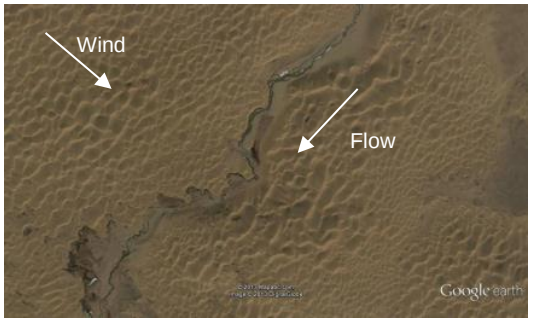

Balanced (*B*). The example is located in Huanghe watershed in China, the uniform sizes of transverse ridges present on both sides of the river bank (35°34'46.91" N 101°01'01.23" E);

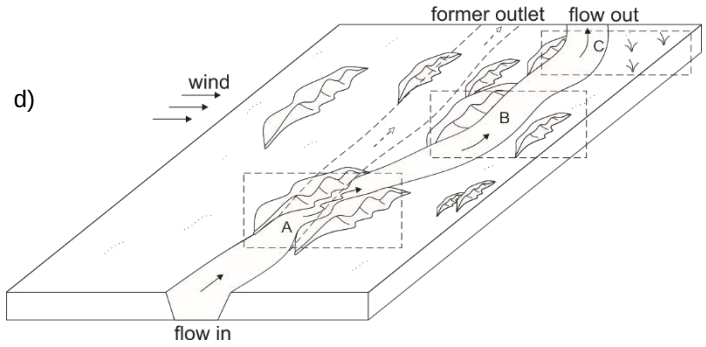

Mostly aeolian dominant (*MA*). In the diagram, area A - dunes dam the river course, area B - dunes divert the river course, area C - dunes push the river course to the margin. The example is located at Himalaya, China, where barchans moving towards the NE dam, divert the channel and thereby change the channel location when crossing the streams (29°55'40.12" N 83°32'35.12" E);

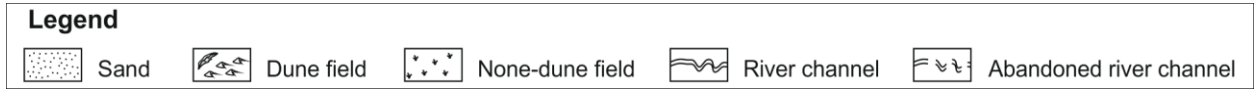

Figure 3-4 Diagrams of different types of interaction (the wind/flow meeting angle, the type of dune and river in real may not exactly as the same as it shows in the graphs).(Landsat image source: Google Earth) (to be continued).

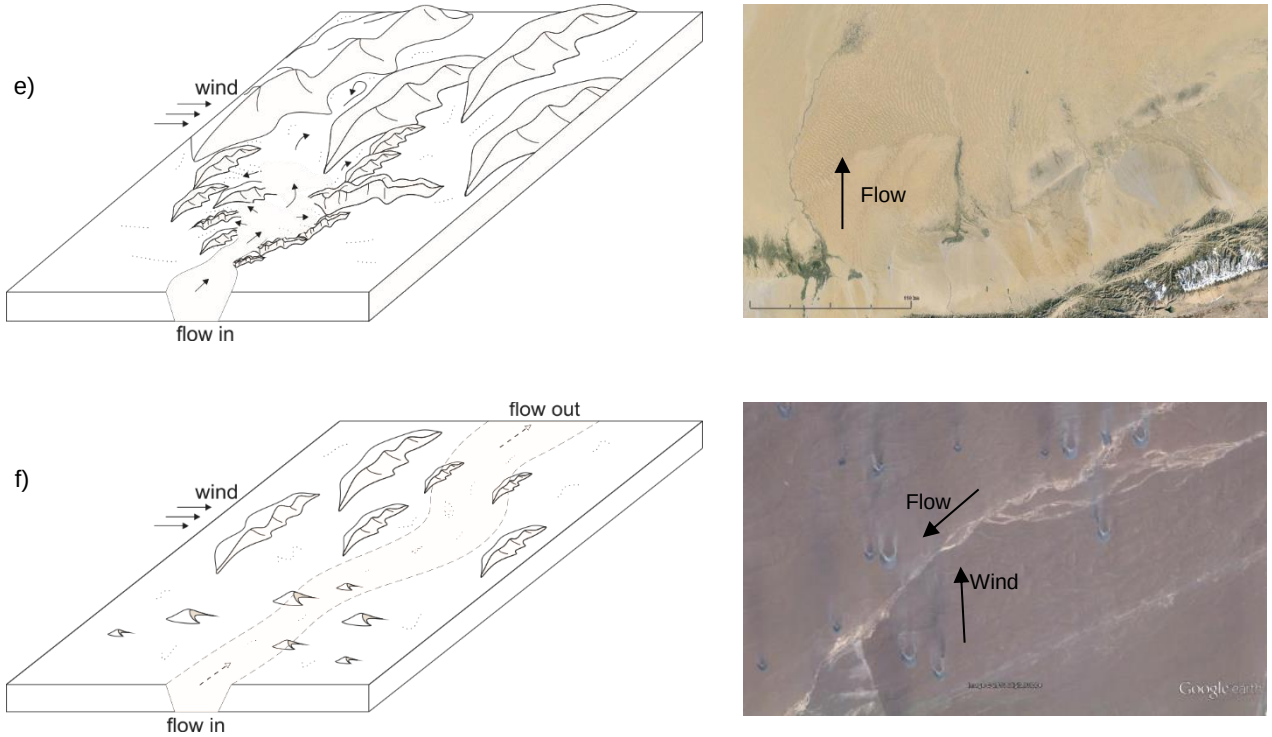

Fully aeolian dominant (*FA*). Examples illustrated are located on the south margin of Taklamakan desert, China, streams flow down from the mountain range into the dune field but have been dammed, diverted and finally diminished into the field (37°33'09.83" N 84°18'30.55" E);

Alternating (*Al*). The example is located in La Joya, Peru. Barchans moving towards north are located on both sides of the ephemeral river bank and even in the channel while no significant change in size so that the dunes may cross the channel during dry season and were eroded when flood in channel occurred (16°39'08.44" S 71°51'23.02" W).

Figure 3-4 Diagrams of different types of interaction (the wind/flow meeting angle, the type of dune and river in real may not exactly as the same as it shows in the graphs).(Landsat image source: Google Earth).

1) ***Fully fluvial dominant:*** When fluvial processes dominate the development of landscape, stream power is sufficient to transport all of the sediment input from aeolian processes (Figure 3-4a). Because of this interception of aeolian sands by the river, the aeolian sand supply is greatly decreased on the downwind side of the river to the extent that no obvious dunes develop. The river channel acts as a boundary preventing the onward dune movement.
2) ***Mostly fluvial dominant***: As the influence of fluvial processes decreases relative to aeolian processes, the interactions become more balanced. Here, rivers have the power to pass through the dune field but are unable to remove all the sediment input from the aeolian system thus allowing some onward dune migration. The resulting landscape is typified by dune fields on both sides of the river but dunes on downwind side of the river are smaller or the dune type changes due to reduced sediment supply (e.g. from transverse ridges to barchans) (Figure 3-4b).
3) ***Balanced:*** The forces between fluvial and aeolian processes become close to equal such that no one process dominates. Therefore, the landscape appears to be in a state of equilibrium where both fluvial and aeolian processes operate without interruption (Figure 3-4c). Here, the river manages to pass through a dune field more or less without change, whilst the dune fields on both sides of the river exhibit parallel development, e.g. similar dune size and pattern.
4) ***Mostly aeolian dominant***: Here, the power of aeolian sediment transport exceeds above that of fluvial action and the sand dunes can partially dam the river channel and/or divert the channel path (Figure 3-4d). From the images this could be observed where the channel became narrower when it was dammed or wider when it was diverted to more open space thus changing its location and length. The dune size and type typically shows little or no change on the downwind side of river.
5) ***Fully aeolian dominant***: As aeolian process become more dominant the river course can be terminated by a dune field and the landscape is dominated by aeolian processes (Figure 3-4e). The landscape dominated by this interaction type can be clearly observed in field that the rivers course is completely obstructed by the dunes.

6) ***Alternating***: Where ephemeral or intermittent rivers intersect with a dune field, the predominant processes can alternate between aeolian and fluvial. For example, in dryer seasons, when river discharge is low or zero, the aeolian process can deposit in the channel, in some cases covering the channel with aeolian features such as dunes. During wetter seasons, flood events can erode part or all of the aeolian features in the channel or the channel location can be diverted because of the dunes obstructing the rivers path (Figure 3-4f). At many study sites, the alternating type can by identified directly from satellite images where dunes were observed located on channel course, for example, the dunes on the left up corner in the image of Figure 3-4f.

3.2.3 Channel pattern

At each location, channel pattern was recorded as this provides information on the river characteristics and behaviour. For example, the relationship between channel form and sediment load may be important in ascertaining the impact of aeolian sediment inputs on fluvial systems due to changes in the channel pattern (Leopold and Wolman, 1957; Schumm, 1985). From the first scoping study it was determined that the most frequently occurring categories of channel patterns were *Straight, Meandering, Wandering* and *Braided* which form the main categories recorded. Some examples of different channel patterns, for example anabranching, anastomosing, and distributive were classified into the group *Others* because of their low occurrence.

3.2.4 Dune field pattern

Satellite imagery limits the amount of morphological information available when classifying dunes. Therefore, four dune categories were adopted during the survey, these include *Transverse ridges, Barchans, Longitudinal ridges and Stars*. These dune patterns are not only readily discernible from satellite images, but their alignment is related to the dominant or resultant sand transport direction, thus reflecting wind regime conditions (Wilson, 1972; Fryberger, 1979; Hunter et al., 1983). As reviewed in Chapter 2, when barchan dunes are formed, this indicates an environment in which the wind regime is unidirectional and sediment supply is limited, and dune migration rates are significant. When transverse ridges are formed, the sediment supply is significantly increased, although the dune migration rate would be decreased relatively,

therefore, the dune field extension would be less significant than the barchan dune field. In terms of longitudinal dunes, the wind regime becomes bidirectional and the dune fields are even more stable, and finally, star dunes are even more stable although the formation of these dune systems indicates that the wind regime is more complicated. Dunes that have low occurrence, or those that are not easily identifiable solely from the GE images, but which can be identified from the literature, were classified into a fifth category of *Others* (this cateogory included oblique, parabolic, reversing, dome, nebkhas, lunettes, and source bordering dunes) (Rendell et al., 2003; Han et al., 2007; Maroulis et al., 2007).

3.2.5 River flow/net aeolian sand transport direction and meeting angle

The river flow direction is measured as the direction along a straight line from the river inflow point to the outflow point within the scale of study area as opposed to the direction of the river thalweg (as illustrated in diagrams and GE images in Figure 3-4). This allows us to assess the general flow direction across the region of study as opposed to the flow direction at a specific location.

The net aeolian sand transport direction is the resultant dune drift potential vector which is identified by the dune pattern or dominant wind regime for a study area. For example, barchan dune migration direction is approximately parallel to the symmetry axis line from its convex point to the horns and the migration direction of transverse ridges is perpendicular to the crest line. For longitudinal dunes which usually develop in wide unimodal or bi-directional wind regimes, the resultant or vector sum transport direction is approximately parallel to the dunes. However, to reduce errors associated with image interpretation where possible these data were verified using information about the local wind direction obtained from meteorological records from existing studies.

The observed river flow direction and net aeolian sand transport direction were classified into 8 equal sized direction categories (ranging from 0° to 180°) (Figure 3-5) with an additional category of “multi-direction” being used to account for features (such as star dunes) that are associated with a multi-directional or complex wind regimes.

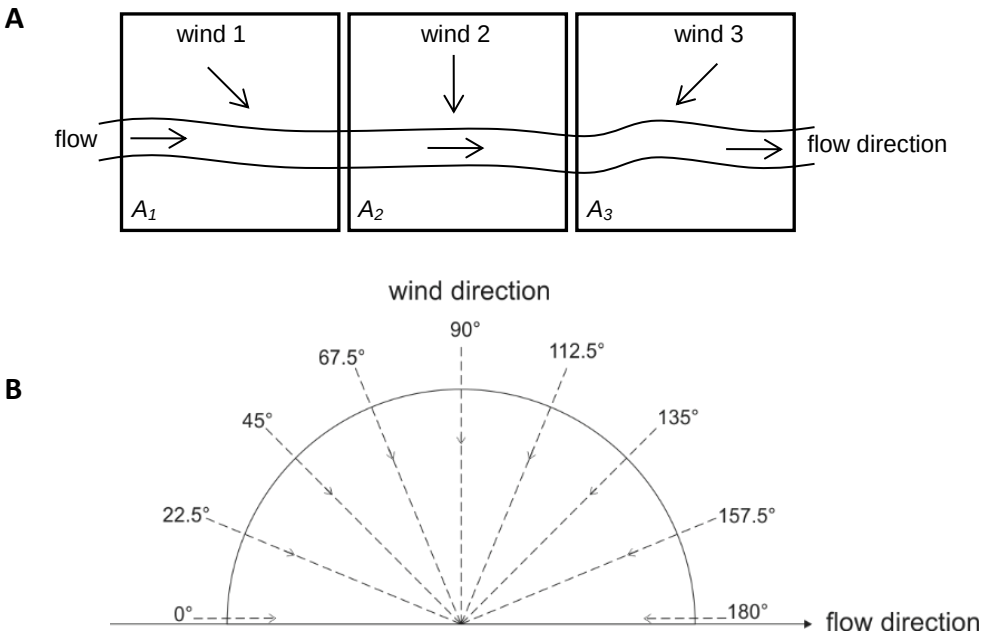

Figure 3-5 Illustration of the meeting angle between flow and net aeolian sand transport direction.

The *Meeting angles* between flow and net aeolian sand transport were also grouped into the same categories as flow/net aeolian sand transport directions (Figure 3-5B). These can be described mainly as either flow with the meeting direction A1, where the aeolian meeting angle is *with* the fluvial flow (e.g. Figure 3-5 (A_1)), direction A2, where the aeolian angle is *perpendicular* to flow (e.g. Figure 3-5 (A_2)) or direction A3, where it is *against* the flow (e.g. Figure 3-5 (A_3)) .

These directional categories were chosen to reflect the sample size and error inherent in the measurement and estimation of the aeolian and fluvial flow angles. For example the angles could be continuously recorded from 0-180 degrees, but with a limited number of sites this would leave a patchy data set, with some angles having no recorded examples. The angle categories also enable the statistical analysis to be reliable, enabling further data analysis and interpretation by combining categories to generate new classifications; see, for example, the results presented in Table 3-2. Furthermore by aggregating the results into categories we can account for some error in the measurement of the angle.

3.3 Results

230 globally distributed study sites were identified where river and dunes were observed to be interacting with each other (Figure 3-6). The majority of these sites are located in Africa, Asia and Australia, with additional sites at the west coast of South America and in North America. Applying the categories described in section 2, the distribution of the categories for each group are presented in Figure 3-7. Some of the categories had a small number of occurrences that were insufficient for any significant statistical analysis. Therefore, these categories were not included in any further analysis. These categories are the channel pattern of *Others* and the dune type of *Star* and *Others* (Figure 3-7a, b), the *Mult* meeting angle category (Figure 3-7c) and the interaction type of *Alternating* (Figure 3-7d). The following sections describe relationships observed between these interacting categories.

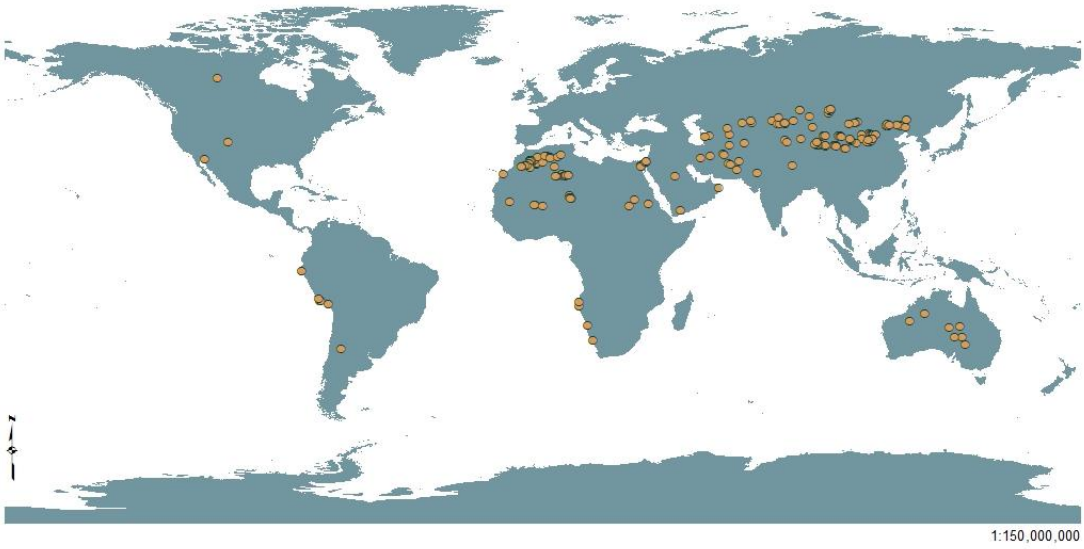

Figure 3-6 Location of 230 study sites.

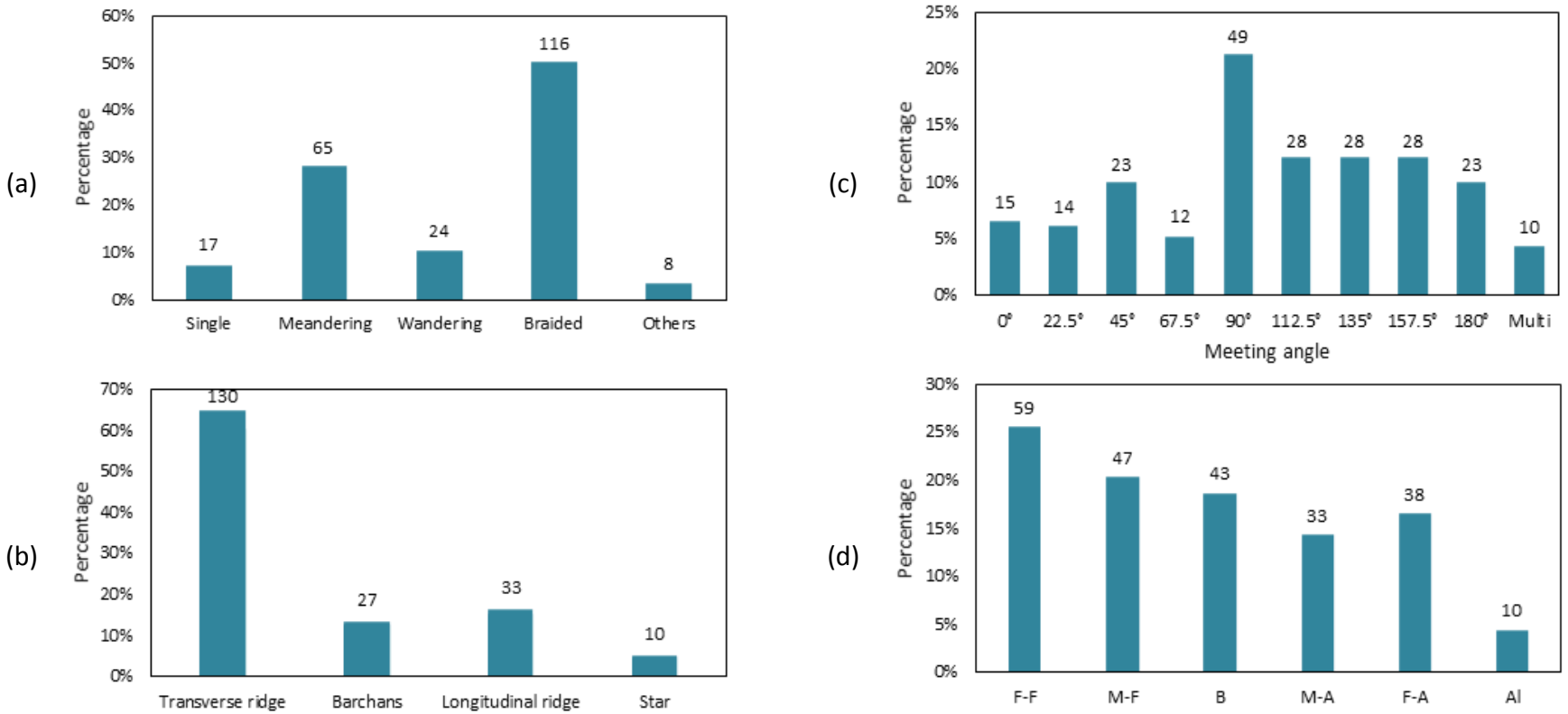

Figure 3-7 Categories distribution in each surveyed factor group, count numbers of each class is labelled. (a) Percentage of all channel patterns; (b) Percentage of all dune types; (c) Percentage of all meeting angle categories; (d) Percentage of all interaction types, where on the x-axis, F-F=Fully fluvial dominant, M-F=Mostly fluvial dominant, B= Balanced, M-A=Mostly aeolian dominant, F-A=Fully aeolian dominant and Al= Alternating.

3.3.1 Dune type vs channel pattern

The relationship between dune type and channel pattern is shown in Figure 3-8. Although *Transverse ridge*s dunes have the greatest occurrence among all dune categories, a similar distribution of channel patterns can be observed for every dune category - with *Braided* channel patterns having the most frequent occurrence followed by *Meandering, Wandering* and then *Straight* river patterns. A chi-square test on the samples indicates that there is no significant association between channel pattern and dune type ($\chi^2 = 12.592, d.f. = 6,\ p > 0.05$).

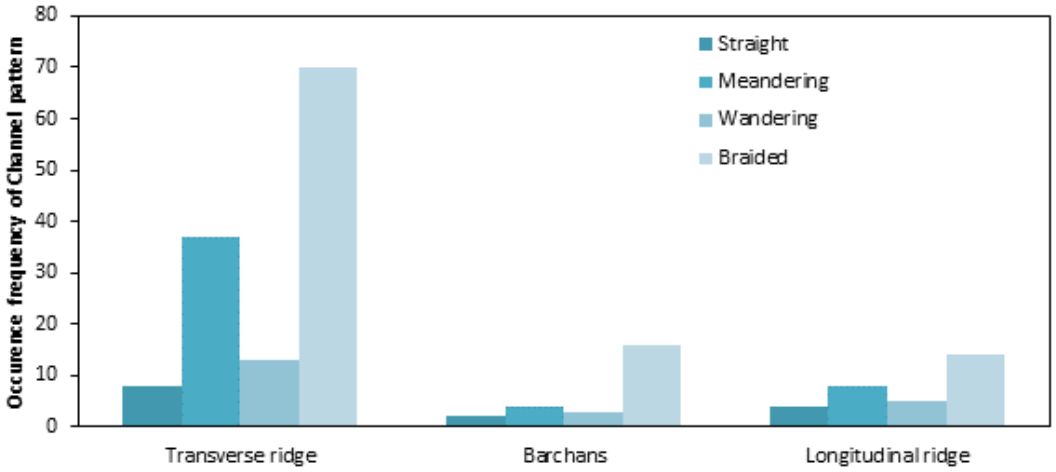

Figure 3-8 Frequency of channel patterns interacting with different dune types. Percentage of dune type is also indicated.

3.3.2 Interaction type vs dune type / channel pattern

No significant relationship between interaction type and dune type was found with our field data ($\chi^2 = 15.507, d.f. = 8, p > 0.05$). However, quite different distributions of the interaction types can be observed between the different dune categories (Figure 3-9), especially between the categories *Barchans* and *Longitudinal ridge*. For *Barchans*, there are very few *Balanced* interaction types with interactions being dominated either by fluvial or aeolian action. Conversely for the *Longitudinal ridge* category there is the inverse distribution of the interaction type compared to *Barchan dunes,* with a high proportion in the balanced interaction type, and a low proportion in fluvial/aeolian dominant interactions.

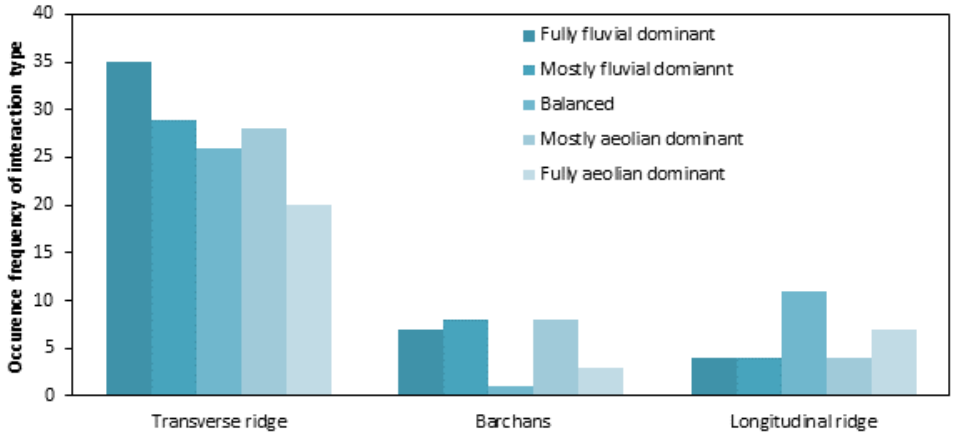

Figure 3-9 Frequency of interaction types in each dune type category.

There is a significant relationship between interaction type and channel pattern (Figure 3-10) ($\chi^2 = 21.026, d.f. = 12, p < 0.05$). With *Straight* and *Meandering* channels, there was a higher frequency of the *Balanced* interaction type but less for all the other Interactions. Conversely for *Wandering* and *Braided* channel categories, the *Balanced* interaction type had the lowest observed frequency.

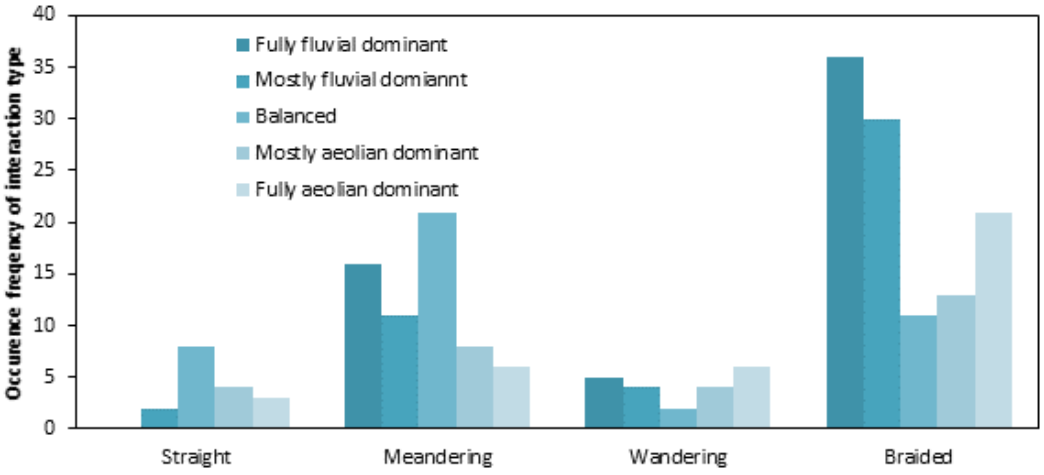

Figure 3-10 Frequency of channel pattern and interaction type in each pattern category of channels.

3.3.3 Meeting angle vs dune type /channel pattern.

Figure 3-11 shows that transverse dunes (*Transverse ridges* and *Barchans*) are most likely to meet the river at right angles, whereas *Longitudinal dunes* are more likely to be parallel to the river direction ([0°, 45°), [157.5°, 180°]). A Chi-square test further supports this with a significant relationship between dune type and the meeting angle ($\chi^2 = 26.296, d.f. = 16, p < 0.05$).

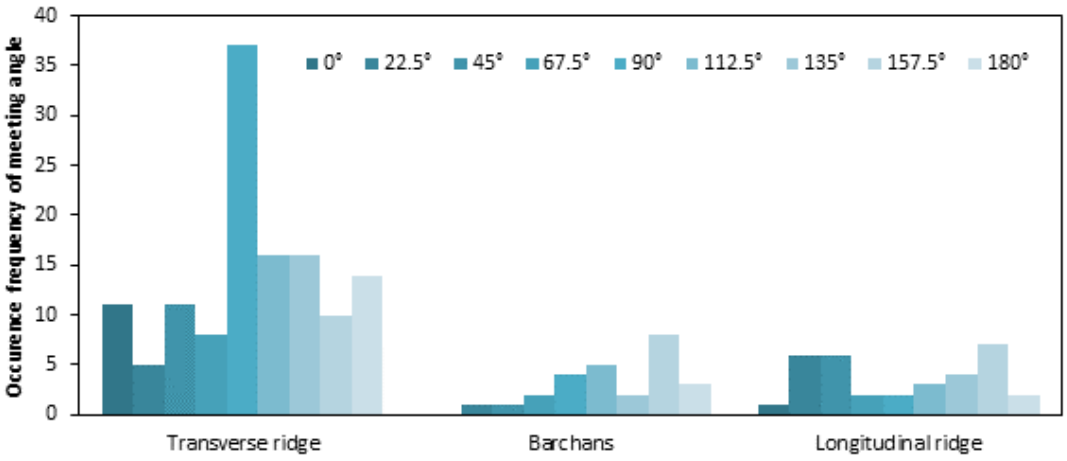

Figure 3-11 Frequency of meeting angle with different dune type.

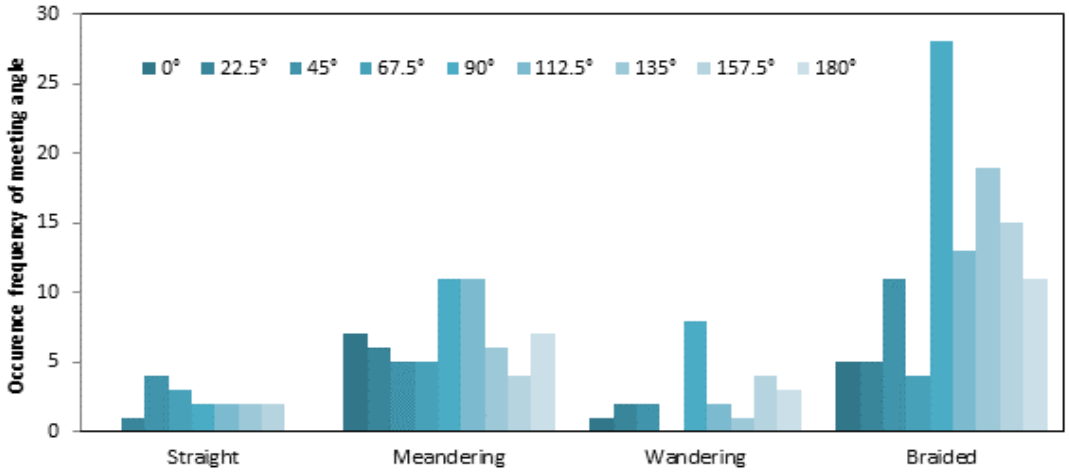

Figure 3-12 Frequency of meeting angle with different channel pattern.

In contrast, there is no significant relationship between channel pattern and meeting angle ($\chi^2 = 12.592, d.f. = 6, p > 0.05$). Though in Figure 3-12, *Straight* rivers appear to interact with dunes at smaller angle, whereas the *Meandering* rivers are more likely to be perpendicular or parallel to the dune movement direction. The *Wandering* and *Braided* river patterns have higher occurrences at 90° and above interaction angles.

It is worth mentioning that the size of the meeting angle categories has no influence on the findings and relationships presented here – the Chi-test results would not change and the occurrences of notable features remains the same. For example, Figure 3-13 illustrates the results of two different size of meeting angle categories by combining the original categories. Using larger category sizes by combining existing categories together can help to simplify the observations, for example, the combined meeting angle categories illustrated in Table 3-2 in section 3.3.4.

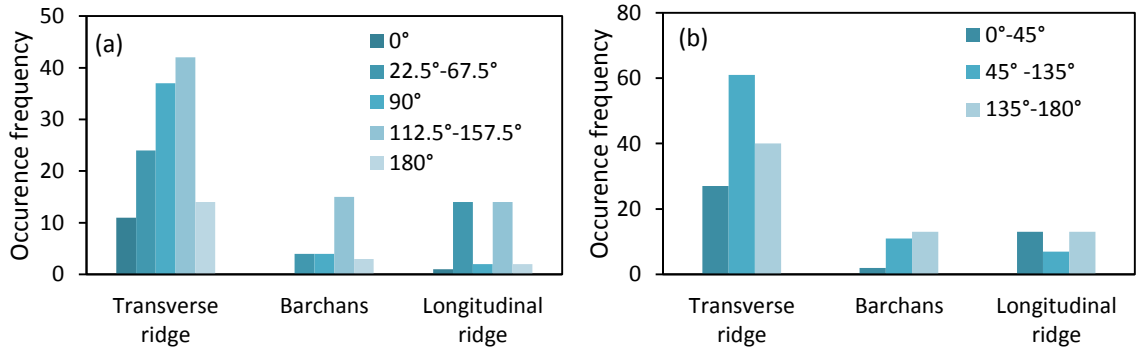

$(\chi^2 = 13.531, d.f. = 4, p > 0.05)$.

$\chi^2 = 15.507, d.f. = 8, p > 0.05)$.

Figure 3-13 Various size of meeting angle categories have no influence on results.

3.3.4 Interaction type vs meeting angle

The relationship between interaction type and meeting angle (Figure 3-14) displays an irregular distribution pattern, however, a Chi-square test shows the interaction type is significantly associated with meeting angle ($\chi^2 = 46.194, d.f. = 32, p < 0.05$). Despite this, we cannot identify whether the interaction type is determined by meeting angle of the interaction or vice versa. But from Figure 3-14 we can observe that fully/mostly fluvial and aeolian dominant interactions have similar distributions of meeting angles that are low for angles from 0° to 90° but higher for 112.5°-180°, whereas in *Balanced* situations the rivers and dunes are more likely to meet at 0°-67.5° followed by 112.5°-180° but less likely to meet at right angles (Table 3-2).

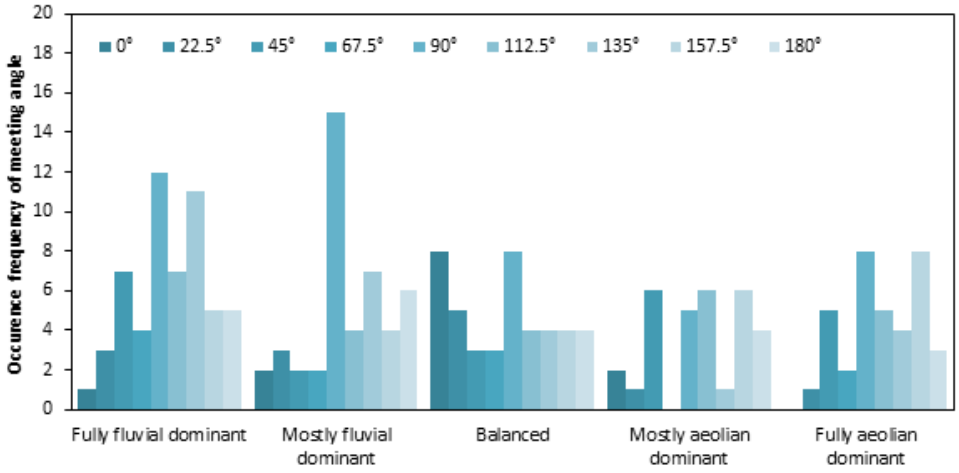

Figure 3-14 Frequency of interaction type and the distribution of meeting angles in each group of interaction type.

Table 3-2 Proportions of combined meeting angles in combined categories of interaction types.

Dominant process	Combined processes	0°-67.5°	90°	112.5°-180°
Fluvial predominant	Fully and mostly fluvial dominant	24%	27%	49%
Balanced	Balanced	44%	19%	37%
Aeolian predominant	Fully and mostly aeolian dominant	25%	19%	55%

3.4 Discussion

The results show significant relationships between aeolian and fluvial systems and these are summarised graphically in Figure 3-15. Here factors connected by black double arrow show a good association between both variables, a blank single arrow shows where there is a dominance between factors (the dominance in the direction of the arrow) and a dashed line reflects no association. For example, *dune type* has a good relationship with *meeting angle* but no significant relationship with *interaction type*.

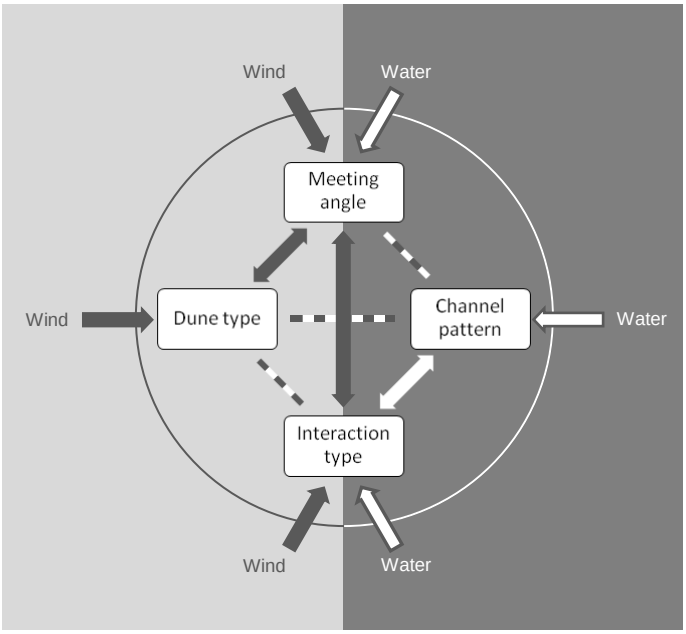

Figure 3-15 Relationships between each two factors.

The most interesting relationships are associated with influences on channel pattern and the dune type/interaction type. *Braided* channel patterns are associated with active sediment erosion and deposition and often found in areas of high sediment supply. Therefore, it is perhaps unsurprising that these were the most commonly observed type of river in this study – as aeolian activity would introduce sand into the fluvial system. Following this assumption we expected to find a larger proportion of braided/wandering streams associated with faster moving, more active dune types (transverse and barchans). But the distribution of channel types was remarkably similar for all dune types (Figure 3-8) and no significant relationship was found. This suggests that enhanced sediment availability from aeolian sources may not be the instigator of change of channel pattern, as has previously been suggested by others

(Huisink, 2000). However, there was a significant relationship between channel pattern and the interaction type (Figure 3-10) where the highest frequency of interactions for *Straight* and *Meandering* channels was related to the *Balanced* type, and *Wandering* and *Braided* patterns were most likely associated with either fully/mostly fluvial or aeolian dominated. This indicates that *Wandering* and *Braided* types are more likely to develop where there is dominance of either aeolian or fluvial processes but not in a balanced situation. This can be interpreted, as more dynamic channel patterns (*Wandering* and *Braided*) are being associated with imbalanced systems and lower energy (*Meandering* and S*traight*) with those in balance indicating a level of stability.

There was also no significant interaction between channel pattern and interaction meeting angle (Figure 3-12). This is an interesting negative result, as we would expect systems where sand transport directions were perpendicular to the river direction would deposit proportionately more sediment into a river than those where the direction was parallel. By running perpendicular to each other, the fluvial and aeolian systems maximise the contact area between them (length of river bank exposed to aeolian transport), thus increasing the potential for transfer for sediment from aeolian to fluvial system. Therefore, we expected sediment added from aeolian sources from perpendicular interactions would lead to a dominance of *Braided*/*Wandering* (more active) channel patterns and parallel interaction angles leading to less active (*Straight*/*Meandering*) patterns.

However, there was evidence for this perpendicular effect and a contrasting interaction with parallel river flow/net aeolian sand transport directions when looking at the meeting angle, interaction type and dune type together. Transverse ridges and barchans are active dune forms and mostly they meet rivers at angles in the range of 90° and 135° (Figure 3-11). These dune types and interaction angles are also associated with systems that are not in balance (Figure 3-9 and Figure 3-14) having either a fluvial or aeolian dominance. In contrast, longitudinal dunes are less dynamic and many extend in parallel with the channel direction (Figure 3-9 and Figure 3-11). This minimises the contact area between the systems contributing to a balanced situation between fluvial and aeolian process. In addition, longitudinal dunes are less active than crescentic dunes, further reducing the available sediment that could be transported

into the river - thus contributing to a low impact interaction between fluvial and aeolian systems.

This raises the question as to whether parallel and perpendicular interactions between dunes and rivers are predetermined (i.e. resulting from the existing topography and wind direction), or if there is some self-organisation within some dune/river systems. For example, this may mean that rivers crossing dune fields perpendicular to the net sand transport direction find it more efficient to be pushed or diverted into flowing parallel to the aeolian sand transport direction (where topography allows). Such an interaction is difficult to ascertain without a time series for the interaction between the two systems, but we can see evidence of this in some field examples. For example Bourke and Pickup (1999) noted that in the Todd River, Australia longitudinal dunes were aligned with the channel pattern. However, it is likely that this interaction will always be one sided, as while deposited sand can alter slopes forcing rivers to take new directions, rivers cannot easily influence the direction of wind driving the aeolian transport.

Looking at the overall balance between fluvial and aeolian dominant systems (Figure 3-7) there is a greater number of sites that are *fully fluvial dominant* compared to *fully aeolian dominant* (26% to 17%). This is also reflected in the next categories of *mostly fluvial dominant* and *mostly aeolian dominant* (20% and 14% respectively). However, these are also be governed by the strength and duration of the wind and water flows which we have not determined in this study. Therefore, whilst the results indicate a greater frequency of fluvial dominance we cannot categorically state that either is greatest.

There are several limitations with this analysis that may have an impact on the findings. Although the study was global, it may not be comprehensive and some areas may have been missed – leading to an incomplete dataset. Additionally, the analysis relies upon the visual identification of aeolian/fluvial features and some of these may be incorrectly identified due to human error. To help minimise such errors all data were verified by two people. The prevailing wind regime is calculated by the dune shape and meteorological records are used where available, but since the sites selected were outside human influence these remote areas often have limited meteorological

records. Whilst much can be extracted from satellite images, it can often be difficult to fully determine the context of a site. A good example of this is provided by the exclusion of channel pattern change - where changes (i.e. from straight to braided) could have been used as an indicator of fluvial/aeolian interactions. Although changes in channel pattern were observed, they were excluded from the analysis since the causes of channel pattern change are complex and involve interactions of multiple factors, (including variables of topography, channel geometry, slope, bank stability, flow discharge). Unfortunately, the satellite images do not provide sufficient information to exclude the influence of alternative factors, in other words the remote sensing does not provide sufficient site context for all types of analysis. Despite access to substantial field data, Huisink (2000) had difficulty in relating historical channel pattern changes in the Vecht Valley (NL) to single driving factors (i.e. aeolian sediment) due to the influence of climate and vegetation changes.

However, the greatest limitation with basing the interpretations on contemporary satellite images which only represent a snapshot in a long history of the interaction at the field site in question. It is quite possible that sites may switch (for example) from being *Mostly aeolian dominant* to *Mostly fluvial dominant*. This makes the *Balanced* category especially difficult to categorise as this state could be static - or it could be in a transition stage from one interaction type to another. Sequential satellite images could be used (dating back to the first Landsat series in the 1970's) though this only allows us to look at a comparatively short period from the past, especially when considering the time scale some dune systems may operate over.

Aeolian and fluvial systems can operate at very different rates and this also makes the interpretation of interactions from snapshot images difficult. Rivers have the capability to change direction (e.g. through avulsion) and move to different courses very rapidly and the destructive nature of large floods can lead to sudden changes (Jones and Schumm, 2009). Conversely, sand dune movement rates are typically low (in the order of less than 1m per year – with some exceptions) and therefore may not be instigators of sudden change (Yao et al., 2007). However, river flow (especially in arid regions) can be ephemeral and aeolian action and dune movement (though slower) may be more continuous. Therefore, this study provides insight into the *static* balance between

aeolian and fluvial geomorphology, but further work is required to investigate the *dynamic* changes between aeolian and fluvial processes.

3.5 Conclusion

This study shows that aeolian and fluvial interactions are clearly widespread – with this survey finding 230 globally distributed sites. Therefore, it is possible to conclude that in many locations aeolian and fluvial processes are having a significant impact upon each other – and on the subsequent landforms and geomorphology. Four variables were analysed to explore possible relationships between fluvial and aeolian systems, including dune type, channel pattern, meeting angle and interaction types. The data showed that certain channel patterns, dune types and interaction angles are most commonly found when there are fluvial and aeolian interactions (e.g. *Braided* rivers: 50%, *Transverse ridges* and *Barchans*: 73%, and a perpendicular meeting angle: 21%). There are significant relationships between meeting angle – dune type, meeting angle – interaction type and channel pattern – interaction type. These relationships indicate that active river channel patterns (braided and wandering) are most common where aeolian or fluvial systems dominate, but not in more stable balanced situations. Unexpectedly there is no relationship between more dynamic crescentic dune systems and active channel patterns, indicating that additional aeolian sediment supply may not be affecting channel pattern. Furthermore, longitudinal dunes tended to flow parallel with river direction, whereas more active crescentic dunes were more often found migrating perpendicular to river flow. This suggests there may be some self-organisation operating between dune type and river flow direction. Finally, all of the results are based on snapshots, from what are often dynamic systems, and further research is required to investigate how the different rates of aeolian and fluvial processes affect their interaction and the resultant geomorphology of the landscape.

However, global mapping by satellite imagery is of limited resolution and can only allow a first-order interpretation of the type of interaction at any one moment and location. Several fundamental questions were raised surrounding fluvial-aeolian interactions (specifically between rivers and sand dunes). Firstly, the field study only showed static snapshots of fluvial-aeolian interactions, so the interaction types

presented in Chapter 3 reflect a comparatively short interaction period, however, it is highly likely that these are dynamic, long-term interactions between rivers and dunes. Therefore, we need a more comprehensive understanding of how sand dunes and rivers interact over *time* and *space*. Further questions include: how do various rates of flow discharge and aeolian sand transport affect the interaction behaviours; what geomorphological landforms are produced; are there critical thresholds for the respective processes to become dominant; and if so, what processes cause the change? An additional question would be, are there any links between the geomorphological changes and other environment factors, such as sediment discharge from aeolian and fluvial systems? This raises a further set of questions surrounding how rapidly the systems change and interact and what the timing, sequence and nature of these fluvial-aeolian interactions are. To answer the questions that arose in Chapter 3, long-term field data would be need to be used, although such data is very hard to obtain due to time and cost limitations. Computational simulation, therefore, can be an effective way of exploring the general long-term dynamic processes between fluvial and aeolian systems.

Chapter 4 Evaluation of DECAL dune model and the Integration with CASAR-Lisflood model

4.1 Introduction

The global inventory presented in Chapter 3 showed how widespread and important interactions between aeolian and fluvial systems are. However, global mapping by satellite image is of limited resolution and can only allow a first-order interpretation of the type of interaction at any one moment and location. To study the long-term dynamic change between fluvial and aeolian processes and the subsequent geomorphological patterns, and to answer the questions arose from the work presented in Chapter 3, ideally, long-term field data would be used. Though such data is very hard to obtain due to time and cost limitations. Computational simulation, therefore, can be an effective way of exploring the general long-term dynamic processes between fluvial and aeolian systems. In this chapter, DECAL sand dune model and the CAESAR-Lisflood morphodynamic model are coupled to allow the dynamic interaction between sand dunes and rivers to be simulated, which will be applied in Chapters 5 and 6.

Among various dune models as introduced in Chapter 2, the DECAL model (Discrete ECogeomorphic Aeolian Landscape model) has been well developed and tested in recent years (Baas, 2002; Eastwood et al., 2011). This model can simulate the development of different sand dunes quickly and comparatively simply. In addition, its cellular grid simulation space eased the linking with the fluvial model CAESAR-Lisflood (Coulthard et al., 2013). However, some amendments were made to the DECAL model so that the required simulation environment can be achieved (section 4.2.1.1). As a result, the behaviours of the implemented DECAL model should and were explored via a series of experiments and a sensitivity analysis, which were presented in this chapter firstly. Furthermore, these analyses will help select the parameters to use with the dune model when combining it with CAESAR-Lisflood in subsequent chapters. For example the dune type, height, width and speed of movement can all be controlled via the DECAL model parameters (section 4.3). Tuning these determines which type of

dune systems will be simulated. In terms of the dune types required for this study, the investigation will be restricted to crescentic dunes, including barchans and transverse ridges. As it is described in Chapters 2 and 3, crescentic dunes, in contrast to longitudinal and star dunes, are one of the most active dune types on earth and the most common type found interacting with river systems. More importantly they form in relatively simple wind regimes – unidirectional - which makes these dune forms suitable for use in simulations in the initial stages of the current preliminary study into fluvial-aeolian interactions.

4.2 DECAL model evaluation method

4.2.1 Model description

The dune model used in this study is based on Werner's (1995) non-dimensional algorithm as implemented by Baas (2002). There are some operational modifications to merge the code with the fluvial CAESAR-Lisflood model but the principal algorithms are the same as DECAL (Baas, 2002; Nield and Baas, 2008). A description of the dune models operation is provided below.

4.2.1.1 Model algorithm

In the combined model, the algorithm relating to dunes is essentially the same as in Werner's (1995) and Baas's (2002) earlier work. The slabs were used to simulate a pack of sand grains, rather than a single grain, movement on a map grid of cells as the model space. Shear stress from the wind was abstracted with a simple shadow zone rule. At each cell a certain angle θ was imposed in upwind direction and any cell that was below the height of this wind shadow was deemed as shadow zone (Figure 4-1). The sand slab transportation was classified into three conditions. Firstly, a grid cell is randomly selected from the modelled domain and if it can be entrained (i.e. does not lie within a shadow zone) it is then moved downwind a constant transport length l which is set to 1 grid cell. At the new location, the slab is deposited or eroded again according to the deposition probability (P_d). This sand slab transportation process is repeated until it is deposited. A slab must be deposited if it falls in the shadow zone which is defined on the leeward side of a dune ($P_d = 1$). In the meantime, the angle of

repose (30°) is enforced through avalanches in the direction of steepest descent with slab that fall into this area being forced to erode ($P_d = 0$).

For each time step of the model operation, the total number of random grid cell selections equals the size of the model domain. This means that on average every cell is polled – but it is possible for cells to be looked at more than once in every model iteration. Previous workers have noted a sensitivity of the DECAL model to input conditions (i.e. the input of sand) (Eastwood et al., 2011).

However, one specific amendament is made to the dune model in the current study in that a non-periodic boundary condition was adapted. This contrasts to the periodic condition used in both Werner's (1995) and Baas's (2002) research. A feature of Werner's original (1995) and subsequent studies is the adaption of periodic boundaries where sand leaving the domain at (for example the bottom edge) is re-introduced or re-cycled at the top of the domain. This enables a conservation of sand within the modelled domain. However, this approach was not used in this study as we aim to mix fluvial and aeolian transport. Therefore sand may be moved by a river over a different boundary (e.g. the right hand edge) disrupting the continuity afforded by a periodic boundary. Therefore, the model was set to have fresh sand entering the model space along the upwind border throughout the simulation and bedforms that migrate off the downwind edge of the model space are not re-introduced along the upwind edge. However, the amount of sand leaving the downwind edge of the simulated field is recorded as the sand output by aeolian process – and sand leaving from other boundaries as fluvially transported sand.

4.2.1.2 Model parameters

There are nine input parameters used in the dune simulations. The value of each parameter has to be set at the beginning of each run and remains constant throughout the simulation. Some parameters have no impact on the dune field boundary conditions but are related to computational operation and efficiency, thus were taken as *Fixed parameters* and were set to the same value for all simulations in this study; whilst some other parameters are based on physical properties associated with the dune field characteristics and thus were categorized as *Controlling Parameters*.

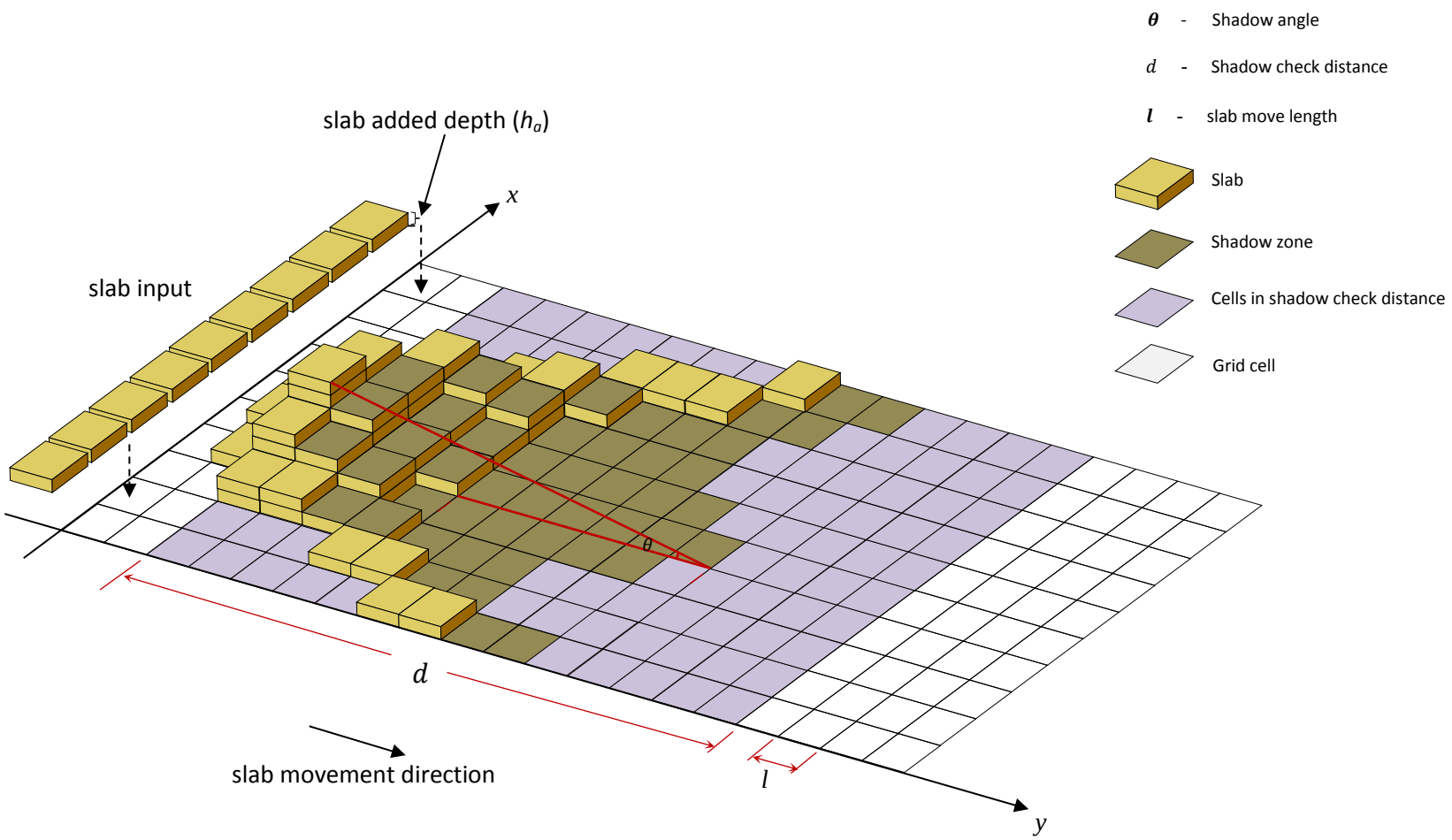

Figure 4-1 Schematic diagram of cellular dune model.

4.2.1.2.1 Fixed parameters

1) Downstream offset (travel distance automatically added)

The downstream offset parameter defines the slab transport length l for each iteration. Although this transport length can be any value, previous researchers found that an increase in effective slab transport distance does not contribute anything additional to the development of dune patterns (Nield and Baas, 2008). Therefore, to ensure that moving slabs interact with all the model space, the downstream offset parameter in this study was set to 1 grid cell.

2) Grid size of dunes (g)

The grid cell size of dune model space can be set independently of the fluvial model grid cell size. This allows the easier scaling of dunes to rivers. The smaller the value, the longer it takes the model run time. Therefore, in this study, this value was set to 10 metres (the same size as the fluvial model) to optimise model run times.

4.2.1.2.2 Controlling parameters

1) Dune landslip angle

As discussed in Chapter 2, the dune landslip angle in real field situation is between 30° and 33°. Typically, in Werner's and subsequent implementation works, this value was set as 30° (Werner, 1995; Baas, 2002; Eastwood et al., 2011; Barchyn and Hugenholtz, 2012). In this study, the dune landslip angle was set to 30° in all simulation tests in order to ensure comparability between this and previous studies.

2) Slab added depth (h_a)

This is a value which describes the height of sand volume ($\boldsymbol{h_a}$) added into the dune simulation per iteration of the dune model. The length of each iteration was determined by the time step (*min*) between dune calls box. This value should not exceed the slab thickness ($\boldsymbol{h_s}$ – below) otherwise sand is added at a faster rate than it can be removed (Table 4-1).

3) Maximum slab thickness (h_s)

The maximum slab thickness is the height of each sand cell which is moved to next cell in metres. In this study, the value of h_s was defined in range of (0, 3) after initial value tests (Table 4-1).

4) Shadow angle (θ)

From each cell of topography, a line is traced down at an angle of θ ($\theta \leq 15°$) to the horizontal surface (Figure 4-1). Any slabs that are below the height of this line are deemed to be in a shadow zone. The shadow zone represent the air flow separation area where the slabs will be forced to deposit (P_d=1). Barchyn and Hugenholtz (2012) found that this parameter can affect the maximum height that dunes form, however, most researchers fix this value at $15°$ (Eastwood et al., 2011).

5) Shadow check distance (d)

Shadow check distance is the distance up wind that the model will check to identify whether a slab is moved into the shadow zone. Slabs in shadow zones are not eroded, otherwise it can be entrained depending on the deposition probability. The value of *d* is confined by the size of the simulation domain, which in this study is between 0 and 200, as illustrated in Table 4-1. The parameter unit is grid cells.

6) Deposition probability (P_d)

This parameter determines whether or not a slab of sand is dropped out or can be moved on to the next cell. The value ranges from 0 to 1. Eastwood et al. (2011) found that a low P_d can result in higher and more variable transport rates but most researchers set this value at 0.6 as this is meant to simulate preferential deposition that occurs on sandy substrates due to momentum absorption.

7) Time step between dune calls (t)

The value of this parameter controls how often the dune model is called to move the slabs. This parameter can therefore exert a strong control over sand transport rates – as it effectively controls when sand is moved within the model. Therefore, *t* could be set at any value (Table 4-1) but the higher the value of *t*, the longer waiting period for

the model to call the slab to the next movement, which would result in slower slab movement rate. This parameter is also important for the integration of the two models and will be discussed in Chapter 5.

4.2.2 Sensitivity analysis set up and configuration

Sensitivity analysis can help to explore how highly correlated the model result is to the value of given input parameters and thus identify the parameters which exert the most influence on the dune formation. Furthermore, once a full understanding of the model performance is gained – parameter values can then be assigned to allow the model to predict realistic rates of sand movement and dune migration – that can be used in the fluvial/aeolian model integration.

To understand the input parameters influence on model results, a range of simulations were carried out to test the sensitivity of each parameter. Although there are nine model parameters listed above, only the controlling parameters affect the simulation results and were therefore considered for this analysis. Even so, seven parameters each with different range of values still constitutes a large combination of parameters that would take a significant amount of run time and generate a great deal of output information. Therefore, *Screening* and *Sampling-based* approaches were applied to determining which input parameters were examined and the experimental design (Muleta and Nicklow, 2005; Helton et al., 2006). This is explained in more detail in Section 4.2.2.2.

4.2.2.1 Simulation domain

The sensitivity tests were carried out over a model domain with a smooth gently sloping but non-erodible surface arbitrarily sized 3000 *m* length in x direction (flow direction) and 1000 *m* length in y direction (downwind direction). There is a small elevation difference between the top and bottom border of 1 *m* which forming a slope of gradient of 0.0005 (Figure 4-2). This slope is introduced for these tests as is the same gradient used in the combined fluvial and aeolian simulations (Chapter 5 and 6).

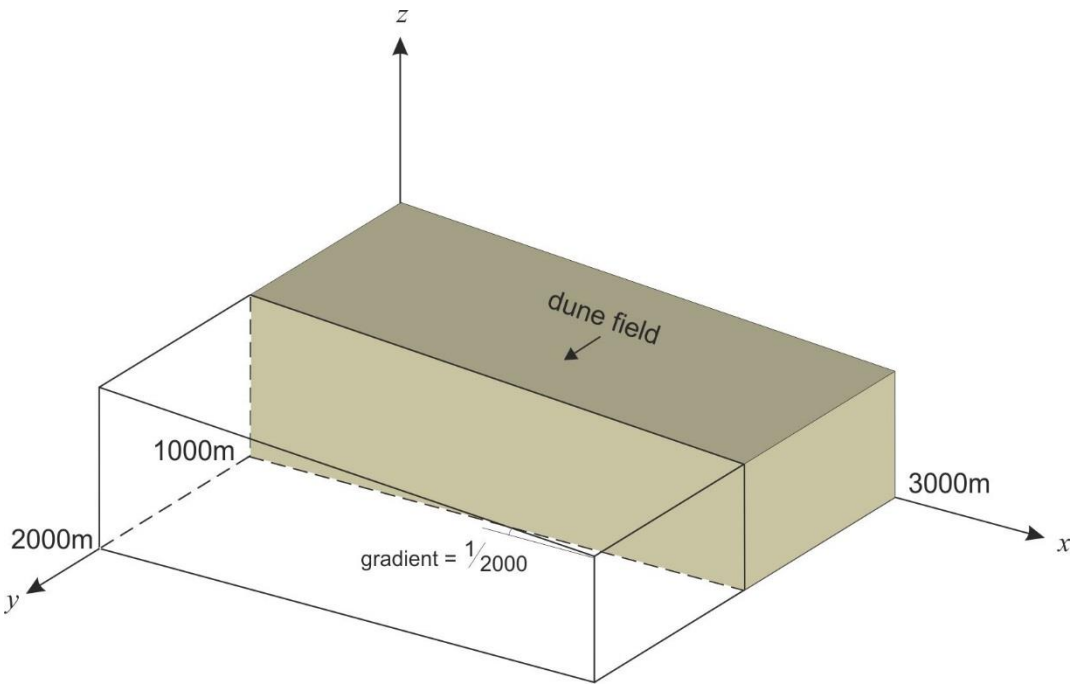

Figure 4-2 Illustration of initial underlain DEM of dune field.

For sensitivity analysis the model run duration was 100 years which was enough for a dynamically stable pattern to form. In each simulation, the first few years represent a "warm-up" period as sand starts to accumulate and form dunes with a relatively stable morphology. The length of this "warm-up" period depends on the sand transport rate. The results of these tests can not only used for sensitivity analysis of the dune modelling, but also provide a control, showing differences in dune field development without interacting with the fluvial.

4.2.2.2 Simulation configuration

All the sensitivity tests were designed with the assumption that all input parameters are independent from each other except the parameter $\boldsymbol{h_a}$ and $\boldsymbol{h_s}$ which are correlated. Therefore, a *local sensitivity analysis method* was applied in this study which required the adjustment of the model input parameters one at a time, whilst all others remained constant so that the influence of each input on the model outputs can be examined (Hamby, 1994).

The parameters involved in sensitivity analysis and the range of values are listed Table 4-1. Even so, the six parameters with a range of values would still require a long computational period when considering the extraction of output image information as explained in section 4.2.3. Sampling-based approaches can reduce computational

demand and, therefore, are adapted in this study (Helton et al., 2006). Some pairs of parameter values were randomly selected first to test the output response. Once a 'sufficient' number of input-output pairs are sampled, further analysis would be performed to explore the input-output mapping and to provide a quantitative measure of output sensitivity due to each input. Scatterplot and correlation analysis are the most common approach used to determine the sensitive of each parameter (Muleta and Nicklow, 2005).

Table 4-1 Model parameters involved in sensitive analysis

Parameter	Unit	Range of values		
		Min.	Max.	Increment
h_a	*metre*	0	h_s	0.1
h_s	*metre*	0	±3	0.1
θ	*degree*	0	15	1
d	cell	0	200 (the vertical length of the simulated field)	10
P_d	%	0	1	0.1
t	*minute*	0	∞	1

4.2.2.2.1 Testing the h_a and h_s

Multiple sensitivity analysis was applied on testing the sensitivity of slab added depth ($\boldsymbol{h_a}$) and slab thickness ($\boldsymbol{h_s}$) whilst the other controlling parameters remained. The values of the other parameters were selected from the ranges of each parameter as listed in Table 4-1. The shadow angle was set at 15° firstly which is the value suggested by most researchers (see section 4.2.1.2); the shadow checking distance d was set at 100 cells which is a mid-level value equals to half of the space cells number in vertical direction; the deposition probability was set at 0.8 which is higher than the recommended value 0.6 in most studies (Eastwood et al., 2011; Barchyn and Hugenholtz, 2012) (see section 4.2.1.2) to increase the rate of dune formation; the time step value was set at 1440 minutes which is one day interval.

Furthermore, as the value range of $\boldsymbol{h_a}$ depend on $\boldsymbol{h_s}$, the test group of $\boldsymbol{h_{si}}$ = [$\boldsymbol{h_{s1}}$, $\boldsymbol{h_{s2}}$, $\boldsymbol{h_{s3}}$, …. , $\boldsymbol{h_{sn}}$] must be decided first and then mapped onto the values of $\boldsymbol{h_{ai}}$ = (0, $\boldsymbol{h_{si}}$). The value of $\boldsymbol{h_s}$ was estimated to be within the range of (0, 3], with the maximum value of 3 being determined from a few pre-simulations that showed there were no well-formed dunes when $\boldsymbol{h_s}$ > 3. The interval value for testing $\boldsymbol{h_{si}}$ was selected as 0.1 for $\boldsymbol{h_{si}}$ ≤ 1.0; 0.2 for 1.0 < $\boldsymbol{h_{si}}$ ≤2.0; and 0.4 for $\boldsymbol{h_{si}}$ > 2.0. For each value of $\boldsymbol{h_s}$, $\boldsymbol{h_a}$ would be tested at intervals of 0.1 within the range given in Table 4-2.

Table 4-2 Test values of h_a and h_s.

h_s	h_a				
	h_{a1}	h_{a2}	h_{a3}	…	h_{ai}
0.1	0.1				
0.2	0.1	0.2			
0.3	0.1	0.2	0.3		
…	…	…	…	…	…
1.0	0.1	0.2	0.3	…	0.9
1.2	0.1	0.2	0.3	…	1.1
1.4	0.1	0.2	0.3	…	1.3
…	…	…	…	…	…
2.0	0.1	0.2	0.3	…	1.9
2.4	0.1	0.2	0.3	…	2.3
2.6	0.1	0.2	0.3	…	2.5
…	…	…	…	…	…
3.0	0.1	0.2	0.3	…	2.9

In addition, to test whether the value of deposition probability (P_d) affect the correlation of h_a and h_s, the influence of deposition probability of the range of [30, 80] was tested on each (h_a, h_s) combination listed in Table 4-2 as well (Table 4-3).

Table 4-3 Test values of P_d.

P_d				
0.3	**0.4**	**0.5**	**…**	**0.8**
(h_{a1}, h_{s1})	(h_{a1}, h_{s1})	(h_{a1}, h_{s1})		(h_{a1}, h_{s1})
…	…	…	…	…
(h_{an}, h_{sn})	(h_{an}, h_{sn})	(h_{an}, h_{sn})		(h_{an}, h_{sn})

From the tests listed in Table 4-2 and Table 4-3, successful pairs of (h_a, h_s) can then be decided if well-formed dunes are observed.

4.2.2.2.2 Testing the shadow angle θ

In this test, θ is the value to change, whilst the other parameter values remained the same. After the test in section 4.2.2.2.1, one successful pair of h_a and h_s was randomly selected from the results and the other parameters were kept the same as when they were tested together. The θ was tested from the maximum value 15°, then reduced by 1° until the minimum value was found when there were no dune pattern can be formed, hence the test group of θ = [15°, 14°, … , θ_n].

4.2.2.2.3 Testing the shadow check distance d

The successful pair of the parameter values selected from the results after simulations designed in section 4.2.2.2.1 and 4.2.2.2.2 were also used to test the shadow check distance d which was varied in range of d = [..., d_i , ..., 100,..., d_j] (d_j<200).

4.2.2.2.4 Testing the deposition probability P_d

In either reality or simulation, it is obvious the higher the deposition probability, the lower the rate of sand transport. A high value of P_d=0.8 was selected to start this test with the deposition probability being tested across the range P_d= [0.8, 0.7, 0.6, 0.5, 0.4, 0.3, 0.2, 0.1].

4.2.2.2.5 Testing the dune recall time step t

With a constant pair value of h_a, h_s, θ, d and P_d, range of t = [1440, 2880, ... , 14400, ... , 36000] with increment of 1440 were tested to find out this parameter's influence on dune formation and field sand dynamics.

4.2.2.3 Simulation output

Three different outputs from the simulations were saved at the same, regular time interval, and were:

1) Screen images of dune field pattern at each time interval saved as a .png image file
2) Land surface elevation information (DEM) saved in ASCII format
3) Rate of aeolian sand transport amount from the field downwind edge at certain time interval were saved

From these data files, six output results could be calculated, including dune height, dune width, dune vertical spacing, dune field pattern, dune migration rate and sand output/transport rate. The processing of these data is described in the following sections.

4.2.3 Quantification of simulation output

To assess correlations between simulation output with model input parameters, a quantitative sensitivity analysis was required. Unlike the input parameter values which can be read directly, some of the output data listed in section 4.2.2.3 needed to be processed further in order to be quantified. Morphological information of the simulated dune field can be obtained using the recorded images and surface elevation data; the dune field sand transport rate and dune migration rate can be obtained from the processed graphical information and the data record.

4.2.3.1 Extracting morphometric information

The images and DEM of the simulated dune field could be processed to obtain the dune field pattern information, e.g. dune height, dune width and length, dune spacing and dune migration distance. All measurements were recorded in an attribute table from which a standard query language macro was used to calculate the dune morphologic information and migrating distance. The measurements were then exported to a spread sheet and plotted on scatter chart to evaluate the relationships between the input parameters and the output morphometric.

4.2.3.1.1 Graphical processing software

To extract information on dune morphology from the images, two programs were applied. *ImageJ* was used to extract the dune width and length, dune spacing and dune migration distance, where ArcGIS was used to identify the dune height.

1) ImageJ

ImageJ is a public domain Java image processing program and runs on any computer with a Java 1.1 or later virtual machine (Schneider et al., 2012).

The function of 'Analyze particles' in *ImageJ* was applied to obtain the dune basal shape and the smallest rectangle enclosing the selected dunes (Figure 4-3).

(a) Simulated dune field pattern:

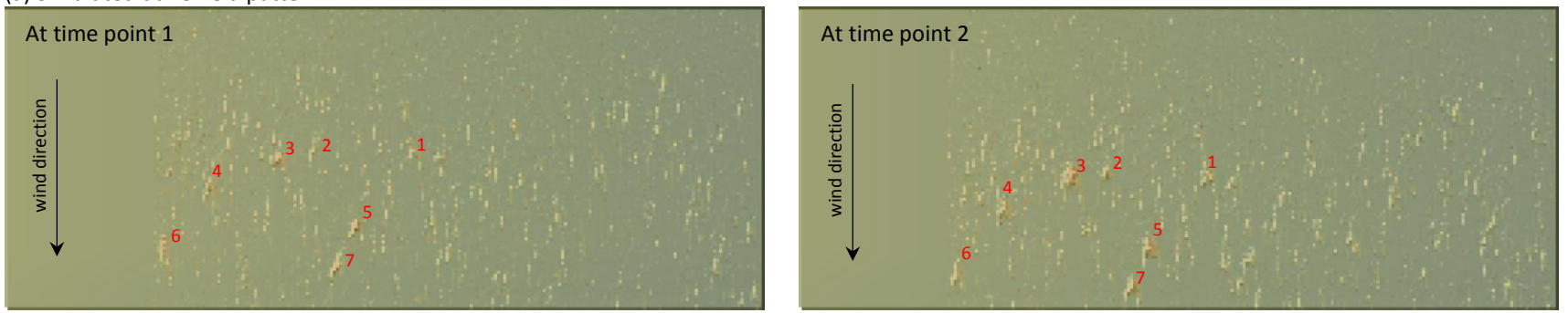

(b) Dune basal outline and coordinate location after been processed in ImageJ:

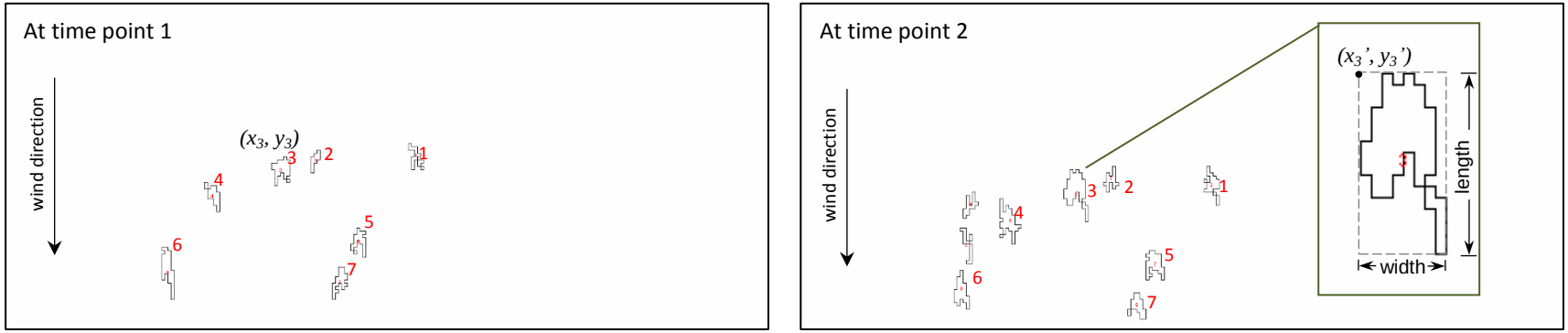

(NB: Images from simulation 0.15-0.3-10-100-80-14400)

Figure 4-3 Illustration of simulated dune width/length and migration distance measurement. (a) Snapshots of a dune field at two sequential time points in raster format; (b) Images in (a) processed into vector format. (Numbers 1-7 in each image represent the seven visible dunes in order to track the dunes movements)

The width and length and the coordinates of the upper left corner of the rectangle that enclosing each dune can be saved automatically by the programme (Figure 4-3). The width and length of the enclosing rectangle can be assumed to equal to the width and length of each dune, and changes in the coordinates of the upper left corner of the enclosing rectangle can be used to calculate the dune advance distance and thus migration rate (e.g. migration distance of dune 3 = y_3'-y_3, as illustrated in Figure 4-3).

However, errors can occur during the image processing. As the images were saved in an RGB format, the dune shapes were outlined mainly by the *Hue* value. As it used a *hue* threshold value, the dune area after a *binary* process in the software may not correspond exactly to the original - as shown in Figure 4-3. But this error results in very small difference of the dune area, usually of 1 to 3 grid cells, which can be ignored. Furthermore, visual identification (between the original image and processed image) was also applied to help reduce the processing errors.

2) ArcGIS

The ArcGIS software is commonly used in geoscience studies. In this study, by applying the *Conversion Tool* function in ArcGIS, the ASCII elevation data were converted to Raster image and then the measurement of each grid cell altitude can be manipulated individually. The dune height measurement is explained in next section 4.2.3.1.2.

4.2.3.1.2 Measurement of simulated dune morphology

In this study, the barchan dunes height/width/length, transverse ridges height and dune field pattern were measured. Transverse ridge width was not considered as they kept increasing by merging processes and would eventually become as wide as the modelled domain width by the end. In addition, there are few field studies describing the relationship between transverse ridge width with other dune field morphologic and dynamics and, therefore, whatever the results obtained from simulation could not be easily compared with field data (see Chapter 2 section 2.2.2.1.2).

1) Barchan dune height

Barchan dune height was measured from the DEM data of the simulation result. It is the distance between the dune crest and the base level. The crest point usually located in the centre of the dune, for example, it could be at the pixel C in Figure 4-4.

Sometimes this point was not the highest one, so the dune height was the average value of the pixels heights in the centre area. For example, in Figure 4-4, the height value at pixel A to D is 63.859425, 64.282669, 62.275402, and 66.289833, respectively, so that the average height value of these four pixels is 62.67140775, which was then taken as the height of this dune.

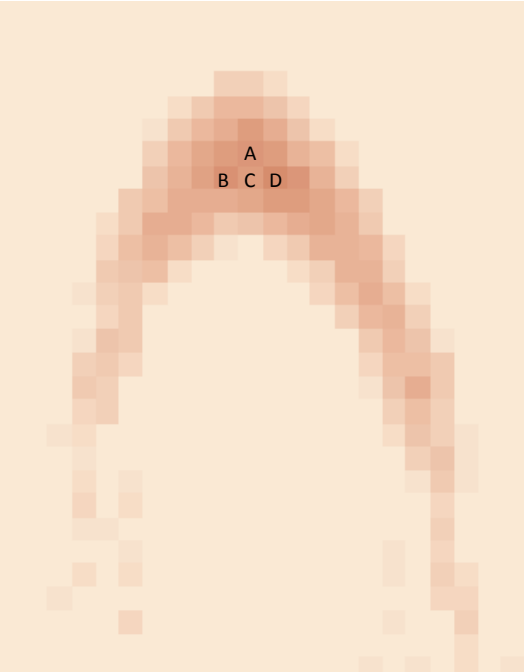

Figure 4-4 Barchan dune height measurement (image from simulation result of h_a=0.2, h_s=0.4, θ=10, d=100, P_d=80, t=1440)

2) Barchan dune length and width

Barchan dune width is defined as the largest distance between the dune horns; barchans length is the horizontal distance along the symmetry line from windward foot of the dune (the trailing edge) to the upper edge of the horns if the barchans are in symmetry condition or the average length in asymmetry condition (Figure 4-5).

The grid in the dune model is 300×100, while the image's pixels are 1500×500 which is 5 times larger than the grids in the model, so after measuring the length in *ImageJ*, the result number is the real pixels number of the image. Then in the model's DEM grid image, the length between dunes should be divided by 5, the result number is the grid cells between dunes. By processing in *ImageJ*, the width and length of the rectangle

that enclosing each dune can be obtained and the values are equal to the width and length of each dune.

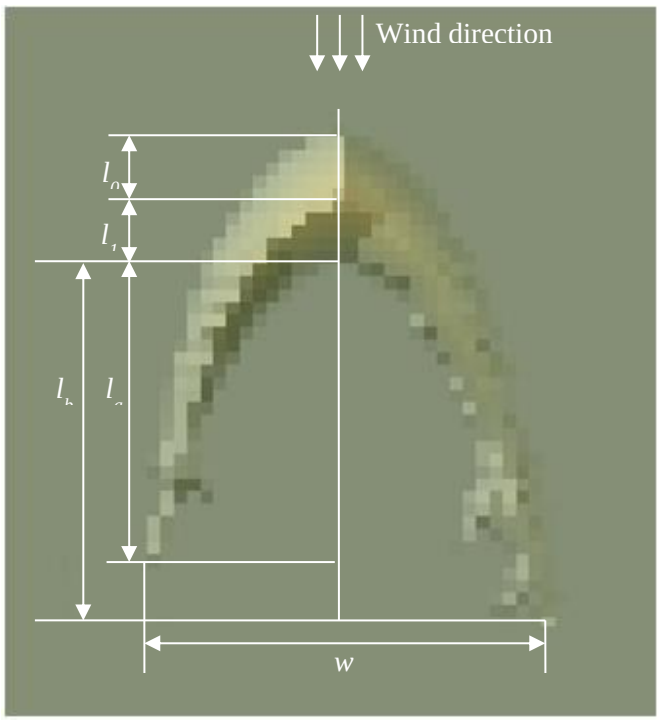

Figure 4-5 Measurement of Barchan dune parameters in model.

3) Transverse ridges height

The transverse ridges are the compound of several barchan dunes coalesced so they may have several crests with different elevations. Therefore, an average value of the elevation of all crests along the main transverse crest line was taken as the ridge height and the crest lines were visually identified on the images and traced manually, as illustrated in Figure 4-6.

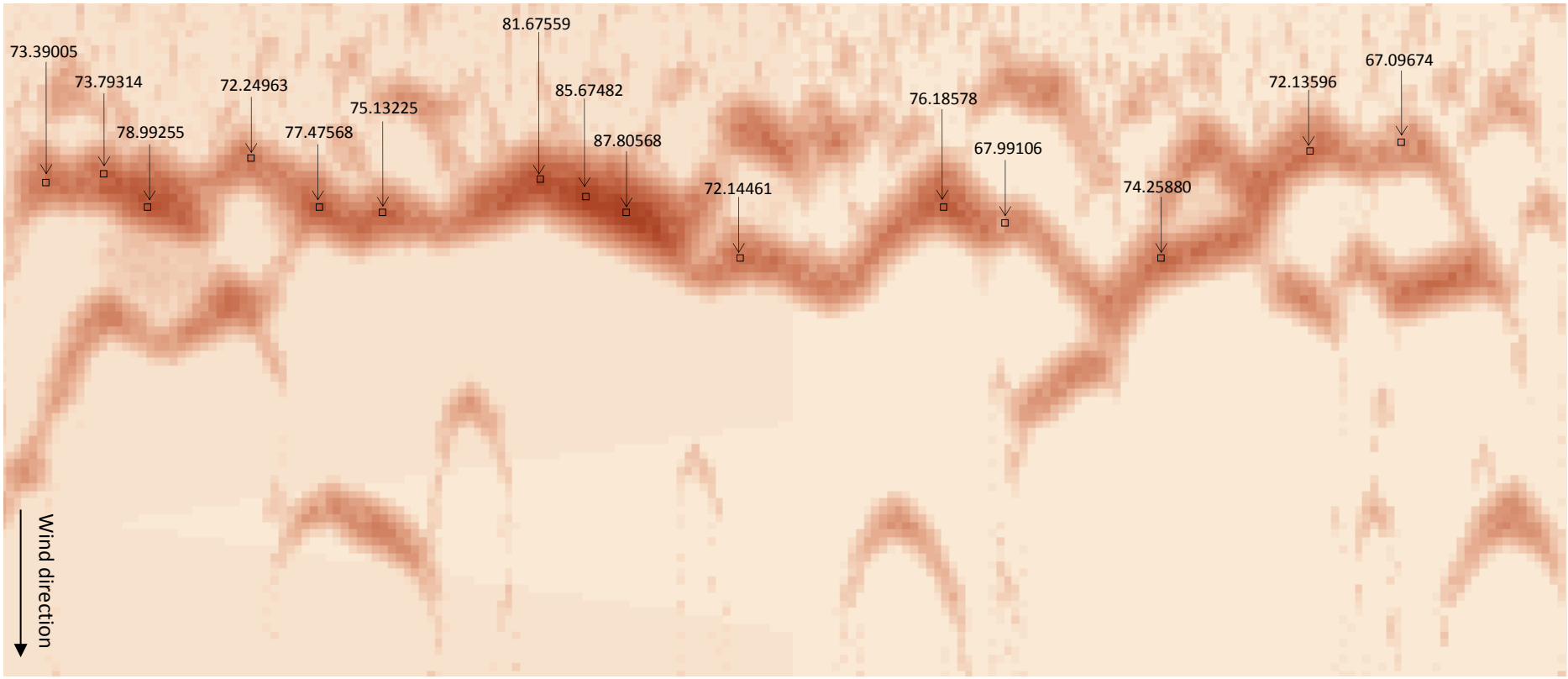

Figure 4-6 Illustration of the measurement of average height of transverse ridge (image from simulation result of h_a=0.2, h_s=0.4, θ=10, d=100, P_d=80, t=1440min).

4) Spatial patterns in dune fields

The spatial pattern of dune field was quantified by two variables, one is the longitudinal distance between dunes and another is the field density as introduced in Chapter 2 section 2.2.3.

a) Longitudinal distance

In this study, the *Longitudinal distance* method, as introduced in Chapter 2 section 2.2.3.2.1 was selected to characterise the dune field due to two reasons. First, the simulated dune field in this study present a crescentic dune field pattern which contains barchans, transverse ridges or combined dunes where the longitudinal distance could be more representative than a combined dune field spacing. Second, it helped to reduce the very heavy workload of processing images. To be more practical, the longitudinal distance between crests, as introduced in the literature review, are replaced by the longitudinal distance between the upper left corner of the rectangle that enclosing each dunes, which can be directly obtained from image processing. In relation to transverse ridges, the crest line were manually traced and then the dune spacing were measured (Figure 4-7).

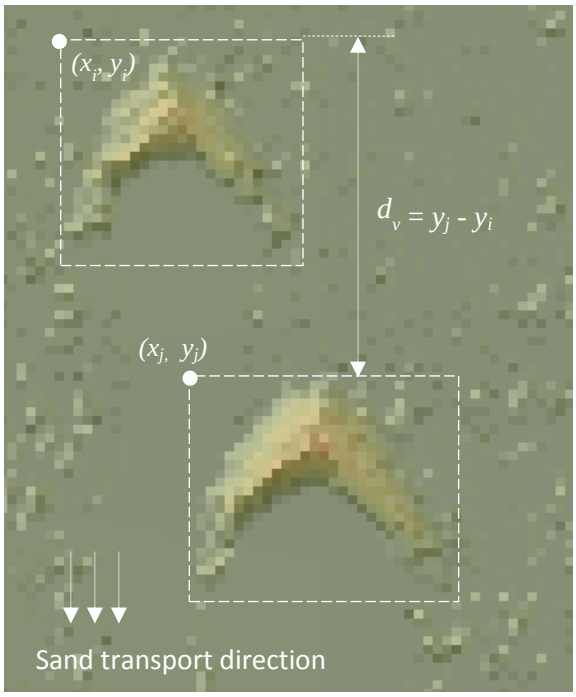

Figure 4-7 Measurement of Barchan dunes spacing pattern in the model (image from simulation result of h_a=0.2, h_s=0.5, θ=10, d=60, P_d=80, t=48000)

Thus, the longitudinal distance between a barchan (x_i, y_i) and its most close barchan in downwind direction (x_j, y_j) can be calculated by:

$$d_v = y_j - y_i \tag{4.1}$$

b) Dune field density

From Equation (2.4), the dune field density can be calculated. This output variable could be used to explore the relationship with input parameters h_s, D_p, d, t.

4.2.3.2 Dune field dynamics

As discussed in Chapter 2 section 2.2.4.1, the aeolian sediment state can be quantified by *sediment supply*, *sediment availability* and the *sand transport* capacity of the wind. However, in the model ALL sand in a slab can be moved if a slab is chosen, so the sediment supply is equal to the sediment availability. The principal limit on sand supply is the amount input, therefore sediment input = sediment supply = sediment availability. Therefore, we calculated the sand input/output rate and the sand transport rate in the model to examine the simulated field dynamics.

4.2.3.2.1 Total aeolian sand input

In these simulations the sediment supply is equal to the sediment input at the upwind edge of the modelled domain. Therefore, the total aeolian sand input volume per iteration via the upwind edge is defined as:

$$Q_{ia} = h_a \times g^2 \times n \tag{4.2}$$

here the h_a is the height of the added slab in each iteration, g is the grid cell size and n is the number of deposition cells along the upwind border and lateral axes of the model space.

The total aeolian sand input rate R_{ia} ($m^3\ m^{-1}\ yr^{-1}$) can be calculated by equation (4.3):

$$R_{ia} = \frac{Sediment\ input\ volume}{per\ width\ per\ unit\ time} = \frac{h_a \times g^2 \times n}{g \times n \times \frac{t}{525600}} = \frac{525600 g h_a}{t} \quad (4.3)$$

here *t* is the dune call time step in minutes.

4.2.3.2.2 Aeolian sand output rate and sand transport rate

The total aeolian sand output volume (Q_{oa}) that leaves the downwind border of the simulated field was saved after each time interval during the simulation. The saving time interval was decided by the dune call time step (*t*) in each simulation test. Hence, the sand output rate R_{oa} ($m^3\ m^{-1}\ yr^{-1}$) from aeolian process can be calculated as:

$$R_{oa} = \frac{\frac{Q_{oa}}{g \times n}}{\frac{t}{525600}} = \frac{525600 Q_{oa}}{ngt} \quad (4.4)$$

On a perfect flat surface, the potential sand transport is defined by:

$$R_p = \frac{P_e \times \frac{h_t}{g} \times l}{P_d \times I} \quad (4.5)$$

Where the P_e is the pre-defined probability of erosion probability (default value is 1.0), $\frac{h_t}{g}$ is the slab height ratio and I is the length of time represented by one iteration (Nield and Baas, 2008; Eastwood et al., 2011).

However, sand slabs will not move on a perfect flat surface throughout of the simulation. To obtain a more practical measure of sand transport rate in this simulated field study, the real sand transport rate (R_s) is defined by:

$$Real\ sediment\ transport\ rate = \frac{sediment\ transport\ volume}{sediment\ transport\ time} \quad (4.6)$$

The sand transport volume is measured from the approximate sand output along the downwind border of the dune field, as illustrated in Figure 4-2, and the sand transport time equals to the data saving interval time.

4.2.3.2.3 Measurement of simulated dune migration rate

The measurement method to calculate dune migration distance was as same as used in measuring the longitudinal spacing in dune field (section 4.2.3.1.2.4). However, tracking the migration of dunes is still difficult because dunes may coalesce or split and new dunes may develop over time. Therefore only dunes that were readily traceable in the output images were measured. Dune migration distance was measured by Equation (2.7) as below:

$$D = y_i' - y_i \tag{4.7}$$

Here y_i is the dune vertical location before the movement and y_i' is the dune vertical location after the movement. Thus the dune migration rate can be gained by:

$$r_d = \frac{D}{\Delta T} \tag{4.8}$$

Where ΔT is the time length during the dune migration from location y_i to y_i'.

4.3 DECAL model sensitivity analysis

Because the dune model is stochastic (the model cells will never be polled in exactly the same order or transported exactly the same distance) every repeat model simulation will be different even when run with identical parameters. However, the general characteristics of dunes created are reproducible. By exploring the relationships of morphologic and dynamic parameters of simulated dunes, it enables the characteristics of the complete dune system to be examined using a few output variables. Scatterplot and regression analysis were applied to explore the input parameters sensitivity and relationships with some representative output variables. In total, 569 different simulations, with different combination of input parameter values, were carried out and analysed.

4.3.1 Simulated dune morphology

4.3.1.1 Simulated dune field pattern

The diversity of simulated patterns can be visually identified and divided into four categories according to the visual characteristics including dune morphology and field pattern: non-development (sand sheet), barchan, transverse ridges and superimposed pattern (Figure 4-8).

(a) Non-development (sand sheet)

(b) Barchan

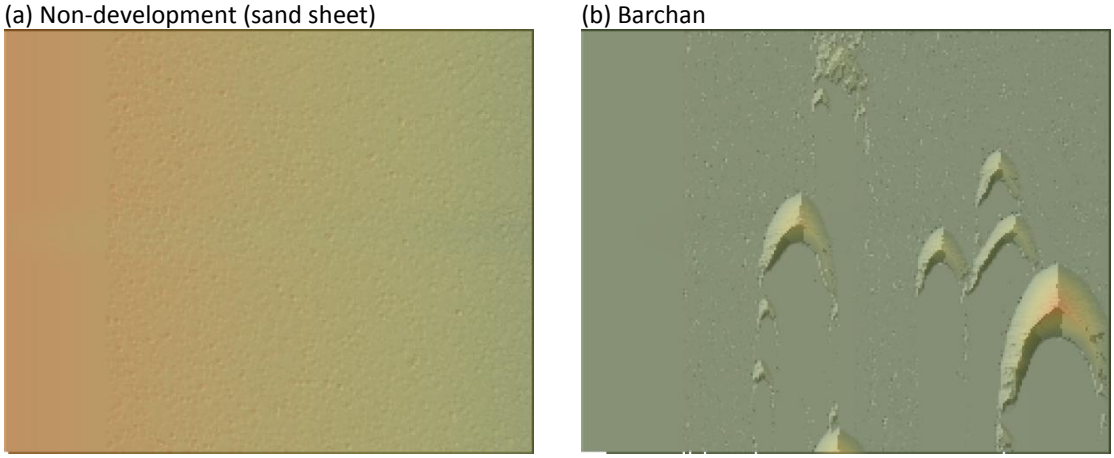

(c) Transverse ridges

(d) Superimposed

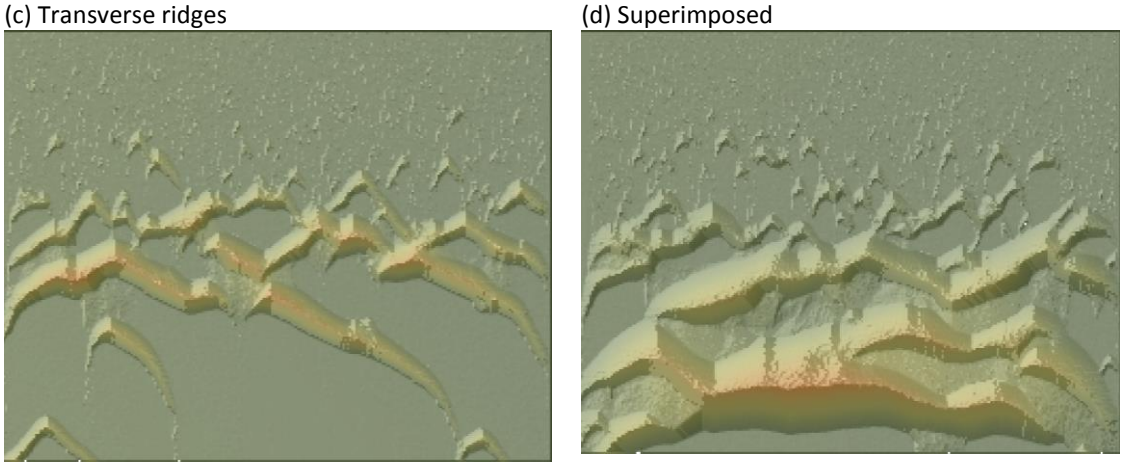

Figure 4-8 Simulated dune field patterns. Sand transport is from top to bottom in each image. (a) Non-developed field (sand sheet); (b) Barchans; (c) Transverse ridges; (d) superimposed dunes.

Among all different simulated dune-field patterns, changes in barchan dunes and transverse ridges are readily traceable from the result images.

Under the static conditions of the system (flat topography, constant flow strength and direction), collisions mainly result in the formation of larger dunes by amalgamation. As a result, the size of barchan dunes is always increasing. Because of the dune-dune interaction with collisions, merging, lateral linking as well as repulsion, the dune field

will develop in stages with different field patterns until ultimately mega ridges form. However, transverse ridge morphology was not analysed as one of output variables to test the model in this study. Most research interest on morphologic characteristics of transverse ridges is mainly focused on the ridge defects and dune spacing, but these two characteristics were not significant features exhibited in the model because of the limited field space (3000m×2000m) compared to the size of well-formed ridges that can be formed as wide as simulation space (Wilson, 1972; Lancaster, 1995; Ewing et al., 2006; Livingstone et al., 2007; Goudie, 2013). Therefore, only the morphometric parameters of single barchan dunes were analysed.

4.3.1.2 Morphometric relationships of simulated barchan dunes

At different time points and for the different movement rates (h_a, h_s , P_d, t), barchan height, length, width and migration rate were measured to test the dune model. Although there are over 569 simulation results, not all of them can be used for analysis in terms of different factors. For example, the dune width/length and field density can be readily obtained or indirectly calculated from the *ImageJ* results, so there are more data for these factors. Whereas, dune height was manually measured in *ArcGIS*, therefore only very well-formed single dune were selected and subsequently there is less data. In terms of dune migration distance, the dunes that can be measured should be not only clearly identifiable but also in the field before and after the movement which further reduced the numbers of available samples.

1) Dune width and height

A general relationship between dune width and height was derived from 193 simulation examples (Figure 4-9). Excluding the four samples that are outliers from the main samples, the equation in Figure 4-10 shows that there is a linear relationship between the simulated dune width and height, which is consistent to other researcher's field works as reviewed in Chapter 2 (section 1)) (Hesp and Hastings, 1998; Wang et al., 2007).

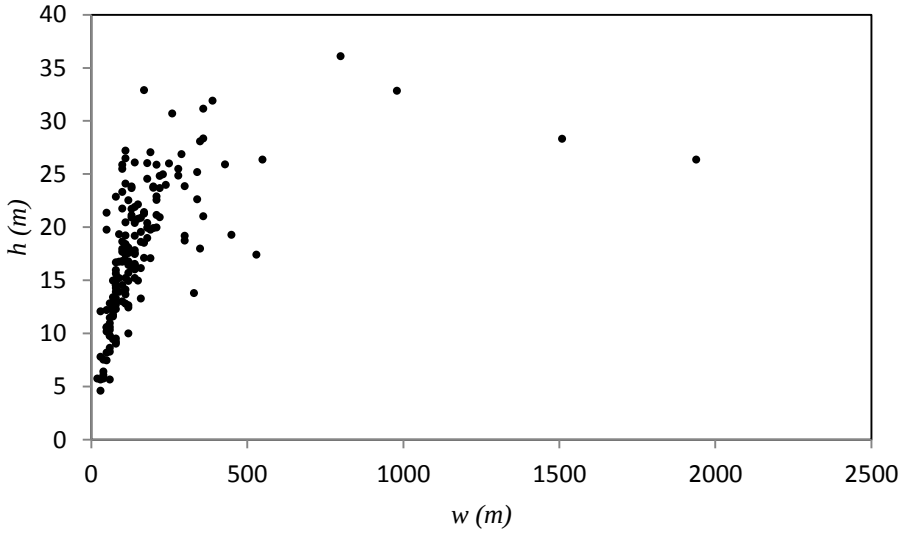

Figure 4-9 Relationship between dune height and width in the simulated field (193 samples).

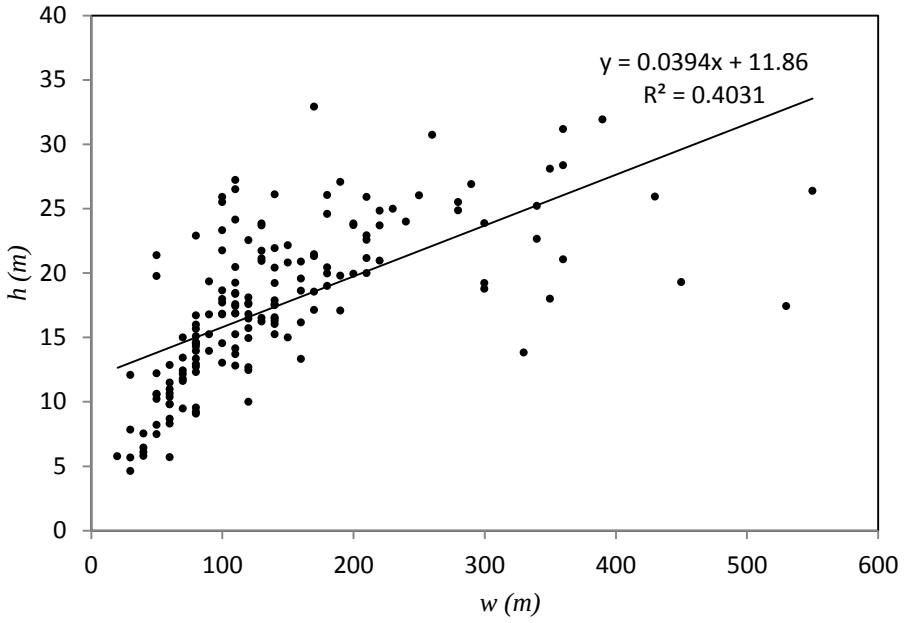

Figure 4-10 Relationship between dune height and width in the model (exclude four samples included in Figure 4-9).

2) Dune length and height

After exploring 193 samples, a proportional linear relationship of barchan dune length and height is demonstrated and is also consistent with some previous field research as discussed in Chapter 2 (Sauermann et al., 2000).

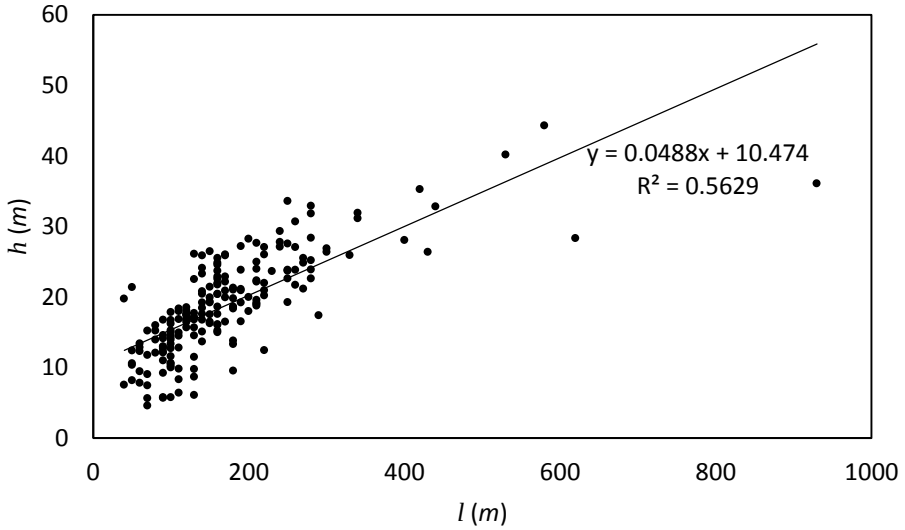

Figure 4-11 Relationship of simulated dune length and height (193 samples).

3) Dune width and length

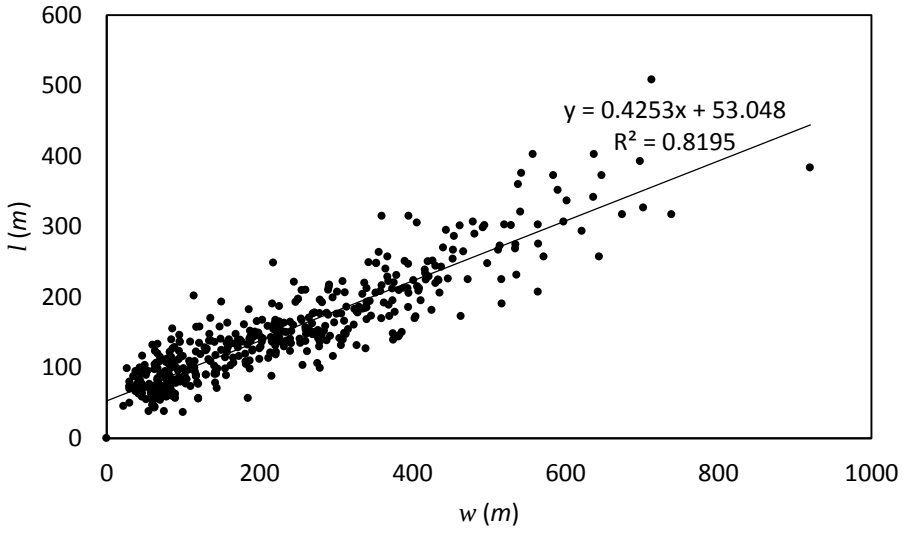

Figure 4-12 Relationship of dune width and length (449 samples).

A good linear relationship has been found between simulated dune width and length which is consistent with previous field data (Hersen et al., 2002).

4) Dune field density

In this study, the dune field density was calculated by the Equation 2.7 (in chapter2, dune number/dune area). To find out whether the dune field density is in related to other dune properties, 407 simulation results were analysed. However, the samples

were all restricted to the image saved at one time point (5-years simulation time) to prevent the dunes growing too large and forming a single large dune.

After plotting the dune field density η against the average dune width w of each sample, no significant relationship has been found, and there is a general limiting trend of lower dune field density as the dune height increases, which means the dune field density will decrease with time (Figure 4-13). However, field data are needed to support the results found in this model investigation.

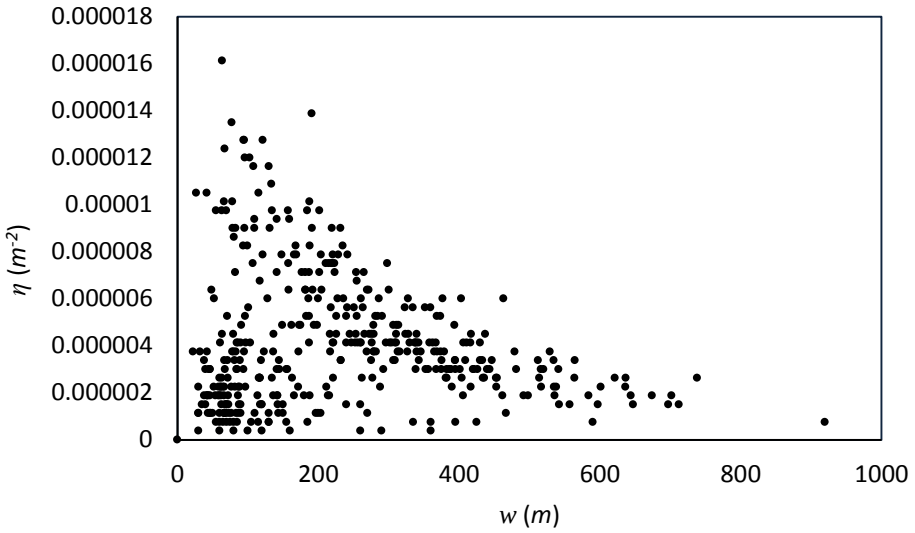

Figure 4-13 Dune field density against dune width (407 samples).

4.3.2 Simulated dune field dynamics

Dune mobility is the most striking property of crescentic dues and this has been studied extensively, Barchans are typically one of the most dangerous of dune types because of their ability to move fast (Cooke et al., 1993). Dune movement can lead to infilling of canals and rivers, overwhelming of vegetation and threatening settlements, which inevitably results in profound changes on local and regional environment. Therefore, it is an important output variable studied in this research. As discussed in Chapter 2, a significant feature of dune movement is its size dependency. The larger the dune the slower the dune movement speed.

236 simulation results were processed to obtain the sample group of dune height and corresponding dune migration rate. As these samples were generated using different input parameters, average dune heights and corresponding migration rates were

calculated using the same value of input parameters h_a, h_s, θ, d, P_d and t, respectively. The relationship between the average dune migration rate and dune height is presented in Figure 4-14. Although some researchers argued that the dune migration rate r_d is more proportional to log h rather than to the liner regression to $1/h$ (Momiji and Warren, 2000), there are very slightly differences between these two regression method as explored in Figure 4-14 and both showed very positive intercept that the dune migration rate r_d decreases monotonically as dune height h increases. This result is consistent with previous field observation (Wilson, 1972). The dune migration rate as a function of dune height in the dune model thus was obtained as below:

$$r_d = 134.46\frac{1}{h} - 3.8116 \tag{4.9}$$

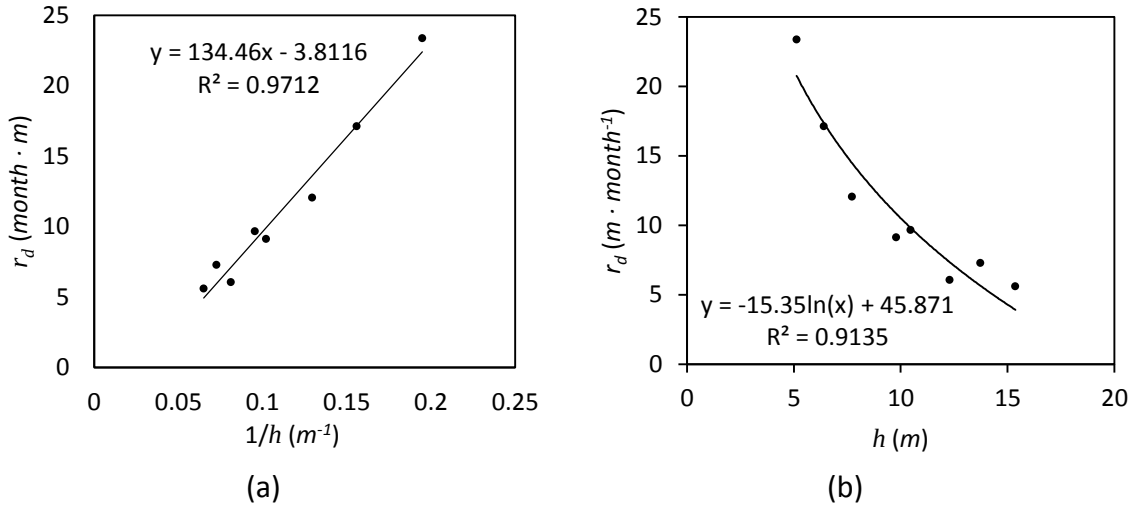

Figure 4-14 Relationship between average dune migration rate and dune height (236 samples): (a) Average dune migration rate against inverse of average dune height; (b) Average dune migration rate against average dune height

Although the dune migration rate can also be measured from the sand transport rate and dune height (Equation (2.6)), there was no relationship have been found between the sand transport rate with any dune morphologic properties. The controlling factors on sand transport rate in model were further explored in section 4.3.3 below.

4.3.3 The effect of model parameters on dune shape and dynamics

The results from sections 4.3.1 and 4.3.2 showed that the simulated dune height/width/length/migration rate can be dependent upon each other, which is consistent with field observation, although the field density could not be expressed by

other dune properties as it is decreases with increasing simulation time. These simulation results are consistent with previous field studies in the height, area and volume of barchans dunes as well as the migration rate which are well characterised by their width *w* solely (Durán *et al.*, 2011). Thus the response from any of these four output variables to input parameters should be considered with regard to the sensitivity of input parameters.

4.3.3.1 Slab added depth (h_a), slab thicknes (h_s) and deposition probability (P_d)

When only considering the single influence of slab added depth ($\boldsymbol{h_a}$) on dune morphology, available samples were limited by the value of slab thickness ($\boldsymbol{h_s}$). Even so, by exploring the limited samples, it is found that the higher the $\boldsymbol{h_a}$ value the higher the dune height so that the dune height is very sensitive to the change of value $\boldsymbol{h_a}$ (Figure 4-15a).

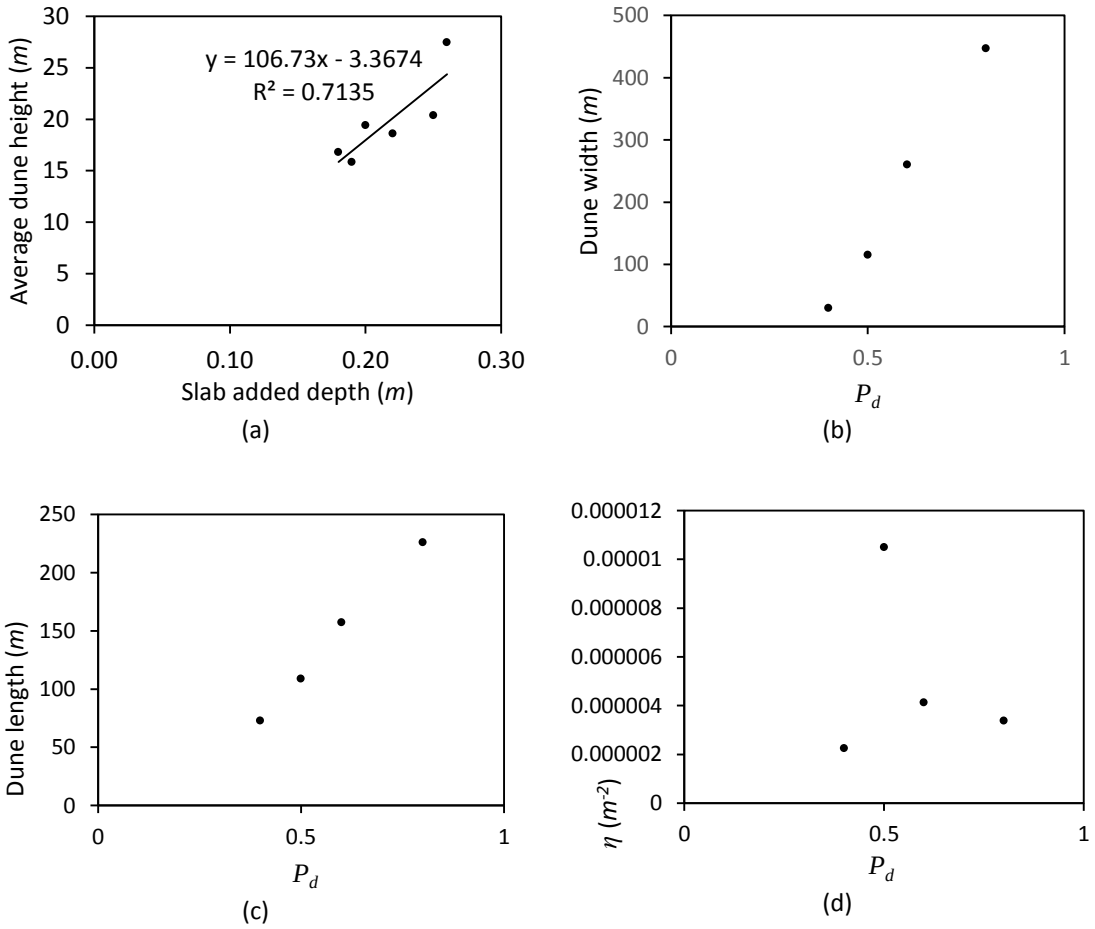

Figure 4-15 Single influence of h_a and P_d on dune morphometry: (a) h_a against h (h_s=0.6, θ=10, d=100, P_d=80, t=1440); (b) P_d against w; (c) P_d against l; (d) P_d against η. (Chart b, c and d are explored after simulation h_a =0.3, h_s=0.6, θ=10, d=100, t=1440)

The single influence of $\boldsymbol{h_s}$ could not be analysed as the $\boldsymbol{h_a}$ value is changing with value of $\boldsymbol{h_s}$ that there are not enough samples available. Likewise to the deposition probability ($\boldsymbol{P_d}$) that the value range of $\boldsymbol{h_a}$ and $\boldsymbol{h_s}$ changed correspondingly to value of $\boldsymbol{P_d}$. A simple scatterplot of $\boldsymbol{P_d}$ against dune width w, length l and field density η were explored with only four samples available (Figure 4-15b, c, d). The results showed that with a certain value of $\boldsymbol{P_d}$, there is a proportional relationships between $\boldsymbol{P_d}$ with dune width w and length l. However, the influence of $\boldsymbol{P_d}$ on dune density can not be identified or have no significant influence on dune field density.

This preliminary exploration of single influence from h_a, h_s and P_d indicates the correlation between the three parameters need to be tested furthermore. A further 535 simulations, therefore, were conducted as designed in Table 4-3. The various range of h_a and h_s under various P_d value thus can be observed from Figure 4-16.

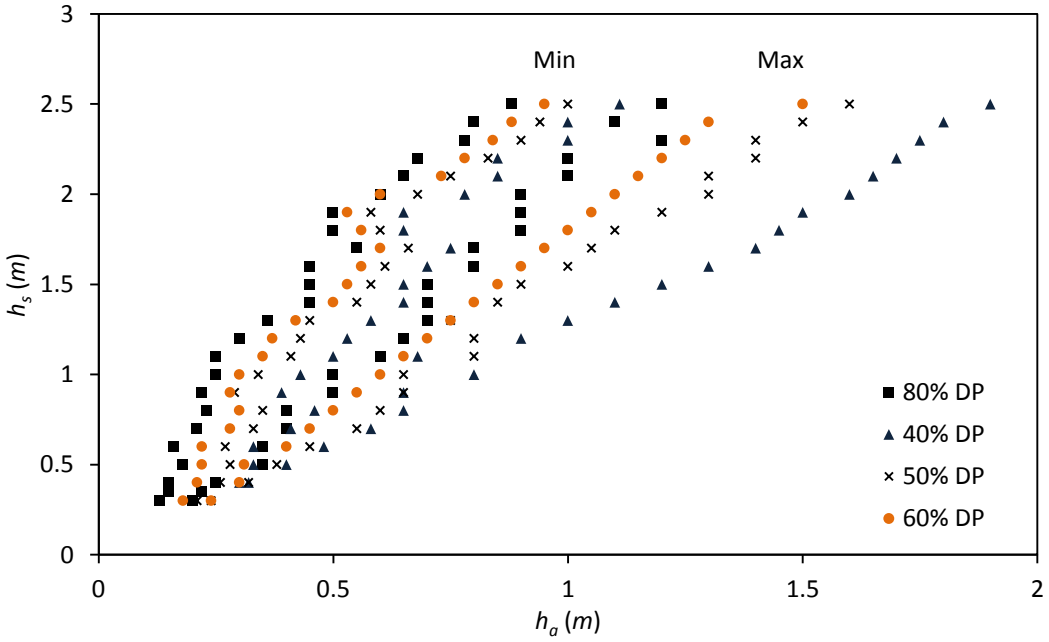

Figure 4-16 Relation between slab added depth and slab thickness when dunes develop under different deposition probability (P_d)

The lines on the left/right side in the chart above showed the minimum/maximum value of h_a and h_s with various deposition probability. The value of h_a is strongly associated with value of h_s. In general, with any value of deposition probability, the h_a is in range between 40-60% of corresponding h_s which is ranged in between [0.3, 2.4] when well-defined dune field with most of the size and density could be well developed. With certain value of h_s, the higher h_a the larger the size of dunes. The

optimal range of h_s is in between [0.3, 1.0] and P_d in between [30, 80], the higher the value of h_a and h_s and P_d, the more possible to form large size dunes and sparse field.

4.3.3.2 Shadow angle θ

A series of simulations were carried out under a range of shadow angle θ value [1, 15] while remain the other parameters the same. It was found that the sand started to accumulate at the upwind edge of the field with θ value in [1, 3] and no dunes were formed with θ value in [14, 15] but only formed well-defined dunes when the shadow angle range between [5, 11] (Figure 4-13). When increasing the θ, there are slight changes in dune height and spacing but these are not great enough to suggest that there is an important influence from θ on dune field development. Therefore, the model output is not sensitive to the change of shadow angle.

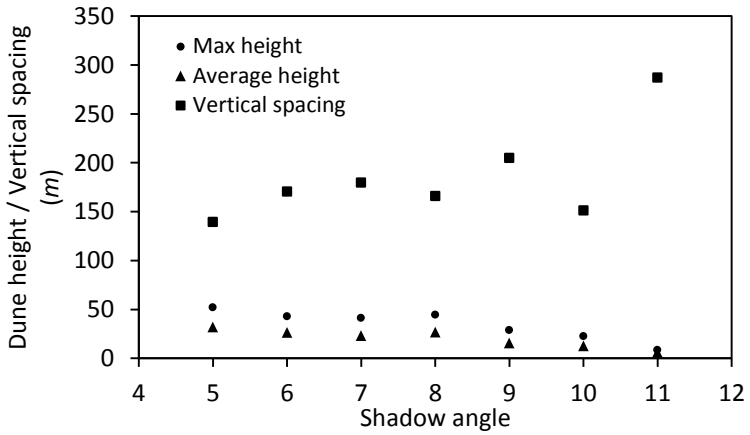

Figure 4-17 Dune pattern change with shadow angle (h_a =0.2, h_s=0.5, d=100, P_d=80, t=1440).

4.3.3.3 Check distance d

Simulations were carried out with the check distance d value between 5 and 103, however, only within value of [10, 103] dunes were formed. Therefore, d clearly has no influence on the dune field development speed (Figure 4-18(a)) and an identifiable influence on dune height and field longitudinal spacing (Figure 4-18(b)). In other words, the model output is not sensitive to the effective value of shadow check distance d.

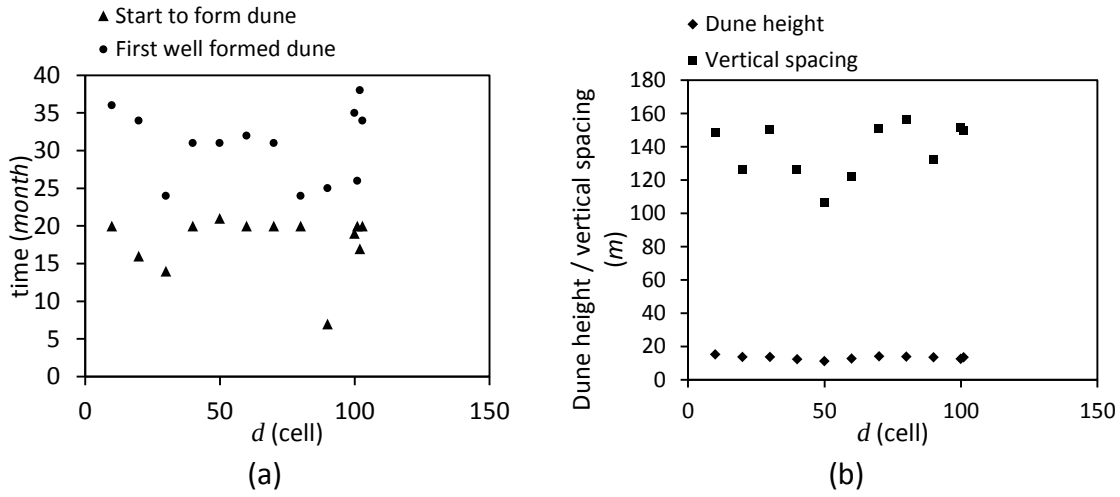

Figure 4-18 Dune formation with various model check distance d value: (a) Influence on dune formation speed; (b) Influence on dune height and field longitudinal spacing at time point 10-yr (h_a =0.2, h_s=0.5, θ =10, P_d=80, t=1440).

4.3.3.4 Dune recall time step t

As observed in the field studies, the formation of dunes are influenced mainly by the sediment supply, sediment availability and sediment transport capability. With the same amount of slabs added into the field per unit time (equal to same sediment input amount Q_{ia}, the sediment output Q_{oa} and transport volume would remain the same, thus the longer the dune recall time step (the unit time) the lower the sediment input rate R_{ia} as well as the sediment transport rate R_s in modelled field when all the other conditions were remained the same. In fact, based on the Equation (2.4), (4.4) and (4.6), the R_{ia}, R_{oa} and R_s would all decrease linearly with increasing time step t. It was found that the t value greatly influenced the dune field formation speed that the longer the t value, the slower the dunes can be developed (Figure 4-19).

Furthermore, the dune field development in all simulations exhibit similar trends that no matter what the t value was. The dune field would always start from a sparse field with similar small size barchans to a field with larger size barchans, then a field with mixed barchans and transverse ridges until, finally, large ridges dominated the field such that single barchans were only be observed at the upwind edge of the field. This shows the influence of t on dune morphology.

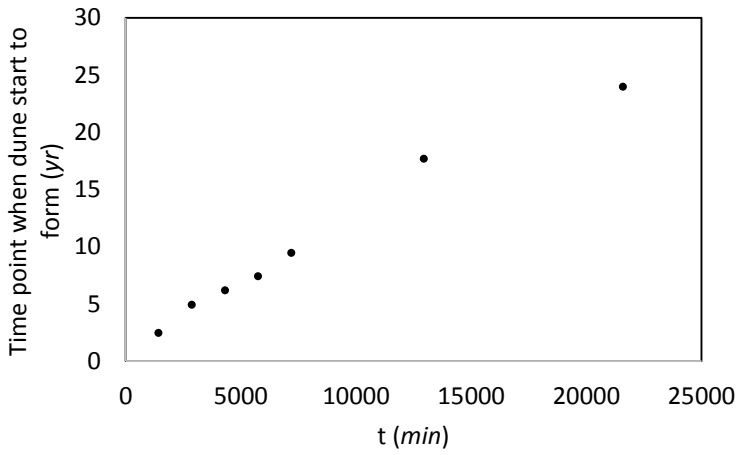

Figure 4-19 The simulated time point when the first indefinable dune was observed with regard to various dune recall time step (h_a =0.32, h_s=0.5, θ =10, d=60, P_d=65).

Above all, the sand transport rate in the model is very sensitive to the change of t value which means by changing the t it is very easily to set up a field that can satisfy the application demand of certain dynamic conditions.

4.3.4 DECAL model discussion

So far, this chapter has shown that the dune model can simulate the formation of crescentic dunes, with relationships between dune morphometric parameters and dune dynamics that are commensurate to those observed in nature. The dune model is more sensitive to the parameters h_a, h_s, t and less influenced by the θ, d, P_d. An important result is that by changing h_a and h_s, different sizes of dunes can be obtained and by changing t the dune formation and movement speed can be adjusted. By being able to adjust the movement speed and the size of the dune, this means we are capable of simulating a wide range of dune sizes *and* sand transport rates. In short, this gives us full control on what size dunes we have, how fast they move and how much sand is moved over modelled time.

However, there is a fundamental weakness in the DECAL model. Over time, with a steady sediment feed, dunes become bigger, slower, coalesce and may merge into one huge dune. From Figure 4-20, it can be observed that the height of dunes increases proportionally with simulation time, while the movement speed decreases inversely with time, and different model parameter combinations have different ratio of dune height and migration rate against simulation time. Furthermore, this is also reflected in space –as towards the base of the modelled domain the larger, slower dunes tend to

form. This is why in Chapter 5, when we link the sand dune and fluvial model together, the river is introduced half way down the modelled domain, so we have some control over the size of the dunes where water and sand meet.

(a)

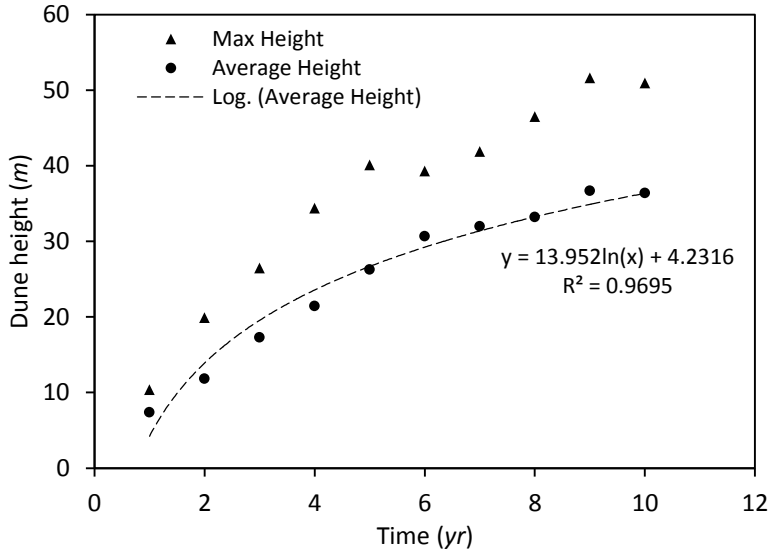

(b)

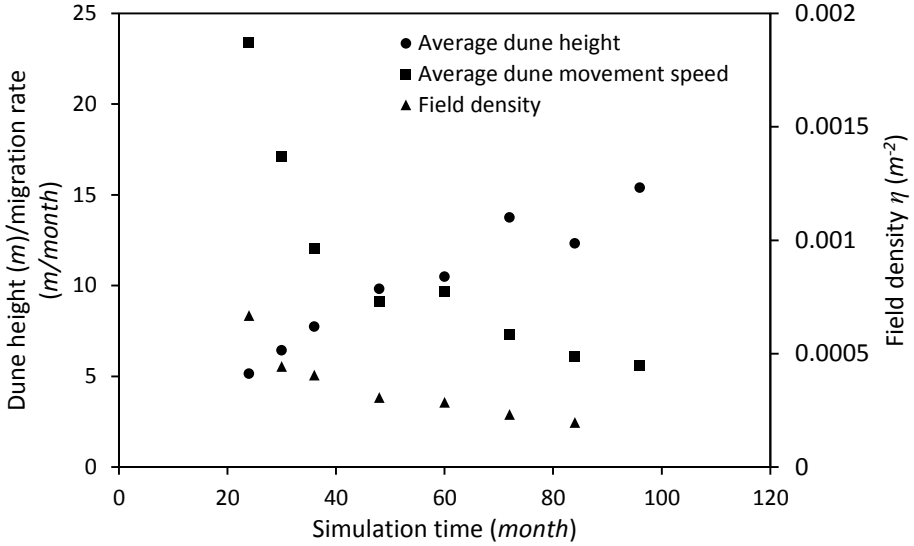

Figure 4-20 Change with simulation time: (a) Change of dune height (h_a =0.26, h_s=0.6, θ =10, d=100, P_d=80, t= 1440); (b) Change of dune height, migration rate and field density (h_a =0.15, h_s=0.3, θ =10, d=100, P_d=80, t= 1440).

4.4 Tuning/calibrating the DECAL model

The results discussed in section 4.3 show that combinations of dune size and migration rate can be obtained by adjusting the model parameters. This allows us to adjust the dune model to simulate a range of dune sizes and movement rates that have been observed in the field as described above.

To determine which parameters to use in future chapters and applications of the model in combination with the fluvial model, measurements of actual dunes was collected to establish real distributions of dune height, field density and dune dynamics. There are two sources of data: one is from the published data, the other is manually measured from satellite data identified previously in Chapter 3. The two sources of data may indicate some differences between the two types of field because: the remote sensed data is where the interaction occurs, whereas the data from literatures are mainly collected from area where aeolian processes are dominant.

The results from published data were listed in Appendix A, whilst the morphometrics of barchan dune fields which were identified in Chapter 3 were manually measured based on the Google Earth images and listed in Table 4-4. In Table 4-4, the dune width, length and space (horizontal and longitudinal) were measured manually from Google Earth, the barchans dune height were calculated by dune width based on the relationship that dune height is generally the 1/10 of dune width (Lancaster, 1995). The barchan field density is the number of dunes per unit surface (Elbelrhiti et al., 2008). The transverse ridges field identified in Chapter 3 were not analysed because of the difficulties in interpreting these data from Google Earth.

4.4.1 Sand dune morphometrics

4.4.1.1 Dune height

From the literature data (as listed in Appendix A), the real barchan heights varied from 0.3 to 55 metres (Figure 4-21c) with median barchan height 13.5 m - which is reasonable compared to Lancaster's (1995) work. However, this result can only give us a general concept of barchan dune height distribution from published research and may not necessarily be the representative value of barchan height distribution in real world as the data sample here is too small to represent the whole population.

The histogram of all mean barchan height values from published data (n=176) shows a skewed distribution with a mean value of 17 m (Figure 4-21(a)), whilst the mean value of transverse ridges height is 31 m (Figure 4-21 (b)).

(a)

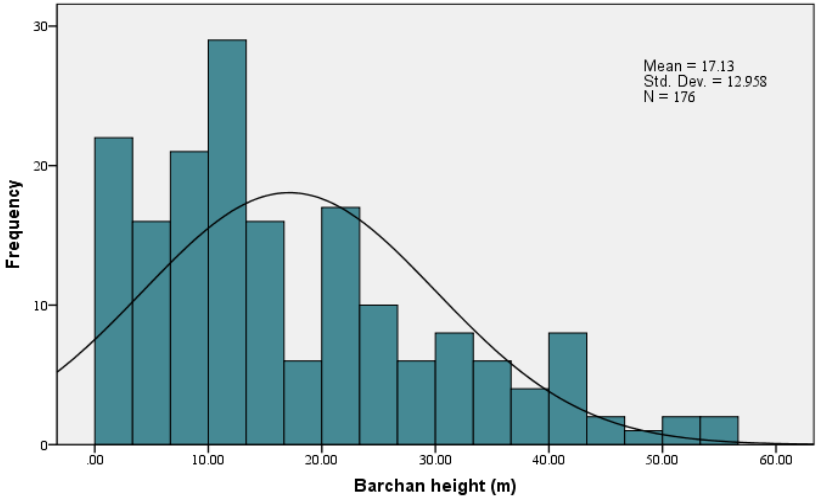

(b)

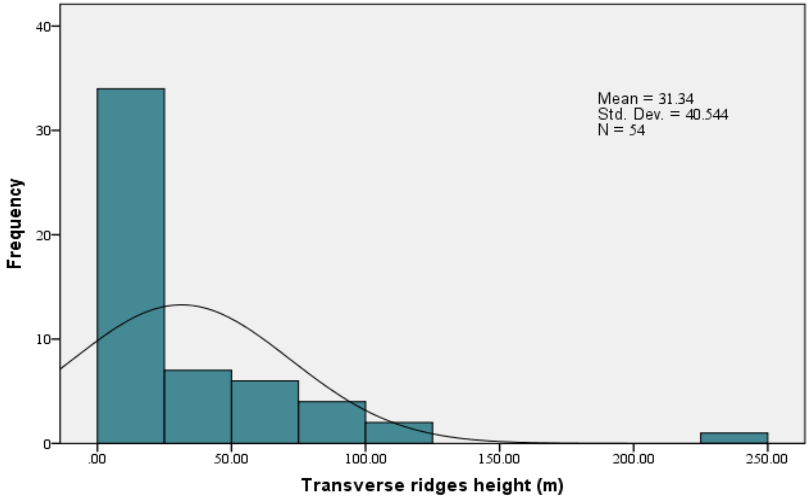

(c)

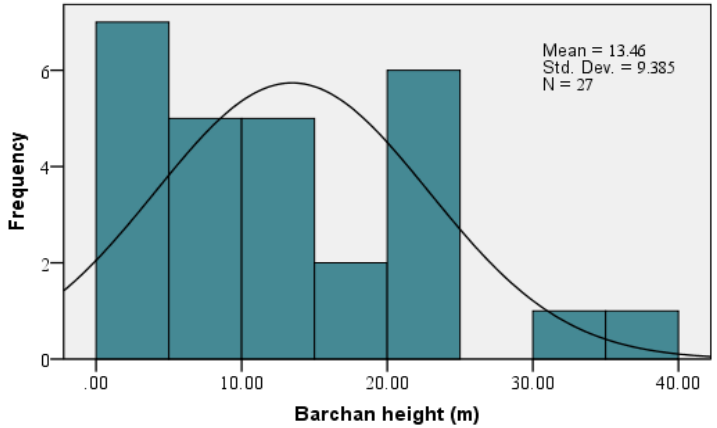

Figure 4-21 Observed dune height distributions: (a) Height of Barchans in non-specific fluvial-aeolian interacting area (data from literature, Appendix A); (b) Height of Transverse ridges from non-specific fluvial-aeolian interacting area (data from literature, Appendix A); (c) Barchans height in fluvial-aeolian interacting field (field observation, Table 4-4).

The height of barchan dunes in fluvial-aeolian interacting fields were measured from the elevation data on Google Earth and the results explored in Figure 4-21(c) shows a mean value of about 13 m and two modes of (1, 5] and (20, 25].Although the distribution of barchan heights in fluvial-aeolian environments is based on a small sample size with unavoidable measurement errors, the data indicates the samples are consistent with a normal distribution. In this study, the simulated dune heights conform to the reasonable range of dune heights found in existing dune systems, where heights ranging from 1 to 50 meters have been observed (Figure 4-21).

4.4.1.2 Dune field density

The dune field density obtained from the manual measurements were analysed using the same measurement method used for determining dune density from the model simulations. A difference was that measuring the longitudinal distance in the field was carried out by measuring the longitudinal distance between the dune crests instead of the distance between the upper left corner of the rectangle enclosing each dune in the simulation (Figure 4-22(a)).

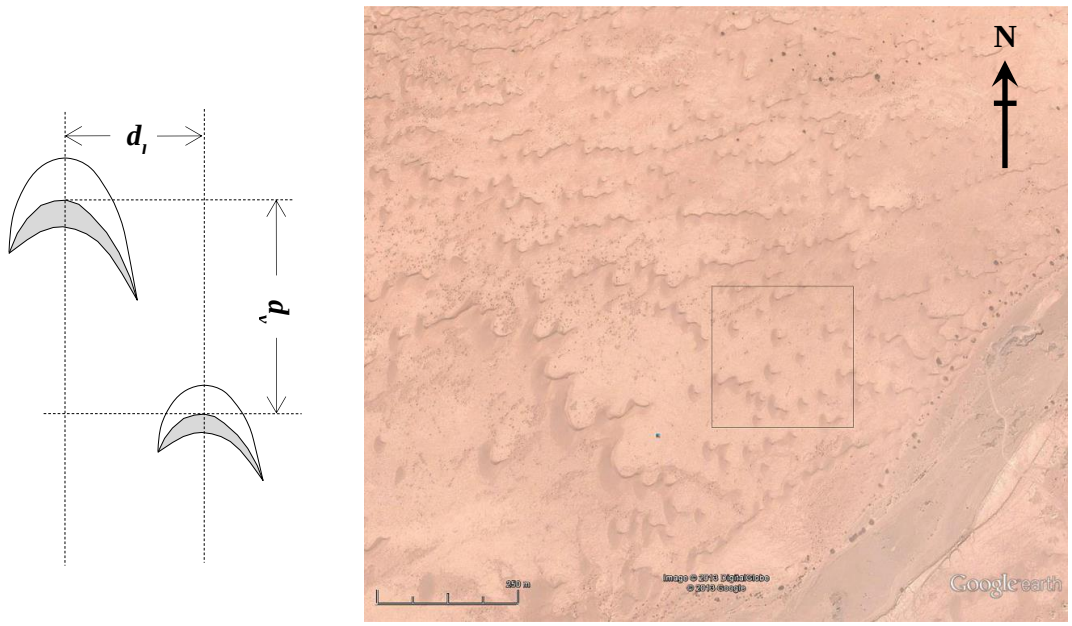

(a) (b)

Figure 4-22 Illustration of the longitudinal distance measurement in the fluvial-aeolian interacting field: (a) longitudinal distance between dunes; (b) field density.

Barchan field density was calculated by Equation (2.4) as introduced in Chapter 2. The dune density measurement on images from Google maps is illustrated in Figure 4-22(b). The image is of the second location listed in Table 4-4, the map scale is 1:250, one 250 *m* ×250 *m* square was selected in the dune field randomly, and the numbers of dunes in the selected square are counted as 20. Thus the density of this dune field is

$$\frac{20}{0.25 \times 0.25} = 320\ km^{-2}$$

Hence, field information at 27 locations were analysed and listed in the table below:

Table 4-4 Measurement result from real fluvial-aeolian interacting field

No.	Main dune (Barchans)						Sub-Dune (Transverse)		
	Width (*m*)	Length (*m*)	Height (*m*)	Horizontal Space (*m*)	Longitudinal Space (*m*)	Density (km^{-2})	Width (*m*)	Height (*m*)	Space (*m*)
1	46.88	45.59	4.69	26.72	34.27	436.65			
2	36.62	38.09	3.66	35.82	60.41	320.00	280.10		46.11
3	49.89	67.21	4.99	32.14	54.95	833.30			
4	27.88	34.18	2.79	17.58	43.05	546.88			
5	126.16	141.49	12.62	100.56	232.41	19.29			
6	65.53	66.15	6.55	24.62	95.92	145.93			
7	226.53	222.03	22.65	105.34	164.61	33.28			
8	232.05	291.97	23.21	145.07	610.48	9.67			
9	204.67	246.92	20.47	73.62	362.44	33.49	1159.68		285.42
10	118.60	107.50	11.86	59.93	163.35	65.68	363.34		103.90
11	64.25	73.53	6.42	43.19	102.84	291.90			
12	63.79	79.58	6.38	44.71	115.51	153.52	495.13		99.40
13	124.88	105.95	12.49	66.63	117.17	87.31			
14	152.10	199.26	15.21	83.54	261.52	26.96			
15	48.37	79.24	4.84	42.11	81.37	160.23			
16	137.03	140.44	13.70	123.32	250.27	34.44			
17	216.52	272.44	21.65	150.61	311.54	8.13			
18	177.90	194.43	17.79	184.19	395.92	6.79			
19	225.39	281.79	22.54	117.77	321.40	24.96	946.88		376.88
20	396.89	434.11	39.69	1067.25	1598.96	0.14			
21	132.95	130.58	13.30	101.71	229.57	23.35			
22	221.98	285.66	22.20	98.54	220.95	1.93			
23	52.44	67.75	5.24	29.55	67.81	59.00			
24	45.08	60.46	4.51	26.48	69.36	32.00			
25	306.41	333.30	30.64	304.07	274.29	4.70			
26	83.58	95.22	8.36	112.20	263.67	3.93			
27	49.56	59.73	4.96	1337.57	2156.29	10.84			

As it can be seen in Figure 4-23(a), a majority of the barchan dunes field density lies between 0 and 200 per km^2, and the distribution of this sub-sample were examined by histogram (Figure 4-23(b)).

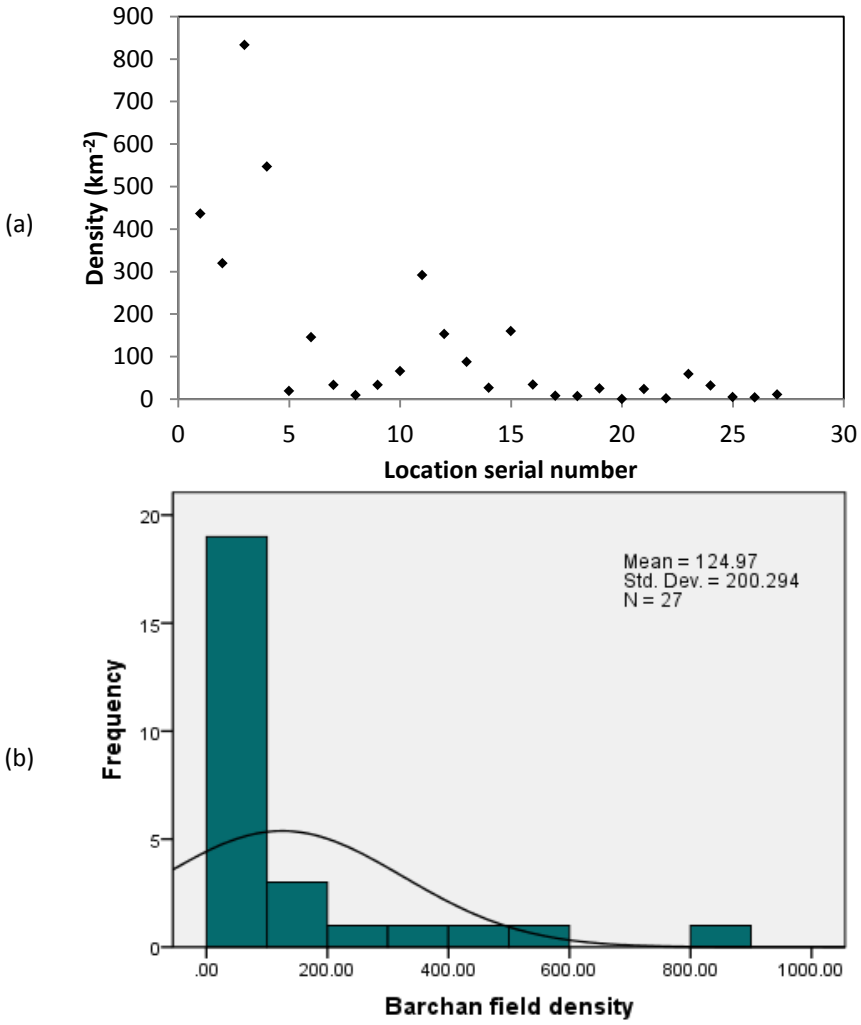

Figure 4-23 Barchan field density: (a) Field density at each location; (b) Histogram of field density distribution.

4.4.1.3 Dune field dynamics

The field sand transport rate varies considerably (Appendix A). For example, the barchans in Chad are considered by some researchers as the fastest barchans in world and the measured sand transport rate is around 76-99 $m^3m^{-1}yr^{-1}$ (Vermeesch and Drake, 2008). Though other researchers have found much higher sand transport rates, for example, the saturated sand transport rate on a 35m-high barchan dune near Jericoacoara in Braizil range between 0-0.035 $kg\ m^{-1}s^{-1}$ which equals to 669 $m^3m^{-1}yr^{-1}$ using an average bulk density 1650 $kg\ m^{-3}$ (Sauermann et al., 2003). In dune fields

intermixed with transverse ridges, the maximum sand transport rate would be even higher than those in uniform barchan fields because of the high sediment availability in compound dune fields (Navarro et al., 2011). Based on the information collected in Appendix A, the maximum value of sand transport rate could be set at about 600 $m^3m^{-1}yr^{-1}$ in model simulation.

The field dune migration rates are only available from published literature as these data cannot be extracted from Google maps. A mean r_d value of 19 $m\ yr^{-1}$ (*Standard Deviation*=35.79) was obtained for barchans dunes after Figure 4-24, and a mean r_d value of 12 $m\ yr^{-1}$ (*Standard Deviation*=15) for transverse ridges (Figure 4-25).

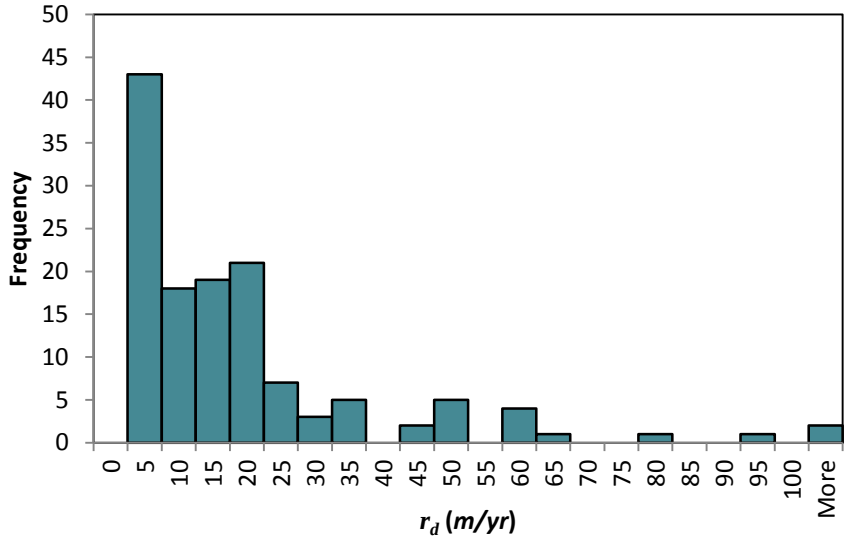

Figure 4-24 The distribution range of Barchans movement speed from different dune area.

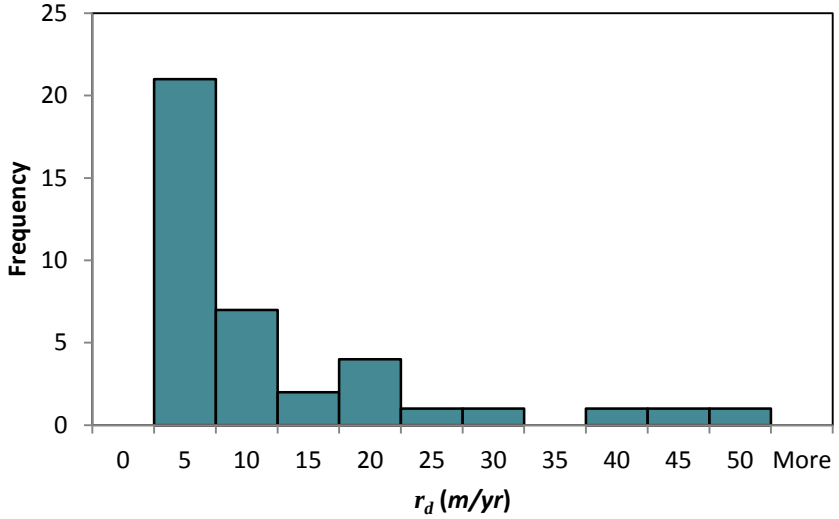

Figure 4-25 Histogram of crescentic ridges height in fields.

4.4.1.4 Translating field data into model parameters

Sections 4.4.1 showed that dunes of height between 0 and 30 *m*, dune density between 0 and 200 per km^2 and dune migration rate of 0 to 30 $m\ yr^{-1}$, were most frequent in the literature and field survey data. These values can be generated by parameter combination h_a =0.32, h_s=0.5, θ =10, d=60, P_d=65, t >11520. Therefore, they are selected to represent real dune field in subsequent studies. For integration with the fluvial model, we will keep parameters controlling the dune size the same, but alter *t* to change the sand transport rate. An example of this is shown in Table 4.5 where a simple exercise measuring sand leaving the end of the modelled domain, for different *t* values was carried out.

Table 4-5 Aeolian sand transport rate in model corresponding to varied model time step *t*.

No.	t (*min*)	R_s ($m^3 m^{-1} yr^{-1}$)
1	144	14351
2	720	2544
3	1440	1207
4	2880	573
5	10080	149
6	11520	129
7	12960	114
8	14400	102
9	15840	92
10	17280	84
11	18720	77

4.4.2 Conclusion

By testing the impact of all model parameters, the model was capable to reproduce the characteristics of dune morphology and dynamics. Three sensitive model parameters, including the model slab added depth (h_a), slab thickness (h_s) and the dune recall time step (t), as well as three less sensitive parameters, which are shadow angle (θ), shadow check distance (d) and deposition probability (P_d), were identified. Of the three sensitive parameters, h_a and h_s can affect the dune morphology whereas the t determines the field dynamics. By adjusting these three parameters, realistic states of dune/sand movement are able to be simulated and will be used to represent sand dune movement in subsequent chapters.

4.5 Integration of the DECAL and CAESAR-Lisflood model

4.5.1 The CAESAR-Lisflood morphodynamic model

The flow model that was applied to simulate the fluvial process in the interaction is a modified version of CAESAR-Lisflood computational landscape evolution model (Coulthard et al., 2013). This model was originally developed to examine the relative importance of climate and land cover change on catchment geomorphology and sediment discharge. It has been further developed by merging hydrological and hydraulic models to allow multiple grainsize erosion and deposition as well as slope process to occur on a sub-event time scale. Many independent field data in a range of river catchments and reaches have been taken in comparison with the model outputs. For example, the patterns of erosion, deposition and lacustrine deposition in Alpine environment (Welsh et al., 2009), the sediment yields and longer term lowering rates from Northern Australia (Hancock et al., 2010), a comparison to field plot experiments (Coulthard et al., 2012), simulating patterns of heavy contaminated sediment dispersal (Coulthard and Macklin, 2003) and modelling 9000 years of drainage basin evolution in the UK (Coulthard and Macklin, 2001).

The simulated domain in CAESAR-Lisflood model is represented by a regular grid of cells, thus the simulated landscape is developed when the cells elevations are changed according to the erosion and deposition from fluvial and slope processes. There are two modes in the model: catchment and reach. In catchment mode, CAESAR-Lisflood uses one rainfall input as the only influx to generate the runoff over the surface; whereas in reach mode, more than one source of water and sediment can be added into the system at user's defined points (as per here). To apply the modes, initial conditions are needed as parameters values in the model including surface elevation, grain sizes and rainfall (catchment) or flow input (reach). The modelled erosion and deposition are driven by the modelled fluvial and hillslope processes as the function of modelled time step. There are four components in CAESAR-Lisflood: a hydrological model, a surface flow model, fluvial erosion and deposition and slope processes.

4.5.1.1 CAESAR-Lisflood flow model

The CAESAR-Lisflood flow model is based on the one-dimensional Lisflood-FP flow model in where the surface flow is routed in four directions (Bates et al., 2010). The flow between cells is calculated by Equation (4.9):

$$q_{t'+\Delta t'} = \frac{q_t - g h_{flow} \Delta t \frac{\partial (h_t + z)}{\partial x}}{\left(1 + g h_{flow} \Delta t n^2 q_t / {h_{flow}}^{10/3}\right)} \quad (4.9)$$

Here, $\Delta t'$ = length of time step (s); t' and $t' + \Delta t'$ are the present time step and the next time step; q = flow per unit width ($m^2 s^{-1}$); g = gravitational acceleration ($m\ s^{-2}$); h' = flow depth (m); z = bed elevation (m); and x = grid cell size (m); $\frac{\partial (h_t + z)}{\partial x}$ = water surface slope and h_{flow} is the difference in elevation between the maximum water surface elevation and maximum bed elevation of the two cells where water is being routed between.

Another part of the flow formulation is the model time step at $t' + \Delta t'$ which is calculated by Equation (4.10):

$$\Delta t'_{max} = \alpha \frac{\Delta x}{\sqrt{g h_t}} \quad (4.10)$$

where α is the Courant number typically defined between 0.3 and 0.7 (Bates et al., 2010; Coulthard et al., 2013). This coefficient enhances the model's robustness by preventing water being moved too fast between cells which is also further controlled by a flow limiter maintaining Froude numbers less than a user specified value (default 0.8).

To increase the model speed in certain circumstances, a modification of the time step has been made. By integrating the Lisflood-FP flow model, CAESAR-Lisflood is able to simulate unsteady flow. However, if the difference between the water input and that leaving the modelled domain (Q_{diff}) is below a certain user-specified threshold, the flow model is deemed to be running in a steady state and the time step is determined by the amount of fluvial erosion as described below. During the stable flow conditions, the time steps can be extended up to one hour if the geomorphic changes are far slower.

By using Equation (4.9) and (4.10), the flow rates between cells can then be calculated, and the water depths for all cells are updated simultaneously so that the model can calculate fluvial erosion and deposition.

4.5.1.2 Fluvial erosion and deposition in CAESAR-Lisflood

CAESAR-Lisflood model uses multiple grainsized sediment (up to nine size fractions) to be fluvial eroded, transported and deposited, and the volumes of the different sizes of grain are recorded within a 3D active layer system, including one surface active layer, multiple buried layers (strata), a base layer and a bedrock layer (Coulthard and Van De Wiel, 2007; Van De Wiel et al., 2007; Hancock et al., 2010; Coulthard et al., 2013). By adopting this 3D layer system, the movement of buried sediments with topographic changes allows the development of stratigraphy. Moreover, this method allows for the development of important processes associated with heterogeneous sediment mixtures, such as the development of an armoured channel bed as a result of selective transport and deposition (Coulthard and Van De Wiel, 2007; Van De Wiel et al., 2007).

A few model parameters can be set by user to define the simulated environment. One parameter termed L_h set the thickness of the strata layers. The thickness of surface active layer can vary between 25% and 150% of L_h and acts as a buffer between erosion and deposition on the channel bed and the strata layers below. If the thickness of the active falls below 0.25 L_h (for example during erosion) then the upper strata layer incorporated into the active layer. Alternatively, if (for example during deposition) the active layer exceeds 1.5 L_h, the active layer is split so the strata layer below receives 1 L_h (Van De Wiel et al., 2007).

Furthermore, there are two options to calculate the amount of sediment eroded by fluvial action based on the transport equation from Einstein (1950) or Wilcock and Crowe (2003) (Coulthard et al., 2012). For the Einstein (1950) method, calculation of sediment transport for each size fraction i requires the calculation of the balance between the forces moving and restraining a particle (Equation (4.11)):

$$\psi = \frac{(\rho_s - \rho)D_i}{\rho dS} \tag{4.11}$$

Where the term ρdS is replaced by τ/g. A dimensionless bedload transport rate ϕ is then estimated from ψ using the relationship (Equation (4.12)) described by Einstein (1950).

$$\phi = 40(1/\psi)^3 \tag{4.12}$$

The value of ϕ is then used in Equation (4.13) to estimate q_i, the rate of sediment transport (m^3s^{-1}):

$$\phi = q_i \sqrt{\frac{\rho}{(\rho_s - \rho) g {D_i}^3}} \tag{4.13}$$

For the Wilcock and Crowe (2003) method, sediment transport rates (q_i) for each sediment fraction (i) are determined by Equation(4.14),

$$q_i = \frac{F_i U_*^3 W_i^*}{\big((\rho_s - \rho) - 1\big) g} \tag{4.14}$$

Here F_i is the fractional volume of the i-th sediment in the active layer, U_* is the shear velocity ($U_* = [\tau/\rho]^{0.5}$) and W_i^* is a function that relates the fractional transport rate to the total transport rate (Van De Wiel et al., 2007). In order to calculate W_i^*, it is first necessary to calculate τ_{rm}, a critical shear stress for the mean size of the bed sediment. τ_{rm} is determined by a function that the relates Shield's parameter for the mean bed material size (τ_{rm}^*) to the percent of sand on the bed surface (F_s) as per Equation (4.15),

$$\tau_{\mathrm{rm}}^* = 0.021 + 0.015 \ \exp[-20F_s] \tag{4.15}$$

The dimensionless value τ_{rm}^* can then be converted to shear stress (Nm^{-2}): $\tau_{\mathrm{rm}} = \tau_{\mathrm{rm}}^* \rho g D_{s50}$ and in Equation (4.16) rearranged to calculate τ_{ri}, the reference or critical shear stress for the i-th size fraction:

$$\frac{\tau_{\mathrm{ri}}}{\tau_{\mathrm{rm}}} = \left(\frac{D_i}{D_{s50}}\right)^b \tag{4.16}$$

Where b is an exponent determined in Equation (4.17),

$$b = \frac{0.67}{1 + \exp\left(1.5 - \frac{D_i}{D_{sm}}\right)} \tag{4.17}$$

W_i^* is then be calculated as per Equation (4.18),

$$W_i^* = \begin{cases} 0.002\phi^{0.75} & \text{for } \phi < 1.35 \\ 14\left(1 - \frac{0.894}{\phi^{0.5}}\right)^{4.5} & \text{for } \phi \geq 1.35 \end{cases} \quad (4.18)$$

Here $\phi = \tau/\tau_{\mathrm{ri}}$. W_i^* is then substituted into the main equation to obtain sediment transport rate q_i (m^3s^{-1}).

The calculation of shear stress (τ) that drives both the Einstein (1950) and Wilcock and Crowe (2003) formulations within CAESAR-Lisflood is determined from square of the resultant flow velocity v^2 (Equation (4.19)) the drag coefficient Ci and a constant (1000).

$$\tau = 1000\ Ci\ v^2 \quad (4.19)$$

The amount of sediment transported is multiplied by the time step ($\mathrm{d}t'$). However, as CAESAR-Lisflood has a variable time-step, $\mathrm{d}t'$ is controlled by a variable that specifies the maximum change in elevation that is allowed during an iteration, ΔZ_{max}. This parameter is used to calculate the time step in Equation (4.20), where q_{max} is the maximum transport rate calculated for a given iteration, and Dx is grid cell size.

$$\mathrm{d}t' = \frac{\Delta Z_{\mathrm{max}} Dx^2}{q_{\mathrm{max}}} \quad (4.20)$$

Equation (4.20) ensures that the time step reduces to sub seconds during periods of intense geomorphic activity, but extends to an hour during periods of stability (Van De Wiel et al., 2007).

4.5.1.2.1 Lateral erosion

Lateral erosion has an important effect on channel geometry as it erodes the sides of the channel leading to channel widen or migration. Here in CAESAR-Lisflood, the lateral erosion rate controls the channel movement, e.g. migration, and is calculated by the local radius of curvature (R_{ca}) on a cell-by-cell basis (Coulthard and Wiel, 2006). Equation (4.21) then determines lateral erosion (ζ) based on R_{ca}, Λ (lateral erosion rate – user defined parameter), τ (shear stress of the cell adjacent to the bank) and T (time).

$$\zeta = \frac{1}{R_{\mathrm{ca}}} \Lambda \tau T \tag{4.21}$$

Material eroded from a bank cell is then deposited in the cell next to the bank and then redistributed via regular fluvial erosion and deposition. Values of R_{ca} can be assigned as negative to cells on the inside bank, or positive to cells on the outside bank, thus a cross-stream gradient can be determined by interpolating the R_{ca} values across the channel to enable the simulation of sediment lateral movement (Van De Wiel et al., 2007). A lateral sediment flux Ψ_n can then be calculated from this cross-stream gradient (Equation (4.22)),

$$\Psi_n = a\left(R_{ca,n} - R_{ca,n-1}\right) h_n \tag{4.22}$$

Here, n and $n-1$ are the donor cell and the receiving cell, a is a coefficient and h is the flow depth. In order to maintain the downstream migration of meanders and lateral erosion, CAESAR-Lisflood shifts the previously calculated cross-channel gradient downstream by a number of cells denoted by the user.

4.5.1.2.2 In-channel lateral erosion

The in-channel lateral erosion, different from the lateral erosion introduced above, is set to control the channel geometry. This process could also be described as a within channel slope failure as it is designed to prevent positive feedback mechanisms that can result in the development of deep, single-thread channels. The in-channel lateral erosion rate and the slope between cells determine the volume of material moved from the donor cell (Equation (4.23),

$$\Delta Z_{n-1} = \frac{E_{n-1}\, \lambda (Z_n - Z_{n-1})}{Dx} \tag{4.23}$$

Here n and $n-1$ denote the donor and the receiving cells, Z is cell elevation, δZ is the change in cell elevation, E is the volume of material eroded, λ is in-channel lateral erosion rate and Dx is grid cell size. The in-channel lateral erosion can be considered as the relative cohesion of the in channel sediment – high values of this parameter represent less cohesive sediments leading to more in-channel lateral transport and wider and shallower channels, and conversely, lower values represent stronger cohesion to allow narrower and deeper channels develop.

4.5.1.2.3 Slope processes

In CAESAR-Lisflood, mass movement in various scales such as bank collapses, landslides can be simulated by two processes. When the slope between two adjacent cells exceeds a defined threshold, material is instantaneously moved from the uphill cell to adjacent downhill until the slope becomes stable (Coulthard et al., 2002). Moreover, soil creep (*m*) is also modelled by using the Equation (4.24), where C_{rate} is the user-specified rate of soil creep ($m\ yr^{-1}$) and T = time (*years*). This represents diffusion-like processes whereby sediment flux is linearly proportional to surface slope (Carson and Kirkby, 1972),

$$Creep = \frac{SC_{\mathrm{rate}}T}{Dx} \tag{4.24}$$

4.5.2 Integration with DECAL model

Merging the DECAL dune model described in 4.2 with CAESAR-Lisflood required a series of modifications and assumptions that are outlined below.

There are several common features that both models share, which significantly eased the linking of models. Firstly, both models are cellular and operate over a regular square grid mesh. The size of sediment transporting between two models is defined equal to the smallest grain faction among the multiple grainsizes within CAESAR-Lisflood. So sand moves as slabs within DECAL can then be moved within CAESAR-Lisflood and *vice versa*. Secondly, both models can share the same DEM of elevations (including any dunes), so changes in elevation caused by one model can easily be fed into the other model. To prevent sand being entrained by DECAL when wet, and to stop sand traversing or being blowing across streams, as bulk of aeolian transport is by saltation, two simple rules are applied to the DECAL model. One is the sand slabs cannot be moved if they are under water, and the other is that they will be instantly deposited encountering water within DECAL model.

However, there are other important issues that need to be overcome in model integration, related to the depth of slabs used by DECAL and the different model time steps. In DECAL, the sand is represented by slabs which could theoretically be set at any size. But, if the slab size is too small, e.g. <0.2 *m*, the shadow areas, which are also

formed by slabs stacking on top of each other, would be negligible and could not perform the reduction in aeolian transport which would result in no dunes forming. In effect sand will move as a sheet. Also, movement of small slabs increases the computational work and hence the model execution time. After the model calibration performed in Chapter 4, blocks of sand 0.5 *m* in thickness were selected as the appropriate slab size considering both the model execution efficiency and the flow-dune model operation. However, with slabs of h_s = 0.5 *m* – this means that substantial volumes of sand are moved for every iteration of DECAL (e.g. on 10 *m* grid cells, a single slab is 10 *m* x 10 *m* x 0.5 *m*) and therefore the dune model has a longer time step, for example, one iteration of the dune model represents 10 days of aeolian transport (Chapter 4). In contrast, the movement of sediment within CAESAR-Lisflood is restricted to a much smaller volume to maintain numerical stability (see Equation (4.20) above) and as a result the fluvial model has far shorter time steps – in the order of seconds. To overcome this difference, CAESAR-Lisflood is run repeatedly until 10 days has elapsed (for example) then the dune model operates – and then CAESAR-Lisflood runs for another 10 days and the process repeats. In other words the two models operate at two different speeds with the dune model called every 10 days whilst the fluvial model operates continuously.

Another problem with operating the models together is that a large volume of sand can be dumped 'instantaneously' into the channel, instantaneously blocking or damming the water flow. Whereas in reality, this process would happen far more gradually. To resolve this problem, sand movement from DECAL is calculated every model recall time step t (e.g. 10 days) but the changes in elevation performed by DECAL are applied gradually over the following 10 days of flow model operation.

One further modification for this study is that sand outputs from the fluvial and aeolian processes are recorded separately – fluvial moved sand leaving from the right hand edge of the modelled domain whereas aeolian sand leaves from the bottom edge. Elevations, images and sediment discharges can be recorded at user-specified intervals.

Chapter 5 Modelling the interaction between sand dunes and perennial rivers

5.1 Introduction

In Chapters 5 and 6, the key questions that arose from the analysis presented in Chapter 3 are explored. Rivers and dunes in the field operate across a spectrum of conditions, e.g. relating to flow regime (ephemeral, intermittent, perennial), sediment calibre (coarse-grained, fine-grained) or boundary characteristics (bedrock, alluvial, indurated or lithified alluvial), long-term behavioural tendencies (incisional, aggradational, migratory, avulsive), riparian vegetation associations (non-vegetated or vegetated with trees, shrubs and/or grasses) and different wind regimes, where changes in all of these can influence outcomes. However, until we can model the fundamental behaviour we do not know how much variation in the above factors will lead to changes. Therefore, to understand some of the basic, fundamental dynamics of the dune/river system a range of simplifications were used. These include simulating a non-vegetation environment; the interacting dunes were prescribed as crescentic types (barchan and transverse ridges); the river flow direction is perpendicular to dune migration and river and aeolian discharges were kept constant to simulate continuous hydrology and aeolian conditions.

The DECAL model described in Chapter 4 was used along with the CAESAR-Lisflood model (section 4.5.1) to conduct a series of experimental simulations examining the balance between perennial water flows of different discharges and continuous aeolian sand transport of different rates. This was carried out with the aim of seeing whether there were points or thresholds where one process became dominant over the other – and to observe and if possible quantify the dynamic interaction between processes.

5.2 Experimental design (model and simulation setup)

After the sensitivity analysis and calibration introduced in Chapter 4, an appropriate set of parameters for the DECAL dune model were chosen to be integrated with the

flow model - to investigate the dynamic fluvial-aeolian interactions in this and next chapter. A series of research aims were set out in the introduction to this chapter and these experiments aim to answer these questions through a simple set of experiments exploring the interactions and dynamics of sand dunes and a perennial flowing river. River and aeolian flows are kept constant, but the rate of aeolian sand transport and the fluvial discharge are varied over a series of experiments. Following the global survey in Chapter 3, crescentic dunes and a perpendicular interaction meeting angle occurred most frequently and therefore this forms the basic set up for the simulations to be carried out. The terrain – or domain that the simulations were carried out over was deliberately simplified to try and reduce any uncertainty in model outcomes that may emerge from using a variable/different topography. Similarly, to reduce uncertainty the fluvial discharges simulated here are kept static – or stable. The simulations are carried out over 100 *yr* to 500 *yr* time scales that are deemed sufficient to enable us to observe a systematic behaviour or dynamic equilibrium between the systems. However, some simulations were restricted due to the time required for them to run.

5.2.1 Space and time

The simulated landscape is a very gentle topography with a flat surface sloping gently in a downstream direction 0.0005 and laterally to the central line of the area 0.0015 (Figure 5-1). The domain area is 3000 *m*×2000 *m* made up of 300 by 200, 10 *m* by 10 *m* grid cells. The channel width is 40 *m*.

Water is introduced from the left of the domain and sand along the top strip (Figure 5-1). No sand is introduced along the first 50 cells (500 *m*) hence the actual area where dunes can form is sized in 2500 *m* × 2000 *m*. The non-dune area was set to prevent dunes/sand blocking the entrance to the domain which would result in flow being direct back over the top left edge. There is no restriction on the size of the domain that can be modelled, however, the larger the domain the longer the model run time. To reduce the run time, a smaller domain could be used, but if too small it would prevent the free formation of dunes. For the two types of dunes simulated in this study, there is usually between 30-100 *m* of width for barchans and between 30-1500 *m* of width, 60-2000 *m* of spacing for simple transverse ridges (Simons, 1956; Lancaster, 1995).

Therefore, the domain was set as small as 2500 *m* × 2000 *m* but large enough to form one simple land unit, a “miniature” of a large landscape.

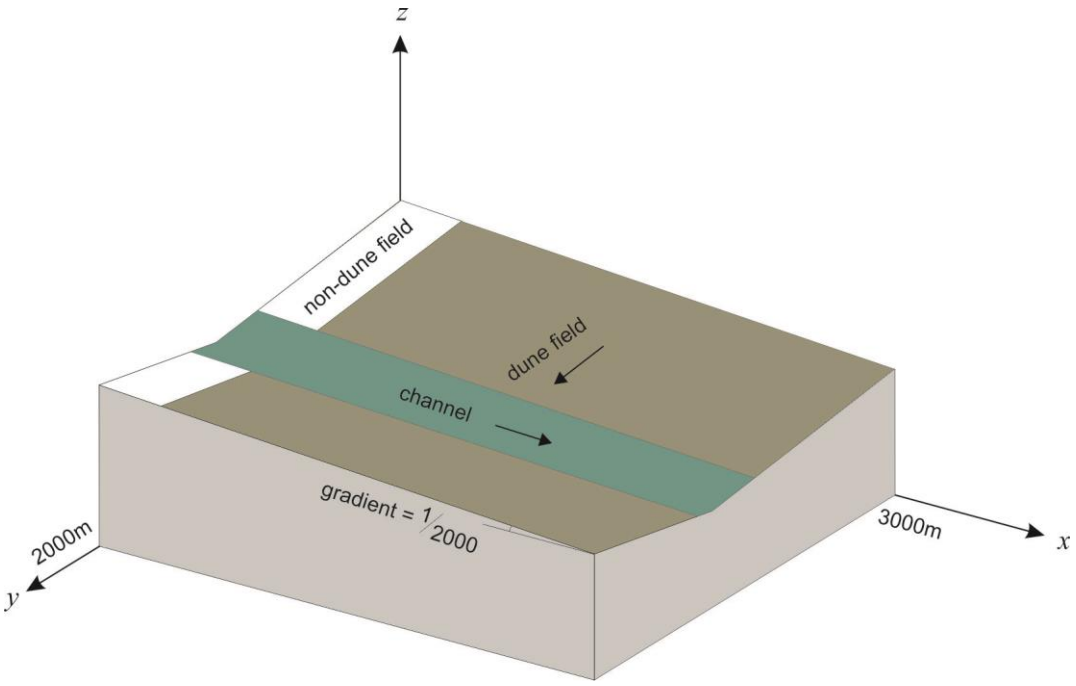

Figure 5-1 Illustration of simulation domain.

5.2.2 Sediment supply

Sediment can be supplied from both fluvial and aeolian sources – but from early exploratory runs it became clear that aeolian inputs were considerably greater than those expected from the fluvial supply. Therefore no sediment is added with the water for the fluvial component – though the fluvial model can erode (or mine) the DEM and generate sediment from the initial surface (as well as from any aeolian material deposited). Subsequently, sediment from the aeolian process becomes the only *external* sediment input into the intermixed fluvial-aeolian system throughout all of the simulations in this study and the sediment budget in the model, therefore, is

$$Q_{ia} = Q_a + Q_{oa} + Q_{of} \tag{4.25}$$

Where, Q_{ia} is the total sediment input volume from aeolian process, Q_{oa} is the total sediment output volume from the dune field and Q_{of} is the total sediment output volume from the flow, as illustrated in Figure 5-2.

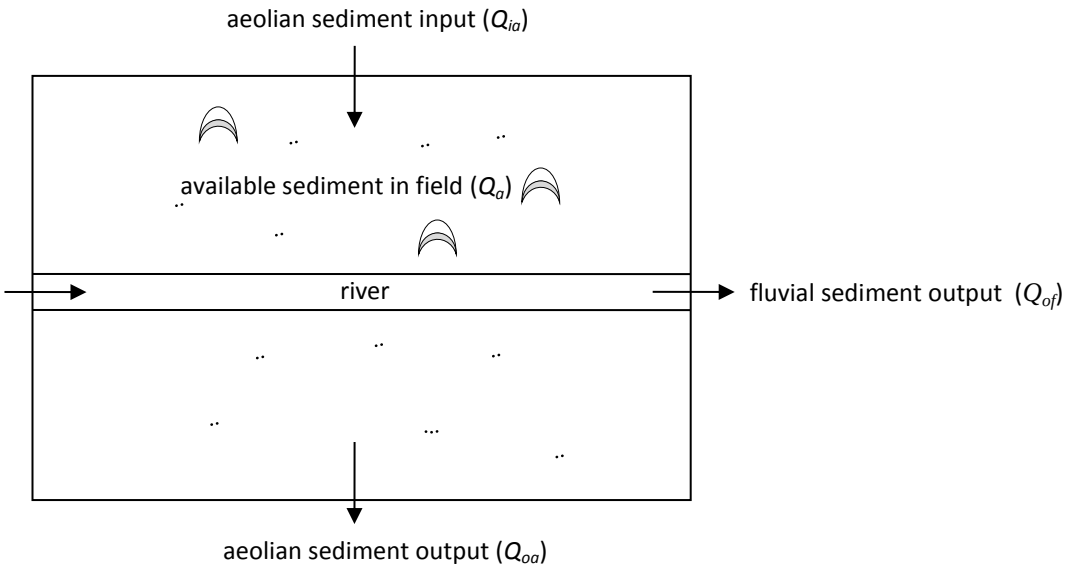

Figure 5-2 Sediment budget in the fluvial-aeolian interacting field.

In each trial of simulations, the rate of Q_{ia} (R_{ia}) can be calculated by Equation (4.3) when the R_{ia} is held constantly, whilst the output amount of fluvial/aeolian sediment (Q_{of} /Q_{oa}) were saved at user defined times during the simulation. For all simulations, outputs were aggregated at 10-day interval (a 10-day interval was used) to calculate the sediment transport rate from flow and dune field (R_{of} /R_{oa}).

5.2.2.1 Dune model setup

Based on the result from Chapter 4 (section 4.4.3), the value of dune model parameters, excluding the value of time step *t*, was set and held constant in all simulations (Table 5-1). The value of time step *t*, as has been explored in Chapter 4, influences the aeolian sand transport rates which characterize the dune field dynamics, and can be decided in corresponding to various sand transport rate R_s.

A group of 29 samples were selected out of the large set of value *t* which represents various levels of sand transport rate (Table 5-1). The maximum simulated sand transport rate was set at 129 $m^3m^{-1}yr^{-1}$, as introduced in section 4.4.1.3, where the corresponding time step *t* is 11520 min. The value of *t* as well as the increasing interval could be set at any value but was set as the times of 1440 *min* (=1 *day*) in this study for convenience of calculation as the model runs on daily or even longer time steps.

Outputs for the simulations were aggregated to the value of time step *t* in each simulation to facilitate analysis and interpretation.

Table 5-1 Values of dune model parameters (values of R_s were rounded).

No.	h_a (*m*)	h_s (*m*)	θ°	d (cell)	P_d (%)	g (*m*)	t (*min*)	R_s ($m^3 m^{-1} yr^{-1}$)
1	0.32	0.5	10	60	65	10	11520	129
2							12960	114
3							14400	102
4							15840	92
5							17280	84
6							18720	77
7							20160	71
8							21600	66
9							23040	61
10							24480	57
11							25920	54
12							27360	51
13							28800	48
14							30240	46
15							31680	44
16							36000	38
17							41760	32
18							50400	26
19							61920	21
20							82080	16
21							93600	14
22							102240	12
23							110880	11
24							120960	10
25							230400	5
26							280800	4
27							361440	3
28							505440	2
29							842400	1

5.2.2.2 Flow model setup

There are two main sets of variables to consider for the flow model – the sediment transport rules and the water discharge rates.

(1) Sediment transport rule

CASEAR-Lisflood provides two options to calculate sediment transport by using Einstein (1950) or the Wilcock and Crowe (2003) equations. A notable difference between these two equations is that the equation of Wilcock and Crowe (2003) reduces the mobility of smaller sizes and increases the mobility of coarser sizes relative to their unisize case, and as such this simulates less erosive channel dynamics than those found when using the Einstein (1950) equation. In this study, all sediments were

supplied by aeolian processes which transport finer sand instead of fluvial-sized coarser sands and gravels. These finer sand sediments have a relatively small median grain size and this sandy channel bed would be very easily eroded and cut down if the Einstein equation were applied. This would enhance the relative strength of fluvial processes relative to the aeolian processes. Therefore, to simulate an environment that is more realistic, the Wilcock and Crowe equation was used in this study.

(2) Discharge

Values of simulated discharge D_c are listed in Table 5-2 below.

Table 5-2 Flow model parameters values.

Flow model parameter	Value
Erosion law	Wilcock and Crowe (2003)
Max erode limit	0.01
Active layer thickness (*m*)	0.05
Lateral erosion rate	0.000002
Water depth threshold above which erosion will happen (*m*)	0.01
Evaporation rate (*m/day*)	0.0005
Courant number	0.3
Hflow threshold	0.00001
Mannings number	0.04
Discharge (m^3s^{-1})	1
	3
	5
	10
	15
	20
	25
	30
	35
	40
	45
	50

Choosing a representative discharge is difficult. Chapter 3 showed there were a wide range of river sizes and different environments where aeolian and fluvial processes interact. Literature detailing river discharges where dunes and rivers meet is sparse (section 2.2.2), with the William River in Canada (Smith and Smith, 1984) having a flow between 5 and 15 m^3s^{-1}. Therefore, for this study we have decided to run with a range of discharges from 1 to 50 m^3s^{-1} as listed in Table 5-2. This spans a wide range of possible flow conditions (given the size of the modelled domain) including those that represent known field conditions.

(3) Model parameters

The model parameters were set as shown above (Table 5-2), which have been validated from previous studies (Coulthard et al., 2002; Coulthard et al., 2013).

5.2.2.3 Run details

The simulation duration is controlled by two model parameters, one is the pre-setting value of "*Max run duration*", and another is the "*Max number of model iterations*". If the pre-set numbers of iterations are run out, the model will stop running even though the pre-set max run duration has not been finished. However, the number of iterations needed in each run is unpredictable. This resulted different length of simulated time in each run, more or less than the pre-set simulation duration which has been set as 480000 hours as the max run duration. As the result, the run durations of all simulations were in the range between 200 to 300 years, which is acceptable as preliminary test runs indicated that this was sufficient for the interactions between rivers and dunes to stabilise. Longer simulation periods are possible but require much longer model run times (up to month for each run) and were therefore not applied in current study. Twelve groups of numerical experiments were conducted, with each experiment consisting of no more than 29 simulations. The simulation matrix is presented in Table 5-3. In fact, it is not realistic to run all of these simulations during the limited research time (12×29 samples), especially when each run can take a long time to finish (over a month). So one group with moderate flow discharge values (5 m^3s^{-1}) was picked out after trial runs and all simulations in this group were tested to find out the transitions between different types of fluvial/aeolian interaction. These transitions gave the first reference to narrow the range of simulations executed. For example, Table 5-3, shows there are two transitions in the group of moderate flow discharges (D_c =5 m^3s^{-1}), one occurs when R_s =16 $m^3m^{-1}yr^{-1}$, and another at R_s =10 $m^3m^{-1}yr^{-1}$. Based on these transitions, when considering a higher flow discharge (D_c= 10 m^3 s^{-1}), one border is likely to be in the range of R_s =14 to 21 m^3 $m^{-1}yr^{-1}$, and the other in range of R_s = 5 to 11 m^3 $m^{-1}yr^{-1}$. Once the transitions for the higher discharge (D_c= 10 m^3s^{-1}) are determined, they can be used as references to find the transitions for in behaviour for the next discharge tested (e.g. D_c =15 m^3s^{-1}). This process means

that not all of the model runs listed in Table 5-3 (section 5.3.2) need to be tested and the modelling time can be reduced.

An additional simulation of river development without aeolian interaction provides a base reference to assess the impact of the changes in external driving conditions. Field investigation results as introduced in Chapter 3 are compared to observe changes on dune field development.

5.3 Simulation results

The results are presented in two formats. Firstly, a qualitative description of the interactions observed between the rivers and dunes (5.3.2) and secondly quantitative data on sediment discharges from aeolian and fluvial systems (5.3.3) and how these reflected the changes observed in 5.5.1.

5.3.1 Interaction behaviours

At the beginning of each simulated scenario, the channel was quickly eroded along the centre of the model domain creating the channel thalweg, meanwhile aeolian sand was added into the domain along the top edge at a constant rate. Depending on the aeolian sediment input rate dunes were formed and moved towards the channel, ultimately encroaching upon the channel which was forced to adjust – largely in response to the high sediment input from the aeolian system. The ability of dunes to cross the channel depended on the simulated flow discharge and aeolian sand transport rate. During this period various landscape patterns developed and these are described in the following sections.

5.3.1.1 Dune development

Developing in an environment with a perennial river, dunes interacting with the river are either eroded, dam the river or rebuild across the river. Dunes located on river banks were unavoidably eroded, either partly or completely (Figure 5-3 a3) by the river flow. When the volume of dunes was sufficiently large, then damming occurred along with the advance of dunes (Figure 5-3 a4, a5). Dune dams could lead to flooding at

different scales along the channel (Figure 5-3 a4, a5). The flooding would cause further erosion of dunes remote from the river banks and also produced some flat inter-dune spaces which redistributed the sediment providing a source for new dune development. Eventually, within the same aeolian regime, dunes in the region of fluvial-aeolian interaction would become smaller than dunes in aeolian only field due to the loss of sediment carried away by the river. Notably this led to no obvious change in the type of dune observed (Figure 5-3 a6).

One distinctive feature about dune migration is the way in which dunes cross the channel. Dunes cannot “fly over” the channel but can “cross” it in two ways. In one situation, some dunes were observed damming the channel to the extent that the river changed its original course from the downwind side to upwind side of the dune (Figure 5-3a8, a9). Thus the dunes appear to “cross” the channel which has actually been diverted. In other situations, new dunes emerged on the downwind bank of channel after flooding events, hence, the crossing is achieved by a mixture of aeolian and fluvial redistribution of sediment.

5.3.1.2 River evolution

Without invasion from aeolian process, the modelled river would develop into a single meander or slightly braided channel downstream (Figure 5-3 a1), and this channel evolution is controlled by river discharge. Whatever the value of the flow discharge, the river was observed to evolve in the same way as it would in the absence of dunes (Figure 5-3 a2). In this condition, the additional aeolian processes were insufficient to change the fluvial processes. However, the rate and frequency of the occurrence of river evolution events were observed to be inversely related to flow discharge, but to increase in relation to aeolian sand transport rates, which suggests that there are threshold values existing in terms of the ratio of river flow discharge to aeolian sand transport rate.

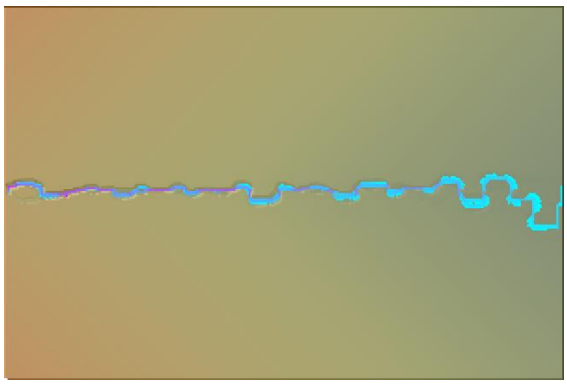

a1) Channel development without interacting with dunes (T=200000d, D_c=5m^3s^{-1})

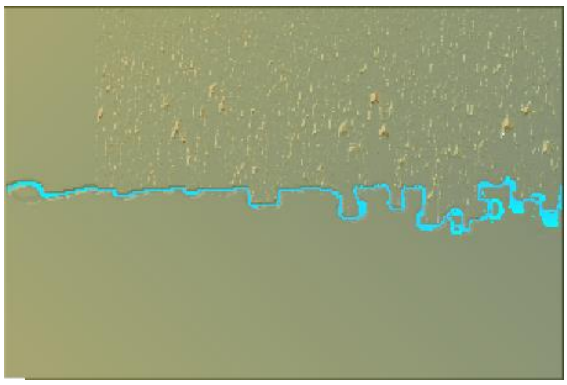

a2) Aeolian process have no or small influence on river development (T=200000d, D_c= 5m^3 s^{-1}, R_s= 3m^3 $m^{-1}yr^{-1}$)

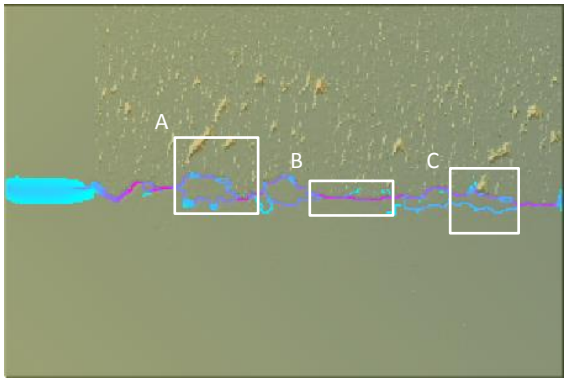

a3) Dunes were encroaching one tribute stream at location A, and some have been eroded at location C. Channels were seen to be narrow and deep without obvious aeolian dames, e.g. location B (T=9449d, D_c= 5m^3s^{-1}, R_s= 92m^3 $m^{-1}yr^{-1}$)

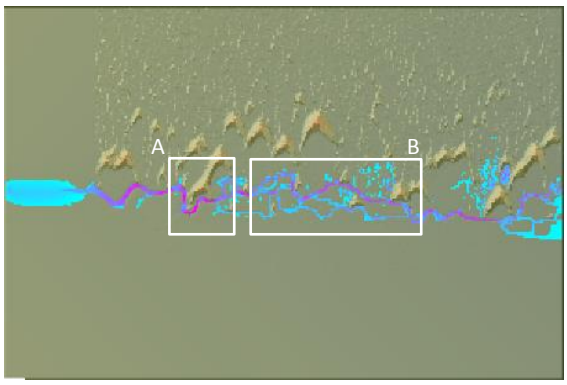

a4) Stream at location A was blocked, the existed stream was diverted, however, overbank floods occurred and some new streams were formed at location B (T=14542d, D_c= 5m^3s^{-1}, R_s= 92m^3 $m^{-1}yr^{-1}$)

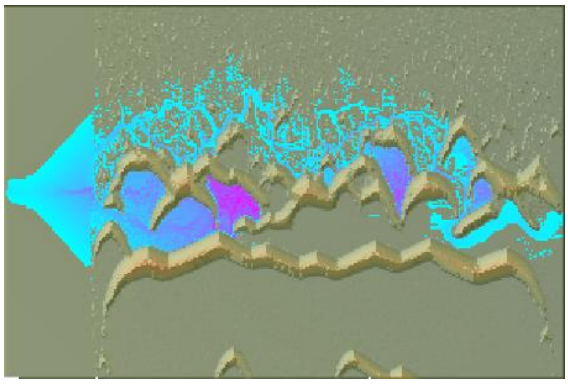

a5) Large scale flooding resulted in avulsion, the whole channel was blocked and ephemeral lakes formed. Wide and shallow channel can be seen at location A (T=71115d, D_c= 5m^3 s^{-1}, R_s=66m^3 $m^{-1}yr^{-1}$)

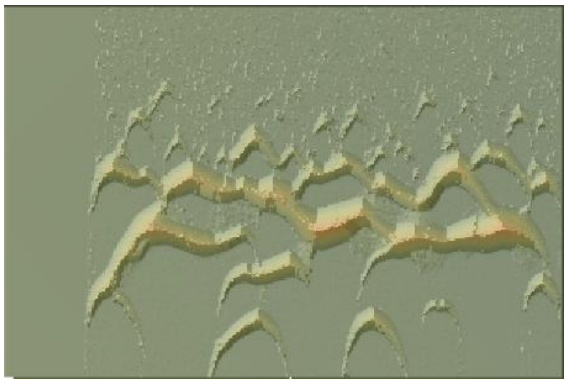

a6) Dune field condition without interfered by fluvial system (T=71115d, R_s=66m^3 $m^{-1}yr^{-1}$)

Figure 5-3 Interaction behaviour (river flow from the left while the sediment were added from the top perpendicular to the channel). a1-a2) scenarios without/with dune interactions; a3-a4) snapshots of one scenario at two sequential time points (higher sand transport rate R_s); a5-a6) scenarios with/without river interactions; a7) scenario with higher river discharge; a8-a12) snapshots of one scenario at sequential time points (with lower sand transport rates when compared to the scenario in image a3-a4). (continued).

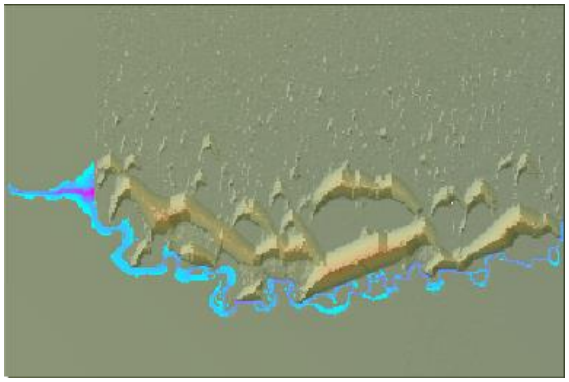

a7) The river managed to intercept the dune advance but was changed obviously in the meantime (T=200000d, D_c= 10$m^3 s^{-1}$, R_s= 44$m^3 m^{-1} yr^{-1}$, t= 31680min)

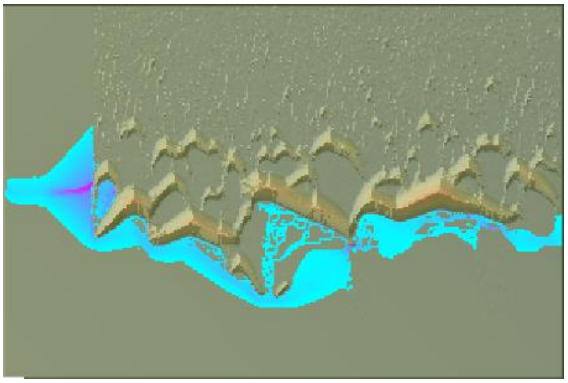

a8) In some situation, the river channel was not blocked suddenly but being slowly pushed away from the centre line in downwind direction during a long period (T=51800d, D_c= 5$m^3 s^{-1}$, R_s= 48$m^3 m^{-1} yr^{-1}$)

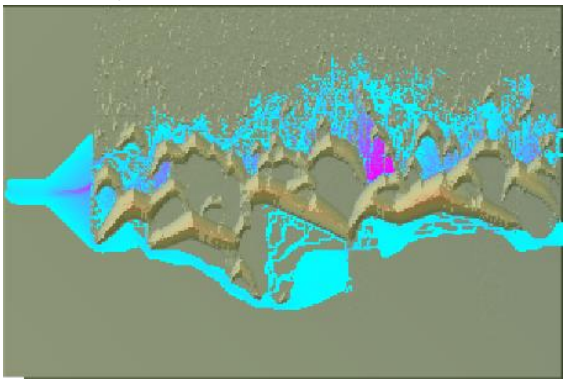

a9) River avulsion occurred, part of the flow were diverted to new location opposite to the parent channel (T=58000d, D_c= 5$m^3 s^{-1}$, R_s= 48$m^3 m^{-1} yr^{-1}$)

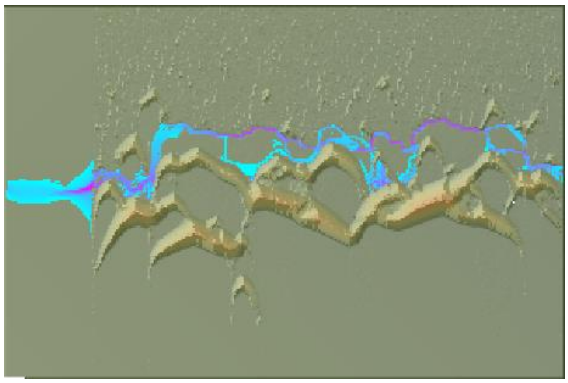

a10) The avulsion channel was established at the new location in upwind direction in single-thread pattern, whereas the previous parent channel was abandoned and occupied by dunes (T=61000d, D_c= 5$m^3 s^{-1}$, R_s= 48$m^3 m^{-1} yr^{-1}$)

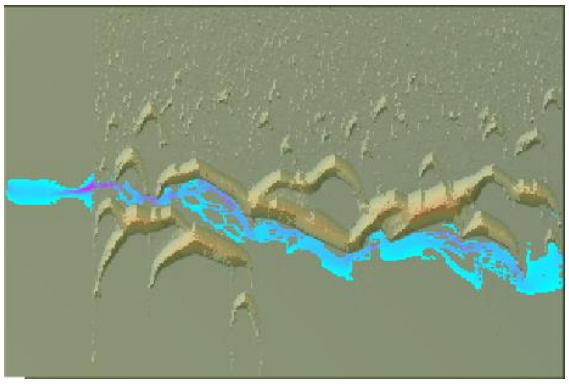

a11) The avulsion channel could be pushed slowly as in the same situation as illustrated in image a6, or being dammed/diverted to flow in downwind direction , until another avulsion occurred (T=67500d, D_c= 5$m^3 s^{-1}$, R_s= 48$m^3 m^{-1} yr^{-1}$)

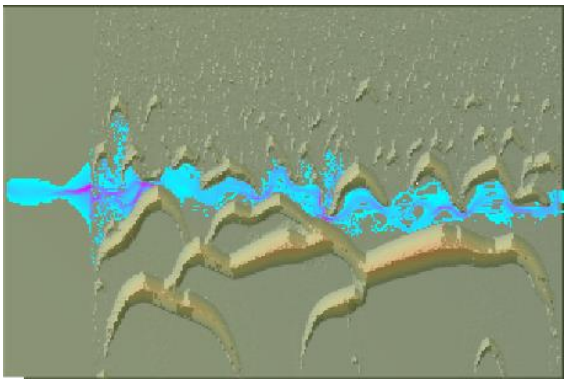

a12) At some time point, the river was pushed or diverted back to the original parent channel location but with similar size and type of dunes presented on both sides of banks (T=95840d, D_c= 5$m^3 s^{-1}$, R_s= 48$m^3 m^{-1} yr^{-1}$)

Figure 5-3 (continued).

Narrowing the difference between the strength of fluvial and aeolian processes produces relatively insignificant changes to the river channel. The higher the value of α, which is ratio of aeolian sand transport rate to flow discharge (R_s/D_c), the more extensive the changes in channel development become. In this situation, most of the interaction behaviours summarized in Langford (1989)'s study can be observed from the simulations. River were observed to be dammed and subsequently diverted, flooding occurrence and scale would increase with increasing aeolian strength, channel width/depth/length hence changed correspondingly and in the most intense situation, catastrophic avulsion would occur which led to channel migration. These behaviours are considered in more detail below.

1) Dammed and diverted

The aeolian topography disrupts the fluvial drainage networks and streams the water flow. This not only controlled the distribution of flooding, but also changed the nature of the flooding. Instead of occupying previously formed channels, streams must erode new channels through the aeolian dams (Figure 5-3 a3, a4). Obstruction of river channels could even form interdune ponds and ephemeral lakes, and in actual fact, similar phenomena have been observed in many field studies (Loope et al., 1995; Bourke, 2002; Bullard and McTainsh, 2003; Barrows et al., 2014). This phenomenon is considered by some researchers to be an important process in many fluvial-aeolian systems (Ahlbrandt and Fryberger, 1981). In the simulations of this study, dammed lakes of the order of hundred to thousand metres in width were very commonly formed (Figure 5-3 a5).

2) Flooding

Aeolian dams led directly to flooding alongside channels (Figure 5-3 a4). Being dammed by dunes, water rushed into hollows and rapidly filled them, creating new streams if there were no more obstructions in front or gradually inundating the blocked interdune space. In the latter condition, the water left in the inter-dune space might evaporate if the water entering was blocked by further dune migration, otherwise it rose until it either overtopped or sapped away part of the dunes that confined the inter-dune area. The resulting outrush of water would breach the inter-

dune space, draining it or flooding any adjoining inter-dune spaces. A good field example has been demonstrated in Krapf et al. (2003)'s work in Namibia desert.

3) Channel morphology

Some channels were observed to show no significant change despite the aeolian process interference (Figure 5-3 a1 and a2). In contrast, some channels underwent a series of fluctuations in width and depth and subsequently the channel pattern: from single to meander, to braided/multi-channels/reticulate or even recovered to single (Figure 5-3 a3-a12). In such type of scenario, the single-thread channel was observed to narrow initially, before its sinuosity then gradually increased. At some locations, the channel became wide and shallow even without aeolian obstructions (Figure 5-3 a5) or narrow and steep at other locations (Figure 5-3 a3). Being dammed by dunes, the rivers could change radically at the meeting points where they encountered a significant number of aeolian dunes. Abundant bedload material and high gradients resulted in multi-various channel morphology. In other instances, sudden events such like flooding rejuvenated the channel pattern from multi-various to single-thread dramatically (Figure 5-3 a10).

4) Channel migration and avulsion

Channel diversions of the order of a hundred metres were a very common phenomenon in all simulations, however, catastrophic change of channel location in reach scale was also observed. This behaviour is illustrated in Figure 5-3 a7, the channel was pushed slowly by dunes in the downwind direction so that the whole thalweg line was completely offset from the centre line. Sudden changes of channel location could also occur when a triggering event, commonly an avulsion caused by flood, forced the river to divert to a completely different location (Figure 5-3 a9, a10).

5.3.2 Interaction types and geomorphological characteristics

The model simulations showed four of the interaction types observed in Chapter 3, including *Fully fluvial dominant* (*FF*), *Mostly fluvial dominant* (*MF*), *Balanced* (*B*) and *Mostly aeolian dominan*t (*MA*). But *Fully aeolian dominant* (*FA*) type were not observed. The main Interaction types occurred in each simulation was marked in Table 5-3.

Table 5-3 Model parameter space (Simulation groups and observed interaction type results).

D_c (m^3s^{-1})	R_s ($m^3m^{-1}yr^{-1}$)																												
	129	114	102	92	84	77	71	66	61	57	54	51	48	46	44	38	32	26	21	16	14	12	11	10	5	4	3	2	1
1	TT				TT																TT	FF	FF	FF	FF				FF
3			TT													TT						FF	FF	MF	FF	FF			
5	TT	TT	TT	TT	TT	TT	TT	TT	TT		TT	TT	TT	TT	TT	TT	TT	TT	TT	MF	MF	MF		MF	FF	FF	FF	FF	FF
10			TT			TT	TT	TT			TT		TT		TT	MF				MF			MF	FF	FF				
15			TT	TT				TT		TT			TT		MF	FF/MF					FF	FF	FF						
20		TT	TT								MF	MF				FF/MF			MF	FF	FF	FF							
25		TT				TT	MF	MF		MF					MF	FF	MF	MF	FF	FF	FF	FF							
30	TT					MF				MF			MF			FF		FF	FF										
35						TT/MF	MF			MF		MF				FF	FF												
40						MF			MF		MF				FF	FF													
45						MF	FF					FF				FF													
50	MF			MF	F				F							F	F							F					

NB: – Fully Fluvial dominant type (FF);
– Mostly Fluvial dominant (MF);
– Transient type (TT) that the interaction type switches among Mostly Fluvial dominant type, Balanced type and Mostly Aeolian dominant type;
– Mostly Aeolian dominant type (MA);
– Unknown.

1) *Fully fluvial dominant* (*FF*)

The *FF* interaction type was commonly observed in simulations as can be seen from the Table 5-3. In these scenarios, the dunes were very unlikely to cross the river but were intercepted by the river. Correspondingly, the river can maintain or slightly change its pattern to accommodate any additional sediment input (as shown in images a1 and a2 of Figure 5-3). The resulting landscape featured the river flowing along the downwind edge of the dune field, and intercepting the aeolian sediment which reduced or even stopped the dune field extension producing different landscapes on either side of the river.

2) Mostly fluvial dominant (*MF*)

In some scenarios, the channel pattern and location had been largely changed although it still managed to intercept most of the additional sediment and reduced the dune field extension rate until the end of the simulated time (Figure 5-3a7, a8). As a result, large and dense dunes were presented on the upwind side of river bank whilst very few small dunes were visible on the downwind side of the river.

3) *Transient types* (*MF/B/MA*)

Balanced (*B*) and *Mostly aeolian dominan*t (*MA*) have been observed many times in the field, however, these two types were not seen in the simulations carried out here. Instead, there was a new category that we have termed transient types (TT) that contains parts of *MF*, *B* and *MA* interaction types (Figure 5-3 image a8-12). In scenarios dominated by *Transient* types (*MF*, *B* and *MA*), the most fundamental geomorphological changes were observed connected with episodic channel avulsion. For example, in Figure 5-3, at earlier time the river can manage to intercept the dunes which should be categorised as *FF*/*MF* interaction type (a8), but sudden avulsion led to vast change of the landform (a9) and as the result large numbers of dunes were seen on the downwind side of the river which interaction type should then be categorised as *MA* (a10). In some instances, *B* interaction type was observed after the river underwent the interaction of *MF* and *MA* (Figure 5-3 a12). As a result, dunes in such scenarios were observed on one side of a single or multi-channel bank at some time but might present on both sides of the banks with same or various size at another time.

Various scales of ponds or lakes were observed to be filled or dried up at different distances to the main channel which could still be located along the middle or the borders of the field.

Furthermore, results in Table 5-3 also show fairly clear zones where one regime dominates – the alteration of different flow discharges and aeolian transport rates led to changes in the behaviour of the modelled domain. For example, in group of D_c = 5 m^3s^{-1}, with the change of ratio α between strength of aeolian and fluvial process (R_s/D_c), the dominant regime changed from *FF* when R_s <10 $m^3m^{-1}yr^{-1}$ to *MF* when R_s was between 10 and 16 $m^3m^{-1}yr^{-1}$, and the dominant interaction types were all *T* when R_s >16 $m^3m^{-1}yr^{-1}$. However, the areas are not completely clear as discussed in 5.4.2.

5.3.3 Sediment output

The combined fluvial – aeolian model allows us to measure sediment that transport out of the modelled domain from fluvial sources (sediment left from the right hand edge of the area) and aeolian sources (sand that has crossed the river and flew out from the bottom edge of the modelled area). This enables us to quantitatively assess how fluvial and aeolian transport rates are affected by the combination of processes. For example how much of sediment were trapped and transported by the river – and how much aeolian sand managed to cross the river. This simple analysis is fundamental for understanding the overall – large scale role of fluvial/aeolian interactions on mass transport rates and correspondingly the impact on landscape development.

Fluvial and aeolian sediment outputs were recorded at the interval of the value of dune model time step in each run. This is because the sand cells in dune model only move after each time step and then there may have sand drop out of field bottom edge which are captured as the aeolian sediment output value at that time point. Therefore, there are no sand movement during the time step duration and no aeolian sediment output records at these times (Chapter 3). Simulated sediment outputs for every run are nonlinear and also varying upon different rate level of fluvial-aeolian regime. However, some common trends in sediment output behaviour were observed among all simulation results. To present and explore these behaviour, one representative group of simulations were selected and analysed in detail (group with D_c=5m^3s^{-1}). In this group, 28 runs showed a transition from fluvial to aeolian dominant

behaviour (Table 5-3). Sediment output results (R_{of} and R_{oa}) from some runs are illustrated Figure 5-4 and Figure 5-5 (results of all runs are listed in Appendix B). These runs are representative as their dominant regimes were observed close to the borders where one interaction type switches to another as shown in Table 5-3. The sediment output data of each simulation was normalized first to allow an easier graphical comparison.

5.3.3.1 Sediment output

Irregular sediment outputs from fluvial and aeolian system were observed in each run. The fluvial outputs contain large pulses of sediment discharge at certain times, for example, the four pulses O, A, B and C marked in Figure 5-4. An initial pulse (e.g. mark O in Figure 5-4) occurs at the beginning of each run when the aeolian processes reach the river channel. At this time, dunes have not yet formed near the channel so the river can intercept and transport away most of the newly arrived aeolian sediment. As the amount of sediment introduced into the field from aeolian system builds up, dunes form and migrate gradually towards the river and begin to interact with the river. The impact of larger bodies of sediment (Dunes - as opposed to the more constant rate of sand previously) can lead to pulses in the fluvial sediment. These pulses (e.g. A, B and C in Figure 5-4) are smaller than the initial pulse detailed above but emerge abruptly and sharply. In each run, the time points when the second and subsequent large pulses occur vary. However, it is noticeable that the lower the aeolian sediment transport rate (the higher the dune model time step value), the greater the delay for the second and subsequent pulses in fluvial sediment discharge (Figure 5-5).

It was also noticed that the sediment yield from both the fluvial and aeolian systems declined with decreasing aeolian transport rates (Figure 5-4 and Figure 5-5), as the decreased aeolian sand transport rate means the total sediment input per unit time decreased. However, the decreasing aeolian transport rate would not lead to noticeable landform change as long as it is maintained in a certain range of values. Comparing the data from all scenarios, it was found that the sediment volume $Q_{oa} < Q_{of}$ when aeolian sediment transport rate is 10 $m^3m^{-1}yr^{-1} < R_s <$16 $m^3m^{-1}yr^{-1}$ ($t >$ 820800 *min*) and nearly no aeolian sediment can cross the river when $R_s <$10 $m^3\ m^{-1}yr^{-1}$ ($t >$120960 *min*).

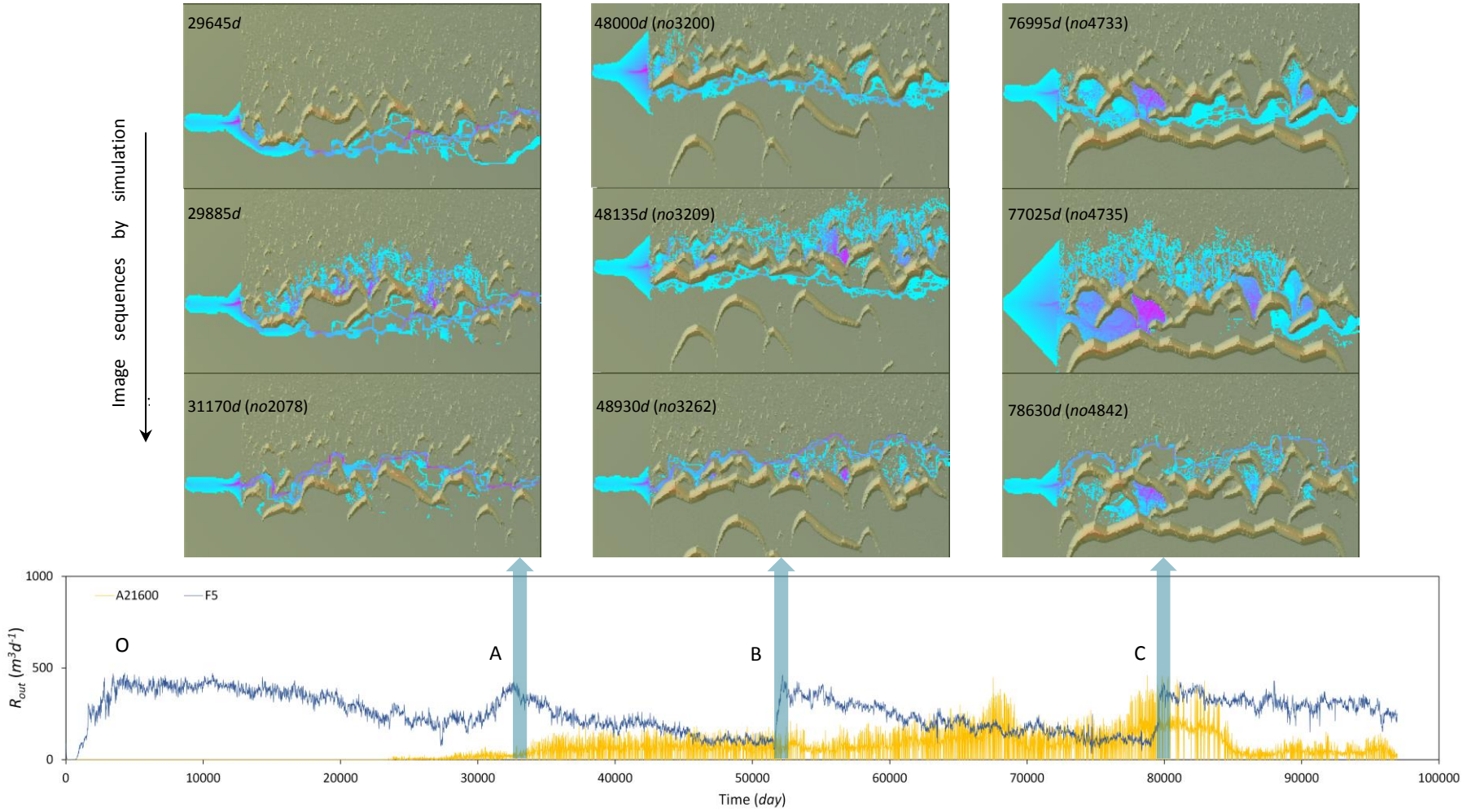

Figure 5-4 Transient events and fluvial sediment yield (D_c =5 m^3s^{-1}, R_s =66 $m^3m^{-1}yr^{-1}$, t= 21600min). O, A, B and C marked in the sediment graph are four significant stages. Sequential snapshots at stage A, B and C are linked to the fluvial sediment output pulses in the sediment output graph by blue arrows. (Image sequences are marked by simulated days and image series numbers in brackets)

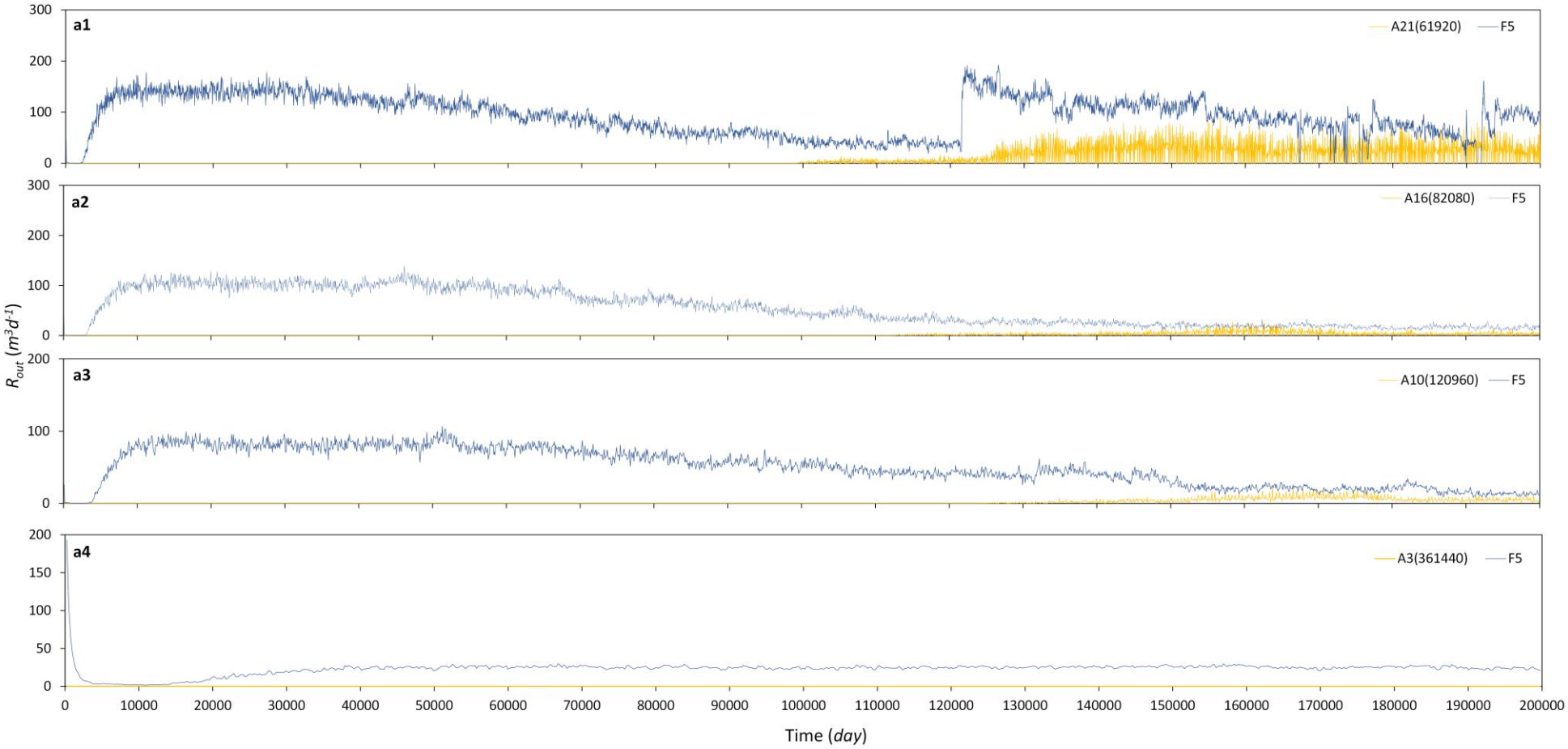

Figure 5-5 Sediment yield in different scenarios dominated by other interaction types, in contrast to the scenario presented in Figure 5-4 (D_c =5 m^3s^{-1}). a1) In *TT* dominant regime (R_s =21 $m^3m^{-1}yr^{-1}$, *t*= 21600*min*); a2) In *MF* dominant regime (R_s =16 $m^3m^{-1}yr^{-1}$, *t*= 82080*min*); a3) In *MF* dominant regime (R_s = *10*$m^3m^{-1}yr^{-1}$, *t*= 120960 *min*); a4) In *FF* dominant regime (R_s = *3*$m^3m^{-1}yr^{-1}$, *t*= 361440 *min*).

5.3.3.2 Ratio of aeolian to fluvial sediment output

From Figure 5-5 and Table 5-3, it can be also seen that with the change of ratio α = R_s/D_c, the contrast δ between sediment yield from aeolian and fluvial system (Q_{oa}/Q_{of}) changed subsequently and were related to the borders of dominant regime. In the group with a flow discharge D_c = 5 m^3s^{-1}, α_{5i} (i=1, 2, …) represents the ratio of sand transport rate R_s to flow discharge D_c in each scenario. In Table 5-3, it can be seen that there are two borders where the dominant regime of interaction type shifts: one border is between scenarios of R_s =21 m^3 $m^{-1}yr^{-1}$ and R_s =16 m^3 $m^{-1}yr^{-1}$, where the dominant interaction type changed from *Transient* (*T*) to *Mostly fluvial* (*MF*), the value of R_s/D_c at this border is marked as α_{5a}; the other is between scenarios of R_s =10 m^3 $m^{-1}yr^{-1}$ and R_s =5 m^3 $m^{-1}yr^{-1}$, where the dominant interaction type changed from *Mostly fluvial* (*MF*) to *Fully fluvial* (*FF*), the value of R_s/D_c at this border is marked as α_{5b}. The regime shifts at these two borders suggest that the corresponding α_{5a} and α_{5b} values could be interpreted as the threshold limits. After calculation by α = R_s/D_c, the values of α_{5i} (i=1, 2, …) when the flow discharge D_c = 5 $m^3s^{-1}$are listed in below.

Hence the value of the first threshold limit α_{5a} is within the range of 3.13 and 4.24, and the second threshold limit α_{5b} is within the range of 1.03 and 2.06 (Table 5-4). These two threshold limits then became the reference points that indicate that:

1) When $\alpha_{5i} > \alpha_{5a}$ (R_s >16 m^3 $m^{-1}yr^{-1}$, t < 82080 *min)*, sediment yield from aeolian output was higher than that of from fluvial regime (δ >0.03), the landscape exhibited the *TT* interaction types;
2) When $\alpha_{5b} < \alpha_{5i} < \alpha_{5a}$ (10 $m^3m^{-1}yr^{-1} < R_s <$21 $m^3m^{-1}yr^{-1}$, 82080 ≤ t ≤ 120960 *min)*, sediment yield from aeolian field would not exceed that of from fluvial regime at any time point (0< δ <0.03), the landscape exhibited the *MF* interaction type;
3) When $\alpha_{5i} < \alpha_{5b}$ (R_s <10 $m^3m^{-1}yr^{-1}$, t >120960 *min)*, there is nearly no sediment yield from aeolian field ($\delta \approx 0$), the landscape exhibited the *Fully fluvial* (*FF*) interaction type.

The existence of the α values indicates that field changes without external forcing may be normal in the development of a fluvial-aeolian interactions, as long as the value of α remains the same.

Table 5-4 Values of ratios $\alpha = R_s/D_c$ in scenario groups of D_c = 5 m^3s^{-1}.

i	D_c (m^3s^{-1})	R_s ($m^3\,m^{-1}yr^{-1}$)	α_{5i} (R_s/D_c)
1	5	129	25.83
2		114	22.76
3		102	20.32
4		92	18.34
5		84	16.70
6		77	15.33
7		71	14.15
8		66	13.14
9		61	12.26
10		57	11.49
11		54	10.80
12		51	10.19
13		48	9.65
14		46	9.15
15		44	8.71
16		38	7.59
17		32	6.47
18		26	5.28
19*		21	4.24
20*		16	3.13
21		14	2.72
22		12	2.26
23		11	2.47
24*		10	2.06
25*		5	1.03
26		4	0.83
27		3	0.64
28		2	0.44
29		1	0.26

(* marks the four scenarios at the borders of dominant interaction regime).

5.4 Discussion

The global survey summarized in Chapter 3 documented a diverse range of fluvial-aeolian interactions over various temporal and spatial scales. This suggests a wide range of possible outcomes from a limited range of environment settings. However, to assess geomorphic characteristics of fluvial-aeolian interactions, rather than focusing on a limited range of environment settings and interpreting the findings as representing a much larger reality, there is a need to step back and look at the 'big picture' across the general fluvial-aeolian environment. The cellular fluvial-aeolian model simulated various geomorphic behaviours which in many ways are similar to the global survey results revealed in Chapter 3. However, several unexpected features were also observed which provide us with considerable insight into the

geomorphological evolution in fluvial-aeolian environments where complete long-term field data is hard to gather.

5.4.1 Non-linear sediment yield

It has been noted that the fluvial and aeolian sediment output from the model were non-linear (Figure 5-4, Figure 5-5). This phenomenon is determined by dune field and the fluvial process properties. Because of the non-linear distribution of sand units in the field, there will be high/low sediment output when bulk of dunes passed by/after the field bottom edge. Even during the passing of dunes, different sizes of dunes or different parts of dune bodies would still result in non-linear sediment yield due to their non-linear shapes. If the channel is considered as another border for the aeolian field, the same situation would occur as it can be expected that non-linear input of aeolian sediments were trapped by the flow and carried away, thus led to the non-linear fluvial sediment output. Furthermore, the dune model is stochastic and this will inevitably introduce an additional level of non-linearity. The non-linear variability of fluvial sediment yields is consistent with previous findings from natural streams and from CAESAR and CAESAR-Lisflood studies (Cudden and Hoey, 2003; Phillips, 2003; Coulthard and Van De Wiel, 2007; Van De Wiel and Coulthard, 2010).

5.4.2 Interaction types

One important finding is that the interaction type classifications are dynamic, instead of the static snap shot observed in the global survey. It is possible for fluvial processes to dominate, or mostly dominate the interactions, but with perennial river flow aeolian processes cannot dominate continuously (simulations dominated by *MF* and *FF* are shown in Table 5-3). Instead a transition state develops as aeolian processes become stronger relative to fluvial processes where the aeolian processes can dominate periodically but not continuously. This leads to the occurrence of transient environments where the dominant processes in the interactions switch between fluvial and aeolian (simulations dominated by *TT* are shown in Table 5-3). The dynamic process in the fluvial-aeolian interacting field will also be considered in section 5.4.4.

It is interesting to find that fluvial process can easily dominate the interaction with even very small fluvial discharges, e.g. scenarios with D_c =1 m^3s^{-1} (Table 5-3), that

dunes could not easily cross the channel. It may be due to the constant work from the perennial river flow. By constant water flow, the channel is a persistent nature barrier to weaken the advancement of aeolian objects. This indicates that even very small but constant fluvial discharges can affect the aeolian process beyond expectation.

5.4.3 Landform evolution

5.4.3.1 Channel morphology and location

Various channel patterns have been observed to develop in the different model runs including the three main channel patterns (single-thread, meandering and braided). However, the history of channel changes in some scenarios exhibited irregular or unusual patterns, for example, the channel change events presented in images a8 to a12, in Figure 5-3. This was particularly significant in scenarios dominated by *Transient* interaction types (*MF*, *B* and *MA*). In *Transient* interaction dominated scenarios, various channel patterns rapidly switched between different types but not in the way associated with traditionally known channel development stages. For example, the river gradually shifted from straight to meandering to braided, but could also rapidly change from braided to single-thread, or the single-thread channel would again developed into network or any other types sooner or later (Figure 5-3 a8-a11). Similar phenomena can be seen in some field studies, for example, at the Morava River in the Czech Republic it has been observed that the environment changed from one of meandering or anastomosing channels to braided fluvial-aeolian systems during MIS 3 at ~48 ka and that this was replaced by a meandering system at ~13 ka, which has been characterised by smaller menaders since the onset of the Holocene (Kadlec et al., 2015). All of these changes can be explained from view of river hydraulics. The constant influence from aeolian processes produces structural instability within the interacting dune field. Over centennial timescale the coupled fluvial/aeolian system is continually subject to this perturbation which eventually leads to a marked unsteadiness in the in-stream sedimentation that cannot be maintained by a single river channel, and so avulsion processes (section 5.4.3.2) create distributary channels or completely relocate the channels. For example, channel changed in the area A from a3 to a4 and flood occurred in a5 of Figure 5-3. After each river reach reforms following the channel breakdown, the channel is smaller, shallower and straighter than

the previous reach and the relatively new channels in transporting and depositing sediment are more rapidly than the discontinuous trunk stream reaches and the multi-channels was gradually straighten and redefined at new locations, e.g. the multi-channels in image a9 changed to small single in image a10 until it become straighter in image a11 (Figure 5-3). However, in all circumstances the river would re-adjust very rapidly after disruptive events to restore stable channel form. Often the river path would be determined by the location of dunes and raised or lowered elevations reflecting past episodes of erosion and deposition. In summary, the irregular and dynamic topography driven by the aeolian process determined the irregular changes of river channel.

Furthermore, the great range of channel morphological changes observed from the model results suggest a strong relationship between channel pattern and sediment input, in contrast to the global survey carried out in Chapter 3. This excluded channel pattern change as one of the geomorphological characteristics in identifying fluvial-aeolian interaction type. This reflects a weakness of the study carried out in Chapter 3 – as this only represented static snap shots of fluvial aeolian environments where here we demonstrate that the interactions can be highly dynamic. By simulating in the simplified model domain, all other possible impact factors, e.g. climate change, bank stability, vegetation, etc., were excluded, and the only impact to channel development is from aeolian process which, therefore, can be taken as one of the determined factors accounting for channel pattern change. Subsequently, change of channel pattern should be considered to be one of the geomorphological characteristics dominated by aeolian process.

5.4.3.2 Avulsion

In field dominated by *Fully fluvial* (*FF*) or *Mostly fluvial* (*MF*) interaction type, there were no significant landform changes, whilst in field of *Transient* (*TT*) interaction types, fundamental geomorphological changes have been observed in all scenarios and were triggered by episodic channel avulsion (as described above). Two avulsion behaviours can be observed include *Nodal* versus *Random* or local versus regional. *Nodal avulsion* were recurring events that originate from a relatively fixed area of a floodplain, e.g. at the apex of the field where river entered whereas *Random avulsions* may occur

anywhere along the active channel (Slingerland and Smith, 2004). The most fundamental landform changes in the simulations were caused by *Nodal avulsion* which is, therefore, the type of avulsion discussed in this study.

The role played by avulsion is considered to be the most important behaviour that discriminate two types of interaction. This is because the relocation of a river would result in very different geomorphic characteristics. For example, in Figure 5-3 image a8, the river was located at the downwind border of the dune field and the interaction type it presented, therefore, was categorized as *MF.* However, after the avulsion as shown in image a9, the channel completely migrated up to the upwind border of the dune field and the interaction type it presented shifted to the category of *Mostly aeolian* dominant (*MA*) (image a10). Superficially, the role of the river shift from the interceptor of dune field to the sediment supplier to the dune field. Avulsion, therefore, is not only the primary process that determines channel location over the long term, but also defines the landform in (Jones and Schumm, 2009). More important is the avulsion would occur repeatedly after every certain time period as long as the same environment setup is retained. Therefore, it seems this behaviour is the norm rather than the exception.

Furthermore, avulsion events can be observed not only from landform change (scenario images) but also the sediment output data (Figure 5-3 and Figure 5-5). By defining the channel location, avulsion has an important effect on the large-scale distribution of river sediment (Jones and Schumm, 2009). This could possibly help to explain some of the phenomena seen in the field, in that flood deposits are absent in lower locations in some river systems when large floods occurred in the upper part of the system (Greenbaum et al., 2014).

When an avulsion occurs, it also results in a sediment pulse moving downstream, and this can be observed by comparing the scenario images with their corresponding sediment output graphs. For example, in the sediment output graph in Figure 5-4, the initial high sediment output period O is caused by the initial input of aeolian sand instead of dune interaction. Subsequently, three significant pulses A, B and C correspond to sudden and rapid avulsion events as illustrated in the images in Figure 5-4 (the event occurred time marked at the up left corner of each image, followed with

image serial numbers in brackets). After comparing the 28 results of sediment outputs from the simulation group with D_c=5 m^3s^{-1} and R_s in the range of 1 to 129 $m^3m^{-1}yr^{-1}$, with the geomorphic changes observed in corresponding scenario images, the same phenomenon seen in Figure 5-4 has been repeatedly seen, in that every avulsion caused significant geomorphic change and the rates of geomorphic activities match with pulses of fluvial sediment discharge from the model (Appendix B). Therefore, the links between geomorphic changes with sediment output change was set up which further help to identify the threshold limits in judging the types of interaction occurred in field.

The recurrences of avulsion events indicate an unexpected cyclic behaviour of abrupt large scale landscape change. Furthermore, this cyclic landscape change could occur in any scenario as long as the corresponding ratio α is higher than a certain threshold limit α_i (e.g. α_{51} is the threshold limit when D_c= 5 m^3s^{-1}, as indicated in section 5.3.3.2). This suggests that the occurrence of cyclic behaviour is insensitive to the change of ratio between force of fluvial and aeolian when $\alpha>\alpha_i$, but the cyclic period is sensitive to α, that the lower the α, the longer the cyclic period (Appendix B for details). Normally, where an abrupt or major landscape change occurs, the explanations are linked to the influence of external factors such as climate change, tectonics or even human activities. Such assumptions may lead to researchers overlooking that large scale of landform instability may be inherent and driven by internal forces of a system in dynamic equilibrium. Hence, the cyclicity found in this study suggests that a sudden landscape change may be normal in the development of a fluvial-aeolian interacting field without any external forcing.

The cyclic behaviours were initiated by avulsion events; therefore the cyclic period is related to the avulsion frequency which is controlled by the rate of fluvial and aeolian processes which move the river toward the avulsion threshold (instability). The cyclic period is one of the important concepts towards the understanding of long-term landscape change. It is the time period required to attain characteristic form (relaxation time) and the length of time over which the characteristic form persists (characteristic form time), since this will identify the ability of the system to adjust in relation to the frequency of any impulse of change (Brunsden and Thornes, 1979).

From the current available data, the sediment output signals indicate the avulsion recurrence interval varies widely in different scenarios, ranging from as low as 10 years (R_s= 129 $m^3m^{-1}yr^{-1}$, t=11520 *min*) to up to 220 years (R_s= 21 $m^3m^{-1}yr^{-1}$, t=61920 *min*) (Appendix B), in contrast to some literature records between 28 years of recurrence for the Kosi River (India) and 1400 years for the Mississippi (Slingerland and Smith, 2004). These examples, however, are for rivers of different size and more importantly in more temperate climates. The inference, therefore, is that avulsion frequency is much greater where there are extensive aeolian/fluvial interactions. Future work is needed to analyse the frequency-magnitude distribution of avulsion events and its threshold to help to further elucidate the factors that control the geomorphic changes (Turcotte, 1997; Jerolmack and Paola, 2007; Jones and Schumm, 2009).

The phenomenon of avulsion occurrences is very important towards understanding the landform evolution in fluvial-aeolian interacting field. Channel avulsions are thought to be an important process in developing alluvial architecture – and form important component of aquifers and hydrocarbon reserves. Therefore, the combined action of fluvial and aeolian processes could have important implications for such features. Especially, river avulsion usually unfolds over relatively long time scales and few avulsions have been observed in modern systems (Hajek and Edmonds, 2014). So numerical modelling provides the ideal tools to study the long-term fluvial-aeolian interaction and the impact on landform change.

5.4.4 Geomorphic thresholds and interaction types

In this study, it was observed that the fundamental landform changes were closely related with channel destabilization which is directly affected by the aeolian activity, conducted by avulsion and the result landforms were presented in different fluvial-aeolian interaction types. To every sudden and radical landform change, there may be a threshold being exceeded. Especially, the sudden landscape changes in a fluvial-aeolian interacting system without external forcing suggests that there may be a intrinsic geomorphic threshold exists (Schumm, 1979).

As it has been seen that the ratio α of sand transport rate to flow discharge (R_s/D_c) is correlated with different landforms, the change of ratio α is closely related to the geomorphological change, which means the geomorphological threshold explored in

this study can be identified by comparing with the qualitative data as well as the sediment yield from fluvial and aeolian field. As it was shown in section 5.3.3.2, among the tests in the group of flow discharge D_c =5 m^3s^{-1}, two threshold limits α_{5a} and α_{5b} were found. Observing the snap shots of the landform, when *Fully fluvial dominant* (*FF*) interaction dominated the landscape change, none of or hardly can sediment yield from aeolian field be observed (Appendix B A25-28 for details). In these conditions, the corresponding ratio α_{5i} (i=1, 2, …) was observed to be lower than threshold limit α_{5b}. When the field exhibited to be dominated by *Mostly fluvial dominant* (*MF*) interaction, the sediment yield per unit time from aeolian field would never exceed the sediment yield from fluvial field during the same period, and corresponding ratio of α_{5i} (i=1, 2, …) was observed to be lower than threshold limit α_{5a} (Appendix B A20-24 for details). In contrast, if the ratio of α_{5i} (i=1, 2, …) was observed to be higher than threshold limit α_{5a}, then the field landforms were observed to be dominated by the three *Transient* interaction types including *Mostly fluvial dominant*, *Balanced* and *Mostly aeolian dominant*. Thus, by comparing the value of α with the threshold limits, the development of the interacting field can be directly predicted.

However, the threshold limits identified above can only be applied in the condition that the flow discharge is 5 m^3s^{-1}. Once the flow discharge is changed to another value, the threshold limits would change correspondingly. In other words, the threshold limits are different in groups of different flow discharge. This is clearly indicated in Table 5-3.

Furthermore, the distribution of dominant regimes shown in Table 5-3 indicates the model parameter space as well as the transition between dominant regimes (Figure 5-6). The dominant regime changes from *FF* to *MF* and then switches between the three *Transient* types with the decreasing R_s and increasing D_c, which is corresponding to the decrease of ratio α (R_s/D_c). Due to the stochastic components of the model transitions between interaction types should be considered as fuzzy boundaries.

In addition, the threshold limits found in this study are all obtained in environment under ideal and controlled conditions, practical threshold values for application should be tested with more field data.

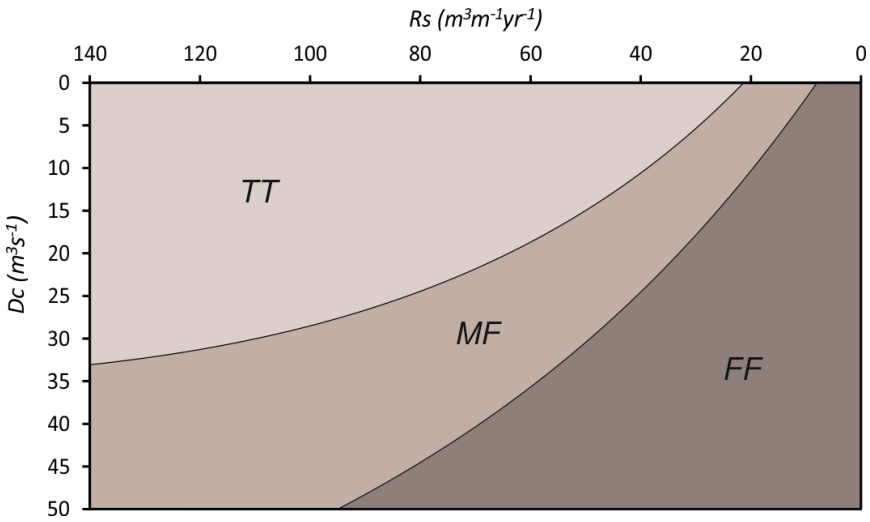

Figure 5-6 Model phase space of interaction types (TT: transient types; MF: mostly fluvial dominant; FF: fully fluvial dominant).

5.5 Conclusion

The findings in this chapter answered most of the questions asked in the introduction but also provide some new findings which are beyond the expectation of this study.

Firstly, the model results certainly support the field observation conducted in Chapter 3 which presented various interactions types, but importantly reveal how important it is to look at the process interactions from dynamic view instead of static. The static interactions types found in the field were not stable in the dynamic system but may be just at one stage of the whole interaction process. Especially, the *Balanced* (B) interaction does not indicate that the landform is absolutely in equilibrium condition but could be the transient state from one interaction type to another. Moreover, scenarios that presented *Balanced* interaction were also involved with another two interaction types including *Mostly fluvial dominant* (MF) and *Mostly aeolian dominant* (MA), and these three interaction types are collectively referred to as *Transient* type (T). These three transient types were found looping between each other in one field as long as the simulation was continued. From this point of view, the landscape dominated under *Transient* type could be considered as in a dynamic equilibrium state, and *Balanced* interaction type classified in Chapter 3 is more like a morpho-equilibrium specification rather than a dynamic-equilibrium.

Importantly, various rates of flow discharge and aeolian sand transport were not found to affect the interaction behaviours and types of interaction. Instead, sudden landscape changes could occur within the same fluvial and aeolian regimes and the trigger that causes the shifting between transient interaction types is a periodic avulsion event occurring without external drivers. Channel avulsion is thought to be an important process in developing alluvial architecture and form important component of aquifer and hydrocarbon reserves. In the simulation, the avulsion events not only caused significant changes to the landform features but they also exhibited cyclic behaviour. This cyclic mode switching can be seen not only from the landform images but also the fluvial sediment yield which provides the opportunity to link the geomorphological characteristics with the field sediment yield data and so to identify the corresponding geomorphic threshold.

The sudden landscape change suggests that it may be normal in the development of a fluvial-aeolian interacting field without any external forcing. The instable landscape is inherent and driven by internal forces of a system in dynamic equilibrium, such that a change in an external variable is not always required for a significant geomorphic event to occur, but that this depends on the systems intrinsic geomorphic threshold. However, in contrast to Schumm's (1979) idea about the threshold discharge of instability, the geomorphic threshold discussed in this study reflects the contrast ratio (α) between fluvial and aeolian process (R_s/D_c) which lead to change of different interaction types and landform features. Threshold discharge of instability is not applicable in this study because it is found that the channels in the fluvial-aeolian interacting field can change epidemically with any constant discharge values as long as α is retained in a certain range of values.

It is very interesting that though with perennial fluvial process seems stronger than aeolian process. There are no *Fully aeolian dominant* scenarios have been identified no matter how low the discharge is and how high the sand transport rate could be, as indicated from the Table 5-3. Nevertheless, it is not easy for dunes to cross the perennial river even with very low discharge such as 1 m^3s^{-1}. The question is subsequently raised as to how landform change and dune migration could be influenced if the fluvial process is further weakened by reducing its flow period, such as in an ephemeral or intermittent environment?

Chapter 6 Modelling the interaction between sand dunes and ephemeral rivers

6.1 Introduction

Chapter 5 showed that with perennial river flow it was difficult for sand dunes to cross the channel, in most cases where sand dunes crossed the channel this was due to the channel avulsing or being diverted. However, Chapter 3 showed that in some field, dunes are present on both sides of the river channel. This suggests that sand dunes must be capable of crossing the channel – possibly during periods when the channel is dry in other words an interaction between aeolian processes and ephemeral rivers. This chapter aims to test this and find out what period of ephemeral flow is required for aeolian processes to begin to dominate – and for sand dunes to be able to cross river channels.

To investigate this, an identical model set up as used in Chapter 5 was used, but the periodicity of flow was varied. These experiment described below aim to investigate a several research questions. Firstly, are different landforms generated by ephemeral flows? Secondly, if four of six interaction types can be observed during the perennial simulations, then what interaction behaviours and types can be observed in an ephemeral environment? Thirdly, the perennial simulations showed sediment outputs that changed with geomorphic events, are such signals – or different – found in ephemeral contexts? Finally, is there a critical threshold value where aeolian processes dominate over fluvial?

6.2 Experiment design

The model set up (DEM, input parameters) are as per section 5.3 except the flow regime is changed from perennial to ephemeral. In an ephemeral environment, changes of wet/dry seasons may change the dominance and formation of resulting landscapes. Therefore, the experiments were designed focusing on the impact from changes of wet/dry seasons instead of the change of ratios between fluvial discharge and sand transport rate. A very simplistic representation of perennial/ephemeral flow

was used where during 'wet' seasons flow was kept continuous – but then stopped completely during 'dry' seasons. The values of sand transport rate (R_s) and flow discharge (D_c), therefore, were retained the same in all scenarios, and the literature and a pilot test was run firstly to determine the experiment water discharge value (section 6.2.1). Once the certain value of R_s and D_c are determined, scenarios of various seasonal changes were designed and simulated (6.2.2).

6.2.1 Aeolian sand transport rate (R_s) and flow discharge (D_c)

To generate as much geomorphic development and interaction as possible in a comparatively short term, the R_s was set at a higher value. As the R_s values in the fastest advancing barchan field is about 76-99 $m^3m^{-1}yr^{-1}$ (Vermeesch and Drake, 2008) (Chapters 2 and 4), the value of dune model time step *t* = 14400 min (giving an R_s = 102 $m^3m^{-1}yr^{-1}$) was selected which was also associated with a water discharge value of D_c = 5 m^3s^{-1} as presented in Chapter 5.

The river discharge of D_c =5 m^3s^{-1} could considered too low for an ephemeral environment as the typical hydrology of dryland/ephemeral environments is of high flow variability - with long periods of little or no flow interspersed with occasional large, sometimes extreme, floods. So an experimental value of D_c needed to be set at higher value than 5 m^3s^{-1}, but very high values, such as over 50 m^3s^{-1}, were excluded since the experiments were designed to represent general environmental conditions rather than extreme examples (see Section 2.3.2.2) (Thoms and Sheldon, 2000; Tooth, 2000; Zhang et al., 2010). Referring to the field value from the William River area (Smith and Smith, 1984), a group of mid-flow discharge values (5/10/20 m^3s^{-1}) were selected and a pilot test was preformed to determine the modelled D_c value (Table 6-1). The three runs in the pilot test were set in the same seasonal change environment. The scenario of the selected seasonal change could be in any condition and was set at half year dry and half year wet in this test to have a general observation.

Table 6-1 Group 1: comparison of impact from flow regime with different flow discharge.

No.	Flow discharge (m^3s^{-1})												t	R_s
	Jan	Feb	Mar	Apr	May	Jun	Jul	Aug	Sep	Oct	Nov	Dec	(*min*)	($m^3m^{-1}yr^{-1}$)
1	5	5	5	5	5	5	0	0	0	0	0	0	14400	102
2	10	10	10	10	10	10	0	0	0	0	0	0	14400	102
3	20	20	20	20	20	20	0	0	0	0	0	0	14400	102

The result of this pilot test showed that the three discharge values did not show any great differences in the landscape development between them. As illustrated in Figure 6-1, the randomly selected images from each run present the landforms at the same modelled time and no significant differences can be distinguished among them. Therefore, value of D_c = 10 m^3s^{-1} was used in ephemeral scenarios in contrast to the D_c = 5 m^3s^{-1} in perennial scenarios, because it is higher but still within a range that can be associated with the R_s value to produce simulations that are generally applicable.

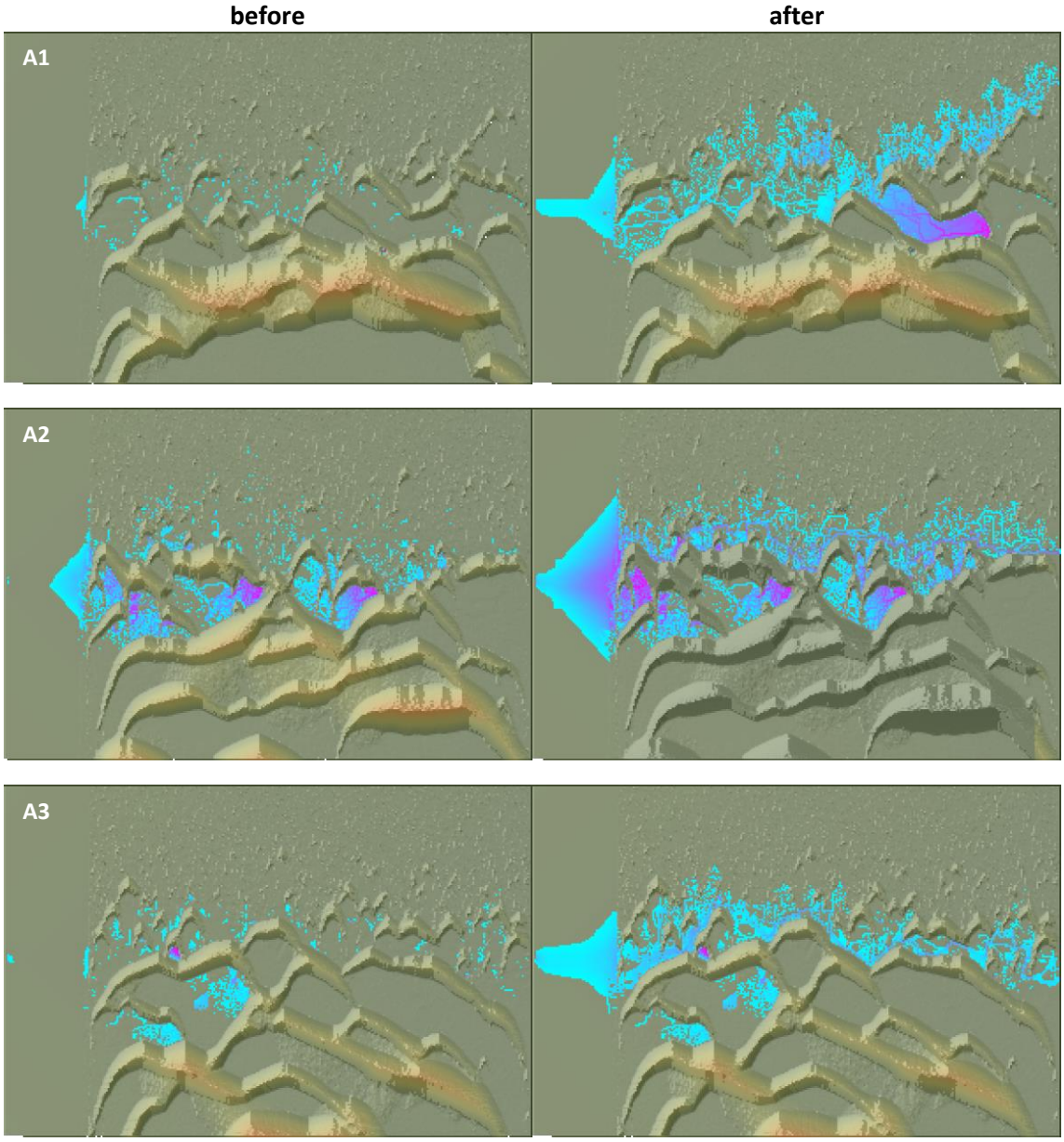

Figure 6-1 The landform before and after the water flow in at *T*=320 year in comparison. A1: D_c = 5 m^3s^{-1}; A2: D_c = 10 m^3s^{-1}; A3: D_c = 20 m^3s^{-1}.

6.2.2 Strategies of seasonal changes

The seasonal changes in this study are defined by the change between wet and dry seasons. The wet and dry periods were set in monthly units. Since there are twelve months in each simulated year and each month could be wet or dry, there are 2^{12} combinations. Considering that wet seasons generally occur during warmer periods in reality, eighteen combinations were selected from the entire range of combinations (Table 6-2). January was selected as an arbitrary starting point for the wet season, though in reality the wet season could start during any month.

An additional test of perennial flow D_c =10 m^3s^{-1} interacting with dunes of R_s =102 $m^3m^{-1}yr^{-1}$was run in comparison with above ephemeral scenarios results.

Table 6-2 Group2 to 4: various wet seasons.

Group	No.	Jan	Feb	Mar	Apr	May	Jun	Jul	Aug	Sep	Oct	Nov	Dec
2	1	×	0	0	0	0	0	0	0	0	0	0	0
	2	×	×	0	0	0	0	0	0	0	0	0	0
	3	×	×	×	0	0	0	0	0	0	0	0	0
	4	×	×	×	×	0	0	0	0	0	0	0	0
	5	×	×	×	×	×	0	0	0	0	0	0	0
	6	×	×	×	×	×	×	0	0	0	0	0	0
	7	×	×	×	×	×	×	×	0	0	0	0	0
	8	×	×	×	×	×	×	×	×	0	0	0	0
	9	×	×	×	×	×	×	×	×	×	0	0	0
	10	×	×	×	×	×	×	×	×	×	×	0	0
	11	×	×	×	×	×	×	×	×	×	×	×	0
3	12	×	0	0	0	0	0	×	0	0	0	0	0
	13	×	×	0	0	0	0	×	×	0	0	0	0
	14	×	×	×	0	0	0	×	×	×	0	0	0
	15	×	×	×	×	0	0	×	×	×	×	0	0
	16	×	×	×	×	×	0	×	×	×	×	×	0
4	17	×	0	0	×	0	0	0	0	0	0	0	0
	18	×	×	0	×	×	0	0	0	0	0	0	0
	19	×	×	×	×	×	×	×	×	×	×	×	×

NB: × represents the discharge value.

6.3 Simulation results

The results from ephemeral interaction experiments are presented first qualitatively and then quantitatively.

6.3.1 Interaction behaviours and geomorphological characteristics

Although most of the interaction behaviours observed in the ephemeral scenarios are similar to those in perennial scenarios, there are still some distinct geomorphological differences.

6.3.1.1 Dune development

The dunes were found to develop more clearly recognisable morphologies and to be able to maintain these well-formed shapes (Figure 6-2 a1) (Appendix C for more details). Although erosion and damming were observed, their extent and persistence were not as significant as observed in the perennial flow experiments (e.g. dune in square A in Figure 6-2 a1) and well-formed dunes were presented alone or surrounded by channels. In contrast, in perennial environment (Figure 6-2 a3) the dunes were only presented on the upwind side of the river bank. Furthermore, the dune field densities were found to be higher than that in aeolian only conditions (Figure 6-2 a4).

It was also found that dune migration paths were influenced less by the fluvial process, in other words, it is easier for dunes to cross the river in an ephemeral environment. By comparing images a1 with a3 (Figure 6-2), some dunes were observed to be already in the channel or to have crossed the channel in ephemeral environments (e.g. dunes in rectangular B in Figure 6-2 a1) whereas no dunes ever crossed the channel but the channel has been forced away from the symmetry axis in downwind direction in perennial environments (Figure 6-2 a3). However, dunes can not only cross the river easily but also avulsions enable the river to change its course so that dune location changes relative to the river channel and appear to move upwind of the channel (Figure 6-2 a2).

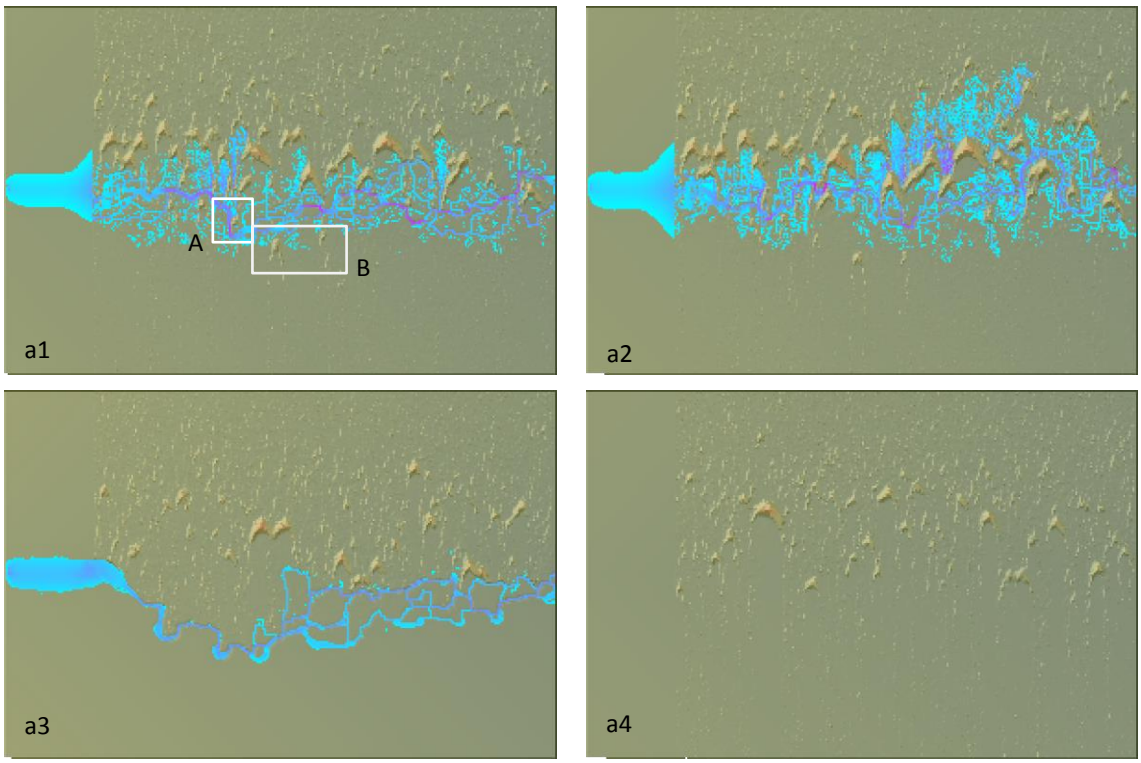

Figure 6-2 Dunes behaviours in fluvial-aeolian interacting field (D_c= 10m^3s^{-1}, R_s= 102$m^3m^{-1}yr^{-1}$). a1-a2) landform snapshots at year of 32 and 35 from scenario 2, respectively (2 continuous wet months and dry at the other time); a3) Perennial scenario (D_c= 10m^3s^{-1}, R_s= 102 $m^3m^{-1}yr^{-1}$, T=32 *yr*); a4) Dune field without flow (R_s= 102 $m^3m^{-1}yr^{-1}$, T=32 *yr*).

6.3.1.2 River evolution

Rivers were found to be less clearly defined in ephemeral scenario (Figure 6-3 and Appendix C for more information). When flowing through the dune field, water immediately filled the open spaces in the interdune areas if the previous channel course had become occupied or cut off by moving sand dunes. As a result, the channel pattern is primarily characterised by the distribution of discrete aeolian landforms rather than fluvial processes. The discontinuous channels appear to be constantly changing as they alternate between two primary modes of operation; either aggradation or degradation may become dominant. The blocked or abandoned channel segments formed many pools and lakes along the channel zone.

Moreover, the avulsion or channel migration events exhibited a higher frequency than was found for perennial simulations, with the channel course in each wet season becoming very unpredictable. Unlike the perennial scenarios where it might take decades or hundreds of years for large scale landform change events, it might take only few years under ephemeral conditions or may occur several times within one year.

For example in Figure 6-3, at year of 62 in scenario 2, a separate water course appeared only after 30 days in the wet seasons (a1 and a2). In the following year (year of 63), the previous new formed channel became the main channel but the previous main channel was nearly disappeared (Figure 6-3 b1). However, the new main channel moved to the middle of the field after the 60-days wet season through avulsion event (Figure 6-3 b2).

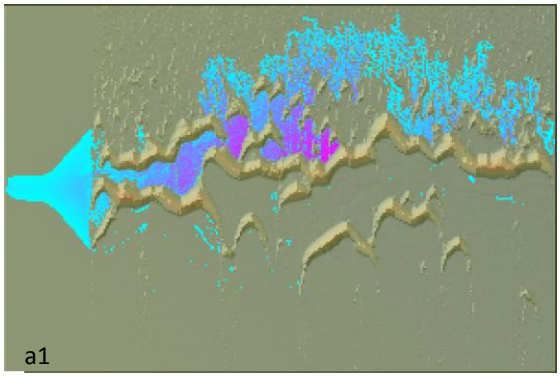

(T=22630d (62 *yr*), *i*=2263, run 2)
Water area at the beginning of one wet season.

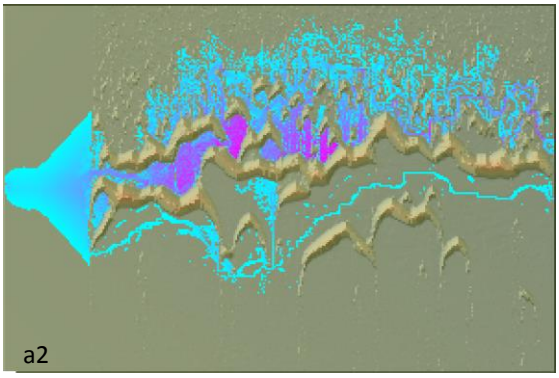

(T=22670d (62 *yr*), *i*=2267, run 2)
After around a month, another channel formed opposite to the main one.

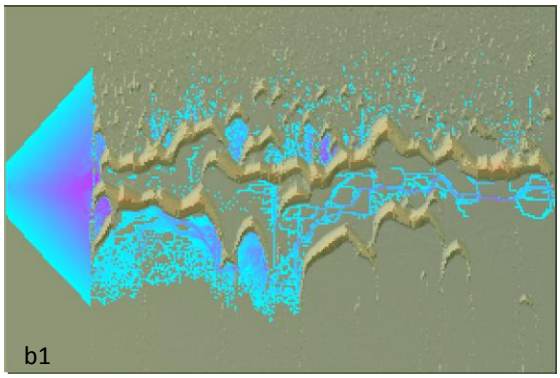

(T=23000d (63*yr*), *i*=2300, run 2)
At the beginning of next wet season, the previous smaller water course became the larger one whilst the previous main course was dried out leaving numerous pools and some lakes.

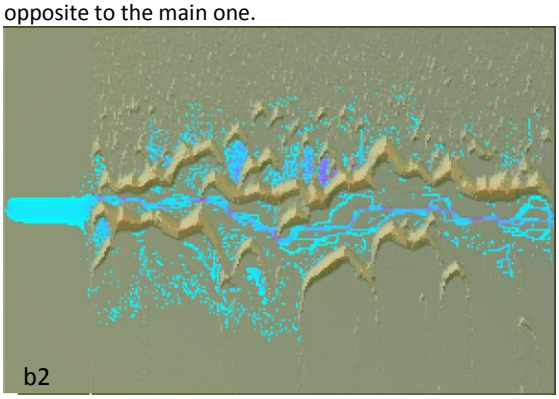

(T=23060d (63*yr*), *i*=2306, run 2)
However, at the end of this wet season (two months later), the new main channel at downwind direction moved to the middle of field, exhibited the *Balanced* interaction type, although there were many pools and lakes presented on both banks, some of them were far away from the present main channel.

Figure 6-3 Rivers behaviours in fluvial-aeolian interacting field (run 2, D_c = 10 m^3s^{-1}, R_s= 102 $m^3m^{-1}yr^{-1}$).

6.3.1.3 Geomorphological characteristics

The geomorphology in ephemeral environments exhibited some distinctive characteristics. Firstly, well-developed dunes were widespread in the field with small channels flowing around the dunes during wet seasons. For example, in the simulation image of Figure 6-2 a1, it exhibited a similar state in comparison with some cases in

field, for example, a site observed in Himalaya area from the preliminary global survey (Chapter3) (Figure 6-4 a1).

Secondly, landform changes were observed rapidly and frequently. The rapid changes of channel locations, such as the example shows in section 6.3.1.2, directly led to large scale landform changes. Moreover, this can be observed frequently throughout all of the simulations. These behaviours are very unlikely to occur in perennial environment simulations where it takes years to one major landform change (Chapter 5 Section 5.4.3.2).

Thirdly, there is a greater frequency of ponding and trench cutting and these features are more widely and uniformly distributed within the model space. The limited water resources were not enough to maintain the flow courses but were instead easily to be diverted into depressions or blocked in previous channel segments. The sand dunes, therefore, became a natural barrier creating numerous separate water bodies of different sizes (Figure 6-4 a2 and Appendix D for more information).

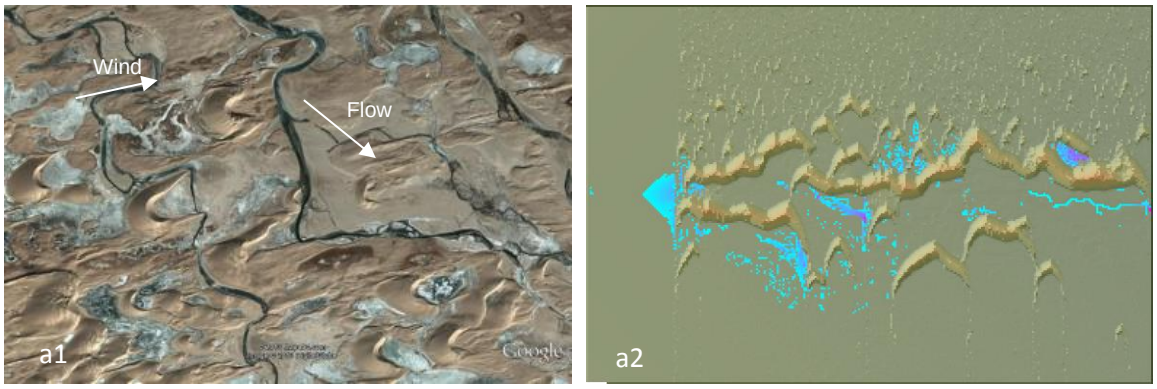

Figure 6-4 Distinctive landforms. a1) Himalaya, China (29°55'40.12" N 83°32'35.12" E); a2) landform after 3-months dry at year of 67.

6.3.2 Interaction types

In general, the interaction type between ephemeral river and dunes are characterised as *Alternating*, switching between fluvial and aeolian dominance when seasons changed. Even so, some features of other interaction types can still be observed under certain conditions. However, there is no *Fully aeolian dominant* (*FA*) interaction type has been observed even in the shortest wet season scenario (one-month wet duration in each year) in this study.

During dry seasons, the river channels dried up except for some small pools or lakes scattered through the dune field as described in section 6.3.1.3 above. These water bodies might or might not last until the next wet season, depending on the storage from previous wet season. Until these water residues had dried up, the areas around it would be affected as sand cannot pass across wet areas in this model configuration.

During wet seasons, the fluvial-aeolian interactions presented complex interaction types. Section 6.3.1.2 identified the unpredictability of the river channel location in each wet season, therefore only the *Alternating* classification from the static satellite images was found to be relevant in this modelled environment. For example, based on the definition of the interaction types, the river was located on the downwind side of the dune field at one time point of 230000-days (Figure 6-3 b1), the corresponding interaction type could be, therefore, characterised as *Mostly fluvial dominant* (*MF*), most of the dunes seemed have not been able to cross the channels. However, after 60 days of the wet period, the channel migrated to the middle of the field with similar dunes presented on both banks (Figure 6-3 b2), the corresponding interaction type at this time point was characterised as *Balanced*. But it was only a year ago, the interaction type exhibited in this land was neither *MF* nor *Balanced* (Figure 6-3 a1, a2). Such phenomena indicate that it is reasonable to set *Alternating* interaction type as one unique type separate from the other five types in terms of ephemeral environment.

6.3.3 Sediment yield

When observing the daily sediment outputs in any scenario, no obvious patterns can be seen. For example, Figure 6-5 presents the sediment output graphs from Group 2, where it can be seen that in scenario 2 it is difficult to identify the regularity from the whole process (Figure 6-5 a2). Focussing in on the first 10 years of the sediment outputs records in scenario 2, the discontinuous fluvial sediment outputs conrrespond to each wet season, and they stop transporting sediment out of the system during dry seasons (Figure 6-5 a1).

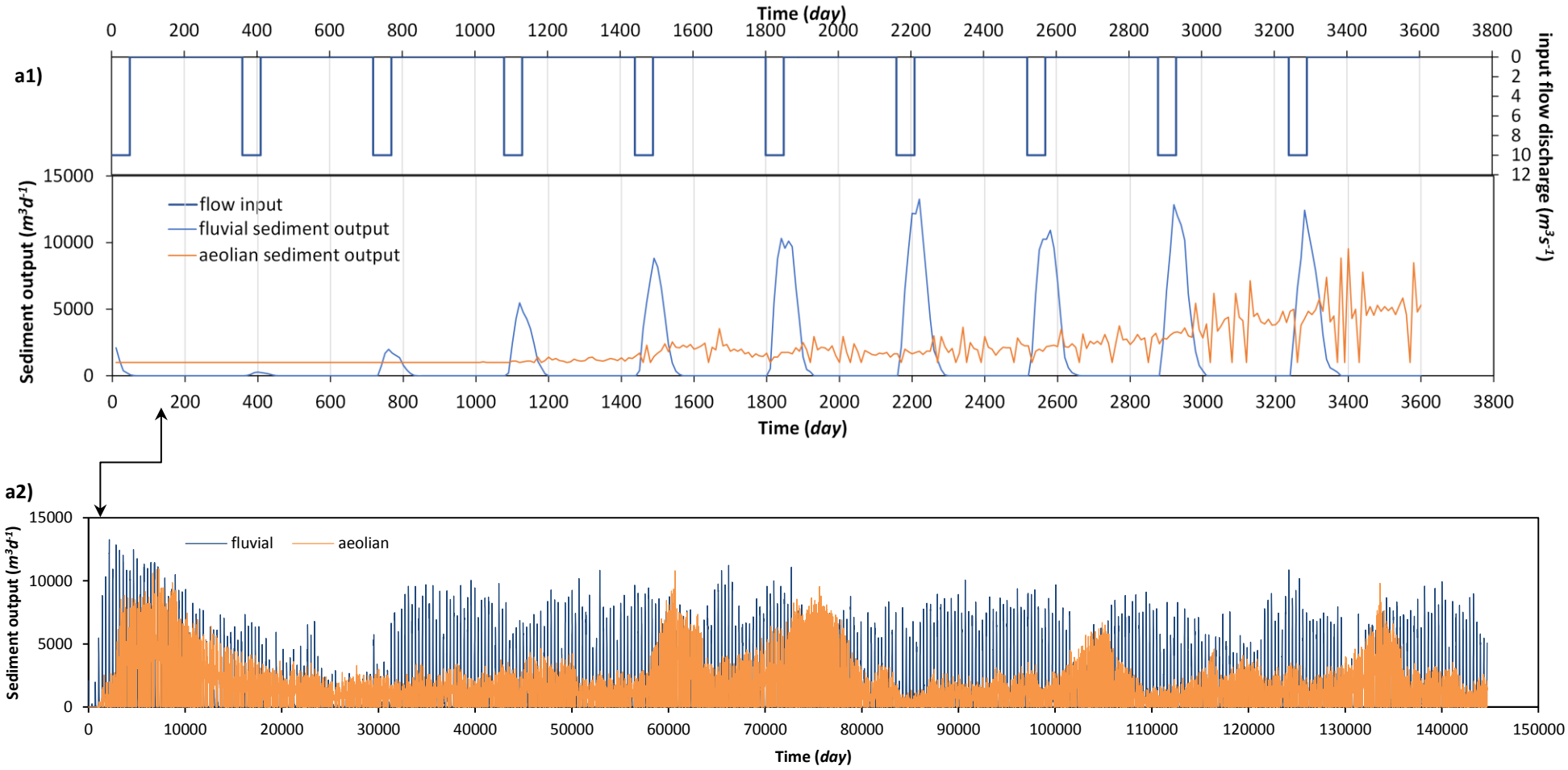

Figure 6-5 Daily sediment output from scenario 2 of group 2 tests. a1) Daily fluvial/aeolian sediment output and flow input during the first 10 years of simulation; a2) Daily fluvial/aeolian sediment output of the whole simulation.

Therefore the annual sediment yield of 20 runs was used to compare (results of all simulations are listed in Appendix E). In each run, relatively large amount of fluvial sediment output, in comparison with those in other periods, was commonly observed at the early stage of interaction. At this stage, the aeolian sediments were just starting to be introduced into the field and no obvious dunes had been formed, therefore, there were no large dune obstructions to disturb the river hydraulics and the sediments were easily transported. Following this period, there are no significant signals that can be observed from fluvial sediment yield in terms of landform change, some peaks of aeolian sediment output occur when large dunes move out of the field edge.

The average annual sediment yield of each group was listed in Table 6-3 and explored separately in Figure 6-6. Results of the three groups all show that the longer the wet duration, the higher sediment amount was transported out of the field by fluvial process. Moreover, group 2 shows a clear cross over where the amount of aeolian sediment transported exceeds that moved by fluvial processes until a threshold between 2 and 3 months of river flow.

Table 6-3 Average annual sediment output in each scenario of group 2 to 4.

No.	D_c (m^3s^{-1})	R_s ($m^3m^{-1}yr^{-1}$)	t (min)	T (day)	Seasonal scenarios	Average sediment output (m^3yr^{-1})	
						Aeolian	Fluvial
1	10	102	14400	130010	01	52643	28125
2	-	-	-	144700	02	59442	46973
3	-	-	-	123250	03	51213	59708
4	-	-	-	58400	04	46201	72504
5	-	-	-	122440	05	41428	84772
6	-	-	-	68370	06	20195	144038
7	20	-	-	59600	-	28474	124176
8	5	-	-	81245	-	45542	85723
9	10	-	-	81280	07	23089	62418
10	-	-	-	109490	08	24518	116250
11	-	-	-	118640	09	44168	129202
12	-	-	-	114790	10	29768	142544
13	-	-	-	125520	11	8647	176033
14	-	-	-	137700	12	58502	54725
15	-	-	-	123300	13	37086	75375
16	-	-	-	112980	14	42095	105869
17	-	-	-	93940	15	21700	112947
18	-	-	-	110240	16	39081	161762
19	-	-	-	146540	17	50277	54550
20	-	-	-	92260	18	51070	79180

N/B: - represents the value as same as the value above it.

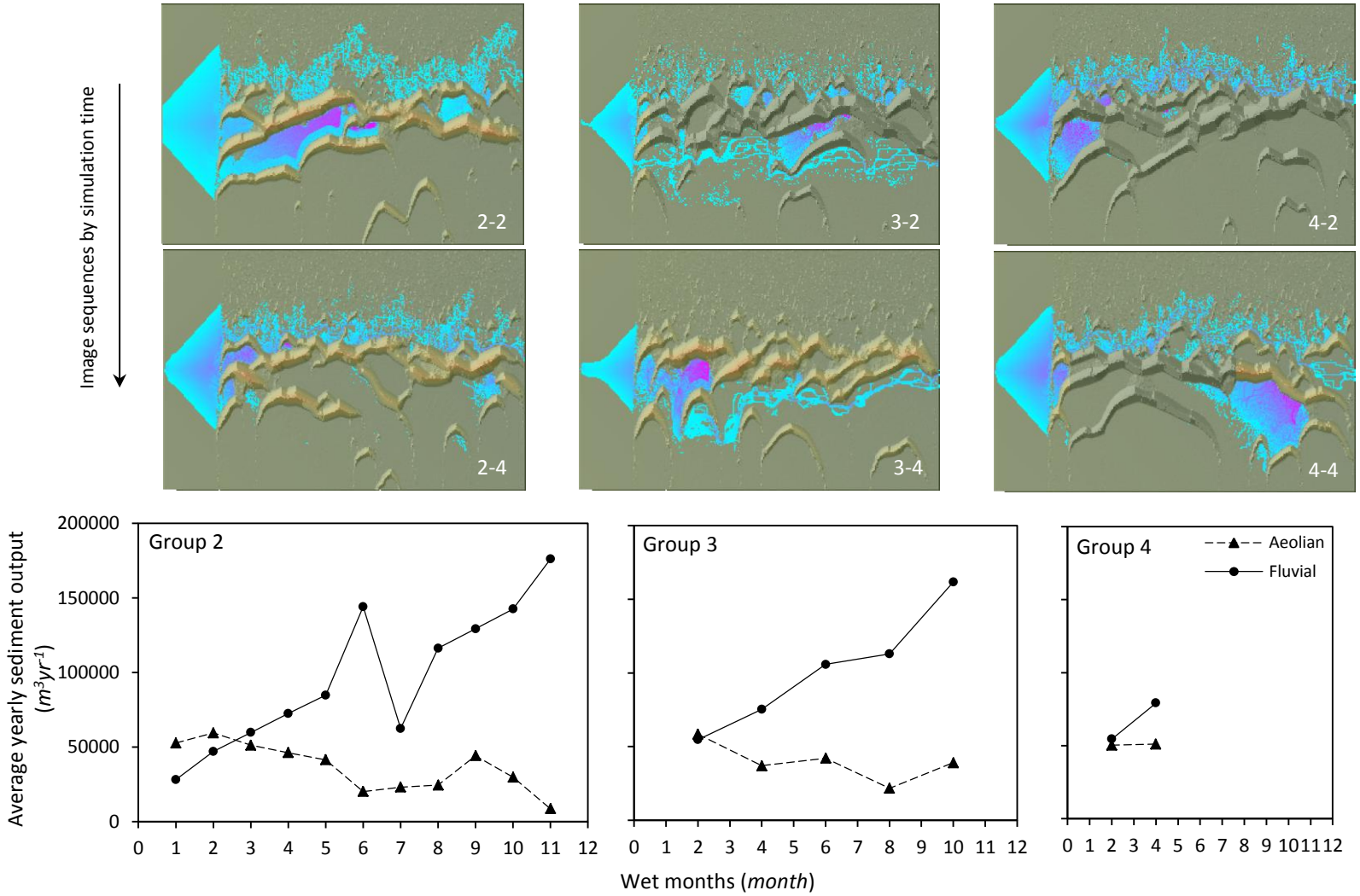

Figure 6-6 Sediment yield reflects landform change. The images show the landforms in runs of wet duration of 2 months and 4 months, separately, in each group.

It was also noticed that the sediment amount from run 2, 12 and 17 and run 4, 13 and 18 from group 2, 3 and 4, respectively, are very similar (Table 6-3 and Figure 6-6). The wet duration in run 2, 12 and 17 and run 4, 13 and 18 are two and four months per year, respectively, but with a different interval (as designed in the section 6.2.2). To observe the corresponding landform features, images from different runs are also illustrated in Figure 6-6. Image 2-2, 3-2 and 4-2 show the landforms developed under 2-months wet duration at different timing, whereas image 2-4, 3-4 and 4-4 show the landforms developed under 4-months wet duration at different timing. There are no great differences visible between the aeolian landforms, although the rivers were flowing through different locations.

6.4 Discussion

6.4.1 Thresholds between aeolian and fluvial processes

Under the seasonal influence, the sediment yields from fluvial and aeolian systems changed correspondingly. It was noticed that with less than three months of river flow, the aeolian model can move more sand than the fluvial - in group 2, the aeolian sediment output is less than that from the fluvial; whereas in group 3 and 4, the fluvial and aeolian sediment outputs are nearly equal (Figure 6-6). This switch over in sediment output indicates a shift between model states: with a shorter wet duration, the aeolian process can dominate over the fluvial. Thus the critical length of the wet duration could be the threshold value determining the dominant regime.

However, this critical threshold in ephemeral scenario is very different from the thresholds found in perennial scenario as presented in Chapter 5. In the perennial environment, it is the ratio between R_s and D_c that was found in association with the dominant regime; whereas in ephemeral environment, the ratio between R_s and D_c is fixed as each value retained the same in all simulations. This means the states in the ephemeral environment is simply determined by the seasons without the influence of the contrast between processes power. Furthermore, it is the wet duration rather than the timing of the seasonal change that has the impact on the critical states, as noted in result 6.3.3. This gives very important implication for field development. The 10 m^3s^{-1}

discharge used in the model is relatively low compared to those we might expect in an ephemeral environment, as reviewed in Chapter 2 (2.3.2.2), but these results suggest that even with higher ephemeral flows, the existence of a flow *duration* threshold provides the aeolian processes with an opportunity to be more dominant.

6.4.2 Geomorphology and landforms, and interaction types generated by ephemeral flows

Some distinctive interaction behaviours are observed which distinguish the fluvial-aeolian interactions in ephemeral environment from those in perennial environment. Though the river flow is alternating between wet and dry seasons, it seems that the role of aeolian process has been greatly enhanced, and correspondingly the fluvial processes are more likely to be affected by the aeolian process in ephemeral environments.

For the dunes, in ephemeral runs their shape was generally more uniform, and their development seems enhanced and they also appear to be better preserved. Furthermore, by comparing the images in Figure 6-2 it can be noticed that the dune field density in the ephemeral environment (a1 and a2) is slightly higher than in perennial environment (a3), or where the dune field is solely dominated by aeolian processes. Why does dune development appear to be improved because of the interaction with the ephemeral fluvial process? In theory this may be due to two factors, which whilst hypothetical and based on the modelled data, may be highlighting interesting patterns of aeolian/fluvial interaction processes. Firstly, there will be less direct interference from the river on the dune – for example by cutting across the trailing legs of barchans – or eroding their sides. Secondly, there is less interference with aeolian transport across the modelled domain – so sand supplies to dunes are less disrupted than they would be in perennial scenarios – where fluvial erosion/deposition and avulsion all alter aeolian supply and transport.

The relative boost in aeolian process afforded by ephemeral water flows increases their impact on rivers by having a stronger role in defining flow paths. Because of the dry seasons, there were more times for the aeolian system to operate without any interference from fluvial processes. For example, dunes reformed and crossed the dry channel beds. This had the additional impact of increasing the difficulty for flow to

resume through these channels. As it can be seen in image a1 or a2, the main channel was separated into small streams flowing around the dune baselines (Figure 6-2). This makes it hard to characterize the channel pattern as it is subject to the aeolian landform which is in dynamic development. However, the temporary break from dry seasons also gives the water an opportunity to find a new way to pass through the field easier, which not only increases the unpredictability of channel paths in each wet season, but also leads to the rapid change of channel location as Jones and Blakey (1997) have observed in south central Utah, USA (section 2.4.1).

The ephemeral flows also led to an increase in the avulsion rates. Dry periods allowed aeolian sand to accumulate on channel beds – blocking them and forcing the river to find a new course when the wet season came again. The frequency of the avulsions in ephemeral scenarios is much higher than in perennial examples. In the ephemeral environment, each wet season is an opportunity for river to select a new path, each dry season is an opportunity for dunes to move easier and transform the fluvial landform. The images presented in Figure 6-3 indicate that in the same scenario, new flow paths appeared in each year (in the 62nd year in images a1-a2, and in 63rd year in images a3-a4). The yearly alternating between wet and dry seasons thus provides much more opportunities for rapid landform change than in perennial environment where it takes years to have one catastrophic avulsion to occur (Chapter 5 section 5.4.3.2).

Furthermore, the frequent rapid change of channel locations and landform can sometimes result in the formation of a wetland environment. The rapid change of channel locations leaves numerous fragments of abandoned channels which fill with water each year. By selecting a new path, the river often unavoidably pours into many interdune spaces which turn out to be the termination points. The moving sand dunes could also block some streams and result in raised water tables, and lead to the formation of lakes or open water bodies of varying sizes. As a result, more pools and lakes are formed than in the perennial environment. Similar phenomena were seen in some field work, such as Loope et al. (1995) who have found that numerous distinct sites with thick marsh and lake sediments in north American were formed due to multiple blockages of sand dune systems during the Holocene.

The above switching between aeolian and fluvial behaviour illustrates the *Alternating* interaction type as defined in Chapter 3. Although the field also exhibited some features that can be seen in other types of interaction, such as the *Mostly aeolian dominant* (Figure 6-3 a1) or *Mostly fluvial dominant* (Figure 6-3 b1) or *Balanced* (Figure 6-3 b2) which are all characterised as *Transient* types as defined in Chapter 5, during wet seasons. However, these seemingly *Transient* interaction types do not reflect the dynamic process as the categories' titles indicated. They are not the results of the constant competition between fluvial and aeolian processes but the new selection of the fluvial system, and the chances are realised via the switching of wet/dry seasons. If the *Transient* interaction types cannot reflect the real dynamic process between ephemeral rivers and dunes then they are not applicable in the relevant environment, but only further support the unique characteristics and necessity of *Alternating* interaction type.

Although no features of *Fully aeolian dominant* interaction type has been observed in this experiment as expected, it is still a very possible type that can occur in ephemeral environment by changing the configuration of fluvial system, for example, the flow discharge, wet duration (e.g. less than a month simulated here) and boundary condition (spatial scale), etc. The likelihood of this interaction type happening can be supported from many field cases such as some channels in Namibia desert (Krapf et al., 2003), the Keriya and other rivers in Tarim desert (Rosso et al., 1991) (Figure 6-7).

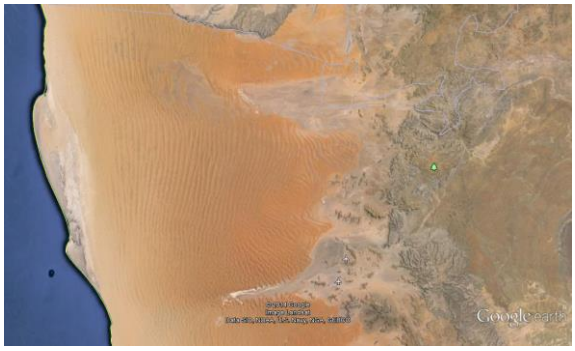

Rivers end in Namibia desert (24°15'02.08" S 15°34'41.07" E).

Keriya and other ephemeral rivers in Tarim desert, China (38°31'44.01" N 83°04'18.71" E).

Figure 6-7 Field cases where *Fully aeolian dominant* interaction type can be observed.

6.4.3 Sediment yield characteristics

As here sediment yields are summed into annual totals that we cannot see changes in sediment yield associated with different landforms or avulsions as shown in Chapter 5 (Figure 5-4). However, two clear findings emerge. Firstly that in terms of sediment output there is a wet duration threshold of 2-3 months above which fluvial processes dominate and below which aeolian prevail. Secondly, that in ephemeral environments the duration of the wet period is more important than the timing. As it was observed in Figure 6-6 in section 6.3.3, with same wet duration but at different timing, the fluvial sediment yield in each run is very close and their corresponding landforms are very similar to each other. It appears that a certain amount of water has certain sediment transport ability, and timing does not have much influence on flow sediment transportation. This suggests that the physics governing hydraulic processes in ephemeral rivers are the same as in other types of rivers, irrespective of flow periodicity (Nanson et al., 2002), such that the sediment outputs by certain hydrologic processes at different times of the year, and for varying durations are the same, and the longer the wet duration the higher the fluvial sediment transport amount, as seen in Table 6-3 and Figure 6-6.

6.5 Conclusions

In ephemeral scenarios, dunes can cross a river more easily than in perennial scenarios even when the flow discharge has been increased as much as two times higher (Figure 6-2). It is without doubt that the break of the flow in each year weakens the fluvial power, and also leaves more time to the dunes to cross the channel during dry seasons and creates more opportunities to the river to select a new path at the beginning of each wet season. These behaviours directly lead to frequent and rapid avulsions and landform changes indicated by the dune field density and the location of the channel. Landscape changes are characterised with more lakes, pools or broken trenches spreading among the aeolian landform, and the channel pattern is less confined to the traditional pattern categories such as straight, meander, braided, anastomosing, etc. (Figure 6-3) because it is more likely to be defined by the aeolian influence.

The interaction types observed in the field can only be classified as *Alternating* because of the intermittent interaction between fluvial and aeolian process - various interaction types can be observed during wet seasons but no interaction at all during dry seasons. Hence, the switching of dominance or the rapid landform change is intrinsic and mainly controlled by the seasonal changes.

By contrast to scenarios with perennial flows (Chapter 5), sediment outputs from both fluvial and aeolian systems in ephemeral contexts were not observed to be linked to either geomorphic events or landscape changes (Figure 6-6). Although a threshold was found from the sediment yield which can indicate the dominant regime, this does not seem to be reflected in a change of the geomorphology. This threshold is determined by the wet duration. In an environment that under the threshold, which means with less than certain length of wet duration, the aeolian process can transport more sediment than the fluvial. The fluvial/aeolian sediment output is proportional with the wet duration and has no association with the timing.

Chapter 7 Conclusions

7.1 Main conclusions

This study has observed the interactions between fluvial and aeolian systems from both static and dynamic perspectives by conducting a global survey and using a highly novel cellular aeolian/dune and fluvial model. The two approaches are adopted in an attempt to provide comprehensive insights into the nature of, and processes involved in, fluvial-aeolian interactions with respect to the five research questions raised after the literature review (as listed in section 2.6), including: 1) how fluvial-aeolian interactions affect landform evolution; 2) what the dominant environmental factors and geomorphic features that characterise these environments are; 3) a comprehensive classification of fluvial-aeolian interaction types that can reflect geomorphological characteristics and corresponding dynamic processes; 4) what numerical simulation can provide in addition to field observation; and 5) what threshold values are exceeded when dominant regimes shift.

The large scale field evaluation, based on current satellite imagery and the available literature provides a preliminary understanding that forms the basis for addressing the first three research questions. This survey identified 230 globally distributed sites where fluvial and aeolian systems interacted. Subsequently a comprehensive classification of fluvial-aeolian interaction types was successively undertaken (Chapter 3). At each site four variables were analysed to explore possible relationships between the fluvial and aeolian processes; these included dune type, channel pattern, meeting angle and interaction types. The worldwide distribution of sites investigated not only strongly supports the necessity for this type of study, but also provides basic information about the processes involved in the interactions.

The fluvial-aeolian interaction types classified in the field investigation were identified based on the modern environmental context, which provide the initial references for evaluating geomorphological characteristics and corresponding dynamic regimes (research questions 1 and 3). This classification includes six types of interaction, namely *Fully fluvial dominant* (*FF*), *Mostly fluvial dominant* (*MF*), *Balanced* (*B*), *Mostly*

aeolian dominant (*MA*), *Fully aeolian dominant* (*FA*) and Alternating (*Al*). In *Fully fluvial dominant* (*FF*) regime, as the category name suggests, fluvial processes are great enough to transport all of the sediment input from the dune fields, so the geomorphological characteristics shown as dunes are located only on the upwind side of river, with the river acting as a barrier to dune movement; in *Mostly fluvial dominant* (*MF*) regime, dunes are present on both sides of the river but are smaller on the downwind side of the river due to sediment depletion. The river flows through the dune field with little or no changes in the channel course.

In the *Balanced* (*B*) regime, the river flows through the dune field and dunes of similar sizes can be observed on both sides of the river channel. There are no obvious changes in channel width/length/location and dune type/size. In *Mostly aeolian dominant* (*MA*) regimes, the power of aeolian action increases above that of fluvial action, so the geomorphological characteristics are shown as the river flows through the dune field but notable changes on channel width/length/location are observed. The channel may be pushed across in the direction of aeolian transport and/or partially obstructed by dunes. In *Fully aeolian dominant* (*FA*) regimes, dunes block or terminate the river. The river flows into the dune field but its path is blocked by sand dunes which prevent it from flowing further. Whereas in the Alternating (*Al*) regime, the dominance alternates seasonally between fluvial and aeolian processes over short timescales (monthly to annually), e.g. dunes may occupy the dry ephemeral/intermittent river bed during dry seasons but are eroded by water flow during wet seasons.

Statistical analysis of the global investigation has demonstrated significant relationships between four variables: meeting angle – dune type, meeting angle – interaction type and channel pattern – interaction type (research question 2). These relationships indicate that active river channel patterns (braided and wandering) are most common in environments where aeolian or fluvial processes dominate, but they are less likely when the fluvial and aeolian systems are in balance with each other. An unexpected outcome was that there is no relationship between more dynamic crescentic dune systems and channel patterns, indicating that additional aeolian sediment supply does not control channel pattern, an observation that contrasts to some previous studies where high sediment input is thought to be the main, or at least the most important, factor influencing changing channel patterns (Smith and Smith,

1984; Huisink, 2000). Furthermore, longitudinal dunes tend to move parallel with river flow direction, whereas more active crescentic dunes were more often found migrating perpendicular to river flow. This suggests there may be some self-organisation operating between dune type and river flow direction. Because the most frequent dune types are found to be crescentic (Barchans and Transverse ridges: 73%), and their most common meeting angle is perpendicular, these were further investigated using a unique combined fluvial and aeolian morphodynamic model to study the dynamic interactions between dunes and rivers.

To address the last two research questions a dune model based on Werner's (1995) algorithm (DECAL) was modified and validated. This was undertaken in order to enable integration of the DECAL model with the CAESAR-Lisflood flow model (Coulthard *et al.*, 2013) (Chapter 4). The modified DECAL model can successively simulate various sizes of barchan and transverse dunes and subsequent dune field patterns by controlling the sand transport rate. The dynamic fluvial process is controlled mainly by the flow discharge and the in-channel erosion mode parameters in the flow model. The coupled flow-dune model can generate both landscape evolution imagery and fluvial/aeolian sediment output records for analysing the dynamic interactions between fluvial and aeolian processes. Two types of fluvial regime – perennial and ephemeral – were simulated at the initial stages of the current study into fluvial-aeolian interactions.

The simulation results were largely consistent with the field survey observations (research questions 4) (Chapter 5 and 6). The fluvial-aeolian interaction behaviours of the six geomorphological landscape types identified in the mapping survey were all observed during the simulations of perennial/ephemeral scenarios, although the *Fully Aeolian dominant* (*FA*) regime is not clearly identified, which may be due to the fact that the FA scenario only occurs for short durations in time. The model results presented in Table 5-3 show a high frequency of *Fully fluvial dominant* (*FF*) or *Mostly fluvial dominant* (*MF*) interaction types, which means there are no or few dunes observed on the river bank on the downwind side, even with very low discharge levels, e.g. 1 or 3 m^3s^{-1}. This result is also consistent with the field survey results, where a greater frequency of fluvial dominance (26% of *FF* and 20% of *MF*) as opposed to aeolian dominance (17% of *FA* and 14% of *MA*) (Figure 3-7 d) is in evidence.

Furthermore, the results from the simulations also provide complementary insights into the dynamics of the fluvial-aeolian interaction processes and how the interactions influence landform evolution (research questions 1 to 4). Firstly, the simulated river patterns correspond to the high frequency of wandering and braided channel patterns as seen in the mapping survey. Secondly, the low frequency of aeolian dominant landform types identified from the global survey (*Fully aeolian dominant* (*FA*) and *Mostly aeolian dominant* (*MA*): 35%) (Figure 3-7d) suggests that it is not easy for dunes to cross river channels, and the simulation results also show a similar pattern of behaviour. Dunes were observed to cross the channel more easily in ephemeral rather than perennial scenarios. Whilst hypothetical and based on the modelled data, this may be due to the dry seasons which enable greater time for dune movement without disturbance from fluvial processes, which thus enhances the impact of aeolian processes. Also, the alternating seasons may provide more opportunities for the river to select a new flow path, which is shorter and results in unpredictable and rapid changes in channel location, without any trigger events such as avulsion, which is required in perennial environments. The redistribution of sediment from fluvial processes then further enhances dune development in ephemeral scenarios.

Thirdly, if the dunes were seen to be able to cross the river, there are two possible processes observed to achieve this result. One possible process is that the dunes that crossed the river are newly formed dunes – it is the sediments redistributed by flood/alluvial deposits which supply material for the formation of new dunes on the downwind side of a river. The other possible process is that the dunes are 'old' dunes but presented on the downwind side of river as a result of channel diversion – the dune movements keep pushing and blocking the river channel in the downwind direction to the extent that channel avulsion occurs; the river may then adopt a new channel on the upwind part of the simulation domain where less dense, smaller sized dunes occur. However, the existence of an active channel has no influence on dune type and the direction of movement in the simulations due to the perpendicular interacting angle simulated in this study. This reinforces the observation made in some studies, which have shown that the perpendicular approach angle between wind and valley is not usually affected by existing channel (Bullard et al., 2000; Wiggs et al., 2002).

In particular, the processes observed in the model simulations improve our understanding of the development of the 'balanced' interaction type seen in the global survey (research questions 3 and 4). The balanced type in the model was found to be transient (Chapter 5), in which the landscape was alternately dominated by *Mostly Fluvial* (*MF*), *Balanced* (*B*) and *Mostly Aeolian* (*MA*) interaction types (*Transient* types). Therefore, the model landscape dominated by the *Transient* types could be considered to be in dynamic equilibrium, and the *Balanced* interaction type classified in Chapter 3 is more like a morpho-equilibrium state. The consistency between the field observations and numerical simulations suggests that various process stages in a dynamic system have modern analogues that are visible in snapshots from the field.

Another important finding from the current study is that there is cyclicity in landform evolution under the influence of fluvial-aeolian interactions (research questions 1 and 4). It was seen that without any external drivers the simulation results presented an unexpected cyclic behaviour of abrupt large scale landscape change where river channels would avulse around dunes significantly altering the river/dune configuration and affecting sediment output. Normally, where an abrupt or major landscape change occurs, the explanations are linked to the influence of external factors such as climate change, tectonics or even human activities. Such assumptions may lead to researchers overlooking the possibility that large scale landform instability may be inherent and driven by the internal forces of a system in dynamic equilibrium. Hence, this study suggests that a sudden landscape change may be normal in the development of a fluvial-aeolian interacting system without any external forcing. If we can identify a cyclicity or metric to describe this behaviour we may start to use this to explain some hydrological, sedimentological and stratigraphic anomalies in aeolian environments and thereby improve the ability of researchers to identify unstable landforms and to predict their change.

A significant result from this study is that there are threshold values in perennial and ephemeral environments, which answers the fifth research question. In the perennial scenario, the ratio of flow discharge and aeolian sand transport rate (R_s/D_c) was found to be associated with different dominant regimes and the subsequent geomorphology. For example, in scenarios with the flow discharge is 5 m^3s^{-1}, two threshold limits α_{5a} and α_{5b} were identified which defined the borders of different dominated regimes

(section 5.3.3.2). As illustrated in Figure 5-5, the dominant regime changes from *Fully Fluvial* (*FF*) to *Mostly Fluvial* (*MF*) and then switches between the three *Transient* types with the decreasing R_s and increasing D_c, which is corresponding to the reduced ratio α (R_s/D_c). The threshold limits in different environments are various in relation to the ratios of flow discharge to aeolian sand transport rate, and the trend of the threshold limits borders are indicated in Figure 5-6. In contrast, for ephemeral environments, the ratio of R_s/D_c was fixed, but the dominant regime was found to be associated with seasonal durations of flow regardless of when the channel flows (timing). In scenarios with flow discharge is 10 m^3s^{-1} but with different wet durations, 3 months of wet duration is found to be the critical period when the dominant regime shifts between fluvial and aeolian systems (Figure 6-6). Similiarly, the threshold value of wet duration in different environmental settings will be various. As long as the total wet duration is below the threshold value, the aeolian processes can transport more sediment than the fluvial processes, although no association has been found between the threshold and geomorphological changes.

7.2 Future work

The study presented in this thesis provides a first step towards understanding the fluvial-aeolian interaction processes and their impact on geomorphology. However, this work could be further developed and will certainly be useful for studying more complicated process and predictions. For example, longer simulation times and more geomorphic measurement work may be helpful to quantify more geomorphological behaviour and identify key threshold values. These thresholds may be at transitions between different behaviours – as well as focused on the cyclicity of avulsions. Exploring different model configurations is also a good potential line of enquiry, such as changing of the meeting angle, dune types, DEM and fluvial/aeolian forcing. The perpendicular meeting angle used in this study means that the relationships between dune type and meeting angle, and interaction types and meeting angle have not been tested and the results from Chapter 3 suggest these may be important in the distribution of landform types. Longitudinal dunes could be also added to the simulations in further studies. Moreover, the stable flow discharge and aeolian sediment transport rate applied in current study could be changed to being unstable,

e.g. by adding a sediment control parameter in the model which has been experimented with during the model development, but not reported in this thesis. Introducing this unsteadiness may make the simulations more realistic.

Another important contribution to this field of study would be to undertake fieldwork to investigate specific cases of fluvial-aeolian interaction. This could be used to help validate the simulation results and improve the modelling of these natural processes.

References

Ackers, P., Charlton, F., 1970. The geometry of small meandering streams. ICE Proceedings, Thomas Telford80.

Ahlbrandt, T.S., Fryberger, S.G., 1981. Sedimentary features and significance of interdune deposits. In: F.G. Etheridge, R.M. Flores (Eds.), Recent and ancient nonmarine depositional environments: models for exploration. Society of Economic Paleontologists and Mineralogists, Tulsa, pp. 293-314.

Ahnert, F., 1976. Brief description of a comprehensive three-dimensional process-response model of landform development. Z. Geomorphol. Suppl, 25, 29-49.

Al-Masrahy, M.A., Mountney, N.P., 2013. Remote sensing of spatial variability in aeolian dune and interdune morphology in the Rub' Al-Khali, Saudi Arabia. Aeolian Research, 11(0), 155-170.

Alabyan, A.M., Chalov, R.S., 1998. Types of river channel patterns and their natural controls. Earth Surface Processes and Landforms, 23(5), 467-474.

Andreotti, B., Claudin, P., Douady, S., 2002. Selection of dune shapes and velocities Part 1: Dynamics of sand, wind and barchans. The European Physical Journal B - Condensed Matter and Complex Systems, 28(3), 321-339.

Ardon, K., Tsoar, H., Blumberg, D.G., 2009. Dynamics of nebkhas superimposed on a parabolic dune and their effect on the dune dynamics. Journal of Arid Environments, 73(11), 1014-1022.

Attal, M., Tucker, G.E., Whittaker, A.C., Cowie, P.A., Roberts, G.P., 2008. Modeling fluvial incision and transient landscape evolution: Influence of dynamic channel adjustment. Journal of Geophysical Research: Earth Surface, 113(F3), F03013.

Baas, A.C.W., 2002. Chaos, fractals and self-organization in coastal geomorphology: simulating dune landscapes in vegetated environments. Geomorphology, 48(1–3), 309-328.

Baas, A.C.W., Nield, J.M., 2007. Modelling vegetated dune landscapes. Geophysical Research Letters, 34(6), L06405.

Bagnold, R.A., 1935. The Movement of Desert Sand. The Geographical Journal, 85(4), 342-365.

Bagnold, R.A., 1941. *The physics of blown sand and desert dunes*. Methuen, London.

Bailey, S.D., Bristow, C.S., 2004. Migration of parabolic dunes at Aberffraw, Anglesey, north Wales. Geomorphology, 59(4), 165-174.

Barchyn, T.E., Hugenholtz, C.H., 2012. A new tool for modeling dune field evolution based on an accessible, GUI version of the Werner dune model. Geomorphology, 138(1), 415-419.

Barnes, J., 2001. Barchan duens on the Kuiseb River delta, Namibia. South African Geographical Journal, 83(3), 283-292.

Barrows, T.T., Williams, M.A.J., Mills, S.C., Duller, G.A.T., Fifield, L.K., Haberlah, D., Tims, S.G., Williams, F.M., 2014. A White Nile megalake during the last interglacial period. Geology, 42(2), 163-166.

Bates, P.D., Horritt, M.S., Fewtrell, T.J., 2010. A simple inertial formulation of the shallow water equations for efficient two-dimensional flood inundation modelling. Journal of Hydrology, 387(1–2), 33-45.

Beadnell, H.J.L., 1910. The Sand-Dunes of the Libyan Desert. Their Origin, Form, and Rate of Movement, Considered in Relation to the Geological and Meteorological Conditions of the Region. The Geographical Journal, 35(4), 379-392.

Beveridge, C., Kocurek, G., Ewing, R.C., Lancaster, N., Morthekai, P., Singhvi, A.K., Mahan, S.A., 2006. Development of spatially diverse and complex dune-field patterns: Gran Desierto Dune Field, Sonora, Mexico. Sedimentology, 53(6), 1391-1409.

Bishop, S.R., Momiji, H., Carretero-Gonz, #225, lez, R., Warren, A., 2002. Modelling desert dune fields based on discrete dynamics. Discrete Dynamics in Nature and Society, 7(1), 7-17.
Bledsoe, B.P., Watson, C.C., 2001. Logistic analysis of channel pattern thresholds: meandering, braiding, and incising. Geomorphology, 38(3–4), 281-300.
Bourke, M.C., 2002. Aeolian-fluvial interaction at paleoflood termini in central Australia, 10th ANZGG meeting, Kalgoorlie.
Bourke, M.C., 2010. Barchan dune asymmetry: Observations from Mars and Earth. Icarus, 205(1), 183-197.
Bourke, M.C., Ewing, R.C., Finnegan, D., McGowan, H.A., 2009. Sand dune movement in the Victoria Valley, Antarctica. Geomorphology, 109(3-4), 148-160.
Bourke, M.C., Pickup, G., 1999. Fluvial form variability in arid central Australia. In: A.J. Miller, A. Gupta (Eds.), Varieties of fluvial form. Wiley, Chichester, pp. 249-271.
Braun, J., Sambridge, M., 1997. Modelling landscape evolution on geological time scales: a new method based on irregular spatial discretization. Basin Research, 9(1), 27-52.
Breed, C.S., Grow, T., 1979. Morphology and distribution of dunes in sand seas observed by remote sensing, United States Geological Survey, Professional Paper.
Breed, C.S., McCauley, J.F., Davis, P.A., 1987. Sand sheets of the eastern Sahara and ripple blankets on Mars. Geological Society, London, Special Publications, 35(1), 337-359.
Bristow, C.S., Lancaster, N., Duller, G.A.T., 2005. Combining ground penetrating radar surveys and optical dating to determine dune migration in Namibia. Journal of the Geological Society, 162(2), 315-321.
Brunsden, D., Thornes, J.B., 1979. Landscape Sensitivity and Change. Transactions of the Institute of British Geographers, 4(4), 463-484.
Bull, L.J., Kirkby, M.J., 2002. Dryland river characteristics and concepts. In: L.J. Bull, M.J. Kirkby (Eds.), Dryland rivers; hydrology and geomorphology of semi-arid channels. Wiley, Chichester, pp. 3-15.
Bullard, J.E., Livingstone, I., 2002. Interactions between aeolian and fluvial systems in dryland environments. Area, 34(1), 8-16.
Bullard, J.E., McTainsh, G.H., 2003. Aeolian-fluvial interactions in dryland environments: examples, concepts and Australia case study. Progress in Physical Geography, 27(4), 471-501.
Bullard, J.E., Nash, D.J., 1998. Linear dune pattern variability in the vicinity of dry valleys in the southwest Kalahari. Geomorphology, 23(1), 35-54.
Bullard, J.E., Wiggs, G.F.S., Nash, D.J., 2000. Experimental study of wind directional variability in the vicinity of a model valley. Geomorphology, 35(1–2), 127-143.
Carson, M.A., Kirkby, M.J., 1972. Hillslope form and process.
Charlton, R., 2008. Fundamentals of Fluvial Geomorphology. Routledge, London and New York.
Chen, X.Y., 1995. Geomorphology, stratigraphy and thermoluminescence dating of the lunette dune at Lake Victoria, western New South Wales. Palaeogeography, Palaeoclimatology, Palaeoecology, 113(1), 69-86.
Church, M., 1983. Pattern of Instability in a Wandering Gravel Bed Channel, Modern and Ancient Fluvial Systems. Blackwell Publishing Ltd., pp. 169-180.
Church, M., Hassan, M.A., 1992. Size and distance of travel of unconstrained clasts on a streambed. Water Resources Research, 28(1), 299-303.
Cooke, R.U., Warren, A., Goudie, A.S., 1993. Desert Geomorphology. Taylor & Francis.
Coulthard, T., Macklin, M., 2001. How sensitive are river systems to climate and land‐use changes? A model‐based evaluation. Journal of Quaternary Science, 16(4), 347-351.
Coulthard, T.J., 2001. Landscape evolution models: a software review. Hydrological Processes, 15(1), 165-173.
Coulthard, T.J., Hancock, G.R., Lowry, J.B.C., 2012. Modelling soil erosion with a downscaled landscape evolution model. Earth Surface Processes and Landforms, 37(10), 1046-1055.

Coulthard, T.J., Kirkby, M.J., Macklin, M.G., 2000. Modelling geomorphic response to environmental change in an upland catchment. Hydrological Processes, 14(11-12), 2031-2045.

Coulthard, T.J., Macklin, M.G., 2003. Modeling long-term contamination in river systems from historical metal mining. Geology, 31(5), 451-454.

Coulthard, T.J., Macklin, M.G., Kirkby, M.J., 2002. A cellular model of Holocene upland river basin and alluvial fan evolution. Earth Surface Processes and Landforms, 27(3), 269-288.

Coulthard, T.J., Neal, J.C., Bates, P.D., Ramirez, J., de Almeida, G.A.M., Hancock, G.R., 2013. Integrating the LISFLOOD-FP 2D hydrodynamic model with the CAESAR model: implications for modelling landscape evolution. Earth Surface Processes and Landforms, 38(15), 1897-1906.

Coulthard, T.J., Van De Wiel, M.J., 2007. Quantifying fluvial non linearity and finding self organized criticality? Insights from simulations of river basin evolution. Geomorphology, 91(3–4), 216-235.

Coulthard, T.J., Van De Wiel, M.J., 2012. Modelling river history and evolution. Philosophical Transactions of the Royal Society A: Mathematical,
Physical and Engineering Sciences, 370(1966), 2123-2142.

Coulthard, T.J., Wiel, M.J.V.D., 2006. A cellular model of river meandering. Earth Surface Processes and Landforms, 31(1), 123-132.

Croke, J.C., Magee, J.M., Price, D.M., 1998. Stratigraphy and sedimentology of the lower Neales River, West Lake Eyre, Central Australia: from Palaeocene to Holocene. Palaeogeography, Palaeoclimatology, Palaeoecology, 144(3–4), 331-350.

Cudden, J.R., Hoey, T.B., 2003. The causes of bedload pulses in a gravel channel: the implications of bedload grain-size distributions. Earth Surface Processes and Landforms, 28(13), 1411-1428.

Daniel, G.B., Alan, F.A., 2007. Digital photogrammetric change analysis as applied to active coastal dunes in Michigan.

David Knighton, A., Nanson, G.C., 1993. Anastomosis and the continuum of channel pattern. Earth Surface Processes and Landforms, 18(7), 613-625.

del Valle, H.F., Rostagno, C.M., Coronato, F.R., Bouza, P.J., Blanco, P.D., 2008. Sand dune activity in north-eastern Patagonia. Journal of Arid Environments, 72(4), 411-422.

Dong, Z., Chen, G., Yan, C., Han, Z., Wang, x., 1998. The sand dune movement along the Tarm desert oil-transportation highway. 18(4), 328-333. (in Chinese).

Dong, Z., Wang, X., Chen, G., 2000. Monitoring sand dune advance in the Taklimakan Desert. Geomorphology, 35(3-4), 219-231.

Draut, A.E., 2012. Effects of river regulation on aeolian landscapes, Colorado River, southwestern USA. Journal of Geophysical Research: Earth Surface, 117(F2), F02022.

Durán, O., Parteli, E.J.R., Herrmann, H.J., 2010. A continuous model for sand dunes: Review, new developments and application to barchan dunes and barchan dune fields. Earth Surface Processes and Landforms, 35(13), 1591-1600.

Durán, O., Schwämmle, V., Lind, P., Herrmann, H., 2009. The dune size distribution and scaling relations of barchan dune fields. Granular Matter, 11(1), 7-11.

Durán, O., Schwämmle, V., Lind, P.G., Herrmann, H.J., 2011. Size distribution and structure of Barchan dune fields. Nonlinear Processes In Geophysics, 4(8), 455-467.

Eastwood, E., Nield, J., Baas, A., Kocurek, G., 2011. Modelling controls on aeolian dune-field pattern evolution. Sedimentology, 58(6), 1391-1406.

Einstein, H.A., 1950. The bed-load function for sediment transportation in open channel flows. US Department of Agriculture.

El-Bana, M.I., Nijs, I., Khedr, A.-H.A., 2003. The Importance of Phytogenic Mounds (Nebkhas) for Restoration of Arid Degraded Rangelands in Northern Sinai. Restoration Ecology, 11(3), 317-324.

El-Baz, F., Maingue, M., Robinson, C., 2000. Fluvio-aeolian dynamics in the north-eastern Sahara: the relationship between fluvial/aeolian systems and ground-water concentration. Journal of Arid Environments, 44(2), 173-183.

Elbelrhiti, H., Andreotti, B., Claudin, P., 2008. Barchan dune corridors: Field characterization and investigation of control parameters. J. Geophys. Res., 113(F2), F02S15.

Evans, I.S., 2003. Scale-specific landforms and aspects of the land surface. Terrapub.

Ewing, R.C., Kocurek, G., 2010a. Aeolian dune-field pattern boundary conditions. Geomorphology, 114(3), 175-187.

Ewing, R.C., Kocurek, G., Lake, L.W., 2006. Pattern analysis of dune-field parameters. Earth Surface Processes and Landforms, 31(9), 1176-1191.

Ewing, R.C., Kocurek, G.A., 2010b. Aeolian dune interactions and dune-field pattern formation: White Sands Dune Field, New Mexico. Sedimentology, 57(5), 1199-1219.

Farraj, A.A., Harvey, A.M., 2004. Late Quaternary interactions between aeolian and fluvial processes: a case study in the northern UAE. Journal of Arid Environments, 56(2), 235-248.

Ferguson, R.I., Werritty, A., 1983. Bar Development and Channel Changes in the Gravelly River Feshie, Scotland, Modern and Ancient Fluvial Systems. Blackwell Publishing Ltd., pp. 181-193.

Field, J.P., Breshears, D.D., Whicker, J.J., 2009. Toward a more holistic perspective of soil erosion: Why aeolian research needs to explicitly consider fluvial processes and interactions. Aeolian Research, 1(1-2), 9-17.

Finkel, H.J., 1959. The Barchans of Southern Peru. The Journal of Geology, 67(6), 614-647.

Fryberger, S.G., 1979. dune forms and wind regimes. In: E.D. McKee (Ed.), A Study of Global Sand Seas. U.S. Government Printing Office.

Fryberger, S.G., Al-Sari, A.M., Clisham, T.J., Rizvi, S.A.R., Al-Hinai, K.G., 1984. Wind sedimentation in the Jafurah sand sea, Saudi Arabia. Sedimentology, 31(3), 413-431.

Garvey, B., Castro, I., Wiggs, G., Bullard, J., 2005. Measurements of Flows Over Isolated Valleys. Boundary-Layer Meteorol, 117(3), 417-446.

Gaylord, D.R., Stetler, L.D., 1994. Aeolian-climatic thresholds and sand dunes at the Hanford site, south-central Washington, U.S.A. Journal of Arid Environments, 28(2), 95-116.

Gibling, M.R., Nanson, G.C., Maroulis, J.C., 1998. Anastomosing river sedimentation in the Channel Country of central Australia. Sedimentology, 45(3), 595-619.

Glennie, K., Pugh, J., Goodall, T., 1994. Late quaternary Arabian desert models of Permian Rotliegend reservoirs. Exploration Bulletin, 274, 1-19.

Gomez, B., Church, M., 1989. An assessment of bed load sediment transport formulae for gravel bed rivers. Water Resources Research, 25(6), 1161-1186.

Good, T.R., Bryant, I.D., 1985. Fluvio-aeolian sedimentation: an example from Banks Island, N. W. T., Canada. Geografiska Annaler. Series A, Physical Geography, 67(1/2), 33-46.

Goren, L., Willett, S.D., Herman, F., Braun, J., 2014. Coupled numerical–analytical approach to landscape evolution modeling. Earth Surface Processes and Landforms, 39(4), 522-545.

Goudie, A.S., 2013. Arid and semi-arid geomorphology. Cambridge University Press, New York.

Goudie, A.S., Colls, A., Stokes, S., Parker, A., White, K., Al-Farraj, A., 2000. Latest Pleistocene and Holocene dune construction at the north-eastern edge of the Rub Al Khali, United Arab Emirates. Sedimentology, 47(5), 1011-1021.

Greenbaum, N., Schwartz, U., Benito, G., Porat, N., Cloete, G.C., Enzel, Y., 2014. Paleohydrology of extraordinary floods along the Swakop River at the margin of the Namib Desert and their paleoclimate implications. Quaternary Science Reviews, 103(0), 153-169.

Habersack, H.M., 2001. Radio-tracking gravel particles in a large braided river in New Zealand: a field test of the stochastic theory of bed load transport proposed by Einstein. Hydrological Processes, 15(3), 377-391.

Hack, J.T., 1941. Dunes of the Western Navajo Country. Geographical Review, 31(2), 240-263.

Hailiang, X., Mao, Y., Yudong, S., 2005. The dynamic variation of water resources and its tendency in the Tarim River Basin. Journal of Geographical Sciences, 15(4), 467-474.

Hajek, E.A., Edmonds, D.A., 2014. Is river avulsion style controlled by floodplain morphodynamics? Geology.

Hamby, D.M., 1994. A review of techniques for parameter sensitivity analysis of environmental models. Environ Monit Assess, 32(2), 135-154.

Han, G., Zhang, G., Dong, Y., 2007. A model for the active origin and development of source-bordering dunefields on a semiarid fluvial plain: A case study from the Xiliaohe Plain, Northeast China. Geomorphology, 86(3–4), 512-524.

Hancock, G.R., Lowry, J.B.C., Coulthard, T.J., Evans, K.G., Moliere, D.R., 2010. A catchment scale evaluation of the SIBERIA and CAESAR landscape evolution models. Earth Surface Processes and Landforms, 35(8), 863-875.

Hancock, G.R., Willgoose, G.R., Evans, K.G., 2002. Testing of the SIBERIA landscape evolution model using the Tin Camp Creek, Northern Territory, Australia, field catchment. Earth Surface Processes and Landforms, 27(2), 125-143.

Harrison, Yair, 1998. Late Pleistocene aeolian and fluvial interactions in the development of the Nizzana dune field, Negev Desert, Israel. Sedimentology, 45(3), 507-518.

Havholm, K.G., Kocurek, G., 1988. A preliminary study of the dynamics of a modern draa, Algodones, southeastern California, USA. Sedimentology, 35(4), 649-669.

Haynes Jr, C.V., 1989. Bagnold's barchan: A 57-yr record of dune movement in the eastern Sahara and implications for dune origin and paleoclimate since Neolithic times. Quaternary Research, 32(2), 153-167.

He, Q., Walling, D.E., Owens, P.N., 1996. Interpreting the 137Cs profiles observed in several small lakes and reservoirs in southern England. Chemical Geology, 129(1–2), 115-131.

Helton, J.C., Johnson, J.D., Sallaberry, C.J., Storlie, C.B., 2006. Survey of sampling-based methods for uncertainty and sensitivity analysis. Reliability Engineering & System Safety, 91(10–11), 1175-1209.

Hermas, E.A., elMagd, I.H.A., K.AlHarbi, measurement of sand dune movements using the Sub-pixel correlation of aster images: a premininary results from North sinai, Egypt.

Herrmann, H.J., Sauermann, G., SchwÃ¤mmle, V., 2005. The morphology of dunes. Physica A: Statistical Mechanics and its Applications, 358(1 SPEC. ISS.), 30-38.

Hersen, P., 2004. On the crescentic shape of barchan dunes. The European Physical Journal B - Condensed Matter and Complex Systems, 37(4), 507-514.

Hersen, P., Andersen, K.H., Elbelrhiti, H., Andreotti, B., Claudin, P., Douady, S., 2004. Corridors of barchan dunes: Stability and size selection. Physical Review E, 69(1), 011304.

Hersen, P., Douady, S., Andreotti, B., 2002. Relevant Length Scale of Barchan Dunes. Physical Review Letters, 89(26), 264301.

Hesp, P.A., Arens, S.M., 1997. Crescentic dunes at Schiermonnikoog, The Netherlands.

Hesp, P.A., Hastings, K., 1998. Width, height and slope relationships and aerodynamic maintenance of barchans. Geomorphology, 22(2), 193-204.

Hesse, P.P., Simpson, R.L., 2006. Variable vegetation cover and episodic sand movement on longitudinal desert sand dunes. Geomorphology, 81(3-4), 276-291.

Hesse, R., 2009a. Do swarms of migrating barchan dunes record paleoenvironmental changes? — A case study spanning the middle to late Holocene in the Pampa de Jaguay, southern Peru. Geomorphology, 104(3–4), 185-190.

Hesse, R., 2009b. Using remote sensing to quantify aeolian transport and estimate the age of the terminal dune field Dunas Pampa Blanca in southern Peru. Quaternary Research, 71(3), 426-436.

Hollands, C.B., Nanson, G.C., Jones, B.G., Bristow, C.S., Price, D.M., Pietsch, T.J., 2006. Aeolian–fluvial interaction: evidence for Late Quaternary channel change and wind-rift linear dune formation in the northwestern Simpson Desert, Australia. Quaternary Science Reviews, 25(1–2), 142-162.

Holliday, V.T., 1997. Origin and Evolution of Lunettes on the High Plains of Texas and New Mexico. Quaternary Research, 47(1), 54-69.

Howard, A.D., Morton, J.B., Gad-el-hak, M., Pierce, D.B., 1978. Sand transport model of barchan dune equilibrium. Sedimentology, 25, 307-338.

Hugenholtz, C.H., Levin, N., Barchyn, T.E., Baddock, M.C., 2012. Remote sensing and spatial analysis of aeolian sand dunes: A review and outlook. Earth-Science Reviews, 111(3–4), 319-334.

Huggett, R., 2007. Fundamentals of geomorphology. Routledge.

Huisink, M., 2000. Changing river styles in response to Weichselian climate changes in the Vecht valley, eastern Netherlands. Sedimentary Geology, 133(1–2), 115-134.

Hunter, R.E., Richmond, B.M., Rho Alpha, T., 1983. Storm-controlled oblique dunes of the Oregon coast. Geological Society of America Bulletin, 94(12), 1450-1465.

Jerolmack, D.J., Paola, C., 2007. Complexity in a cellular model of river avulsion. Geomorphology, 91(3–4), 259-270.

Jones, L.S., Blakey, R.C., 1997. Eolian-fluvial interaction in the Page Sandstone (Middle Jurassic) in south-central Utah, USA — a case study of erg-margin processes. Sedimentary Geology, 109(1–2), 181-198.

Jones, L.S., Schumm, S.A., 2009. Causes of avulsion: an overview, Fluvial Sedimentology VI. Blackwell Publishing Ltd., pp. 169-178.

Kadlec, J., Kocurek, G., Mohrig, D., Shinde, D.P., Murari, M.K., Varma, V., Stehlík, F., Beneš, V., Singhvi, A.K., 2015. Response of fluvial, aeolian, and lacustrine systems to late Pleistocene to Holocene climate change, Lower Moravian Basin, Czech Republic. Geomorphology, 232(0), 193-208.

Kar, A., Felix, C., Rajaguru, S.N., Singhvi, A.K., 1998. Late Holocene growth and mobility of a transverse dune in the Thar Desert. Journal of Arid Environments, 38(2), 175-185.

Khalaf, F.I., Al-Ajmi, D., 1993. Aeolian processes and sand encroachment problems in Kuwait. Geomorphology, 6(2), 111-134.

Kirkby, M.J., 1978. The stream head as a significant geomorphic threshold. School of Geography, University of Leeds, Leeds.

Klaus, K., Sebastian, F., Benedikt, O., 2005. The shape of barchan dunes. Journal of Physics: Condensed Matter, 17(14), S1229.

Kleinhans, M., van Rijn, L., 2002. Stochastic Prediction of Sediment Transport in Sand-Gravel Bed Rivers. Journal of Hydraulic Engineering, 128(4), 412-425.

Knighton, A.D., Nanson, G.C., 1994. Waterholes and their significance in the anastomosing channel system of Cooper Creek, Australia. Geomorphology, 9(4), 311-324.

Knighton, D., 2014. Fluvial forms and processes: a new perspective. Routledge.

Kocurek, G., Carr, M., Ewing, R., Havholm, K.G., Nagar, Y.C., Singhvi, A.K., 2007. White Sands Dune Field, New Mexico: Age, dune dynamics and recent accumulations. Sedimentary Geology, 197(3–4), 313-331.

Kocurek, G., Ewing, R.C., 2005. Aeolian dune field self-organization – implications for the formation of simple versus complex dune-field patterns. Geomorphology, 72(1–4), 94-105.

Kocurek, G., Ewing, R.C., Mohrig, D., 2010. How do bedform patterns arise? New views on the role of bedform interactions within a set of boundary conditions. Earth Surface Processes and Landforms, 35(1), 51-63.

Kocurek, G., Lancaster, N., 1999. Aeolian system sediment state: theory and Mojave Desert Kelso dune field example. Sedimentology, 46(3), 505-515.

Krapf, C.B.E., Stollhofen, H., Stanistreet, I.G., 2003. Contrasting styles of ephemeral river systems and their interaction with dunes of the Skeleton Coast erg (Namibia). Quaternary International, 104(1), 41-52.

Kroy, K., Sauermann, G., Herrmann, H.J., 2002. Minimal model for sand dunes. Physical Review Letters, 88(5), 543011-543014.

Lancaster, N., 1982. Dunes on the skeleton coast, Namibia (South West Africa): Geomorphology and grain size relationships. Earth Surface Processes and Landforms, 7(6), 575-587.

Lancaster, N., 1985. Variations in wind velocity and sand transport on the windward flanks of desert sand dunes. Sedimentology, 32(4), 581-593.
Lancaster, N., 1989. The dynamics of star dunes: an example from the Gran Desierto, Mexico. Sedimentology, 36(2), 273-289.
Lancaster, N., 1995. *Geomorphology of desert dunes*. Routledge, London.
Lancaster, N., 2008. Desert dune dynamics and development: insights from luminescence dating. Boreas, 37(4), 559-573.
Lancaster, N. (Ed.), 2011. Desert dune processes and dynamics. Arid zone geomorphology: process, form, and change in drylands. Wiley.
Lancaster, N., Nickling, W.G., Neuman, C.K.M., Wyatt, V.E., 1996. Sediment flux and airflow on the stoss slope of a barchan dune. Geomorphology, 17(1-3), 55-62.
Langford, R.P., 1989. Fluvial-aeolian interactions: Part I, modern systems. Sedimentology, 36(6), 1023-1035.
Langford, R.P., Chan, M.A., 1989. Fluvial-aeolian interactions: Part II, ancient systems. Sedimentology, 36(6), 1037-1051.
Lenzi, M.A., Mao, L., Comiti, F., 2003. Interannual variation of suspended sediment load and sediment yield in an alpine catchment. Hydrological Sciences Journal, 48(6), 899-915.
Leopold, L.B., Wolman, M.G., 1957. River channel patterns: braided, meandering and straight. Geological Survey professional paper;no. 282-B. U.S. Dept. of the Interior, Washington.
Li, S., Dong, G., Shen, J., Yang, P., Liu, X., Wang, Y., Jin, H., Wang, Q., 1999. Formation mechanism and development pattern of aeolian sand landform in Yarlung Zangbo River valley. Science in China Series D: Earth Sciences, 42(3), 272-284.
Lima, A.R., Sauermann, G., Herrmann, H.J., Kroy, K., 2002. Modelling a dune field. Physica A: Statistical Mechanics and its Applications, 310(3-4), 487-500.
Link, S.O., Waugh, W.J., Downs, J.L., Thiede, M.E., Chatters, J.C., Gee, G.W., 1994. Effects of coppice dune topography and vegetation on soil water dynamics in a cold-desert ecosystem. Journal of Arid Environments, 27(3), 265-278.
Liu, B., Coulthard, T., 2014. Mapping the interactions between rivers and sand dunes-implications for fluvial and aeolian geomorphology. Geomorphology.
Liu, L.Y., Skidmore, E., Hasi, E., Wagner, L., Tatarko, J., 2005. Dune sand transport as influenced by wind directions, speed and frequencies in the Ordos Plateau, China. Geomorphology, 67(3-4), 283-297.
Livingstone, I., 1989. Monitoring surface change on a Namib linear dune. Earth Surface Processes and Landforms, 14(4), 317-332.
Livingstone, I., 2003. A twenty-one-year record of surface change on a Namib linear dune. Earth Surface Processes and Landforms, 28(9), 1025-1031.
Livingstone, I., 2012. Aeolian geomorphology of the Namib Sand Sea. Journal of Arid Environments(0).
Livingstone, I., Wiggs, G.F.S., Weaver, C.M., 2007. Geomorphology of desert sand dunes: A review of recent progress. Earth-Science Reviews, 80(3-4), 239-257.
Long, J.T., Sharp, R.P., 1964. Barchan-dune movement in Imperial Valley, California. Geological Society of America Bulletin, 75(2), 149-156.
Loope, D.B., Swinehart, J.B., Mason, J.P., 1995. Dune-dammed paleovalleys of the Nebraska Sand Hills: Intrinsic versus climatic controls on the accumulation of lake and marsh sediments. Geological Society of America Bulletin, 107(4), 396-406.
Mabbutt, J.A., 1977. Desert landforms. MIT Press.
Mainguet, M., 1984. A classification of dunes based on aeolian dynamics and the sand budget. Deserts and arid lands, 31-58.
Marín, L., Forman, S.L., Valdez, A., Bunch, F., 2005. Twentieth century dune migration at the Great Sand Dunes National Park and Preserve, Colorado, relation to drought variability. Geomorphology, 70(1â€“2), 163-183.

Maroulis, J.C., Nanson, G.C., Price, D.M., Pietsch, T., 2007. Aeolian–fluvial interaction and climate change: source-bordering dune development over the past ~100ka on Cooper Creek, central Australia. Quaternary Science Reviews, 26(3–4), 386-404.

Martin, Y., Church, M., 2004. Numerical modelling of landscape evolution: geomorphological perspectives. Progress in Physical Geography, 28(3), 317-339.

McIntosh, R.J., 1983. Floodplain Geomorphology and Human Occupation of the Upper Inland Delta of the Niger. The Geographical Journal, 149(2), 182-201.

McKee, E.D., 1979. A Study of Global Sand Seas. U.S. Government Printing Office.

McKee, E.D., Douglass, J.R., 1971. Growth and Movement of Dunes at White Sands National Monument, New Mexico U.S. Geological Survey Professional Paper 750-D, D108–D114.

Melton, F.A., 1940. A tentative classification of sand dunes its application to dune history in the Southern High Plains. The Journal of Geology, 48(2), 113-174.

Miao, X., Hanson, P.R., Wang, H., Young, A.R., 2010. Timing and origin for sand dunes in the Green River Lowland of Illinois, upper Mississippi River Valley, USA. Quaternary Science Reviews, 29(5–6), 763-773.

Mingxiang, M.E.I., Bingsong, Y.U., Weiguang, J.I.N., 2004. Sequence Stratigraphy of the Desert System: A Case Study of the Lower Cretaceous in the Kuqa Basin in Xinjiang, Northwestern China. Acta Geologica Sinica - English Edition, 78(3), 744-755.

Momiji, H., Carretero-González, R., Bishop, S.R., Warren, A., 2000. Simulation of the effect of wind speedup in the formation of transverse dune fields. Earth Surface Processes and Landforms, 25(8), 905-918.

Momiji, H., Warren, A., 2000. Relations of sand trapping efficiency and migration speed of transverse dunes to wind velocity. Earth Surface Processes and Landforms, 25(10), 1069-1084.

Mountney, N., Howell, J., Flint, S., Jerram, D., 1998. Aeolian and alluvial deposition within the Mesozoic Etjo Sandstone Formation, northwest Namibia. Journal of African Earth Sciences, 27(2), 175-192.

Mousavi, S.H., Dorgouie, M., Vali, A.A., Pourkhosravani, M., Ameri, A.R.A., 2010. Statistical Modeling of Morphological Parameters of Barchan Dunes (Case Study: Chah Jam Erg in South of Haj Ali GHoli Playa, in Central Part of Semnan Province, IRAN). Journal of Geography and Geology, 2(1), 98-113.

Muhs, D.R., Reynolds, R.L., Been, J., Skipp, G., 2003. Eolian sand transport pathways in the southwestern United States: importance of the Colorado River and local sources. Quaternary International, 104(1), 3-18.

Muhs, D.R., Swinehart, J.B., Loope, D.B., Been, J., Mahan, S.A., Bush, C.A., 2000. Geochemical Evidence for an Eolian Sand Dam across the North and South Platte Rivers in Nebraska. Quaternary Research, 53(2), 214-222.

Muleta, M.K., Nicklow, J.W., 2005. Sensitivity and uncertainty analysis coupled with automatic calibration for a distributed watershed model. Journal of Hydrology, 306(1–4), 127-145.

Mulligan, K.R., 1988. Velocity profiles measured on the windward slope of a transverse dune. Earth Surface Processes and Landforms, 13(7), 573-582.

Muñoz-Perez, J.J., Navarro, M., Roman-Sierra, J., Tejedor, B., Rodriguez, I., Gomez-Pina, G., 2009. Long-term evolution of a transgressive migrating dune using reconstruction of the EOF method. Geomorphology, 112(1â€“2), 167-177.

Murray, A.B., Paola, C., 1994. A cellular model of braided rivers. Nature, 371(6492), 54-57.

Murray, A.B., Paola, C., 1997. Properties of a cellular braided ‐ stream model. Earth Surface Processes and Landforms, 22(11), 1001-1025.

Nanson, G.C., Knighton, A.D., 1996. ANABRANCHING RIVERS: THEIR CAUSE, CHARACTER AND CLASSIFICATION. Earth Surface Processes and Landforms, 21(3), 217-239.

Nanson, G.C., Tooth, S., Knighton, A.D., 2002. A global perspective on dryland rivers: perceptions, misconceptions and distinctions, 388. John Wiley and Sons: Chichester.

Narteau, C., Zhang, D., Rozier, O., Claudin, P., 2009. Setting the length and time scales of a cellular automaton dune model from the analysis of superimposed bed forms. Journal of Geophysical Research: Earth Surface, 114(F3), F03006.

Navarro, M., Muñoz-Pérez, J.J., Román-Sierra, J., Tsoar, H., Rodríguez, I., Gómez-Pina, G., 2011. Assessment of highly active dune mobility in the medium, short and very short term. Geomorphology, 129(1-2), 14-28.

Neal, J., Villanueva, I., Wright, N., Willis, T., Fewtrell, T., Bates, P., 2012. How much physical complexity is needed to model flood inundation? Hydrological Processes, 26(15), 2264-2282.

Necsoiu, M., Leprince, S.b., Hooper, D.M., Dinwiddie, C.L., McGinnis, R.N., Walter, G.R., 2009. Monitoring migration rates of an active subarctic dune field using optical imagery. Remote Sensing of Environment, 113(11), 2441-2447.

Newell, A.J., 2001. Bounding surfaces in a mixed aeolian–fluvial system (Rotliegend, Wessex Basin, SW UK). Marine and Petroleum Geology, 18(3), 339-347.

Nicholas, A.P., 2005. Cellular modelling in fluvial geomorphology. Earth Surface Processes and Landforms, 30(5), 645-649.

Nickling, W.G., Wolfe, S.A., 1994. The morphology and origin of Nabkhas, Region of Mopti, Mali, West Africa. Journal of Arid Environments, 28(1), 13-30.

Nield, J.M., Baas, A.C.W., 2008. Investigating parabolic and nebkha dune formation using a cellular automaton modelling approach. Earth Surface Processes and Landforms, 33(5), 724-740.

Nielson, J., Kocurek, G., 1987. Surface processes, deposits, and development of star dunes: Dumont dune field, California. Geological Society of America Bulletin, 99(2), 177-186.

Nishimori, H., Ouchi, N., 1993. Formation of ripple patterns and dunes by wind-blown sand. Physical Review Letters, 71(1), 197-200.

Nishimori, H., Yamasaki, M., Andersen, K.H., 1998. A simple model for the various pattern dynamics of dunes. International Journal of Modern Physics B, 12(3), 257-272.

Norris, R.M., 1966. Barchan Dunes of Imperial Valley, California. The Journal of Geology, 74(3), 292-306.

Ojeda, J., Vallejo, I., Malvarez, G.C., 2005. Morphometric evolution of the active dunes system of the Doñana National Park, Southern Spain (1977-1999) Journal of Coastal Research, 40-45.

Ouchi, N.B., Nishimori, H., 1995. Modeling of wind-blown sand using cellular automata. Physical Review E, 52(6), 5877-5880.

Ould Ahmedou, D., Ould Mahfoudh, A., Dupont, P., Ould El Moctar, A., Valance, A., Rasmussen, K.R., 2007. Barchan dune mobility in Mauritania related to dune and interdune sand fluxes. Journal of Geophysical Research: Earth Surface, 112(F2), F02016.

Parker, G., 1990. Surface-based bedload transport relation for gravel rivers. Journal of Hydraulic Research, 28(4), 417-436.

Parker, G., Dhamotharan, S., Stefan, H., 1982. Model experiments on mobile, paved gravel bed streams. Water Resources Research, 18(5), 1395-1408.

Parker Gay Jr, S., 1999. Observations regarding the movement of barchan sand dunes in the Nazca to Tanaca area of southern Peru. Geomorphology, 27(3â€“4), 279-293.

Parsons, D.R., Wiggs, G.F.S., Walker, I.J., Ferguson, R.I., Garvey, B.G., 2004. Numerical modelling of airflow over an idealised transverse dune. Environmental Modelling & Software, 19(2), 153-162.

Parteli, E.J.R., Durán, O., Herrmann, H.J., 2007. Minimal size of a barchan dune. Physical Review E, 75(1), 011301.

Parteli, E.J.R., Schwämmle, V., Herrmann, H.J., Monteiro, L.H.U., Maia, L.P., 2006. Profile measurement and simulation of a transverse dune field in the Lençóis Maranhenses. Geomorphology, 81(1–2), 29-42.

Pelletier, J.D., 2004. Persistent drainage migration in a numerical landscape evolution model. Geophys. Res. Lett., 31(20), L20501.

Pelletier, J.D., 2009. Controls on the height and spacing of eolian ripples and transverse dunes: A numerical modeling investigation. Geomorphology, 105(3–4), 322-333.
Peterov II, M., 1959. The mineral components and genesis of the aeolian sand on the Ordos, in eastern Alaxan and the middle reaches of the Yellow River. 25, 1-20. (in Russian).
Phillips, J.D., 2003. Sources of nonlinearity and complexity in geomorphic systems. Progress in Physical Geography, 27(1), 1-23.
Price, W.A., 1950. Saharan Sand Dunes and the Origin of the Longitudinal Dune: A Review. Geographical Review, 40(3), 462-465.
Ramsey, M.S., Christensen, P.R., Lancaster, N., Howard, D.A., 1999. Identification of sand sources and transport pathways at the Kelso Dunes, California, using thermal infrared remote sensing. Geological Society of America Bulletin, 111(5), 646-662.
Refice, A., Giachetta, E., Capolongo, D., 2012. SIGNUM: A Matlab, TIN-based landscape evolution model. Computers & Geosciences, 45(0), 293-303.
Reid, I., Laronne, J.B., Powell, D.M., 1998. Flash-flood and bedload dynamics of desert gravel-bed streams. Hydrological Processes, 12(4), 543-557.
Rendell, H.M., Clarke, M.l.L., Warren, A., Chappell, A., 2003. The timing of climbing dune formation in southwestern Niger: fluvio-aeolian interactions and the role of sand supply. Quaternary Science Reviews, 22(10-13), 1059-1065.
Rice, S.P., Church, M., Wooldridge, C.L., Hickin, E.J., 2009. Morphology and evolution of bars in a wandering gravel-bed river; lower Fraser river, British Columbia, Canada. Sedimentology, 56(3), 709-736.
Robinson, C.A., El-Baz, F., Al-Saud, T.S.M., Jeon, S.B., 2006. Use of radar data to delineate palaeodrainage leading to the Kufra Oasis in the eastern Sahara. Journal of African Earth Sciences, 44(2), 229-240.
Roskin, J., Porat, N., Tsoar, H., Blumberg, D.G., Zander, A.M., 2011. Age, origin and climatic controls on vegetated linear dunes in the northwestern Negev Desert (Israel). Quaternary Science Reviews, 30(13–14), 1649-1674.
Rosso, R., Bacchi, B., La Barbera, P., 1991. Fractal relation of mainstream length to catchment area in river networks. Water Resources Research, 27(3), 381-387.
Rust, B.R., 1972. STRUCTURE AND PROCESS IN A BRAIDED RIVER. Sedimentology, 18(3-4), 221-245.
Sauermann, G., Andrade, J.S., Maia, L.P., Costa, U.M.S., Araújo, A.D., Herrmann, H.J., 2003. Wind velocity and sand transport on a barchan dune. Geomorphology, 54(3-4), 245-255.
Sauermann, G., Rognon, P., Poliakov, A., Herrmann, H.J., 2000. The shape of the barchan dunes of Southern Morocco. Geomorphology, 36(1–2), 47-62.
Schatz, V., Herrmann, H.J., 2006. Flow separation in the lee side of transverse dunes: A numerical investigation. Geomorphology, 81(1–2), 207-216.
Schneider, C.A., Rasband, W.S., Eliceiri, K.W., 2012. NIH Image to ImageJ: 25 years of image analysis. Nature methods, 9(7), 671-675.
Schumm, S.A., 1979. Geomorphic Thresholds: The Concept and Its Applications. Transactions of the Institute of British Geographers, 4(4), 485-515.
Schumm, S.A., 1981. Evolution and response of the fluvial system, sedimentologic implications.
Schumm, S.A., 1985. Patterns of Alluvial Rivers. Annual Review of Earth and Planetary Sciences, 13(1), 5-27.
Sharp, R.P., 1963. Wind Ripples. The Journal of Geology, 71(5), 617-636.
Sierputowski, P., Ostrowski, J., Cenedese, A., 1995. Experimental study of wind flow over the model of a valley. Journal of Wind Engineering and Industrial Aerodynamics, 57(2–3), 127-136.
Simons, F.S., 1956. A Note on Pur-Pur Dune, Virú Valley, Peru. The Journal of Geology, 64(5), 517-521.
Slingerland, R., Smith, N.D., 2004. River avulsions and their deposits. Annual Review of Earth and Planetary Sciences, 32(1), 257-285.

Smith, N.D., Smith, D.G., 1984. William River: An outstanding example of channel widening and braiding caused by bed-load addition. Geology, 12(2), 78-82.
Stokes, S., Bray, H.E., 2005. Late Pleistocene eolian history of the Liwa region, Arabian Peninsula. Geological Society of America Bulletin, 117(11-12), 1466-1480.
Sweet, M.L., Nielson, J., Havholm, K., Farrelley, J., 1988. Algodones Dune Field of Southeastern California - Case-History of a Migrating Modern Dune Field. Sedimentology, 35(6), 939-952.
Telfer, M.W., Thomas, D.S.G., 2006. Complex Holocene lunette dune development, South Africa: Implications for paleoclimate and models of pan development in arid regions. Geology, 34(10), 853-856.
Tengberg, A., Chen, D., 1998. A comparative analysis of nebkhas in central Tunisia and northern Burkina Faso. Geomorphology, 22(2), 181-192.
Thomas, D.S.G., 1991. Arid geomorphology. Progress in Physical Geography, 15(2), 157-163.
Thomas, D.S.G., Stokes, S., Shaw, P.A., 1997. Holocene aeolian activity in the southwestern Kalahari Desert, southern Africa: significance and relationships to late-Pleistocene dune-building events. The Holocene, 7(3), 273-281.
Thomas, D.S.G., Tsoar, H., 1990. The geomorphological role of vegetation in desert dune systems. In J.B. Thornes (ed.), Vegetation and Erosion, 471-489.
Thoms, M.C., Sheldon, F., 2000. Water resource development and hydrological change in a large dryland river: the Barwon–Darling River, Australia. Journal of Hydrology, 228(1–2), 10-21.
Tooth, S., 2000. Process, form and change in dryland rivers: a review of recent research. Earth-Science Reviews, 51(1–4), 67-107.
Tricart, J., 1965. Rapport de la Mission de Reçonnaissance Géomorphologique de la Vallée Moyenne du Niger (Janvier-Avril 1957).
Troendle, C.A., Wilcox, M.S., Bevenger, G.S., Porth, L.S., 2001. The Coon Creek Water Yield Augmentation Project: implementation of timber harvesting technology to increase streamflow. Forest Ecology and Management, 143(1–3), 179-187.
Tsoar, H., 1983. Dynamic processes acting on a longitudinal (seif) sand dune. Sedimentology, 30(4), 567-578.
Tsoar, H., Blumberg, D.G., 2002. Formation of parabolic dunes from barchan and transverse dunes along Israel's Mediterranean coast. Earth Surface Processes and Landforms, 27(11), 1147-1161.
Tsoar, H., Blumberg, D.G., Stoler, Y., 2004. Elongation and migration of sand dunes. Geomorphology, 57(3–4), 293-302.
Tsoar, H., Moller, J.T., 1986. The role of vegetation in the formation of linear sand dunes.
Tucker, G.E., Bras, R.L., 2000. A stochastic approach to modeling the role of rainfall variability in drainage basin evolution. Water Resources Research, 36(7), 1953-1964.
Tucker, G.E., Hancock, G.R., 2010. Modelling landscape evolution. Earth Surface Processes and Landforms, 35(1), 28-50.
Tucker, G.E., Slingerland, R.L., 1994. Erosional dynamics, flexural isostasy, and long-lived escarpments: A numerical modeling study. Journal of Geophysical Research: Solid Earth, 99(B6), 12229-12243.
Turcotte, D.L., 1997. Fractals and chaos in geology and geophysics. Cambridge university press, New York.
Van Boxel, J.H., Arens, S.M., Van Dijk, P.M., 1999. Aeolian processes across transverse dunes. I: Modelling the air flow. Earth Surface Processes and Landforms, 24(3), 255-270.
Van De Wiel, M.J., Coulthard, T.J., 2010. Self-organized criticality in river basins: Challenging sedimentary records of environmental change. Geology, 38(1), 87-90.
Van De Wiel, M.J., Coulthard, T.J., Macklin, M.G., Lewin, J., 2007. Embedding reach-scale fluvial dynamics within the CAESAR cellular automaton landscape evolution model. Geomorphology, 90(3–4), 283-301.

Van De Wiel, M.J., Coulthard, T.J., Macklin, M.G., Lewin, J., 2011. Modelling the response of river systems to environmental change: Progress, problems and prospects for palaeo-environmental reconstructions. Earth-Science Reviews, 104(1–3), 167-185.

van den Berg, J.H., 1995. Prediction of alluvial channel pattern of perennial rivers. Geomorphology, 12(4), 259-279.

Van Dijk, P.M., Arens, S.M., Van Boxel, J.H., 1999. Aeolian processes across transverse dunes. II: modelling the sediment transport and profile development. Earth Surface Processes and Landforms, 24(4), 319-333.

Vermeesch, P., Drake, N., 2008. Remotely sensed dune celerity and sand flux measurements of the world's fastest barchans (Bodélé, Chad). Geophysical Research Letters, 35(24), L24404.

von Karman, T., 1947. Sand ripples in the desert. Technion Yearbook, 6, 52-54.

Walker, I.J., Nickling, W.G., 2003. Simulation and measurement of surface shear stress over isolated and closely spaced transverse dunes in a wind tunnel. Earth Surface Processes and Landforms, 28(10), 1111-1124.

Wang, X., Dong, Z., Zhang, J., Chen, G., 2002. Geomorphology of sand dunes in the Northeast Taklimakan Desert. Geomorphology, 42(3â€“4), 183-195.

Wang, X., Wang, T., Dong, Z., Liu, X., Qian, G., 2006. Nebkha development and its significance to wind erosion and land degradation in semi-arid northern China. Journal of Arid Environments, 65(1), 129-141.

Wang, Y., Wang, J., Chi, Z., Xiao, X., Zhang, Z., 2004. Formation of Keriya river terraces and uplift of western Kunlun. 3(3), 207-209. (in Chinese).

Wang, Z.-T., Tao, S.-C., Xie, Y.-W., Dong, G.-H., 2007. Barchans of Minqin: Morphometry. Geomorphology, 89(3–4), 405-411.

Wang, Z.T., Zhao, H., Zhang, K.C., Ren, X.Z., Chen, F.H., Wang, T., 2009. Barchans of Minqin: quantifying migration rate of a barchan.

Ward, J., 1987. The Cenozoic succession in the Kuiseb valley, central Namib Desert. Geological Survey, Department of Economic Affairs (Windhoek, South West Africa/Namibia).

Warren, A., 1972. Oberservations on dunes and bi-modal sands in the Tenere Desert. Sedimentology, 19(1-2), 37-44.

Wasson, R.J., Hyde, R., 1983. Factors determining desert dune type. Nature, 304(5924), 337-339.

Weather Underground, 2013. Weather Underground. http://www.wunderground.com/?MR=1, 2011-2013.

Welsh, K.E., Dearing, J.A., Chiverrell, R.C., Coulthard, T.J., 2009. Testing a cellular modelling approach to simulating late-Holocene sediment and water transfer from catchment to lake in the French Alps since 1826. The Holocene, 19(5), 785-798.

Werner, B.T., 1995. Eolian dunes: Computer simulations and attractor interpretation. Geology, 23(12), 1107-1110.

Werner, B.T., Kocurek, G., 1999. Bedform spacing from defect dynamics. Geology, 27(8), 727-730.

Wiggs, G.F.S., 2001. Desert dune processes and dynamics. Progress in Physical Geography, 25(1), 53-79.

Wiggs, G.F.S., Bullard, J.E., Garvey, B., Castro, I., 2002. Interactions Between Airflow and Valley Topography with Implications for Aeolian Sediment Transport. Phys. Geogr., 23(5), 366-380.

Wiggs, G.F.S., Livingstone, I., Warren, A., 1996. The role of streamline curvature in sand dune dynamics: evidence from field and wind tunnel measurements. Geomorphology, 17(1–3), 29-46.

Wilcock, P., Crowe, J., 2003. Surface-based Transport Model for Mixed-Size Sediment. Journal of Hydraulic Engineering, 129(2), 120-128.

Willgoose, G., 2005. Mathematical Modeling of Whole Landscape Evolution. Annual Review of Earth and Planetary Sciences, 33(1), 443-459.

Willgoose, G., Bras, R.L., Rodriguez-Iturbe, I., 1991. A coupled channel network growth and hillslope evolution model: 1. Theory. Water Resources Research, 27(7), 1671-1684.

Willgoose, G., Bras, R.L., Rodriguez-Iturbe, I., 1994. Hydrogeomorphology modelling with a physically based river basin evolution model. Process Model and Theorethical Geomorphology, 3-22.

Wilson, I.G., 1971. Desert Sandflow Basins and a Model for the Development of Ergs. The Geographical Journal, 137(2), 180-199.

Wilson, I.G., 1972. Aeolian bedforms - their development and origins. Sedimentology, 19(3-4), 173-210.

Wippermann, F.K., Gross, G., 1986. The wind-induced shaping and migration of an isolated dune: A numerical experiment. Boundary-Layer Meteorol, 36(4), 319-334.

Wu, Z., 1987. Aeolian Geomorphology. Science Press, Beijing.

Xu, J., Yang, J., Yan, Y., 2006. Erosion and sediment yields as influenced by coupled eolian and fluvial processes: The Yellow River, China. Geomorphology, 73(1-2), 1-15.

Xu, Z.X., Chen, Y.N., Li, J.Y., 2004. Impact of Climate Change on Water Resources in the Tarim River Basin. Water Resources Management, 18(5), 439-458.

Yang, X., Zhu, Z., Jaekel, D., Owen, L.A., Han, J., 2002. Late Quaternary palaeoenvironment change and landscape evolution along the Keriya River, Xinjiang, China: the relationship between high mountain glaciation and landscape evolution in foreland desert regions. Quaternary International, 97–98(0), 155-166.

Yang, Y., 1990. The geomorphology development of Keriya River, China. 13(1), 37-45. (in Chinese).

Yao, Z.Y., Wang, T., Han, Z.W., Zhang, W.M., Zhao, A.G., 2007. Migration of sand dunes on the northern Alxa Plateau, Inner Mongolia, China. Journal of Arid Environments, 70(1), 80-93.

Zhang, Q., Xu, C.-Y., Tao, H., Jiang, T., Chen, Y., 2010. Climate changes and their impacts on water resources in the arid regions: a case study of the Tarim River basin, China. Stoch Environ Res Risk Assess, 24(3), 349-358.

Zhu, Z., Guo, H., Wu, G., 1964. The dune migration along the oasis in the south-west of Taklamkan,China. 30(1), 35-50. (in Chinese).

Zhu, Z.D., Wu, Z., Liu, S., Di, X.M., 1980. Introduction to the Sand Deserts in China. Science Press, Beijing.

Appendices

Appendix A Crescentic dunes height and dynamics in field (continues to page 184).

Experiment taken date	Location	Dune type	Dune height (*m*)	Dune migration speed (myr^{-1})		Sand transport rate ($m^3m^{-1}yr^{-1}$)		References
				Range	Average	Range	Average	
1991-1992	Tarim, China	Barchans	0.84-2.0	4.81-10.87	7.29		4.374	(Dong et al., 1998)
1992-1993	Tarim, China	Barchans		3.33-8.89	5.56		3.336	(Dong et al., 2000)
1964	Tarim, China	Barchans	0.8-3.5	6.8-61.4	17.2	23.65-25.7675		(Zhu et al., 1964)
1930-1987	Northwestern Sudan				7.5			(Haynes Jr, 1989)
2002	Taklimakan, China					2.2-4.4	3.3	(Wang et al., 2002)
2009	Great Kobuk Sand Dunes, Alaska, USA			0.5-1.5				(Necsoiu et al., 2009)
1967-1988	Algodones, CA, USA	crescentic	≤ 80	0.0135-80				(Sweet et al., 1988)
2002	NE, Taklimakan, China	crescentic	8-15	1-20				(Wang et al., 2002)
2005	Ordos Plateau, China					0.01-40.1		(Liu et al., 2005)
1999	South Peru	Barchans		13.5-45.75				(Parker Gay Jr, 1999)
1973-2000	Alxa, Inner Mongolia, China	Transverse/barchan	6-22	4-7.4	5.3			(Yao et al., 2007)
1961-2001	Victoria Valley, Antarctica		5.3		1.5			(Bourke et al., 2009)
1952		Draa	35-240	0.016-0.34		3.6-8		(Wilson, 1972)
1948-1964	Hanford Site, USA	Crescentic	3-5.8	0.9-3.3				(Gaylord and Stetler, 1994)
2011	Valdevaqueros, Spain		40			318.75–456.25		(Navarro et al., 2011)
1995-2006	Valdevaqueros, Spain	transgressive	40	≤ 38	17.5			(Muñoz-Perez et al., 2009)
1940-1993	Aberffraw, North Wales,	parabolic	12	≤3.6	1			(Bailey and Bristow, 2004)
1977-1999	SW Spain	Transgressive		≤ 5.35	1.21			(Ojeda et al., 2005)
0-1998	Thar desert, India	Transverse	7	0.025-0.09				(Kar et al., 1998)

Appendix A (continued).

Experiment taken date	Location	Dune type	Dune height (*m*)	Dune migration speed (myr^{-1})		Sand transport rate ($m^3m^{-1}yr^{-1}$)		References
				Range	Average	Range	Average	
1680-2005	Liwa,UAE	Transverse	20	≤ 0.91	0.78			(Stokes and Bray, 2005)
1969-2005	Valdes Peninsula, Argentina	Compound transverse	7-15	9.1±2.7				(del Valle et al., 2008)
1936-1999	Great Sand, USA	barchans		(2.2±1.7)-22				(Marín et al., 2005)
2008-2009	Chah Jam erg, Iran	Barchans			20			(Mousavi et al., 2010)
1916-1958	South Peru	Barchans	1-7	3.6-91				
1953	Pru-dune, south of Trujillo, Peru	Barchans	55		5			(Finkel, 1959)
1957-1964	South Peru	Barchans	7-20	13-157				(Parker Gay Jr, 1999)
1941-1956	West side of Salton Sea, California	Barchans	3-40	15.24-60				(Long and Sharp, 1964)
1955-1964			9.33-11.22	8.78-44.62				(Norris, 1966)
1974-2003	South Peru			0.95-1.98				(Hesse, 2009b)
	White sands, New Mexico, US		15	1-7	1.6			(Kocurek et al., 2007) (McKee and Douglass, 1971)
1958-2005	La Joya, Peru	Barchans	10-80	9-25				(Elbelrhiti et al., 2008)
	North Sinai, Egypt	Barchans		0.9-21				(Hermas et al.)
		Transverse	11.7-47.1		19			(Fryberger et al., 1984)
2000-2007	Chad	Barchan	3-50			76-99		(Vermeesch and Drake, 2008)
1907-1908	Libyan Bellaida dune	Barchans	1-40	10.8-15				(Beadnell, 1910)

Appendix A (continued).

Experiment taken date	Location	Dune type	Dune height (*m*)	Dune migration speed (myr^{-1})		Sand transport rate ($m^3m^{-1}yr^{-1}$)		References
				Range	Average	Range	Average	
		Barchans	10-30	0.8-350				(Hesp and Hastings, 1998)
		Barchans	0.3-0.6					(Hesp and Arens, 1997)
	Namib South	Barchans		4.2-60				(Livingstone, 2012)
1961-2000	Namib	Barchans		4.24-18.9	13.15			(Barnes, 2001)
2007	Minqin, China	Barchans	1.509 - 9.382					(Wang et al., 2007)
2007				1.78-3.42				(Wang et al., 2009)
1993	Kuwait	Barchans	3		26.7		20	(Khalaf and Al-Ajmi, 1993)
1980	Sahara	Barchans			7.5			(Haynes Jr, 1989)
1996	california	Barchan	5			5.38-465.8		(Lancaster et al., 1996)
2000	Jericoacoara, Brazil	Barchan	35	20		0-668.9455		(Sauermann et al., 2003)
2003	Brazil	Transverse Barchan	6.9-9.7 0.5-1					(Parteli et al., 2006)
	Mojave desert, USA					7.86		(Kocurek and Lancaster, 1999)
2000		transverse	0.4-19	6-50				(Momiji and Warren, 2000)

NB: Sand bulk density = 1700 $kg\ m^{-3}$ when the local sand bulk density were not specified in each study (Wilson, 1972).

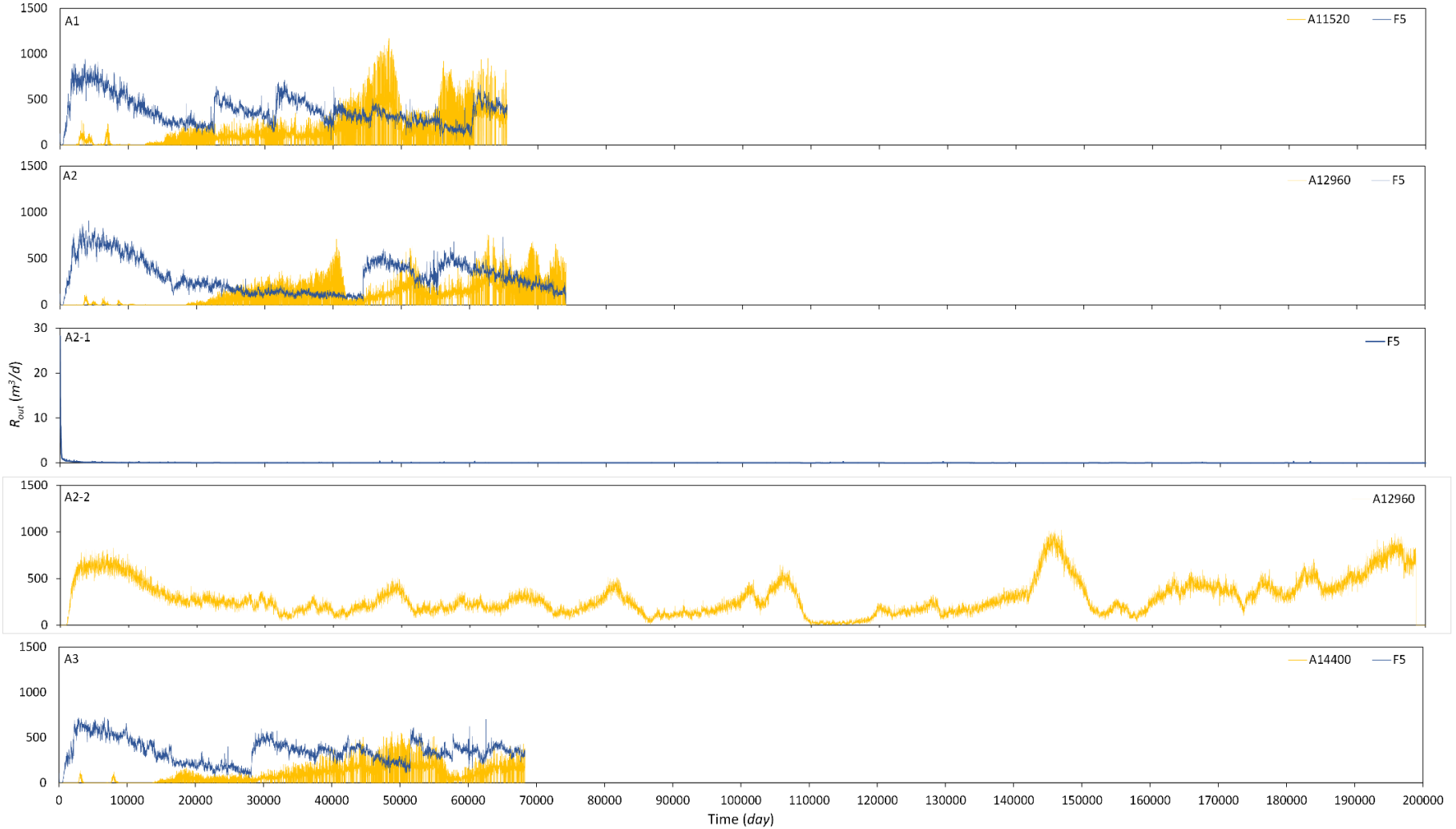

Appendix B Daily fluvial/aeolian simulated sediment output rate in perennial context. Graphs A1- A28 shows the sediment output from fluvial-aeolian interacting field, while graphs A2-1 shows fluvial sediment discharge in field without aeolian system and A2-2 shows aeolian sediment output in field without fluvial system (continues to page 190).

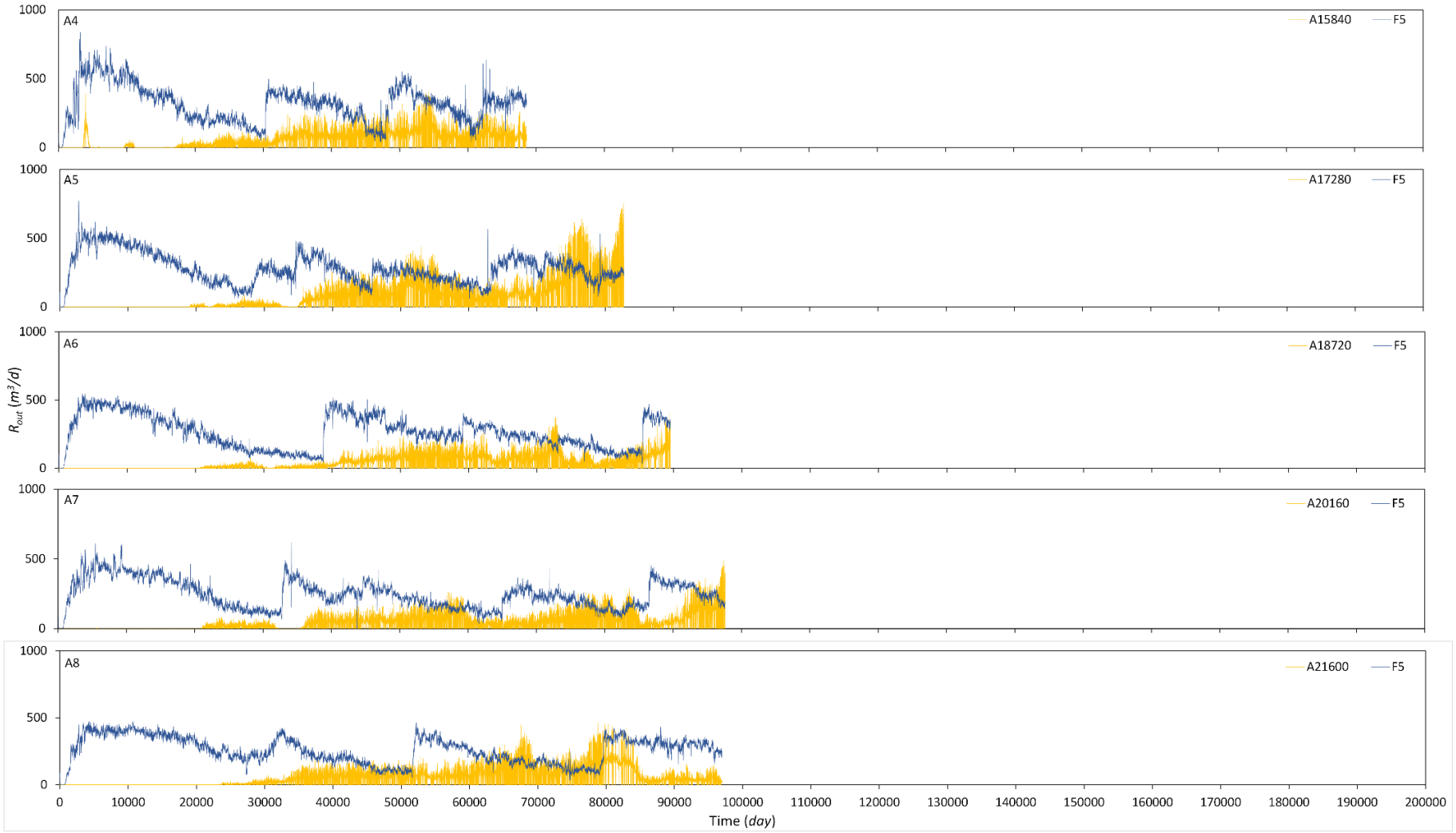

Appendix B (continued).

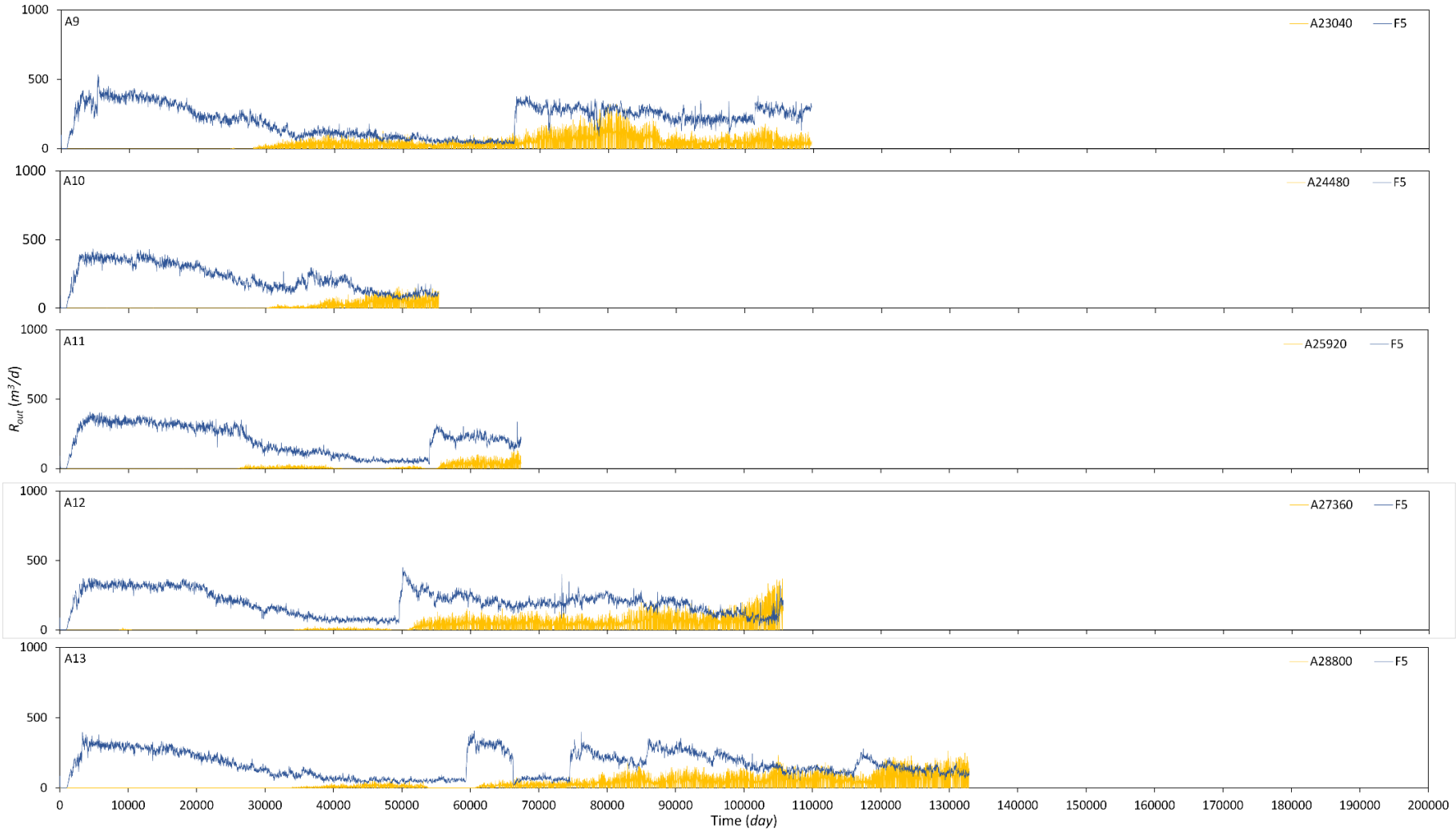

Appendix B (continued).

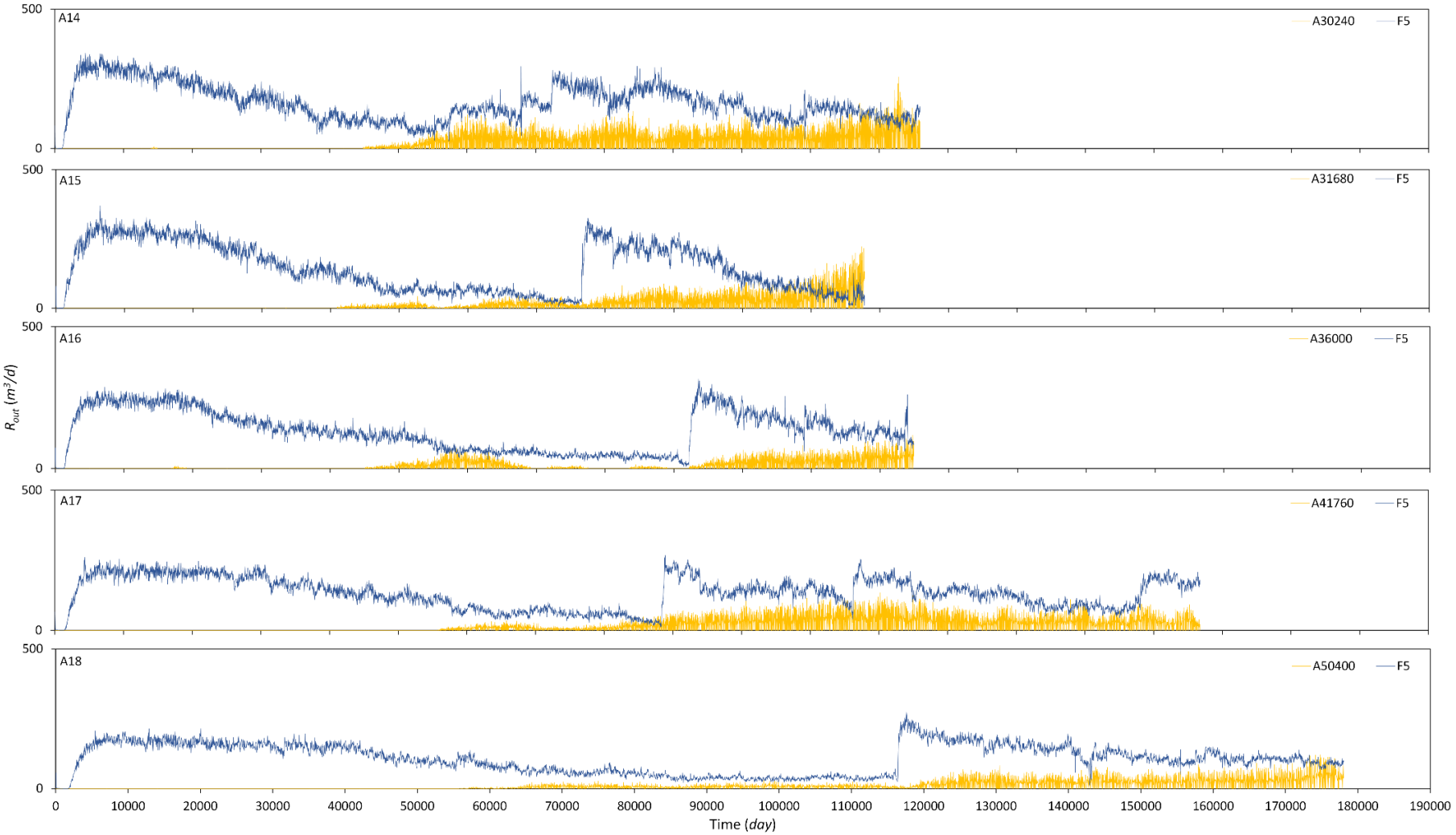

Appendix B (continued).

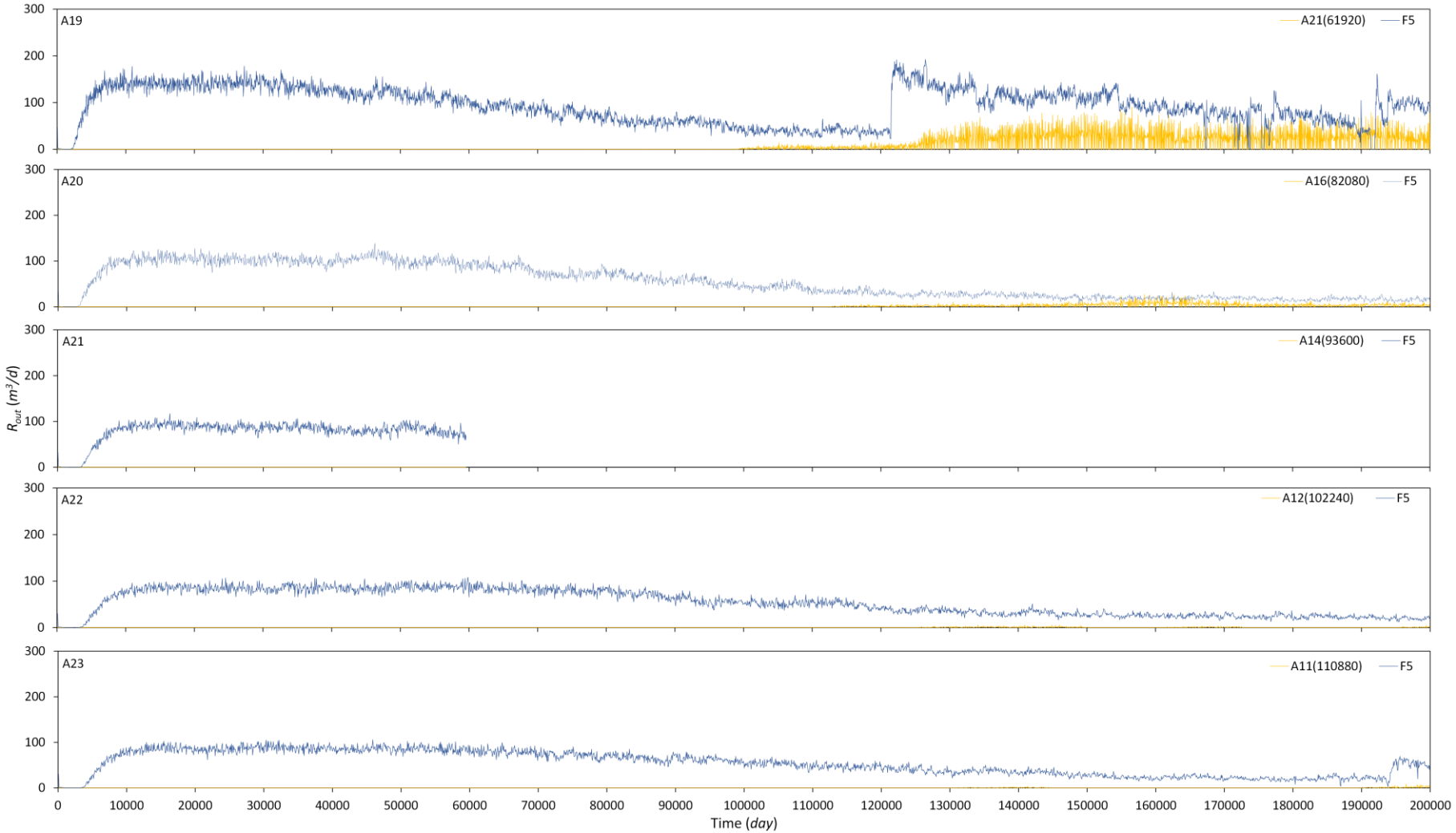

Appendix B (continued).

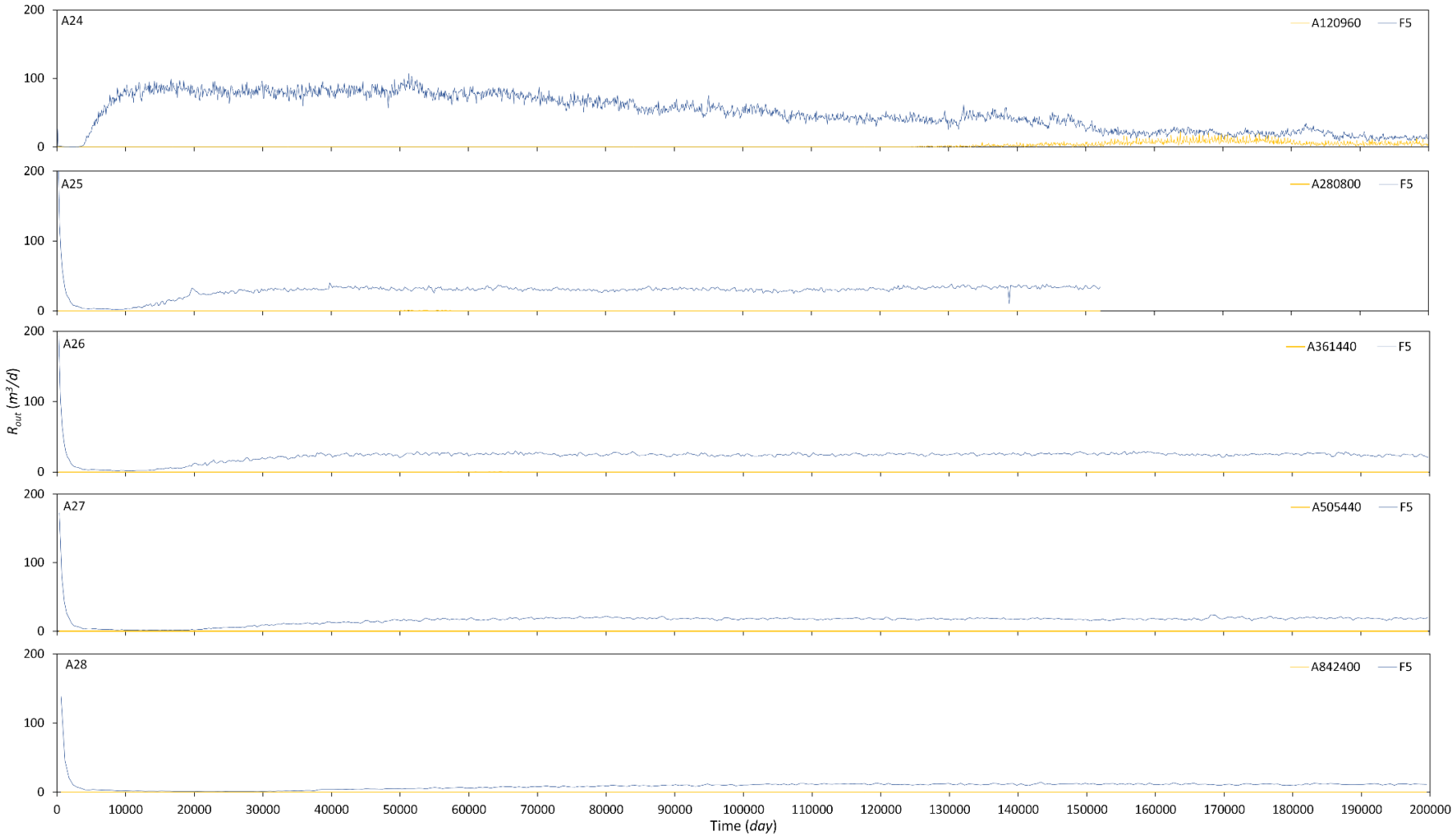

Appendix B (continued).

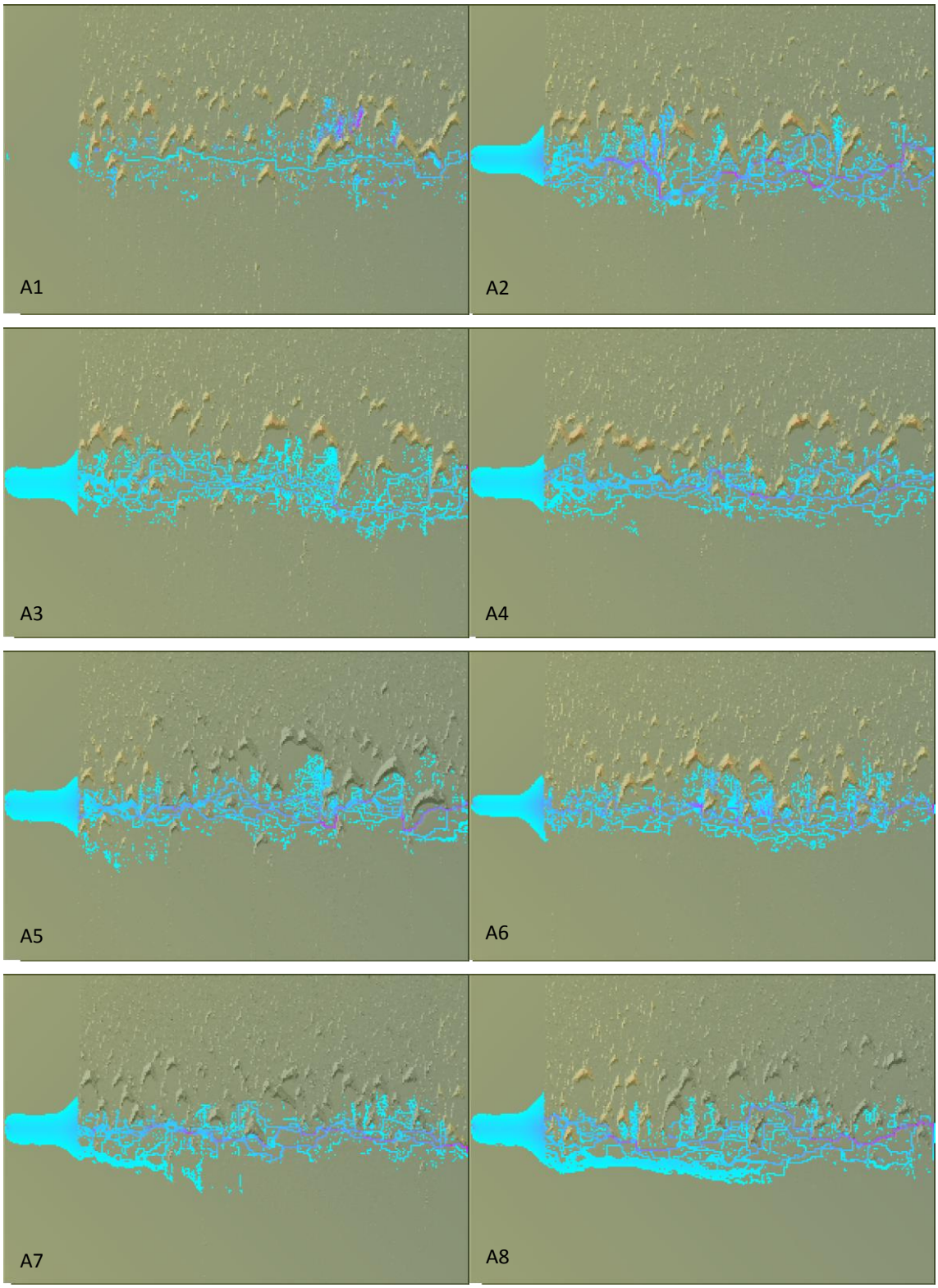

Appendix C Dunes behaviours in fluvial-aeolian interacting field in perennial context (D_c= 10m^3s^{-1}, R_s= 102$m^3m^{-1}yr^{-1}$, T=32 *yr*, *i*=1153). A1-A11) landform snapshots from scenario 1 to 11, respectively; A12) Himalaya, China (29°55'40.12" N 83°32'35.12" E); A13) Perennial scenario (D_c= 10m^3s^{-1}, R_s= 102 $m^3m^{-1}yr^{-1}$); A14) Dune field without flow interfering (R_s= 102 $m^3m^{-1}yr^{-1}$) (continues to page 192).

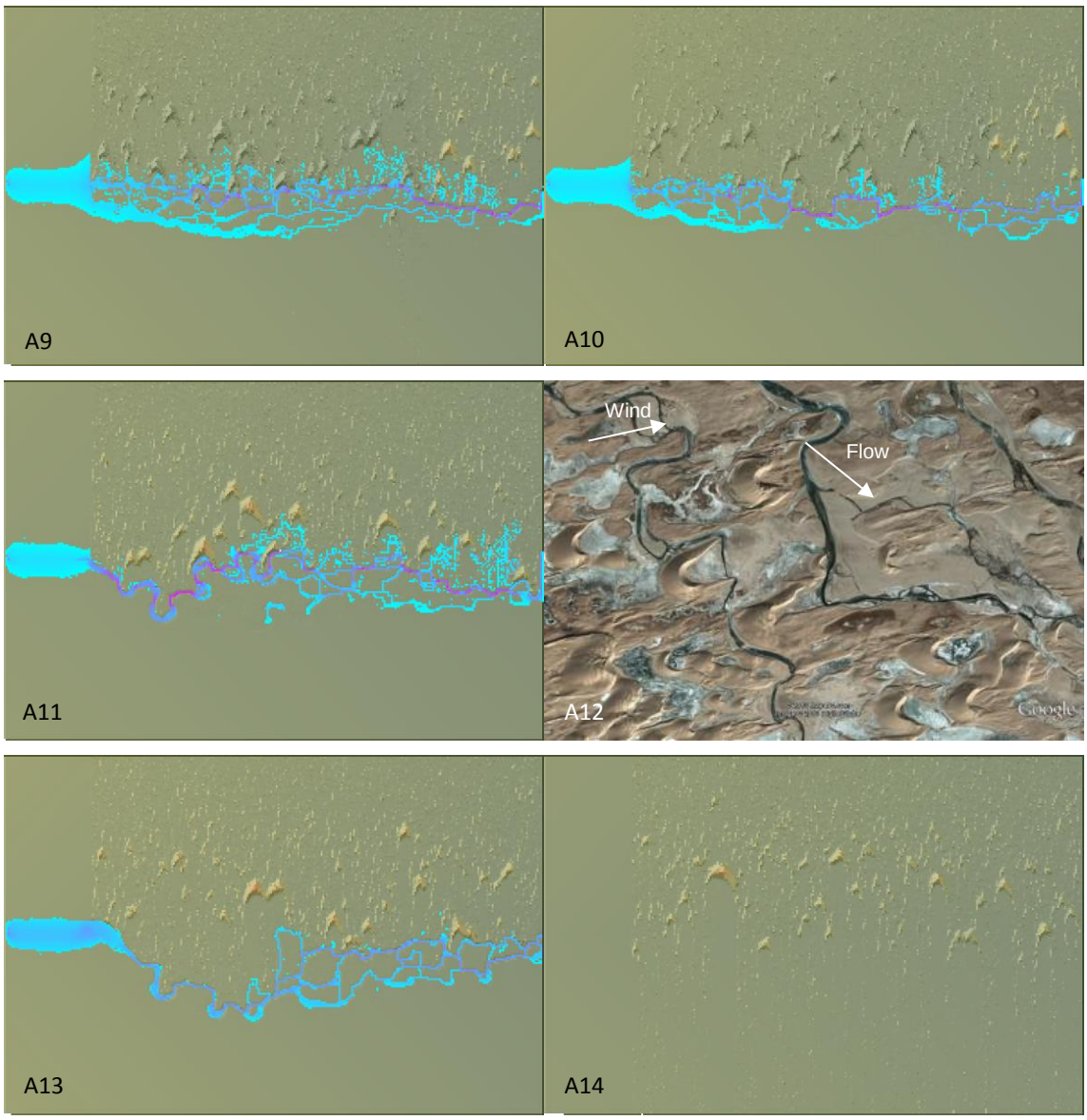

Appendix C (continued).

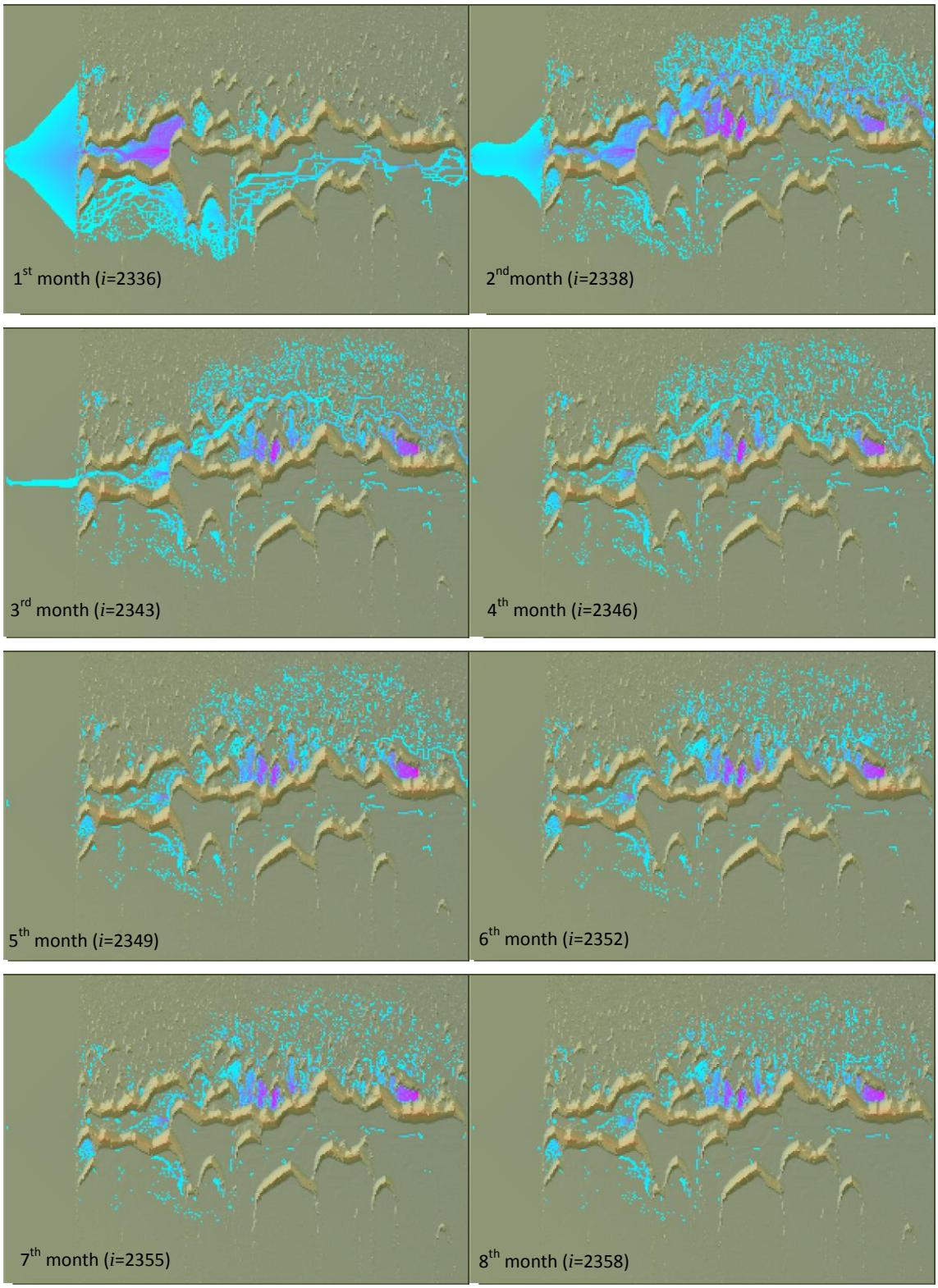

Appendix D Landform in each month of scenario 2 in ephemeral context (D_c= 10m^3s^{-1}, R_s= 102$m^3m^{-1}yr^{-1}$, T=64 *yr*) (continues to page 194).

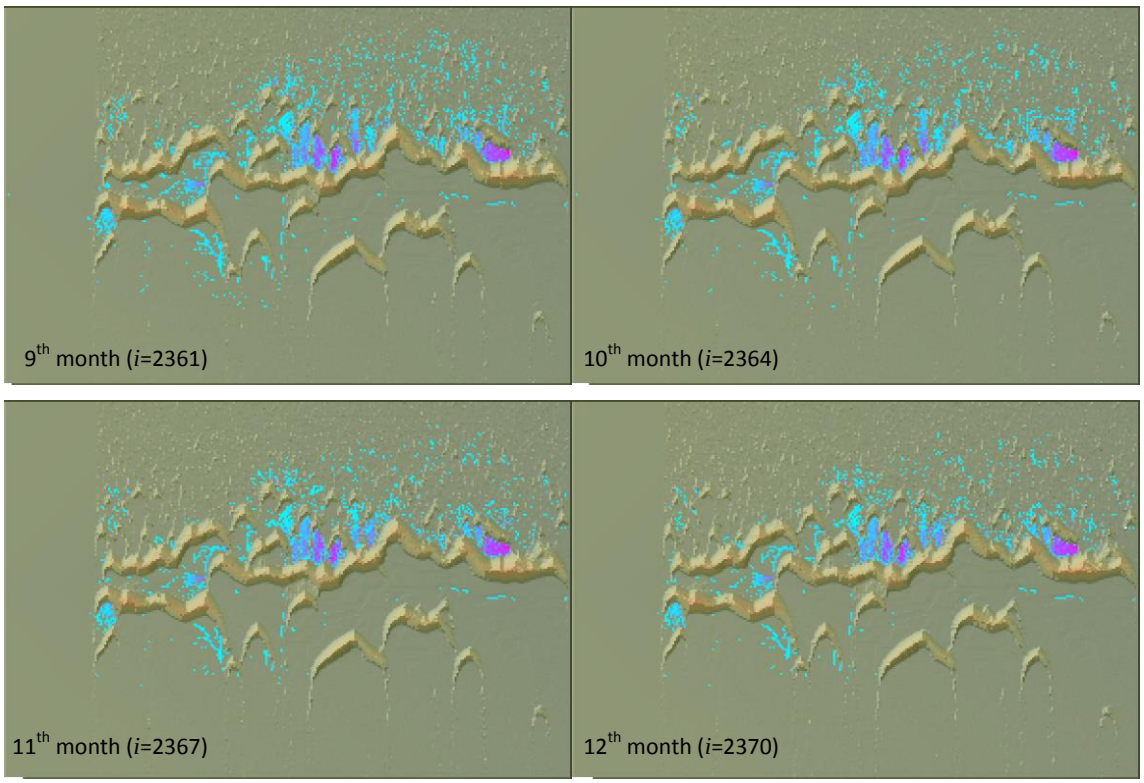

Appendix D (continued).

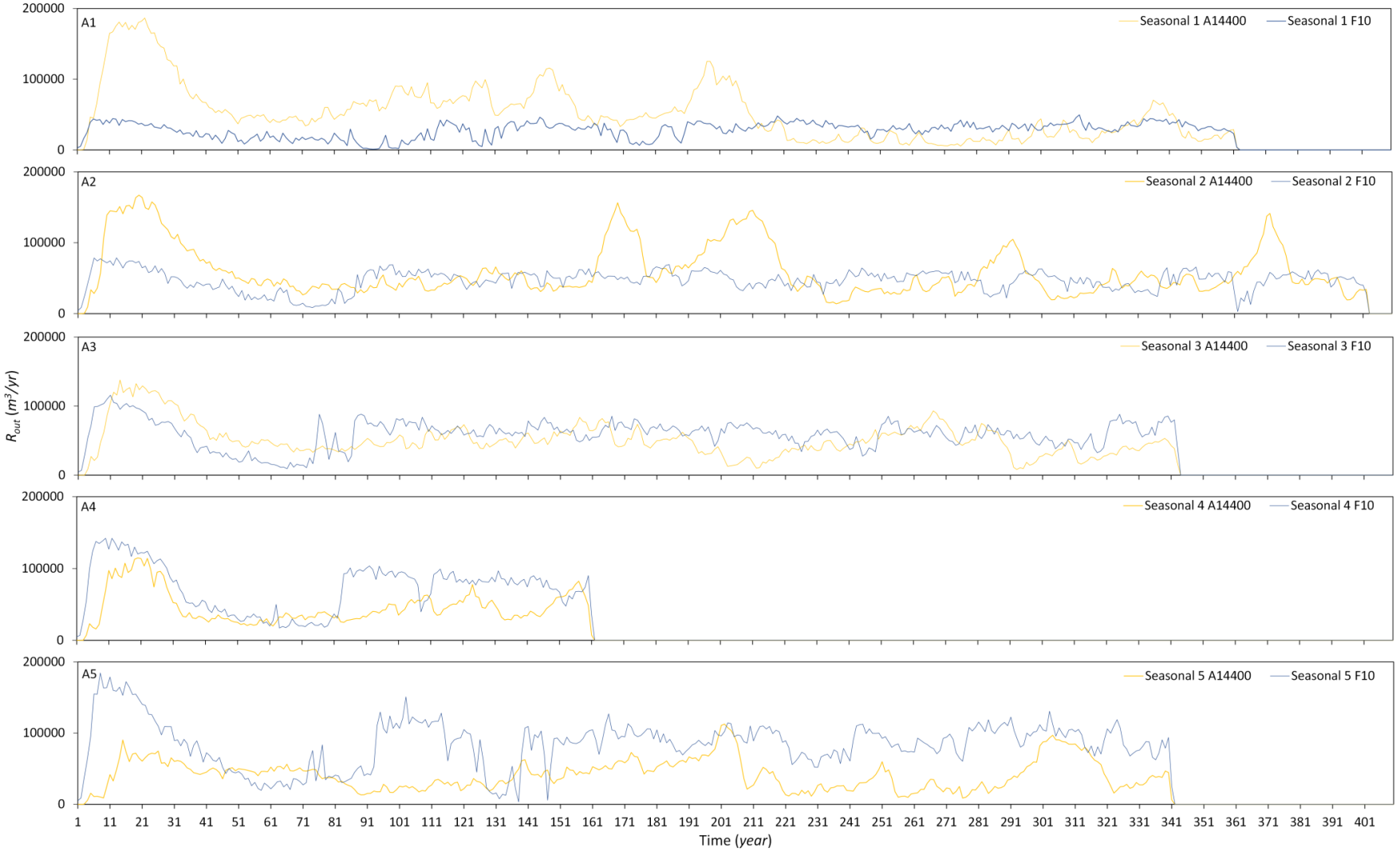

Appendix E Annual sediment output in each scenario of seasonal change of group 2 (continues to page 198).

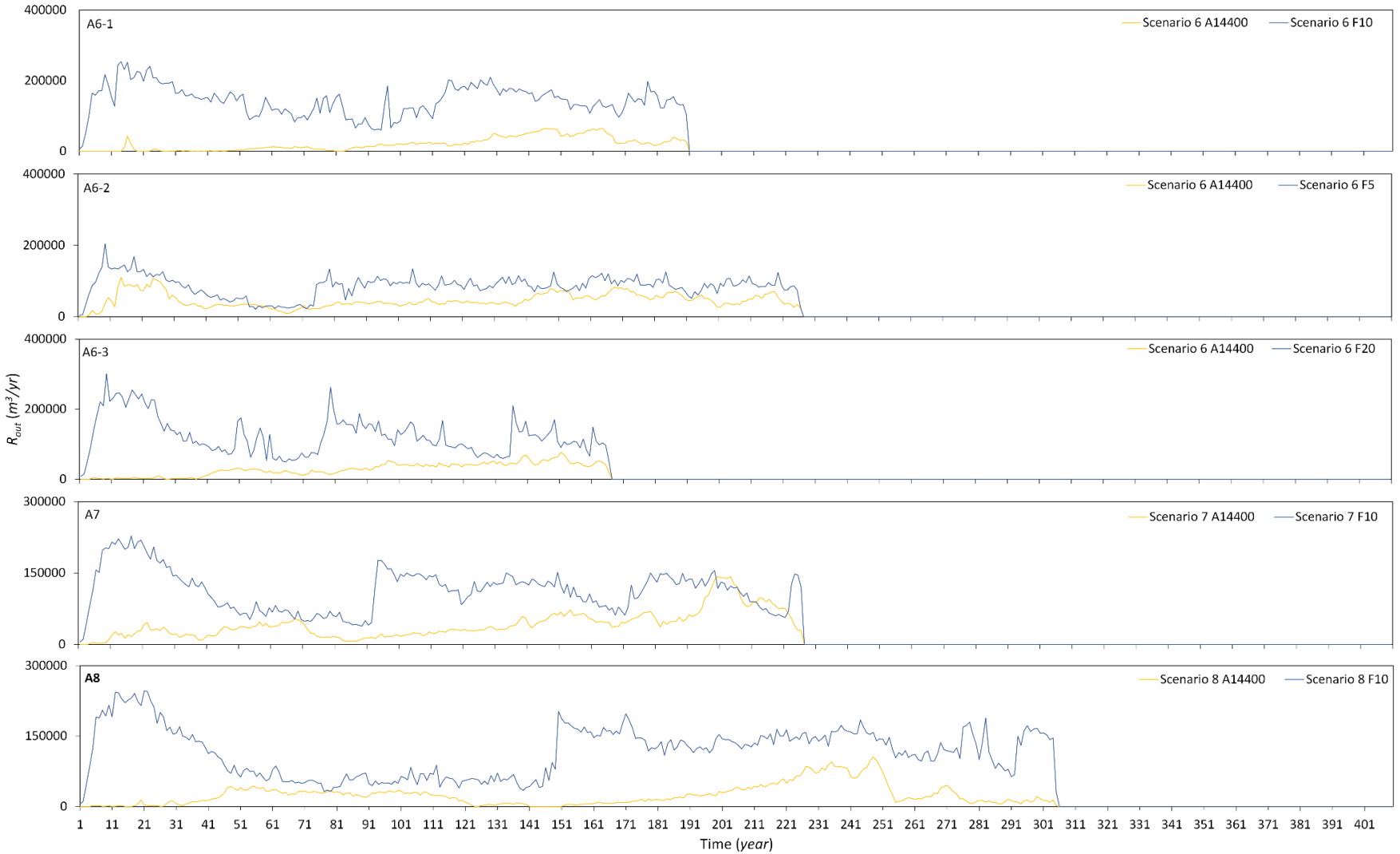

Appendix E (continued).

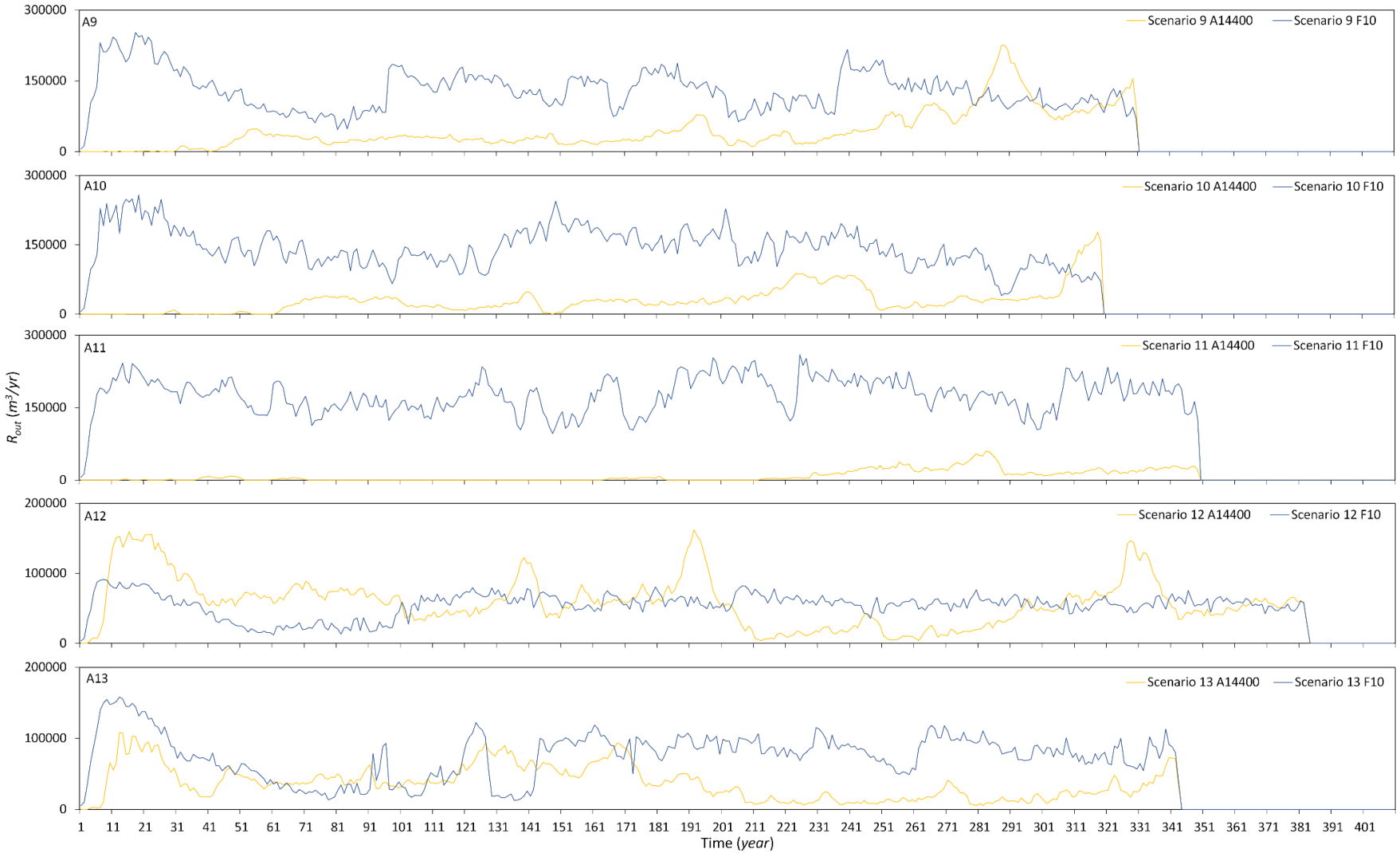

Appendix E (continued).

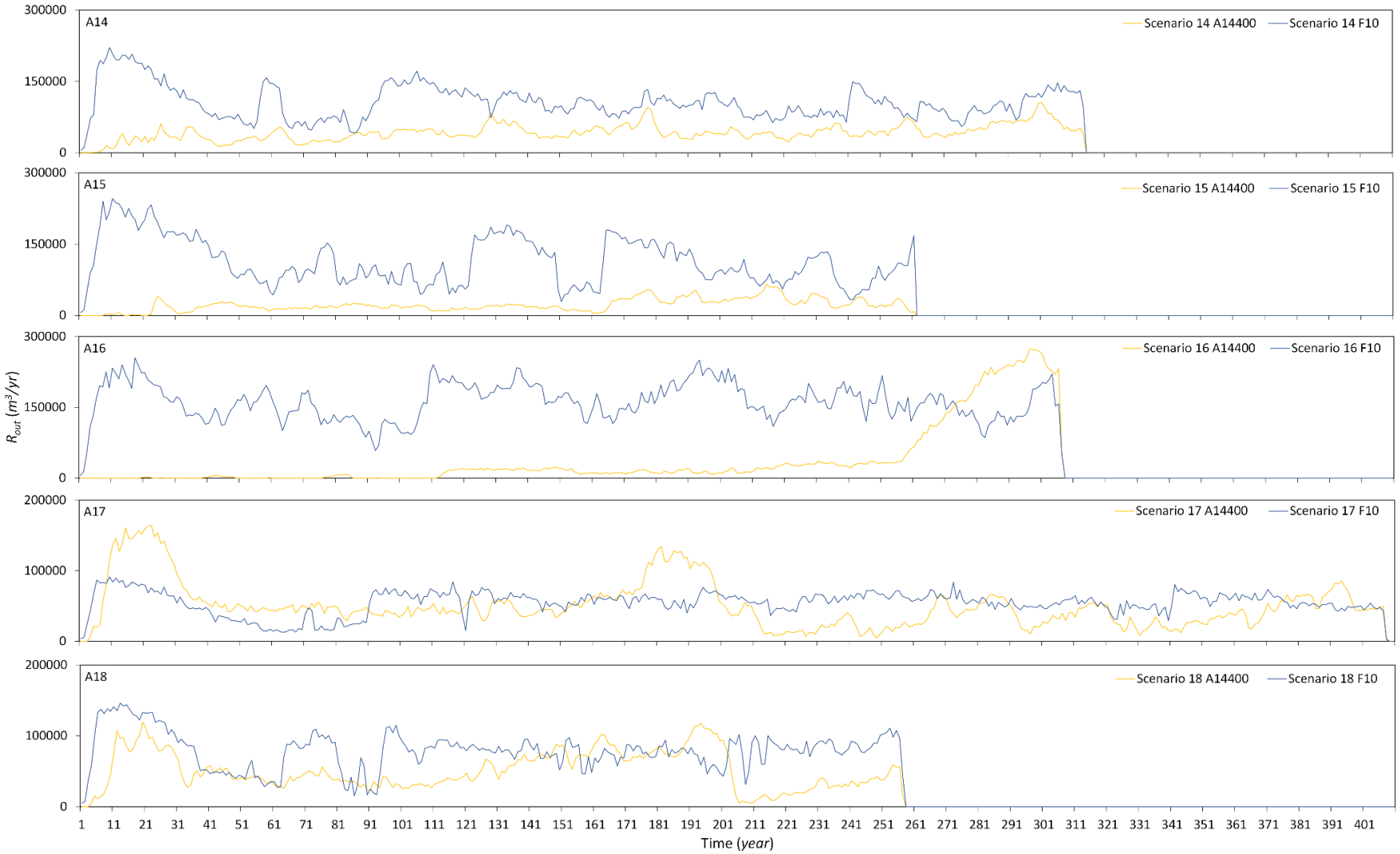

Appendix E (continued).